

Polytechnic of Turin

THESIS OF MASTER'S DEGREE IN
AEROSPACE ENGINEERING



Virtual Shaker Testing (VST) approach and its application to a spacecraft

(In collaboration with Thales Alenia Space)

LM-20 (DM270)

Supervisors:

Egr. Prof. Erasmo Carrera

Dr. Pietro Nali (Thales Alenia Space Italia)

Candidate:

Davide Pederbelli

A.A 2018/2019

"Part of the journey is the End"
The Avengers

Alla mia Famiglia

Ringraziamenti

Abstract

(In **English** language)

Into the design and verification framework of a S/C, a fundamental milestone is provided by the qualification and acceptance tests during which the capability of the platform to withstand the mechanical environment, reproduced by proper devices with suitable load values, is observed.

Focusing on sinusoidal vibration tests, also called *sine sweep*, the aim is to impose low frequency loads on three axes, between 5÷100 Hz, through a shaker placed at the base of the S/C. Mechanical proper interfaces connect the slip table to the S/C.

Typically, the curves acquired during the test are different with respect to the ones predicted in the classical numerical sine test prediction. In general, the anomalies unforeseen in the numerical sine test prediction can imply test aborts and schedule issues to complete the test campaign.

The detailed study of these anomalies, between the sine test numerical predictions and the corresponding test acquisitions, shows that differences are mainly attributable to an inconsistent imposition of the boundary conditions (BCs) into the numerical model, “Hard mounted” (HM), where translations and rotations are constrained to the base of the S/C. Moreover, the transient phenomena neglected in the Frequency Response Analysis (FRA) are an additional source of discrepancy.

Precisely, the geometrical and mechanical characteristics of the shaker as mass, inertia, elasticity and constructive elements (seismic mass, struts, and supports), are completely omitted into the classical approach. It follows the inability to model and study the phenomenon observed during the test phase as dynamic couplings (“rockling”, “saddle”, “bending”) between shaker and S/C, the dynamic effect of the seismic mass and “Cross-talks”.

In addition, the “sweep rate”, the rate of climb of the forcing frequency during the test, increases the gap between model and reality, separating the stationary predictions based on FRA, compared to the extracted transient. As result, the natural frequencies observed during the vibration test are distorted through a frequency shift.

A low sweep rate is critical for the S/C because forces it to oscillate subjected to a forcing function with a frequency close to the natural one of the S/C itself. For these reasons, the classical approach based on FRA with HM conditions is inconsistent due to an incomplete modelling of the problem.

In this framework, the innovative transient approach called “Virtual Shaker Testing” (VST), extends the BCs beyond shaker, modelling the complex shaker –S/C. It allows to perform the sine test prediction anticipating the dynamic transient behaviours, sweep rate effects and coupling issues between S/C and shaker-assembly that are impossible to recognize though the steady state approach.

From the applicative point of view, a MATLAB/Simulink© model, called *Vibration controls*, provided by SIEMENS®, has been used. These routines are able to automatically integrate the *Notching* criteria, i.e. the reduction of the forcing amplitude when dedicated acceleration thresholds are exceeded, into the computational loop of a transient analysis.

For this reason, the preparation of a computational framework capable to setup and carry out the VST with dynamic structural models, in a state-space form using condensed models in Craig-Bampton formulation, is possible. In this way, the real transient prediction is performed for two satellites with a comparison between numerical and experimental possible results.

Sommario

(In *Italian* language)

Nell'ambito del design e verifica di uno S/C, una tappa fondamentale è appresentata dalle prove di qualifica ed accettazione durante le quali si osserva la capacità della piattaforma nel sopportare l'ambiente meccanico riprodotto da opportuni dispositivi, con valori di carico adeguati.

Focalizzandosi sulle prove vibrazionali sinusoidali ("sine sweep"), l'obiettivo è imporre carichi a bassa frequenza lungo tre assi distinti, tra 5 – 100 Hz, tramite uno shaker posto alla base dello S/C. Apposite interfacce meccaniche collegano la tavola vibrante ("slip table") con lo S/C stesso.

Tipicamente, le curve estratte in fase di testing risultano diverse da quanto previsto dalle classiche predizioni numeriche basate su analisi di risposta in frequenza (FRA), tramite codici agli elementi finiti. Come conseguenza vi è la generazione aborti (stop dei test) a cui seguono alti costi di affitto della facility per completare il ciclo di prove.

Lo studio accurato di tali discrepanze afferma che la loro origine sta nell'imposizione delle condizioni al contorno nella modellazione numerica, "Hard mounted" (HM), in cui traslazioni e rotazioni sono tutte bloccate, ed alla natura stessa dell'analisi di risposta in frequenza con cui si trascurano gli effetti di transitorio.

Più nel dettaglio, le caratteristiche geo-meccaniche dello shaker come massa, inerzia, elasticità ed elementi costruttivi non trascurabili (massa sismica, montanti e supporti), sono completamente omesse. Ne consegue l'incapacità di modellare e studiare le fenomenologie riscontrate in fase di test, quali accoppiamenti dinamici ("rockling", "saddle", "bending") tra shaker e S/C, effetto della dinamica della massa sismica e "Cross-talks".

Inoltre, il cosiddetto "sweep rate", il rateo di salita della frequenza della forzante durante il test, aumenta il gap tra realtà e modello, separando le predizioni stazionarie basate sulla FRA, con quelle transitorie estratte. Vengono così falsate le frequenze naturali monitorate a valle del test rispetto le previsioni numeriche, il "frequency shift". Uno "sweep rate" basso risulta critico per lo S/C poiché lo obbliga ad oscillare sottoposto ad una forzante la cui frequenza è prossima a quella naturale dello S/C stesso.

Per i detti motivi, l'approccio analitico classico basato sulla FRA con condizioni HM, risulta dunque fallace poiché basato su una incompleta modellazione del problema.

In tale ottica, l'innovativo approccio transitorio "Virtual Shaker Testing" (VST), basandosi su una estensione delle condizioni al contorno, in cui il complesso shaker – S/C è totalmente modellato, permette di estendere e migliorare la qualità delle predizioni numeriche anticipando virtualmente le problematiche di accoppiamento non analizzabili per via convenzionale, anticipandone gli effetti dovuti al transitorio.

Dal punto di vista applicativo ci si è concentrati nell'uso di un modello MatLab/Simulink fornito da SIEMENS, capace di integrare il criterio del "Notchig", ovvero la riduzione dell'ampiezza dell'eccitante in caso di superamento di adeguate soglie di accelerazione, automaticamente all'interno di una analisi transiente. Ciò ha reso possibile la creazione un framework computazionale atto a compiere il VST di modelli dinamici in formato stato-spazio usando condensati nella formulazione Craig-Bampton, effettuando, dunque, la vera e propria predizione dinamica di due satelliti comparando i risultati numerici con eventuali curve da test sperimentale.

Table of contents

Ringraziamenti.....	3
Abstract.....	4
Sommario.....	5
Table of contents	6
Nomenclature	8
List of figures.....	9
List of tables	12
Introduction	13
Introduzione	15
Part I	17
Chapter 1: Background on structural dynamics	18
1.1 SINGLE DOF UNDER FORCED DAMPED MOTION	20
1.2 SINGLE DOF UNDER BASE EXCITATION	22
1.3 MULTI DEGREES OF FREEDOM (MDOF)	24
1.4 FREQUENCY RESPONSE FUNCTION (FRF).....	26
1.5 MODAL EFFECTIVE MASSES (MEMS).....	29
Chapter 2: The State space systems	32
2.1 THE STATE VARIABLE MODEL AND CONTINUOUS STATE SPACE SYSTEMS	33
2.2 DISCRETE STATE SPACE SYSTEMS	35
Chapter 3: The Craig-Bampton dynamic condensation method	37
Part II.....	40
Chapter 4: The launch environment.....	41
4.1 OVERVIEW OF THE TYPICAL LOADS DURING THE LAUNCH	44
4.1.1 <i>Quasi-static</i>	44
4.1.2 <i>Sinusoidal</i>	45
4.1.3 <i>Random and vibro-acoustics</i>	45
4.1.4 <i>Shocks</i>	46
4.2 EXAMPLE OF LAUNCH LOADS THROUGH ARIANE 5	47
Chapter 5: Sine vibration	51
5.1 SHOCK RESPONSE SPECTRUM (SRS), EQUIVALENT SINE DYNAMICS AND EQUIVALENT SINE LEVEL (ESL) 54	
Chapter 6: Sine testing for S/Cs	60
6.1 TEST PREPARATION: CONFIGURATION AND SEQUENCE	62
6.2 PRIMARY AND SECONDARY NOTCHING DURING SINE VIBRATION TEST	62
Part III	65
Chapter 7: The issue of the coupling between shaker and test-item	66
7.1 SINE SWEEP EXCITATION.....	67
7.1.1 <i>The effect of sweep rate</i>	68
7.1.2 <i>Beating phenomena</i>	69

7.2 MECHANICAL AND DYNAMIC COUPLING BETWEEN SHAKER AND IUT	72
Chapter 8: The Virtual Shaker Testing approach (VST)	73
8.1 ELECTRO-MECHANICAL LUMPED ANALYTICAL MODEL OF THE SHAKER	76
Chapter 9: Description of Siemens LMS Vibration Control Routines in Simulink environment	83
9.1 LMS- MATLAB FILES DESCRIPTION	84
9.1.2 “Set_Control_parameters.m”	84
9.1.2 “Flow.m”	84
9.2 SIMULINK MODEL DESCRIPTION	87
Chapter 10: Setup and definition of VST methodology and framework using pre-existing experimental data	94
10.1 MATLAB STATE SPACE CONVERTER DESCRIPTION: S_S_CONVERTER.M	94
10.2 EVALUATIONS BASED ON DIFFERENT DAMPING MODELS	95
10.2.1 Notch prediction using viscous damping models with mass and stiffness matrices extracted from the condensed model	99
10.2.2 Notch prediction updating using viscous damping models with mass and stiffness matrices from the condensed model	106
10.2.3 Notch prediction using structural damping matrix provided by NASTRAN	111
10.3 EVALUATIONS BASED ON SEVERAL CONTROL AND TESTING PARAMETERS	117
10.3.1 Influence of the compression factor	118
10.3.2 Influence of the sweep rate	120
10.3.3 Influence of the electrical parameters	121
Chapter 11: Application of VST to a S/C and results	123
11.1 TRANSIENT ANALYSIS INTO VST ENVIRONMENT OF S/C 01	123
11.1.1 S/C_01 notching prediction using H.M. boundary conditions	125
11.1.2 S/C_01 VST along Y direction	128
11.1.3 S/C_01 VST along X direction	130
11.1.4 S/C_01 Comparison between notched input from FRA, VST prediction and experimental test results	131
11.2 TRANSIENT ANALYSIS INTO VST ENVIRONMENT OF S/C 02	134
11.2.1 S/C_02 notching prediction using H.M. boundary conditions	135
11.2.2 S/C_02 VST setup and analysis	141
11.2.2 .1 S/C_02 VST along Y direction	144
11.2.2.2 S/C_02 VST along X direction	149
Chapter 12: Future trends and applications	156
Chapter 13: Conclusions	157
Appendix	159
References	162

Nomenclature

VST	Virtual Shaker Testing
IUT	Item Under Test
S/C	Spacecraft
L/V	Launch Vehicle
CLA	Coupled Load Analysis
FE	Finite Elements
FRF	Frequency Function Response
SDoF	Single Degree Of Freedom
MDOF	Multi Degree Of Freedom
HIL	Hardware In The Loop
MOS	Margin Of Safety
B.C.	Boundary Conditions
MEMs	Modal effective masses
MMOD	Micro Meteoroids Or Debris
SEA	Statistic energy analysis
QSL	Quasi-static loads
CoG	Centre of gravity
SPL	Sound pressure level
GTO	Geostationary Transfer Orbit
OASPL	Overall Acoustic Sound Pressure Level
SRS	Shock response spectrum
FT	Fourier transform
FFT	Fast Fourier transform
ODE	Ordinary differential equations
LTI	Linear time invariant
SV	State variables
ODE	Ordinary Differential Equation
SISO	Single Input-Single Output
SIMO	Single Input-Multiple Output
MIMO	Multiple Input-Multiple Output
A, B, C, D	State variables Matrix, Control Matrix, Observation Matrix, Control Matrix, Observation Matrix, Feed forward Matrix

List of figures

Figure 1: Chart for structural analysis [Ref. 10]	18
Figure 2: Main analysis strategies [Ref. 14]	19
Figure 3: SDoF with fixed base [Ref. 12]	20
Figure 4: Typical curves [Ref. 12]	21
Figure 5: Transient, steady-state and total response	22
Figure 6: Enforced motion at the base [Ref. 12]	22
Figure 7: Three examples of MDoF [Ref. 10, 12]	24
Figure 8: Mode superposition in a time domain signal [Ref. 16]	25
Figure 9: Modal technique: from one MDoF to a different SDoF systems (a), (b) [Ref. 16]	26
Figure 10: Representation of FRF [Ref. 10]	26
Figure 11: FRFs superposition [Ref. 16]	28
Figure 12: Continuous and discrete state space formulations [Ref. 29]	36
Figure 13: Craig-Bampton indices [Ref.12]	37
Figure 14: Different sources acting on a S/C [Ref. 13]	41
Figure 15: Loads in term of frequency content (a) [Ref. 9]	43
Figure 16: Loads in term of frequency content (b) [Ref. 9]	44
Figure 17: Quasi-static longitudinal acceleration [Ref.14]	45
Figure 18: Acoustic loads [Ref.12]	46
Figure 19: Example of time history for shock loads [Ref.12]	46
Figure 20: Close-up (on left) and exploded view of the LV (on right) [Ref.30]	47
Figure 21: Ariane 5 typical mission profile [Ref.30]	48
Figure 22: Quasi-static longitudinal acceleration during time [Ref.30]	48
Figure 23: Sine excitation at spacecraft base [Ref.30]	49
Figure 24: Acoustic noise spectrum [Ref.30]	49
Figure 25: Envelope shock spectrum for clamp-band release at spacecraft interface and for fairing and L/V stage separation events (left) L/V acceptable shock spectrum at launcher bolted interface (right) [Ref.30]	50
Figure 26: Swept sine wave [Ref.31]	51
Figure 27: Time vs frequency ratio for different exponential rate of sweep [Ref.31]	53
Figure 28: Enforced motion at the base [Ref.13]	55
Figure 29: Construction of SRS [Ref. 12, 32]	56
Figure 30: Simplified 1 DoF models [Ref.14]	57
Figure 31: Brief scheme of ESI definition [Ref.9]	58
Figure 32: Comparison between ESI and SRS curves [Ref.9]	58
Figure 33: IXV (left) and Bepi Colombo (right) on shaker [Curtesy of ESA]	61
Figure 34: Representation of a notched profile [Ref.12]	63
Figure 35: Views of the shaker facility, (a)-(b) describes the keys elements involved,	67
Figure 36: Peak shift caused by the sweep rate [Ref. 4]	68
Figure 37: Beating from the superposition of two frequency sinusoidal excitations [Ref. 4]	69
Figure 38: Dynamic amplification factor at different damping ratio (a), Response at various damping and input levels (b) [Ref. 4]	70
Figure 39: The effect of sweep rate (up) and damping [Ref. 4]	70
Figure 40: The effect of sweep rate (down) and damping [Ref. 4]	71
Figure 41: Ringing after the peak [Ref. 4]	71
Figure 42: Example of collocation of pilots and notchers on a platform [Ref.26]	74
Figure 43: VST based on modal analysis [Ref. 27, 26] saddle, bending and rockling modes	75

Figure 44: Cross section of the shaker (left), example of electromechanical model (right) [Ref.5]	76
Figure 45: The implemented electro-mechanical model [Ref.33]	77
Figure 46: Pilot curves	80
Figure 47: Acceleration profile reached up from the pilots (time and frequency)	81
Figure 48: Coil and Body time variation	82
Figure 49: Coil and Body frequency variation	82
Figure 50: Hardware and software in the loop (a), Simple scheme of the vibration controller (b) [Ref.7], Principle control-loop virtual shaker testing (c) [Ref. 25]	84
Figure 51: Main control environment	88
Figure 52: Detailed sine control environment	89
Figure 53: Modification to the Simulink model: before (a), after (b)	90
Figure 54: Sine control block parameters	91
Figure 55: Simulink block for Discrete State Space	92
Figure 56: Viscous vs structural damping force (a), equivalent hysteresis process in structural damping (b) [Ref.34]	96
Figure 57: Variation of viscous damping with natural frequencies (a), damping coefficients Vs natural frequency [Ref.34]	98
Figure 58: DTM structural model as a reference (a), location of accelerometers and condensed node, entire structure (c) [Courtesy of Thales Alenia Space IT]	101
Figure 59: Pre-existing experimental data. Excitation along Y+ and acquisition along Y+ and frequency range of interest (5-35 Hz) [Courtesy of Thales Alenia Space IT]	102
Figure 60: Acceleration control profile in frequency domain (a), pilot curves in time domain (b) {Pure proportional damping model}	103
Figure 61: Acceleration control profile in frequency domain (a), pilot curves in time domain (b) {Pure modal damping model}	104
Figure 62: Acceleration control profile in frequency domain (a), pilot curves in time domain (b) {Partial proportional Case 1}	104
Figure 63: Acceleration control profile in frequency domain (a), pilot curves in time domain (b) {Partial proportional Case 3}	105
Figure 64: Acceleration control profile in frequency domain (a), pilot curves in time domain (b) {Hybrid case}	106
Figure 65: Location of the notching Dofs attached on the DTM structure	107
Figure 66: View of the DTM FEM model (a), nodes used for the dynamic condensation using Nastran superelements (b) and (c), global view of the structure with the nodes used for the condensation (d)	108
Figure 67: Frequency range of interest of the updating model	108
Figure 68: Pure proportional damping model	109
Figure 69: Pure modal up to 150 Hz	109
Figure 70: Pure modal up to 200 Hz	109
Figure 71: Partial proportional Case 1	110
Figure 72: Partial proportional Case 3	110
Figure 73: Hybrid model	110
Figure 74: Pilots curves: EqVd on components (a), decoupled method (b), SDCB method (c), EqVd on system (d)	116
Figure 75: Analysis with variable compression factor.	119
Figure 76: Analysis with variable sweep rate [oct/min]	120
Figure 77: Analysis with variable electrical parameters	122
Figure 78: S/C_01 artist impression [Curtesy of spacenews.com]	123
Figure 79: Damping ration for S/C_01	125

Figure 80: Hard Mounted (HM) sine prediction, X (a), Y (b)	127
Figure 81: Pilot curves during VST along Y direction of S/C_01: comparison with steady state	128
Figure 82: Notched responses for Sine Y	129
Figure 83: Pilot curves during VST along X direction of S/C_01: comparison with steady state	130
Figure 84: Notched responses for Sine X	131
Figure 85: Notched steady state HM Vs VST prediction Vs experimental test: Sine Y (a), Sine X (b)	132
Figure 86: S/C_02 Curtesy of ESA	134
Figure 87: S/C_02, Curtesy of TAS-I	134
Figure 88: S/C_02 overview [Ref. 38]	135
Figure 89: SSH main X bending mode ($f=16.96$ Hz)	138
Figure 90: Global mode Y ($f= 20.9$ Hz)	138
Figure 91: Main PLM lateral mode X with SSH out-of-phase ($f=22.97$ Hz)	138
Figure 92: HGAMA Z mode, SSH wing Y mode, upper and middle panel Out-of-Phase ($f=47.91$ Hz)	138
Figure 93: Lateral (X-Y) HM input profile	139
Figure 94: Lateral (X) Steady state HM notched input profile	140
Figure 95: Lateral (Y) Steady state HM notched input profile	141
Figure 96: Mass and stiffness matrix from NASTRAN Craig-Bampton condensation, pattern visualization	142
Figure 97: Proportional damping ratio (light blue), modal damping ratio (res) at given frequency	143
Figure 98: S/C_02 mounted on shaker along Y	144
Figure 99: Sensitivity analysis to different VST compression factor Vs Steady state HM input on Y	146
Figure 100: VST Y curve at CF=6 Vs steady state HM	147
Figure 101: Tank response on Y, Steady state from NASTRAN/SYNEPOST (a) Vs VST (b)	148
Figure 102: S/C_02 mounted on shaker along X	149
Figure 103: Sensitivity analysis to different VST compression factor Vs Steady state HM input on X	151
Figure 104: VST X curve at CF=6 Vs steady state HM	152
Figure 105: Tank response on X, Steady state from NASTRAN/SYNEPOST (a) Vs VST (b)	153
Figure 106: PCDU response on X, Steady state from NASTRAN/SYNEPOST (a) Vs VST (b)	154
Figure 107: Sine Y - Pilots along X (Cross talks)	159
Figure 108: Sine Y - Pilots along Z (Cross talks)	160
Figure 109: Sine X - Pilots along Y (Cross talks)	160
Figure 110: Sine X - Pilots along Z (Cross talks)	161
Figure 111: VTA adapter on shaker	161

List of tables

Table 1: Different kinds of motion	20
Table 2: Level of damping and related motion.....	20
Table 3: Short schematic relationship between FRFs	27
Table 4: Symbols used infrequency response function.....	27
Table 5: Name of FRFs at given output/input.....	29
Table 6: MEMs symbols	31
Table 7: Discretization useful approaches [Matworks.com]	36
Table 8: Division by load paths	42
Table 9: Division by vibration sources	42
Table 10: Division by frequency content.....	43
Table 11: Origin of some loads [Ref. 12].....	44
Table 12: Some technical information (a), (b) about Ariane 5 [Ref.30].....	48
Table 13: Sine excitation at spacecraft base [Ref.30].....	49
Table 14: Acoustic noise spectrum under the fairing [Ref.30].....	49
Table 15: Verification by analysis and test for each load cases [Ref.14].....	50
Table 16: sweep rate in aerospace field.....	53
Table 17: Sinusoidal environment for different units [Ref.14].....	53
Table 18: Mechanical test usually performed.....	60
Table 19: Difference between pilots and notchers	74
Table 20: Adopted symbols.....	78
Table 21: Implemented values	80
Table 22: Set_control_paramenters.m.....	85
Table 23: parameters into Flow.m	86
Table 24: Differences between structural and viscous damping	98
Table 25: Input/ output parameters from test.....	102
Table 26: condensation and control parameters	113
Table 27: General parameters simulation independent	117
Table 28: Fixed and variable parameters, first case of study	118
Table 29: Fixed and variable parameters, second case of study	120
Table 30: Fixed and variable parameters, third case of study.....	121
Table 31: Notching plan for "S/C_01"	124
Table 32: Proposed sine input level along X and Y axis	124
Table 33: Further instruction about S/C_01 VST	125
Table 34: Modal effective masses with the main contributions	126
Table 35: Frequency requirement imposed by the launcher and S/C_01 PFM Prediction ..	128
Table 36: Sine Y comparison between experimental, VST and FRA with HM conditions	132
Table 37: Sine X comparison between experimental, VST and FRA with HM conditions	133
Table 38: Modal effective mass table (up to 30th mode) and normal modes.....	136
Table 39: Most critical modes and the effective masses involved HM.....	137
Table 40: Description of the characteristics of each mode HM	137
Table 41: Nominal qualification Lateral input profile (X-Y)	139
Table 42: Notched qualification input in X.....	140
Table 43: Notched qualification input in Y.....	140
Table 44: Control parameter and instruction into S/C_02 VST analysis	143
Table 45: Notching plan for S/C_02	143
Table 46: Frequency shift along sine Y	145
Table 47: Frequency shift along sine X.....	150

Introduction

(In **English** language)

The need to perform qualification and acceptance tests at the component, subsystem or system level of an S / C, or a platform in general, commonly requires to submit the considered apparatus to specific tests, capable to confirm its capacity to resist to the mechanical environment expressed by the launcher, once it has detached from the launch pad. Each type of load acting during the ascent requires different procedures, techniques and devices to be properly replicated.

Typically, the so-called "quasi-static" loads require very rigid platforms capable of imparting an equivalent load to the centre of gravity (C.o.G.) of the S / C. The inherent tests to the sinusoidal and random low frequency loads are usually conducted by means of seismic excitation at the base of the S / C, with different time and frequency laws. In this context, the classic devices adopted are electrodynamic shakers. At the same time, the high frequency "random" and the acoustics are properly simulated into special rooms equipped with loudspeaker microphones capable of imparting sound waves onto the surfaces of the S / C, thus recreating the appropriate environment. Finally, the shock tests provide dedicated equipment or procedures designed to produce excitement at the base of the analysed component or system of extreme importance in terms of amplitude. These include, for example, *Drop-testing* or *Free-fall techniques*.

All these tests are connected by the fact that the test values are greater than actually perceived during the launch by the S / C as a whole or by the investigated equipment.

Focusing on the peculiarities and specificities of sinusoidal tests, these are aimed at verifying the compliance of the S / C to the low-frequency mechanical environment, between 5 - 100 Hz, typically encountered during launch.

The phases and procedures which these tests are carried out are different. Classically, in fact, today's practice provides separate tests on 3 axes, each of them with theoretically different excitation levels, respecting what expressed during the launch phase. Moreover, the level of excitation at the base also varies according to the philosophy of test, qualification or acceptance: peak of excitation and speed of execution ("sweep rate") of the tests are among the fundamental characteristics that have the greatest impact on the structural dynamic response of the analysed object.

In particular, the so-called "sweep rate", the rate of increase of the frequency of the forcing function during the test, increases the gap between reality and model, separating the stationary predictions based on *Frequency Response Analysis* (FRA) in *Hard mounted* (HM) conditions, with the transient ones extracted. The natural frequencies monitored after the test are thus distorted compared to the numerical forecasts, the "frequency shift". A low sweep rate is critical for the S/C since it forces it to oscillate subjected to a forcing whose frequency is close to the natural frequency of the S/C itself.

For these reasons, the classical analytical approach based on FRA with HM conditions is therefore fallacious because it is based on an incomplete modelling of the problem.

It also causes test abort (test stop) from which is necessary to proceed with low excitation tests in order to experimentally characterize the S / C dynamics.

However, the genesis of the problems during the tests lies in having deliberately neglected the characteristics of the shaker, such as mass, inertia, elasticity and the presence of constructive elements such as seismic mass, struts and supports.

The innovative approach called "Virtual Shaker Testing" (VST) introduced in 2007 by Apolloni and Cozzani of ESA-ESTEC, extends the boundary conditions beyond the shaker, modeling the shaker-S/C assembly in a single FEM model able to anticipate the typical problems of the test as dynamic couplings between satellite modes and shaker modes ("rockling", "saddle", "bending"), effect of the dynamics of the seismic mass on the structural response, effect of the "sweep rate" on the natural frequencies of the S / C and the Cross-talks.

From the application point of view, a MATLAB/Simulink© model was used, called Vibration controls, provided by SIEMENS®. These routines simulate a Hardware In the Loop (HIL) system capable to simulate the implemented control system into the real test facility. They are also able to automatically integrate the Notching criterion, i.e. the reduction of the forcing function amplitude when appropriate acceleration thresholds are exceeded into a computational cycle integrated in a transient analysis.

In conclusion, the analysed work not only aims to apply this VST methodology to the study of structural transient responses for two satellites, possibly comparing the response with test data, but also intends to doing it through an autonomous control system, able to anticipate all possible problems.

The approach that has been followed to achieve this objective consists on the preparation of a computational framework capable of setting up and implementing the VST and its preliminary approach through reduced mass-spring-damper models. In this context, the capabilities and limitations of the code itself are evaluated, as well as the type of output and their quality. Subsequently, an important and consistent post-correlation work is carried out on a dynamic state-space model, starting from the Craig-Bampton formulation, which experimental data were already available.

At the same time, a consistent research, investigation and implementation is also carried out about advanced damping models, mostly based on a equivalent viscous formulation, that can be implemented during the preparation of the mechanical matrices to be supplied as input to the solver integrated in the Simulink model.

Finally, the heritage of the preliminary analyses was useful for predicting the transient structural responses of two satellites, comparing the results with any vibrational test outputs.

Lastly, for the sake of clarity, from a purely methodological point of view is specified that the VST represents a general approach to sinusoidal testing not only in aerospace field, but also for any apparatus or devices under examination. In fact, as introduced just before, its aims are reached by an approach focused on the generalization of the boundary conditions which often are a source of discrepancy between numerical and experimental results.

Introduzione

(In **Italian** language)

La necessità di eseguire prove di qualifica ed accettazione a livello di componente, sottosistema o sistema di uno S/C, o di una piattaforma in genere, richiede comunemente di sottoporre l'apparato considerato a specifici test, atti a confermare la sua capacità nel resistere all'ambiente meccanico espresso dal lanciatore una volta staccatosi dalla piattaforma di lancio. Ogni tipologia di carico agente durante l'ascesa richiede procedure, tecniche e dispositivi differenti per essere opportunamente replicato.

Tipicamente, i cosiddetti carichi "quasi statici" richiedono piattaforme molto rigide capaci di imprimere un carico equivalente al baricentro (C.o.G.) dello S/C. I test inerenti ai carichi sinusoidali e random di bassa frequenza sono usualmente condotti tramite eccitazione sismica alla base dello S/C, con leggi temporali ed in frequenza diverse. In questo contesto, i classici apparati adottati sono gli shaker elettrodinamici. Parallelamente, i "random" di alta frequenza e gli acustici sono opportunamente simulati in camere speciali dotate di microfoni ad altoparlanti in grado di imprimere onde sonore sulle superfici dello S/C, ricreando quindi l'opportuno ambiente ricercato. Gli "shocks", infine, prevedono apparati o procedure dedicate ed atte a produrre un'eccitazione alla base del componente o sistema analizzato di estrema importanza in termini di ampiezza. Tra queste vanno citati, ad esempio, i *Drop-testing* o le *Free-fall techniques*.

Tutti questi test sono tra loro accomunati dal fatto che i valori sperimentali sono maggiori di quanto effettivamente percepiti in fase di lancio dallo S/C complessivamente o dall'equipaggiamento investigato.

Soffermendosi sulle peculiarità e specificità dei test sinusoidali, questi sono tesi a verificare la *compliance* dello S/C all'ambiente meccanico di bassa frequenza, tra 5 – 100 Hz, tipicamente incontrato durante il lancio.

Le procedure e le fasi con cui tali test vengono svolti sono molteplici. Classicamente, infatti, la pratica odierna prevede test *sine* su 3 assi distintamente, ognuno dei quali con livelli di eccitazione teoricamente differenti, rispettando quanto espresso in fase di lancio. Inoltre, il livello di eccitazione alla base varia anche in funzione della filosofia di test, qualifica o accettazione: picco di eccitazione e velocità di esecuzione ("sweep rate") dei test sono tra le caratteristiche fondamentali che incidono maggiormente sulla risposta dinamica strutturale dell'oggetto analizzato.

In particolare, il cosiddetto "sweep rate", il rateo di salita della frequenza della forzante durante il test, aumenta il gap tra realtà e modello, separando le predizioni stazionarie basate sulla *Frequency Response Analysis* (FRA) in condizioni *Hard mounted* (HM), con quelle transitorie estratte. Vengono così falsate le frequenze naturali monitorate a valle del test rispetto le previsioni numeriche, il "frequency shift". Uno "sweep rate" basso risulta critico per lo S/C poiché lo obbliga ad oscillare sottoposto ad una forzante la cui frequenza è prossima a quella naturale dello S/C stesso.

Per i detti motivi, l'approccio analitico classico basato sulla FRA con condizioni HM, risulta dunque fallace poiché basato su una incompleta modellazione del problema.

Esso inoltre è causa di aborti (interruzioni del test) da cui la necessità di procedere con test a basso livello di eccitazione in modo da caratterizzare sperimentalmente la dinamica dello S/C.

Tuttavia, la fonte delle problematiche durante i test sta proprio nell'aver deliberatamente accantonato le caratteristiche dello shaker, quali massa, inerzia, elasticità, presenza di elementi costruttivi come massa sismica, armature e supporti.

A questo proposito l'innovativo approccio denominato "Virtual Shaker Testing" (VST) introdotto nel 2007 da Apolloni e Cozzani di ESA-ESTEC, estende le condizioni al contorno oltre lo shaker, modellando il complesso shaker-S/C in un unico modello FEM capace di anticipare i problemi tipici del test quali accoppiamenti dinamici tra modi di satellite e modi di shaker ("rockling", "saddle", "bending"), effetto della dinamica della massa sismica sulla risposta strutturale, effetto dello "sweep rate" sulle frequenze naturali dello S/C ed i "Cross-talks" (o risposte incrociate).

Dal punto di vista applicativo, è stato utilizzato un modello MATLAB/Simulink®, chiamato *Vibration controls*, fornito da SIEMENS®. Queste routine sono in grado di integrare automaticamente il criterio del *Notching*, ovvero la riduzione dell'ampiezza di forzante quando vengono superate opportune soglie di accelerazione in un ciclo computazionale integrato in una analisi transitoria.

In conclusione, il lavoro in esame, non solo si prefigge l'obiettivo di applicare tale metodologia del VST allo studio di transitori strutturali a due satelliti, comparandone eventualmente la risposta con dati di test, ma di farlo tramite un sistema di controllo autonomo, scritto in MatLab/Simulink® e distribuito da SIEMENS®, in grado di anticipare tutte le possibili problematiche.

L'approccio che si è seguito per raggiungere quest'obiettivo consta della preparazione di *framework* computazionale in grado di impostare e realizzare il VST e di un suo preliminare avvicinamento tramite modelli ridotti massa-molla-smorzatore. In questo contesto sono valutate capacità e limiti del codice stesso, nonché la tipologia delle risposte in output e la loro qualità. Successivamente, viene condotta un'importante e consistente opera di post correlazione su un modello dinamico in formato stato-spazio, partendo dalla formulazione alla "Craig-Bampton", di cui erano già disponibili i dati sperimentali.

Parallelamente, viene eseguita una altresì consistente ricerca, indagine ed implementazione sui modelli di smorzamento attuabili in sede di preparazione delle matrici meccaniche da fornire come input al solutore integrato nel modello Simulink®.

Infine, quanto appreso dalle analisi preliminari è stato utile per predire le risposte strutturali transienti di due satelliti, comparandone i risultati con gli eventuali output di test vibrazionale.

Dal punto di vista puramente metodologico si precisa che il VST rappresenta un approccio generale al testing sinusoidale non solo in ambito aerospaziale, quanto per qualsivoglia apparato o dispositivo in esame. Infatti, come introdotto pocanzi i suoi obiettivi vengono raggiunti da un approccio teso alla generalizzazione delle cosiddette condizioni al contorno le quali spesso sono fonte di discrepanza tra risultati numerici e sperimentali.

Part I

Theoretical background

Chapter 1: Background on structural dynamics

Structural dynamics is a branch of vibration mechanics. It studies how the structures response to a mechanical input e.g. applied force or imposed motion in terms of displacements, speeds, acceleration or internal stresses.

In fact, how is described by Figure 1, a structure transforms any kind of input in an output. This is a general idea, the output can be understood in terms of natural frequencies, mode shapes, or response (in frequency or time domain).

However, all the parameters as mass, stiffness, damping, boundary condition and initial conditions shall be completely defined for launching an appropriate analysis.

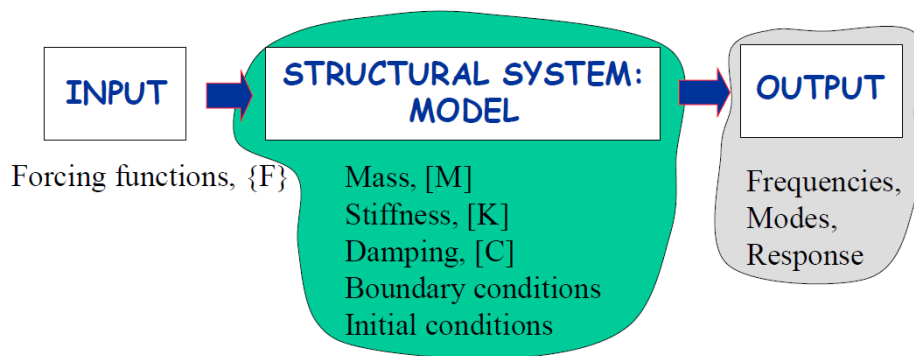


Figure 1: Chart for structural analysis [Ref. 10]

Particularly, vibration is a mechanical oscillation around the equilibrium configuration. It can be induced by different kind of sources as mechanical or acoustic and classified according to the regimes (harmonic, transient, random) or based on frequency content (low, medium, high frequency). Nevertheless, these concepts will be discussed in “Chapter 4: The launch environment”

Typically, from an engineering point of view, many problems are treated ad liner. Linearity, if fact, allows an “easy” way to solve complex problem developing some strategies that avid iteration and loop into the theories.

Not only, different problems have a stochastic and probabilistic content hence, in order to be solved in an appropriate way, they must be approached with particular techniques. An example of this topic is represented by vibration. At medium and low frequency the can be treated with deterministic approach (FEM, for instance), but at high frequency is necessary to change the resolution mode.

In Figure 2 the most important analysis, are recollected.

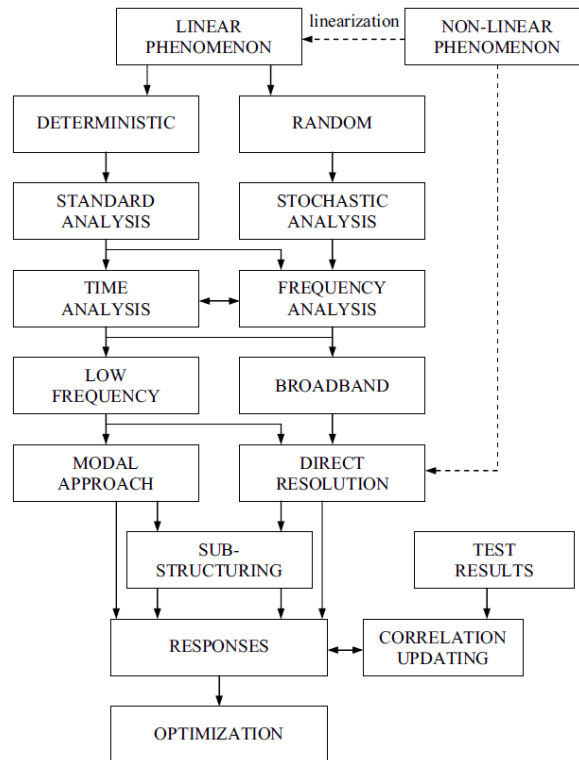


Figure 2: Main analysis strategies [Ref. 14]

Particularly, according to “ECSS-E-HB-32-26A Spacecraft mechanical loads analysis handbook” structural dynamic analysis depends on various factors as:

- Linear vs. Nonlinear Analysis – The behaviour of the structure may be linear or nonlinear for several reasons. Typically, nonlinearity is approached through the linearization.
- Low frequency vs. Wide band – In the low frequency range, the modal approach provides an efficient analysis technique known as mode superposition. In the wide band range, the number of modes becomes excessive, requiring the use of more suitable analysis techniques which are in general more complex, less accurate and used less widely.
- Time vs. Frequency Domain – Analyses may be performed in the time or frequency domains. In the frequency domain the relations between excitations and responses are called frequency response functions (FRF) which can be manipulated with ease leading to several advantages.
- Continuous vs. Discrete – Apart from particular cases, it is advantageous to represent a structure using a mathematical model discretised using a finite element approach in which case the equations of motion are expressed in terms of matrices.
- Global vs. Modular – Direct analysis using finite elements can become numerically burdensome when dealing with a large number of DOF. If the structure is modular (i.e. composed of distinct components connected at localized interfaces), each component may be analysed separately before assembly. This coupling technique known as substructuring, may be performed using FRF (Frequency Response Synthesis) or modes (Component Mode Synthesis).

1.1 Single DoF under forced damped motion

Starting from a single DoF system (SDoF) in which the equation of motion could be deduced by Newton or Lagrange equation:

$$m\ddot{x} + c\dot{x} + kx = f(t) \quad (1.1)$$

This is the simplest mechanical model able to describe the dynamic of a general system

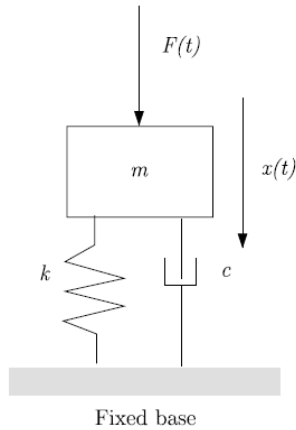


Figure 3: SDof with fixed base [Ref. 12]

	$c = 0$	$c \neq 0$
$f(t) = 0$	Undamped free vibrations	Damped free vibrations
$f(t) \neq 0$	Undamped forced vibrations	Damped forced vibrations

Table 1: Different kinds of motion

In the field of sine vibrations $f(t)$ has the expression $f(t) = f_0 \sin(\omega t)$.

Typically, the time response is $u(t) = u_f(t) + u_p(t)$, in which:

- $u_f(t)$ is the General solution of the homogeneous part (free motion): complementary solution; it is associated with the initial conditions
- $u_p(t)$ is the Particular solution (integral) of the full equation

Firstly, the resolution of the general solution is necessary to defining the following quantities

$$\omega_n = \sqrt{\frac{k}{m}} \quad \text{Natural circular frequency} \quad (1.2)$$

$$\zeta = \frac{c}{2m\omega_n} \quad \text{Damping ratio} \quad (1.3)$$

$$\omega_d = \omega_n \sqrt{1 - \zeta^2} \quad \text{Damped natural circular frequency} \quad (1.4)$$

In this way it is possible to quantify the three kinds of motion according to the value of ζ

Level of damping ratio	Description of the motion
$\zeta > 1$	Over damped
$\zeta = 1$	Critically damped
$0 < \zeta < 1$	Under damped
$\zeta = 0$	Undamped

Table 2: Level of damping and related motion

Particularly, the most interesting regime in motion is represented by the under damped because it previews the evolution of the motion through more than one oscillation.

In this case the time response of the homogeneous is represented by

$$u_f(t) = e^{-\zeta\omega_n t} \left(U_0 \cos \omega_d t + \frac{\dot{U}_0 + \zeta\omega_n U_0}{\omega_d} \sin \omega_d t \right) \quad (1.5)$$

In which \dot{U}_0 and U_0 are the initial condition in terms of speed and displacement.

(1.5) is also called transient response.

Secondly, the particular solution of the full equation (1.1), also called steady state response, is written assuming

$$f(t) = F_0 e^{j\omega t} ; \quad u(t) = U_0 e^{j\omega t} ; \quad \beta = \omega/\omega_n \quad (1.6)$$

In which F_0 and U_0 represent the peak force and displacement.

Substituting the previous expressions in (1.1), is possible to identify $U_0 = \frac{F_0/k}{1-\beta^2+j2\zeta\beta}$.

Then, the steady state equation of motion is

$$u_p(t) = F_0/k \frac{\sin(\omega t + \phi)}{\sqrt{(1-\beta^2)^2 + 4\zeta^2\beta^2}} \quad (1.7)$$

And the phase

$$\phi = \tan^{-1} \left(-\frac{2\zeta\beta}{1-\beta^2} \right) \quad (1.8)$$

In this context is definable D_{max} : Maximum dynamic amplification factor.

$$D_{max} \cdot \left| \frac{u_p(t)}{F_0/k} \right| = \frac{1}{\sqrt{(1-\beta^2)^2 + 4\zeta^2\beta^2}} \quad (1.9)$$

It represents the ratio between the steady state and the static response. Particularly, doing a frequency response analysis D_{max} occurs at $\beta = 1$.

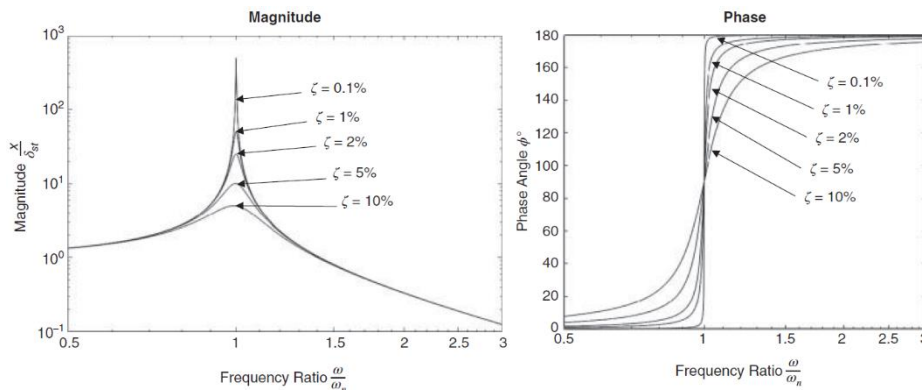


Figure 4: Typical curves [Ref. 12]

In this case the peak undergoes at $Q = 1/2\zeta$ (quality factor).

How is possible to see in Figure 4, when the damping ratio is low, the shape of the peak of the frequency response is very sharp. On the contrary, if it is significant, the peak is smoother. Similarly, the phase when damping ratio is roughly negligible, has a discontinuity for $\beta = 1$

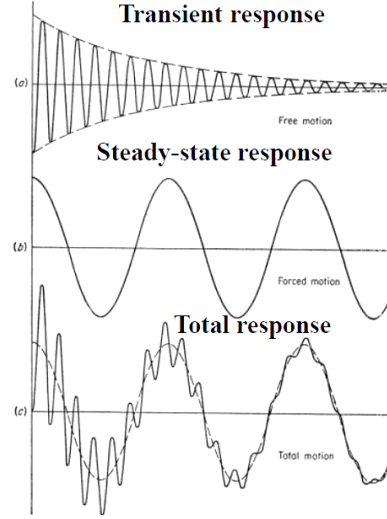


Figure 5: Transient, steady-state and total response

To sum up, the total response for a SDoF due to damped and forced motion is defined as

$$u(t) = e^{-\zeta\omega_n t} \left(U_0 \cos \omega_d t + \frac{\dot{U}_0 + \zeta\omega_n U_0}{\omega_d} \sin \omega_d t \right) + F_0/k \frac{\sin(\omega t + \phi)}{\sqrt{(1 - \beta^2)^2 + 4\zeta^2\beta^2}} \quad (1.10)$$

And well explained in a graphical way in Figure 5

1.2 Single DoF under base excitation

Previously in paragraph 1.1 has been discussed the influence of a force acting on a single DoF. In that case the base of the considered DoF was fixed on the ground and the excitation was applied on top of the mass.

In this section will be treated the case of enforced motion at the base of DoF.

Let consider the simple mechanical system shown in Figure 6. It could represent various kind of states for the system, for instance an object putted on top on a moving base. Particularly, this configuration allows the discussion of sine sweep test and environment. Not only, this elementary approach can be utilized in terms of VST.

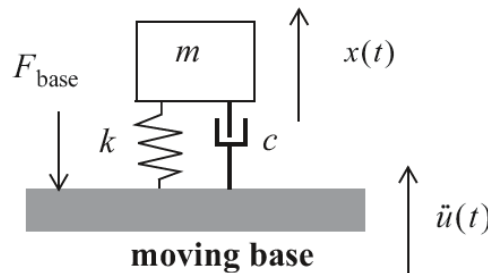


Figure 6: Enforced motion at the base [Ref. 12]

Introducing the relative displacement

$$z(t) = x(t) - u(t) \quad (1.11)$$

In which $z(t)$ represents the relative motion; $x(t)$ the displacement of the mass; $u(t)$ the displacement of the base.

The equation of motion for the sDoF shown in Figure 6 is

$$m\ddot{x}(t) + c(\dot{x}(t) - \dot{u}(t)) + k(x(t) - u(t)) = 0 \quad (1.12)$$

Rewrite (1.12) using (1.11) is possible to impose the acceleration at the base as external source

$$\ddot{z}(t) + 2\zeta\omega_n\dot{z}(t) + \omega_n^2z(t) = -\ddot{u}(t) \quad (1.13)$$

The absolute displacement can be calculated from

$$\ddot{x}(t) = \ddot{z}(t) + \ddot{u}(t) = -\zeta\omega_n\dot{z}(t) - \omega_n^2z(t) \quad (1.14)$$

And the force at the base due to the acceleration $\ddot{u}(t)$ is merely the sum of the forces expresses by spring and the damper

$$F_{base}(t) = kz(t) + c\dot{z}(t) = -m\ddot{x}(t) \quad (1.15)$$

Assuming $\ddot{u}(t) = A \sin \omega t$ for (1.13) and non-homogeneous initial condition, the relative displacement can be written as

$$\begin{aligned} z(t) = z(0)e^{-\zeta\omega_nt} \left(\cos \omega_d t + \frac{\zeta}{\sqrt{1-\zeta^2}} \sin \omega_d t \right) + \dot{z}(0)e^{-\zeta\omega_nt} \frac{\sin \omega_d t}{\omega_d} \\ - A \int_0^t e^{-\zeta\omega_n\tau} \frac{\sin \omega_d \tau}{\omega_d} \sin(\omega(t-\tau)) d\tau \end{aligned} \quad (1.16)$$

On the other way, using homogeneous initial condition is possible to write

$$z(t) = e^{-\zeta\omega_nt} (B \cos \omega_d t + C \sin \omega_d t) - \frac{A}{\omega_n^2} \left[\frac{(1-\beta^2) \sin \omega t - 2\zeta\beta \cos \omega t}{(1-\beta^2)^2 + (2\zeta\beta)^2} \right] \quad (1.17)$$

The interesting terms is the acceleration, in fact,

$$\begin{aligned} \ddot{z}(t) = e^{-\zeta\omega_nt} \{ [(B\omega_d^2\zeta^2 - 2C\omega_d\omega_n\zeta - B\omega_d^2) \cos \omega_d t] + [(C\omega_d^2\zeta^2 - 2B\omega_d\omega_n\zeta - C\omega_d^2) \sin \omega_d t] \} + \\ A\beta^2 \left[\frac{(1-\beta^2) \cos \omega t - 2\zeta\beta \sin \omega t}{(1-\beta^2)^2 + (2\zeta\beta)^2} \right] \end{aligned} \quad (1.18)$$

In which

$$\begin{aligned} B = -\frac{A}{\omega_n^2} \left[\frac{2\zeta\beta}{(1-\beta^2)^2 + (2\zeta\beta)^2} \right] \\ C = \frac{1}{\omega_d} \left[B\omega_n\zeta + \frac{A}{\omega_n} \beta \frac{1-\beta^2}{(1-\beta^2)^2 + (2\zeta\beta)^2} \right] \end{aligned} \quad (1.19)$$

1.3 Multi Degrees of Freedom (MDoF)

How the heading suggests, MDoF, shown in Figure 7, are systems composed by more than 1 DoF. This kind of system allows a better compression of complex structures. In fact, we can divide the properties of the considered structures in different parts, in terms of mass, stiffness and damping and give them the role of degree of freedom.

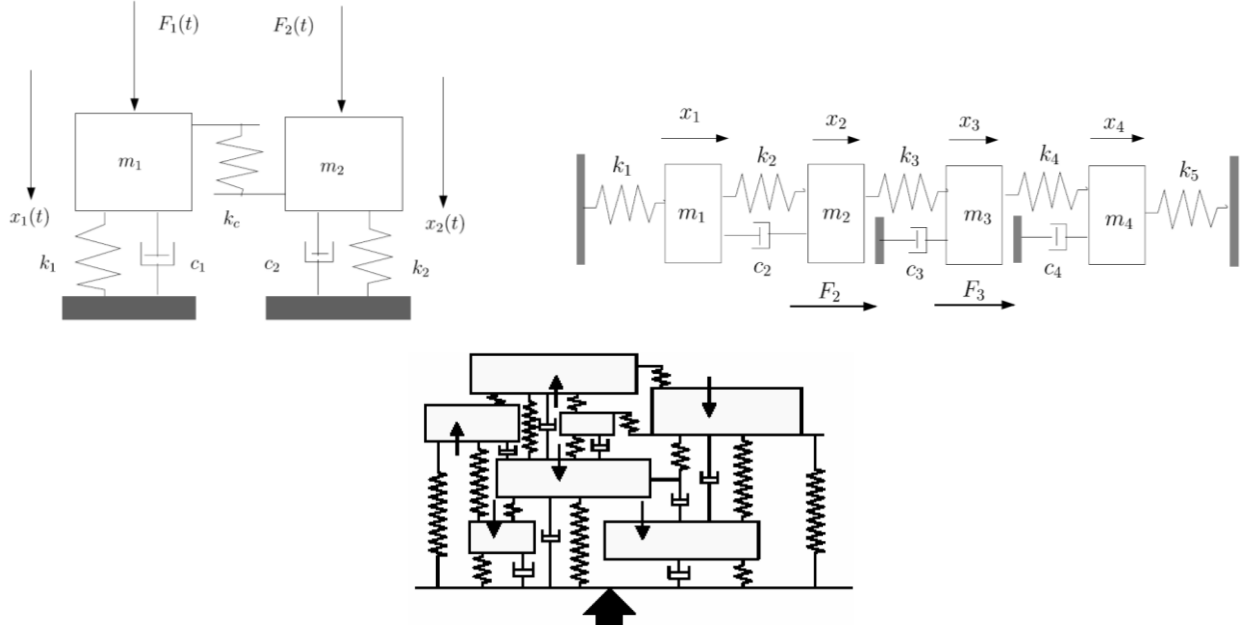


Figure 7: Three examples of MDoF [Ref. 10, 12]

The typical mathematical description associates to this systems is in matrix form. In compact form

$$[M]\{\ddot{x}\} + [C]\{\dot{x}\} + [K]\{x\} = \{F\} \quad (1.20)$$

Where

$[M]$	Mass matrix	Diagonal matrix
$[C]$ (or $[D]$)	Damping matrix	Un-symmetrical matrix
$[K]$	Stiffness matrix	Symmetrical matrix
$\{F\}$	Source vector	Column vector

Obviously, the inner structure of each matrix depends on the mechanical configuration of the system.

Particularly, this notation is very useful when we are working in Finite Element field. In fact, after the discretization we obtain the description of the system as is shown in (1.19).

How introduced in Table 1: Different kinds of motion for a SDoF system, we can have different kind of motion. In this context of lumped systems, take an important role the undamped free vibration analysis.

Particularly, if we perform it, we are doing a “Normal modes analysis”. In fact, how is well known in theory, this approach represents the first step in a more complex field as “Dynamic analysis”. In fact, recognising the natural frequencies and the mode shapes of the considered structure is possible to manage more complex and detailed analysis such as Frequency response and Transient analysis thanks to a procedure based on the number of the extracted mode shapes with which uncoupled the equations, rather than a direct integration. Obviously, this is valid for linear systems.

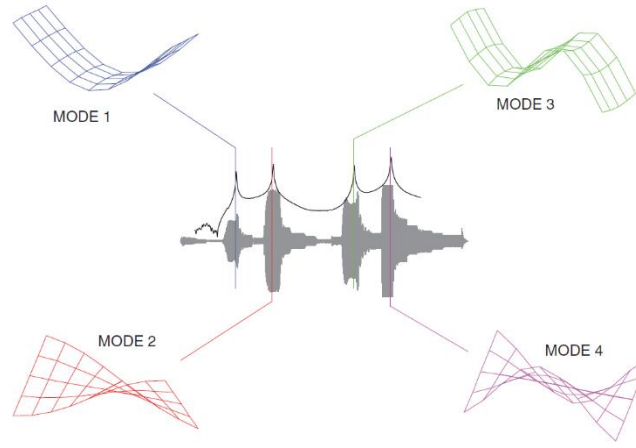


Figure 8: Mode superposition in a time domain signal [Ref. 16]

From a mathematical point of view the aim of a normal modes analysis is to find the so-called modal matrix in which are recollected the eigenvectors of the problems: the modes shapes. Obviously, each eigenvector is associated to an eigenvalue: the natural frequency.

In fact, considering the equation of motion for an undamped forced system

$$[M]\{\ddot{x}\} + [K]\{x\} = \{F\} \quad (1.21)$$

Assuming known $[\Phi]$ modal matrix, the response in terms of displacement can be written as

$$\{u(t)\} = [\{\phi_1\}|\{\phi_2\}|\dots] \begin{Bmatrix} q_1 \\ q_2 \\ \dots \end{Bmatrix} \quad (1.22)$$

In which $\begin{Bmatrix} q_1 \\ q_2 \\ \dots \end{Bmatrix}$ are the so-called modal participation factor (or modal coordinates).

After simple passages is possible to write for each DoF the following equation

$$\ddot{q} + \omega_i q = a_i \quad (1.23)$$

In this way the MDoF system is solved in terms of multi SDoF into the modal coordinates frame, Figure 9.

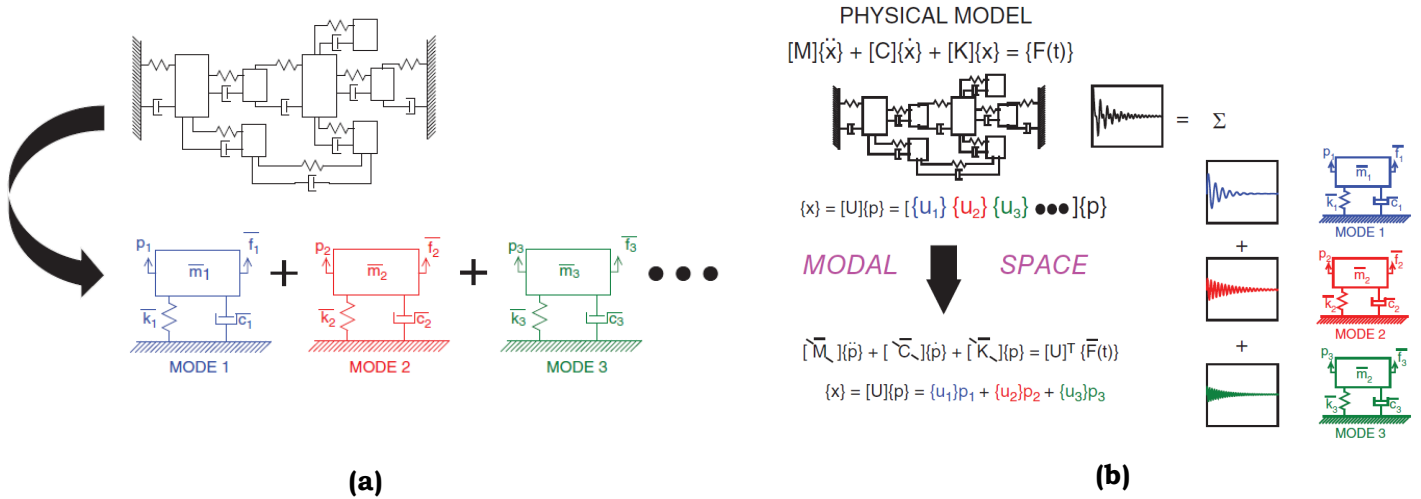


Figure 9: Modal technique: from one MDoF to a different SDoF systems (a), (b) [Ref. 16]

After that, using the motion superposition the response is reconstructed.

1.4 Frequency Response Function (FRF)

The Frequency Response Function, also called transfer function, is one of the most important concepts and tool, for the dynamic analysis of the mechanical systems.

It is able to produce, and represent, an output for the system only knowing the input.

In fact, it is defined in frequency domain as the ratio between the output and the input, as

$$H(\omega) = \frac{Y(\omega)}{X(\omega)} \quad (1.24)$$

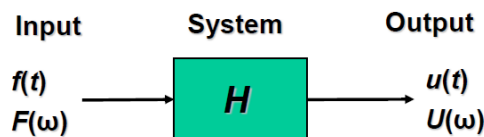


Figure 10: Representation of FRF [Ref. 10]

However, it is an idea that relates and leads the dynamic systems in general and grouping them into the signal processing field.

Obviously, we will discuss about FRFs strictly speaking about structural dynamic.

Using the theory provided by Fourier we are able to write transfer function in order to understand the response of the system (output) in terms of displacement, speed or acceleration in frequency domain at given input.

For instance, considering the elementary system mass-spring-damper with fixed base

$\ddot{u} + 2\zeta\omega_n\dot{u} + \omega_n^2 u = \frac{f(t)}{m} = a(t) \rightarrow$ <p style="text-align: center;">↓</p>	$U(\omega)[1 - \beta^2 + j2\zeta\beta] = \frac{1}{\omega_n^2} A(\omega)$ $U(\omega) = \frac{1}{\omega_n^2[1 - \beta^2 + j2\zeta\beta]} A(\omega)$ $H_{UA}(\omega) = \frac{1}{\omega_n^2[1 - \beta^2 + j2\zeta\beta]}$	<p>The transfer function $H_{UA}(\omega)$ connects the displacement in output and the acceleration in input in frequency domain</p>
$\ddot{U}(\omega)[1 - \beta^2 + j2\zeta\beta] = -\beta^2 A(\omega)$ $\ddot{U}(\omega) = -\frac{\beta^2}{[1 - \beta^2 + j2\zeta\beta]} A(\omega)$ $H_{\ddot{U}A}(\omega) = -\frac{\beta^2}{[1 - \beta^2 + j2\zeta\beta]}$ <p>The transfer function $H_{\ddot{U}A}(\omega)$ connects the acceleration in output and the acceleration in input in frequency domain</p>	$H_{\ddot{U}A}(\omega) = -\omega^2 H_{UA}(\omega)$	

Table 3: Short schematic relationship between FRFs

In general, this concept can be extended also for lumped systems with “N” DoFs, or continuous systems. In this case, FRF is represented by a matrix.

$$\begin{Bmatrix} Y_1(\omega) \\ Y_2(\omega) \\ Y_3(\omega) \\ \vdots \\ Y_N(\omega) \end{Bmatrix} = \begin{bmatrix} H_{11} & \dots & H_{1N} \\ \vdots & \ddots & \vdots \\ H_{N1} & \dots & H_{NN} \end{bmatrix} \begin{Bmatrix} X_1(\omega) \\ X_2(\omega) \\ X_3(\omega) \\ \vdots \\ X_N(\omega) \end{Bmatrix} \quad (1.25)$$

As for SDoF, the transfer function depends on the types input and output.

For example, measuring the displacement due to an applied force: $U(\omega) = H(\omega)F(\omega)$,

$$H_{\alpha,\beta}(\omega) = \sum_{k=1}^N \frac{\phi_{k,\alpha}\phi_{k,\beta}}{m_k(\omega_k^2 - \omega^2 + j2\zeta_k\omega_k\omega)} \quad (1.26)$$

In which

Symbol	Meaning
$H_{\alpha,\beta}(\omega)$	Occupy just one position into transfer function matrix
$\phi_{k,\alpha}, \phi_{k,\beta}$	Are the α -th and β -th component of the k-th eigenvector
ω_k	k-th natural circular frequency
m_k, ζ_k	k-th modal mass and modal damping

Table 4: Symbols used infrequency response function

For a better comprehension, let considering s 2DoF system mass-spring-damper, in order to measure the previous quantities, we re-write (1.24) as

$$\begin{Bmatrix} U_1(\omega) \\ U_2(\omega) \end{Bmatrix} = \begin{bmatrix} H_{11} & H_{12} \\ H_{21} & H_{22} \end{bmatrix} \begin{Bmatrix} F_1(\omega) \\ F_2(\omega) \end{Bmatrix} \quad (1.27)$$

$$\begin{aligned} U_1(\omega) &= H_{11}F_1(\omega) + H_{12}F_2(\omega) \\ U_2(\omega) &= H_{21}F_1(\omega) + H_{22}F_2(\omega) \end{aligned} \quad (1.28)$$

And applying (1.25)

$$\begin{aligned} H_{11} &= \frac{\phi_{1,1}\phi_{1,1}}{m_1(\omega_1^2 - \omega^2 + j2\zeta_1\omega_1\omega)} + \frac{\phi_{2,1}\phi_{2,1}}{m_2(\omega_2^2 - \omega^2 + j2\zeta_2\omega_2\omega)} \\ H_{12} &= \frac{\phi_{1,1}\phi_{1,2}}{m_1(\omega_1^2 - \omega^2 + j2\zeta_1\omega_1\omega)} + \frac{\phi_{2,1}\phi_{2,2}}{m_2(\omega_2^2 - \omega^2 + j2\zeta_2\omega_2\omega)} \\ H_{21} &= \frac{\phi_{1,2}\phi_{1,1}}{m_1(\omega_1^2 - \omega^2 + j2\zeta_1\omega_1\omega)} + \frac{\phi_{2,2}\phi_{2,1}}{m_2(\omega_2^2 - \omega^2 + j2\zeta_2\omega_2\omega)} \\ H_{22} &= \frac{\phi_{1,2}\phi_{1,2}}{m_1(\omega_1^2 - \omega^2 + j2\zeta_1\omega_1\omega)} + \frac{\phi_{2,2}\phi_{2,2}}{m_2(\omega_2^2 - \omega^2 + j2\zeta_2\omega_2\omega)} \end{aligned} \quad (1.29)$$

The subscripts are divided based on colours criteria:

- “black” means the degree of freedom
- “red” means the component in which we are measure
- “blue” means the excited component

Using this simple case is easy to understand that the calculus based on frequency response (transfer) function, induce a huge amount of calculus.

Furthermore, we have to remind that each $H_{\alpha\beta}$ represent a curve, thus is a vector.

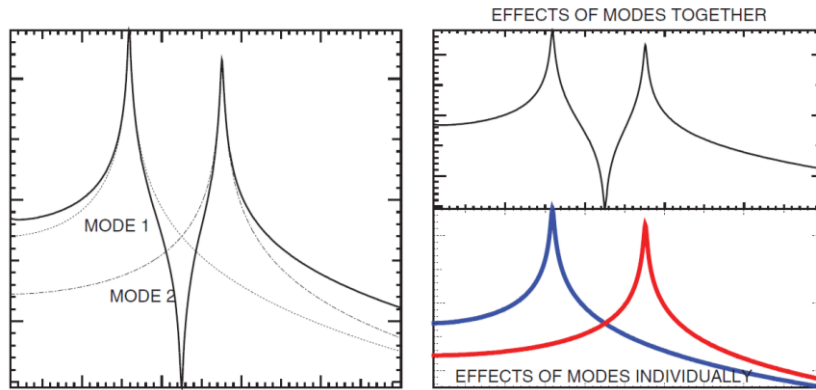


Figure 11: FRFs superposition [Ref. 16]

The response characteristics may be plotted in terms of displacement $U(\omega)$, speed $\dot{U}(\omega)$, or acceleration $\ddot{U}(\omega)$ for a given input, as it shown in Table 5.

Ratio		Attributes of transfer function
Displacement/ Force:	$\frac{U(\omega)}{F(\omega)}$	Receptance or Dynamic compliance
Speed/ Force:	$\frac{\dot{U}(\omega)}{F(\omega)}$	Mobility or Mechanical Admittance
Acceleration/ Force:	$\frac{\ddot{U}(\omega)}{F(\omega)}$	Inertance, Accelerance
Force/ Displacement	$\frac{F(\omega)}{U(\omega)}$	Dynamic stiffness
Force/ Speed	$\frac{F(\omega)}{\dot{U}(\omega)}$	Mechanical Impedance
Force/ Acceleration	$\frac{F(\omega)}{\ddot{U}(\omega)}$	Dynamic mass, Apparent Mass
Acceleration/ Acceleration	$\frac{\ddot{U}_l(\omega)}{\ddot{Z}(\omega)}$	Dynamic Transmissibility

Table 5: Name of FRFs at given output/input

Particularly, will be very useful for VST the FRF called transmissibility that in this case leads the input acceleration at the base of the SDoF with the corresponding output

$$Tr\left(\frac{\omega}{\omega_n}\right) = \frac{1 + i2\zeta \frac{\omega}{\omega_n}}{1 - \left(\frac{\omega}{\omega_n}\right)^2 + i2\zeta \frac{\omega}{\omega_n}} \quad (1.30)$$

Finally, using transfer functions, is possible to rebuild the time history for a given quantity through the inverse Fourier transformation, as for instance

$$u(t) = T^{-1}[H(\omega)F(\omega)] = \int_0^t f(\tau)h(t - \tau)d\tau \quad (1.31)$$

Obviously, neglecting the initial condition for the same theory.

1.5 Modal Effective Masses (MEMs)

Modal Effective Masses is a dynamic important topic strongly tied with modal properties as mode shapes, damping, natural frequencies and participation factors.

Particularly, it is defined in case of base enforced motion how discussed in paragraph 1.2. How J.Wijker says “The modal effective mass is a measure to classify the importance of a mode shape when a structure will be accelerated via its base”, despite this topic is related to the mass, is suggested to avoid to say “it is the mass which participates to the mode”.

MEMs is a 6x6 matrix and it allows the analysis of coupling between translational and rotational modes in fact, is a useful tool: permit a good schedule of the tests setup and enable the correlation between the mathematical model and the test.

In this framework, recalling what has been done in paragraph 1.2, we can write the following quantities, assuming harmonic vibration

$$\begin{aligned}
\ddot{u}(t) &= \ddot{U}(\omega)e^{j\omega t} && \text{the enforced acceleration} \\
z(t) &= Z(\omega)e^{j\omega t}, \dot{z}(t) = j\omega Z(\omega)e^{j\omega t}, && \text{the relative motion} \\
\ddot{z}(t) &= -\omega^2 \ddot{Z}(\omega)e^{j\omega t} \\
\ddot{x}(t) &= -\omega^2 \ddot{X}(\omega)e^{j\omega t} && \text{the absolute acceleration}
\end{aligned} \tag{1.32}$$

In this context, equation (1.13) can be transformed in terms of frequency and relative motion

$$\begin{aligned}
[-\omega^2 + 2j\zeta\omega_n\omega + \omega_n^2]Z(\omega) &= -\ddot{U}(\omega) \\
&= \omega^2 U(\omega)
\end{aligned} \tag{1.33}$$

Then

$$Z(\omega) = \left(\frac{\omega}{\omega_n}\right)^2 H\left(\frac{\omega}{\omega_n}\right) U(\omega) \tag{1.34}$$

Where, the frequency response function is

$$H\left(\frac{\omega}{\omega_n}\right) = \frac{1}{1 - \left(\frac{\omega}{\omega_n}\right)^2 + 2j\zeta\left(\frac{\omega}{\omega_n}\right)} \tag{1.35}$$

Is now possible to write the absolute acceleration

$$\ddot{X}(\omega) = -\omega^2[Z(\omega) + U(\omega)] = -\omega^2 \left[1 + \left(\frac{\omega}{\omega_n}\right)^2 H\left(\frac{\omega}{\omega_n}\right)\right] U(\omega) \tag{1.36}$$

Or

$$\ddot{X}(\omega) = \left[1 + \left(\frac{\omega}{\omega_n}\right)^2 H\left(\frac{\omega}{\omega_n}\right)\right] \ddot{U}(\omega) \tag{1.37}$$

In conclusion, the force at the base

$$F_{base}(\omega) = m\ddot{X}(\omega) = m \left[1 + \left(\frac{\omega}{\omega_n}\right)^2 H\left(\frac{\omega}{\omega_n}\right)\right] \ddot{U}(\omega) \tag{1.38}$$

Particularly, in this case $m = M_{eff}$ the effective mass, and the acting force is proportional to M_{eff} , and the base excitation in frequency domain multiplying by the amplification factor.

For a single DoF at the resonance:

$$|F_{base}(\omega)| = M_{eff} Q \ddot{U}(\omega_n) \tag{1.39}$$

Analogous relationships are writable for MDoF systems in which

$$\{F_{base,k}(\omega)\} = [M_{eff,k}] \left[1 + \left(\frac{\omega}{\omega_k}\right)^2 H_k\left(\frac{\omega}{\omega_k}\right)\right] \ddot{X}_j(\omega) \tag{1.40}$$

Where

$$[M_{eff,k}] = \frac{[L_k]^T [L_k]}{m_k} \tag{1.41}$$

$$[L_k] = \{\phi_{p,k}\}^T [M] [\Phi_r] \tag{1.42}$$

Symbol	Meaning
$[L_k]$	k-th Modal participation factor
$[M]$	Mass matrix
$\{\phi_{p,k}\}$	k-th mode
$[\Phi_r]$	Rigid body modes matrix
m_k	k-th generalized mass

Table 6: MEMs symbols

The effective mass characterises the mode and it is independent from the eigenvector normalization.

Chapter 2: The State space systems

The discipline of control systems takes part into the automation science. Its aim is to modify a dynamic system in terms of the output, subsequently to its observation, working on its input variables.

Typically, the control of the system is entrusted to a control system, exactly. Without going into detail, a control system is a mathematical model properly written and designed after the analysis of the physical system itself.

From a mathematical point of view a control system requires, as necessary, to solve a set of ODE in time domain. This task could be difficult due to the presence of ODE indeed.

For this reason, is a common practice to refer to the frequency domain using Laplace or Fourier transformation when the control system works. Practically, instead of a number of coupled differential equation is possible to determine the algebraic coefficient involved into the frequency transformation. Thanks to them, using the anti-transformation the control is expressed.

Commonly, the controllable systems are divided as follow:

- “SISO”: Single input- single output. Each element of the FRF matrix is analysed individually and by everyone of them the modal parameters are estimated
- “SIMO”: Single input- multiple output. A "set" of elements of a column (row) of the FRF matrix is analysed individually and from each one them the modal parameters are estimated
- “MIMO”: Multiple input- multiple output. A "set" of elements of the FRF matrix is obtained by exciting the structure in different points and analysed individually and from each of them the modal parameters are estimated

In this framework, the modelling using the “State Variables” represents a useful technique thanks to which is possible to monitoring the evolution in time, or frequency domain, of a prescribed system without the passage through a direct solving of an ODE.

Particularly, the state space approach represents one of the involved tools of the modern control theory.

They are effective into the dynamic system environment, for mechanical and electro-mechanical devices or scheme and, in general, if the considered model ha time-dependant variables.

Particularly, in this field, are common considered the so- called LTI (Linear time invariant) namely system in which their properties don't vary with the time (e.g. mass or stiffness for the application of VST). For this kind of systems, in past, the most common classical methods as root locus were used.

2.1 The State Variable Model and Continuous State Space systems

The state variables (or SV), or just the “state”, of a dynamic system represent the minimum set of variables thanks to which is possible to describe, and uniquely determinate, the system at every moment of its evolution when it is excited by a forcing function.

For this reason, calling

$$\mathbf{x} = \{x_1(t), x_2(t), \dots, x_n(t)\}^T \in \mathbb{R}^{n \times 1} \quad \text{The state vector/ variables} \quad (2.1)$$

$$\mathbf{u} = \{u_1(t), u_2(t), \dots, u_m(t)\}^T \in \mathbb{R}^{m \times 1} \quad \text{Input vector} \quad (2.2)$$

$$\mathbf{y} = \{y_1(t), y_2(t), \dots, y_n(t)\}^T \in \mathbb{R}^{l \times 1} \quad \text{Output vector} \quad (2.3)$$

For a generic system characterized by one, or more, differential equation, the modelling using the SV leads to the following mathematical systems

$$\begin{cases} \dot{x}_1 = f_1(x_1(t), x_2(t), \dots, x_n(t), u_1(t), u_2(t), \dots, u_m(t)) \\ \dot{x}_2 = f_2(x_1(t), x_2(t), \dots, x_n(t), u_1(t), u_2(t), \dots, u_m(t)) \\ \vdots \\ \dot{x}_n = f_n(x_1(t), x_2(t), \dots, x_n(t), u_1(t), u_2(t), \dots, u_m(t)) \end{cases} \quad (2.4)$$

Then, how is possible to see in (2.4) this modelling strategy makes equal the first derivate of a specific SV to a prescribed function.

At the same time, output system

$$\begin{cases} y_1 = g_1(x_1(t), x_2(t), \dots, x_n(t), u_1(t), u_2(t), \dots, u_m(t)) \\ y_2 = g_2(x_1(t), x_2(t), \dots, x_n(t), u_1(t), u_2(t), \dots, u_m(t)) \\ \vdots \\ y_n = g_n(x_1(t), x_2(t), \dots, x_n(t), u_1(t), u_2(t), \dots, u_m(t)) \end{cases} \quad (2.5)$$

Then writing in vector form

$$\begin{cases} \dot{\bar{x}}(t) = \bar{f}(\bar{x}(t), \bar{u}(t)) \\ \bar{y}(t) = \bar{g}(\bar{x}(t), \bar{u}(t)) \end{cases} \quad (2.6)$$

If the system allows the linearization process, (2.6) is writable as

$$\begin{cases} \dot{\bar{x}}(t) = A\bar{x}(t) + B\bar{u}(t) & \text{State equation} \\ \bar{y}(t) = C\bar{x}(t) + D\bar{u}(t) & \text{Output equation} \end{cases} \quad (2.7)$$

(2.7) is also called the State space representation of a system, or the state space system.

Where

- A: State variables Matrix
- B: Control Matrix
- C: Observation Matrix
- D: Feed forward Matrix

For better understand practically what is a “state space system”, how is possible to derive for a given differential equation, let consider the following ODE

$$\frac{d^n y}{dt^n} + a_1 \frac{d^{n-1} y}{dt^{n-1}} + \dots + a_n y = u \quad (2.8)$$

The State Space modelling requires the variables transformation

$$\begin{aligned} y &= x_1 \\ \frac{dy}{dt} &= x_2 \\ &\vdots \\ \frac{d^n y}{dt^n} &= -a_1 x_{n-1} - a_2 x_{n-2} - \dots - a_n x_1 + u \end{aligned} \quad (2.9)$$

Rewriting

$$\begin{aligned} \dot{x}_1 &= x_2 \\ \dot{x}_2 &= x_3 \\ &\vdots \\ \dot{x}_n &= -a_1 x_{n-1} - a_2 x_{n-2} - \dots - a_n x_1 + u \end{aligned} \quad (2.10)$$

Then, using the matrix form as in (2.7)

$$\begin{Bmatrix} \dot{x}_1 \\ \dot{x}_2 \\ \vdots \\ \dot{x}_n \end{Bmatrix} = \begin{bmatrix} 0 & 1 & 0 & \dots & 0 \\ 0 & 0 & 1 & \dots & 0 \\ \vdots & & & \dots & \vdots \\ -a_1 & -a_2 & \dots & -a_{n-1} & -a_n \end{bmatrix} \begin{Bmatrix} x_1 \\ x_2 \\ \vdots \\ x_n \end{Bmatrix} + \begin{bmatrix} 0 \\ 0 \\ \vdots \\ 1 \end{bmatrix} u \quad (2.11)$$

Based on what we desire to observe the output equation change.

For example, if we want to observe $y = x_1$

$$y = [1 \ 0 \ 0 \ \dots \ 0] \begin{Bmatrix} x_1 \\ x_2 \\ \vdots \\ x_n \end{Bmatrix} \quad (2.12)$$

Particularly, this kind of modelling is characterized by the continuous operators, for this reason they are usually called “Continuous state space system”.

Using continuous operators, the solution of the state equation (2.7) is provided by the following equation.

$$\mathbf{x}(t) = e^{A(t-t_0)}\mathbf{x}(t_0) + \int_{t_0}^t e^{A(t-\tau)}B\mathbf{u}(\tau)d\tau \quad (2.13)$$

$$e^{At} = \Phi \quad \text{The transition matrix} \quad (2.14)$$

Continuous state space formulation is an useful tool, but in control system environment usually is preferable to consider the discrete formulation.

2.2 Discrete State Space systems

Modern control systems are characterized by having electronic devices that require a sampling criterion in order acquire a correct signal and impose the appropriate action.

For this reason, the mathematical operator (continuous) are usually manipulated so as to be discrete and sampled.

Into this field, also called digital control environment, the State space system descried by (2.7) has to be converted to a sampled and discrete formulation.

Digital control techniques allow different types of conversions from continuous operators to discrete.

For this reason, let consider the time sampling $kT \leq t < (k+1)T$ together to the hypothesis $u = \text{constant at times}$. From these assumptions it follows the “Exact sampling”.

Using (2.13) and applying $t = (k+1)T$, $t_0 = KT$, $\mathbf{x}(t_0) = \mathbf{x}(kT)$, and being $u = \text{constant at times}$ this mean $u(\tau) \equiv \bar{u}(k)$, $kT \leq \tau < (k+1)T$.

Then

$$\mathbf{x}((k+1)T) = e^{AT}\mathbf{x}(kT) + \left(\int_0^T e^{A(T-\tau)}d\tau \right) B\bar{u}(k) \quad (2.15)$$

Rewriting

$$\bar{\mathbf{x}}(k+1) = e^{AT}\bar{\mathbf{x}}(k) + \left(\int_0^T e^{A\tau}d\tau \right) B\bar{u}(k) \quad (2.16)$$

This means

$$\begin{aligned} \bar{A} &\triangleq e^{AT} & \bar{B} &\triangleq \int_0^T e^{A\tau}d\tau B \\ \bar{C} &\triangleq C & \bar{D} &\triangleq D \end{aligned} \quad (2.17)$$

Obviously, this is just one possibility. In MatLab/ Simulink environment is possible to adopt different strategies in order to achieve the own best discretization strategy.

Table below recollects the most common strategies of discretization proposed in MatLab

Discretization strategy	Comment
ZOH	Zero-order hold,
FOH	Triangle approximation (modified first-order hold)
IMPULSE	Impulse-invariant discretization
TUSTIN	Bilinear (Tustin) approximation.
MATCHED	Zero-pole matching method.
LEAST- SQUARED	Least-squares method. Minimize the error between the frequency responses of the continuous-time and discrete-time systems up to the Nyquist frequency.

Table 7: Discretization useful approaches [Matworks.com]

The following images describe, in a graphical way, the differences between continuous and discrete state space formulation

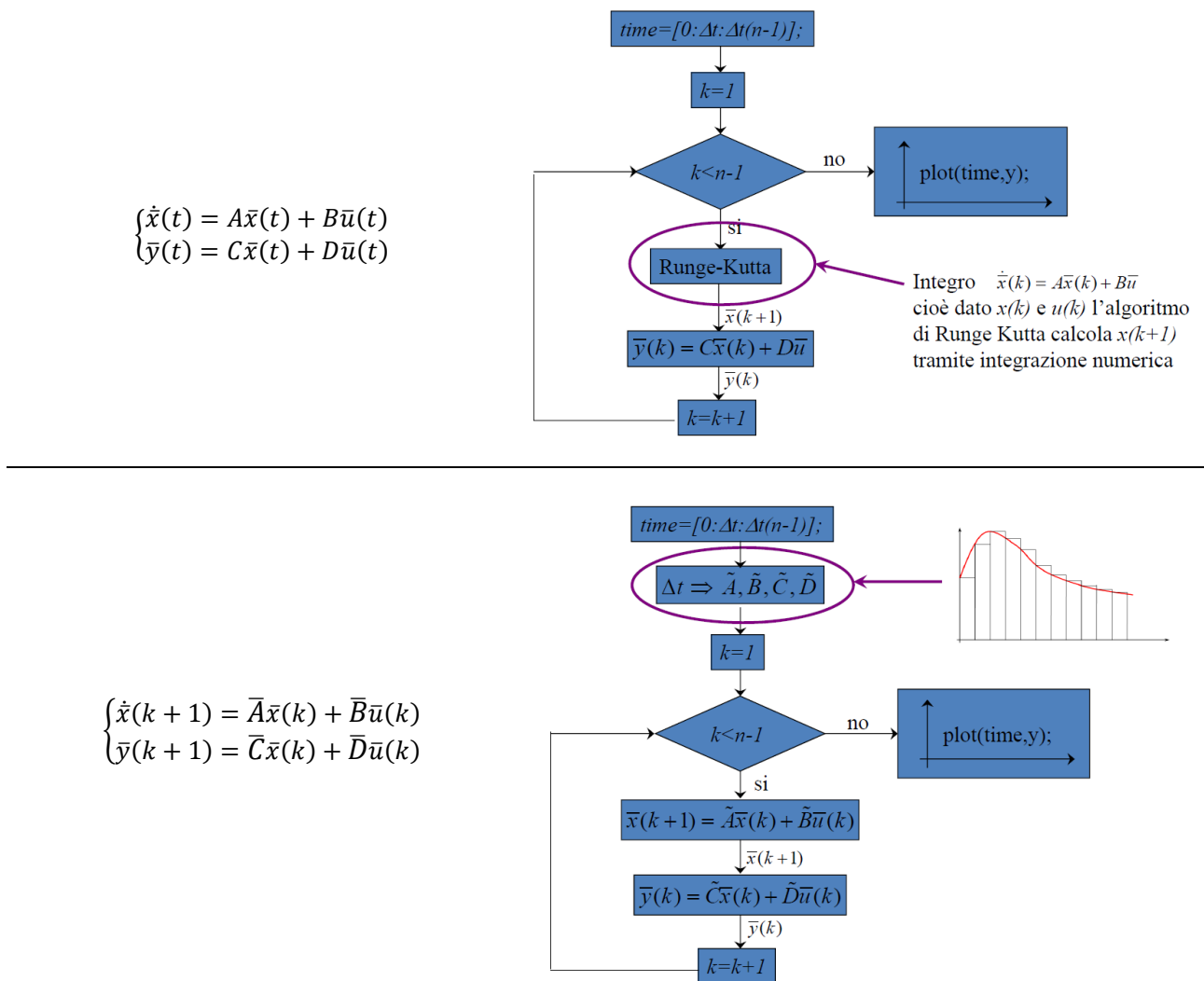


Figure 12: Continuous and discrete state space formulations [Ref. 29]

Particularly, continuous state spaces are usually solved with Runge-Kutta algorithms. On the contrary, discrete formulation involves schemes as finite differences. In addition, assuming the Runge-Kutta as the exact solution for a discrete problem, the discrete formulation represents the approximation of the previous.

Chapter 3: The Craig-Bampton dynamic condensation method

Finite Element Method (FEM) are distinguished by a huge number of elements inside the matrices that represent the structure. In fact, usually they are composed of millions of rows and columns having a sparse characteristic. When the simulation is running, all the terms are considered, however not always they are strictly required.

From a dynamic point of view, is not convenient to manage this “heavy” model in order to extrapolate the natural frequencies. How is well known, in fact, they are a global property of the system. For this reason, is useful to consider a reduced model capable to provide the same (or very close) values of the natural frequency.

This kind of consideration suggests the possibility in the use of a dynamic condensation method in which the DoFs into mass and stiffness matrices are less than the original provided by FEM. One of the main techniques is represented by Craig- Bampton condensation method.

Let considering the undamped equation of motion

$$[M]\{\ddot{x}\} + [K]\{x\} = \{F(t)\} \quad (3.1)$$

Denotating the external (or boundary) degrees of freedom with the index “j” and the internal degrees of freedom with the index “i”, is possible to deconstruct and partitioned (3.1) in accordance to different sub-blocks.

$$\begin{bmatrix} M_{ii} & M_{ij} \\ M_{ji} & M_{jj} \end{bmatrix} \begin{Bmatrix} \ddot{x}_i \\ \ddot{x}_j \end{Bmatrix} + \begin{bmatrix} K_{ii} & K_{ij} \\ K_{ji} & K_{jj} \end{bmatrix} \begin{Bmatrix} x_i \\ x_j \end{Bmatrix} = \begin{Bmatrix} F_i \\ F_j \end{Bmatrix} \quad (3.2)$$

Is common practice to depict the displacement vector $\{x(t)\}$ on a basis of 6 rigid-body modes (or static modes) $[\Phi_r]$ and elastic mode shapes $[\Phi_p]$.

We can express $\{x\}$ as

$$\{x\} = [\Phi_r]\{x_j\} + [\Phi_p]\{\eta_p\} = \begin{bmatrix} [\Phi_r], [\Phi_p] \end{bmatrix} \begin{Bmatrix} x_j \\ \eta_p \end{Bmatrix} = [\Psi]\{X\} \quad (3.3)$$

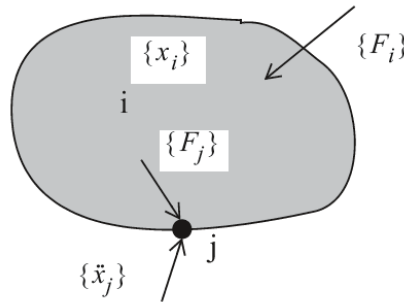


Figure 13: Craig-Bampton indices [Ref.12]

The two matrices $[\Phi_r]$ and $[\Phi_p]$ are evaluated in different ways.

Firstly, the static modes can be obtained, neglecting the inertia effects and $\{F_i\} = \{0\}$ and introducing a unit displacement for 6 boundary DoFs, $\{x_j\} = [I]$.

$$\begin{bmatrix} K_{ii} & K_{ij} \\ K_{ji} & K_{jj} \end{bmatrix} \begin{Bmatrix} x_i \\ x_j \end{Bmatrix} = \begin{Bmatrix} 0 \\ 0 \end{Bmatrix} \quad (3.4)$$

Considering the first equation of (3.4)

$$[K_{ii}]\{x_i\} + [K_{ij}]\{x_j\} = 0 \quad (3.5)$$

$$\{x_i\} = -[K_{ij}]^{-1}[K_{ii}]\{x_j\} \quad (3.6)$$

Therefore, introducing

$$[\Phi_{ij}] = -[K_{ij}]^{-1}[K_{ii}][I] = -[K_{ij}]^{-1}[K_{ii}] \quad (3.7)$$

Then, the static transformation

$$\{x\} = \begin{Bmatrix} x_i \\ x_j \end{Bmatrix} = \begin{bmatrix} \Phi_{ij} \\ I \end{bmatrix} \{x_j\} = [\Phi_r]\{x_j\} \quad (3.8)$$

Secondly, the elastic mode shapes assume fixed external degrees of freedom $\{x_j\} = \{0\}$ and harmonic motion $x(t) = X(\omega)e^{j\omega t}$. In this way, the eigenvalues problem can be formulated as

$$([K_{ii}] - \lambda_k[M_{ii}])[\Phi_{ip}] = \{0\} \quad (3.9)$$

Introducing the modal coordinates

$$\{x\} = \begin{Bmatrix} x_i \\ x_j \end{Bmatrix} = \begin{bmatrix} \Phi_{ip} \\ 0 \end{bmatrix} \{\eta_p\} = [\Phi_p]\{\eta_p\} \quad (3.10)$$

The Craig- Bampton transformation matrix $[\Psi]$ is

$$\{x\} = \begin{bmatrix} [\Phi_r], [\Phi_p] \end{bmatrix} \begin{Bmatrix} x_j \\ \eta_p \end{Bmatrix} = [\Psi]\{\chi\} \quad (3.11)$$

In which, using the same nomenclature proposed by Wijker [Ref 12, 13]:

- $[\Phi_r]$: the rigid body modes
- $[\Phi_p]$: the modal matrix
- $\{x_j\}$: the external or boundary degrees of freedom ($j \leq 6$)
- $\{\eta_p\}$: the generalised coordinates
- $[M_{rr}]$: the 6x6 rigid body mass matrix with respect to the boundary DOFs

- $[\widetilde{K}_{JJ}]$: the Guyan reduced stiffness matrix (j-set)
- $[m_p]$: diagonal matrix of generalised masses
- $[K_p]$: the diagonal matrix of generalised stiffnesses
- $[M_{jp}] = [L]^T$: matrix with the modal participation factors

Particularly,

$$\begin{aligned}
[m_p] &= [\Phi_p]^T [M] [\Phi_p] \\
[K_p] &= [\Phi_p]^T [K] [\Phi_p] = < \lambda_p > [m_p] = < \omega^2 > [m_p] \\
[K_{ip}] &= [\Phi_{ij}]^T [K_{ii}] [\Phi_{ij}] + [K_{ij}] [\Phi_p] = \left(-[K_{ij}]^T [K_{ii}]^{-1} [K_{ii}] + [K_{ij}] \right) [\Phi_p] = [0] \\
[K_{pi}] &= [K_{ip}]^T = [0] \\
[\widetilde{K}_{JJ}] &= [\Phi_r]^T [K] [\Phi_r] = [0] \\
&\text{(only if the structure is statically determinate)}
\end{aligned} \tag{3.12}$$

Rewriting

$$[\Psi]^T [M] [\Psi] \{\ddot{\chi}\} + [\Psi]^T [K] [\Psi] \{\chi\} = [\Psi]^T \{F(t)\} = \{f(t)\} \tag{3.13}$$

From (3.13) is possible to deduce

$$\begin{bmatrix} M_{rr} & M_{jp} \\ M_{pj} & m_p \end{bmatrix} \begin{Bmatrix} \ddot{x}_j \\ \ddot{\eta}_p \end{Bmatrix} + \begin{bmatrix} \widetilde{K}_{JJ} & K_{jp} \\ K_{pj} & K_p \end{bmatrix} \begin{Bmatrix} x_i \\ x_j \end{Bmatrix} = \begin{bmatrix} [\Phi_{ij}] & [\Phi_p]^T \\ I & 0 \end{bmatrix} \begin{Bmatrix} F_i \\ F_j \end{Bmatrix} \tag{3.14}$$

And, introducing (3.12)

$$\begin{bmatrix} M_{rr} & L^T \\ L & m_p \end{bmatrix} \begin{Bmatrix} \ddot{x}_j \\ \ddot{\eta}_p \end{Bmatrix} + \begin{bmatrix} \widetilde{K}_{JJ} & 0 \\ 0 & < \lambda_p > m_p \end{bmatrix} \begin{Bmatrix} x_i \\ x_j \end{Bmatrix} = \begin{bmatrix} [\Phi_{ij}] & [\Phi_p]^T \\ I & 0 \end{bmatrix} \begin{Bmatrix} 0 \\ F_j \end{Bmatrix} = \begin{Bmatrix} F_j \\ 0 \end{Bmatrix} \tag{3.15}$$

As adjunction, is possible to consider the modal damping matrix in addition to (3.15)

$$\begin{bmatrix} M_{rr} & L^T \\ L & m_p \end{bmatrix} \begin{Bmatrix} \ddot{x}_j \\ \ddot{\eta}_p \end{Bmatrix} + \begin{bmatrix} 0 & 0 \\ 0 & < 2\zeta\omega_p > m_p \end{bmatrix} \begin{Bmatrix} \dot{x}_j \\ \dot{\eta}_p \end{Bmatrix} + \begin{bmatrix} \widetilde{K}_{JJ} & 0 \\ 0 & < \lambda_p > m_p \end{bmatrix} \begin{Bmatrix} x_i \\ x_j \end{Bmatrix} = \begin{Bmatrix} F_j \\ 0 \end{Bmatrix} \tag{3.16}$$

Particularly, (3.16) will be implemented further.

Part II

Applicative background

Chapter 4: The launch environment

During a typical mission there are usually two critical periods: the launch and re-entry phase. In this context we are interested only about the first because second one produces above all thermal and aero-thermodynamics problems. In addition, each S/C are subjected to launch, but not everybody is interested in re-entry phase, for instance unmanned missions without any interests of retrieval.

Launch environment is the most critical setting in which a S/C could operate in terms of mechanical solicitations and stresses.

In fact, even if, the outer space is dangerous for all the equipment due to radiations, high difference of temperatures during the orbit and the presence of MMOD, the launch phase is distinguished by high values of acting forces coming from different sources.

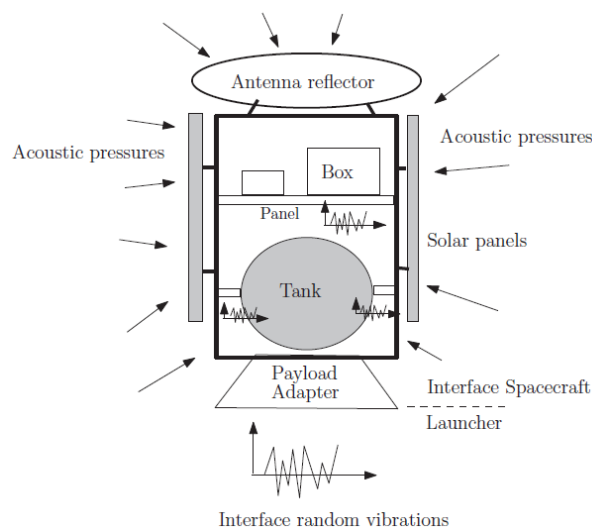


Figure 14: Different sources acting on a S/C [Ref. 13]

These solicitations, in particular, act during the ascent but they are especially critical during the firsts 120-200 second.

They produce induced vibration, noise, dynamic loads and could start any unwanted breaks for the L/V and the S/C.

For this reason, engineers involved in mechanical design have to be able to satisfy all the mechanical requirements in order to guarantee that the S/C could withstand to launch loads.

Briefly, mechanical requirements are usually imposed in terms of:

- Strength
- Structural life
- Structural response
- Stiffness, damping and mass properties
- Dynamic envelope
- Positional stability
- Mechanical interface

From a mechanical point of view, launch environment is possible to classify the dynamic environment in terms of:

- Load path
- Vibration sources
- Frequency content

Firstly, load path represents the “vehicle” with which the solicitation could be transmitted from its source to the S/C.

It can be divided in two categories as is shown in Table 8

Load Paths	
<u>Structural</u> (or mechanical-borne)	<u>Acoustic</u> (or air-borne)
Transmission via the launcher structure in which the spacecraft is excited by mechanical forces at its interface with the launcher.	Transmission via the ambient air in which the spacecraft is excited by the acoustic pressure field inside the fairing and acting on all exposed surfaces.

Table 8: Division by load paths

Obviously, during the ascent, they are involved simultaneously. During the lift-off and transonic flight the sum of structural and acoustic environment produces the so-called vibro-acoustic environment.

Secondly, in term of vibration sources, Table 9 offers an appropriate classification

Regimes of vibration sources		
<u>Harmonic</u>	<u>Transient</u>	<u>Random</u>
Very important due to high amplification, but also rare	Very short periods affect this kind of vibration (e.g. millisecond or seconds) but they can produce high excitation (e.g. pyrotechnic events or burst)	They are produced from different sources but at the same time they can be independent. A deterministic analysis is no sufficient

Table 9: Division by vibration sources

Last type of classification is based on frequency content, Table 10

Frequency content	
Low frequency	Wide band
<p>Usually, low frequency involves quasi-static loads and sine-sweep.</p> <p>In this case, the excitation produces a clear and predictable response</p>	<p>When the frequency increases the number of shapes increase too.</p> <p>The mode shapes are very close respectively and the analysis become more difficult.</p> <p>Typical loads are shock and acoustic loads</p>

Table 10: Division by frequency content

In fact, according to the last classification, Figure 15 shows a useful representation of launch environment in terms of loads as a function of frequency.

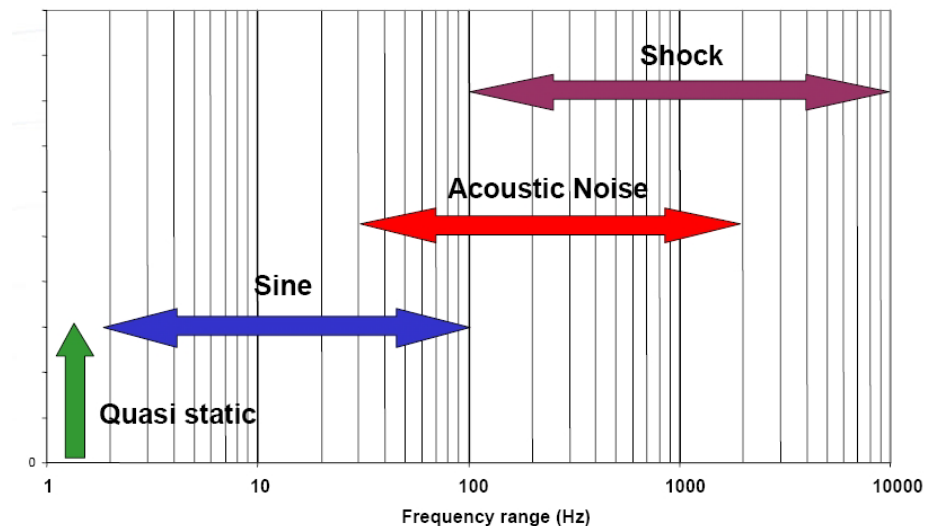


Figure 15: Loads in term of frequency content (a) [Ref. 9]

More precisely, they are usually categorized as follows:

- Static accelerations generate by external and constants forces (e.g gravity) or by forces that has very slow rate of change during a period
- Low frequency acceleration and dynamic response, typically from 0 to 100 Hz
- High frequency random vibration environment, typically defined from 20 to 2000 Hz, the solicitations are transmitted through the interfaces
- High frequency acoustic pressure environment, typically from 20 to 8000 Hz inside the fairy
- Shock events, in this case the frequency content is defined from 500 to 10 KHz.

In the following paragraph 4.1 a brief overview of the common loads encountered during the launch phase and the ascent is provided.

4.1 Overview of the typical loads during the launch

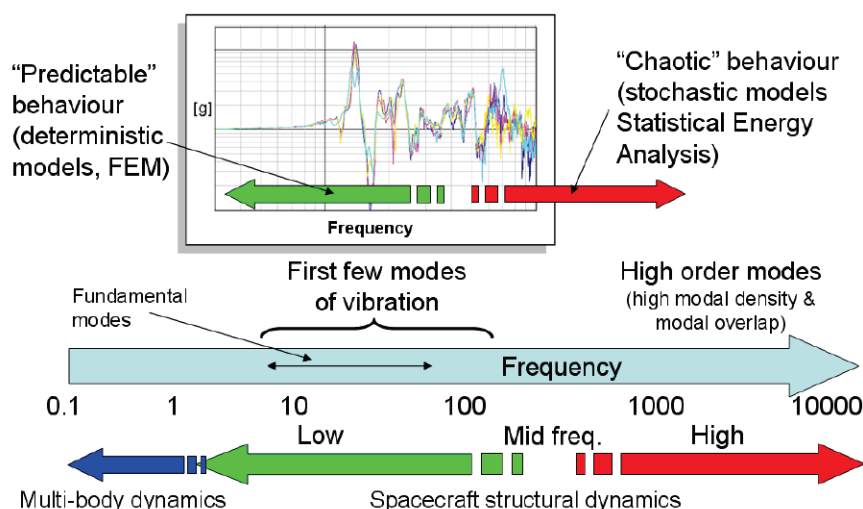


Figure 16: Loads in term of frequency content (b) [Ref. 9]

To have a good knowledge of the different load affecting the S/C during launch allows the better prediction in terms of analysis and test of the different load cases. In fact, how has been introduced before, and is possible to see in Figure 166, at low frequency and very low frequency ($\approx 0.1 \div 100 \text{ Hz}$) the prediction based on FEM is accepted and gives reliable results. In this context they are defined the so- called “Quasi static”, “Sinusoidal” and “Acoustic” (at low frequency) loads .

When the LV arise, frequency grows and the loads change their nature becoming “Random”, “Acoustic” (at high frequency) or with a very high energy content, called “Shocks”.

In this cases chaos affect the global motion, therefore any other methos have to be used as SEA.

	Acoustics	Random Vibration	Sine vibration	Shock
Lift-off	x	x		
Aerodynamic	x	x		
Separation (stage, fairing, spacecraft)				x
Motor burn, POGO		x	x	

Table 11: Origin of some loads [Ref. 12]

4.1.1 Quasi-static

Quasi-static loads (QSL) is a combination of static and dynamic loads into an *equivalent* static applied at CoG, typically expressed as positives or negatives accelerations and representatives of the maximum and minimum values perceived at CoG.

Actually, they are not fully adequate for a complete and precise design of a S/C nevertheless they are suitable for preliminary design.

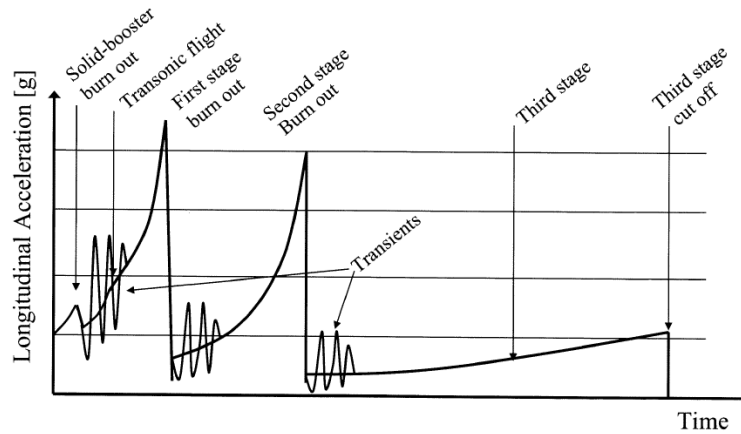


Figure 17: Quasi-static longitudinal acceleration [Ref.14]

4.1.2 Sinusoidal

Sinusoidal loads, or sine loads, are typically mechanical loads with low frequency content. Usually they come from engines combustion during which sine waves ascend from structure load path.

Particularly, is common to identify this kind of vibration in the range up to 100 Hz. In addition, it is usual to classify them whit different specification levels: for S/C and for payloads and equipment.

Firstly, sine loads for S/C is defined from the launcher's user manual. Secondly, at equipment level, they are designed and qualified for typical sine loads and not only for one specific mission.

4.1.3 Random and vibro-acoustics

During the ascend, acoustic pressure affect the structure and could induce acoustic vibration and random response. The interested structures in this case are those which are light in weight and large in surface area (e.g. skin panels and solar array).

Is an usual approach the use of “ sound pressure level “ or SPL, defined as

$$SPL = 10 \log \left(\frac{p}{p_{ref}} \right)^2 \quad (4.1)$$

Where “p” is the rms pressure at certain frequency band and $p_{ref} = 2 \times 10^{-5} \text{Pa}$.

Normally, vibro-acoustic and random vibration are defined over the range of 20 Hz to 10 KHz and they have to be studied in terms of statistic analysis.

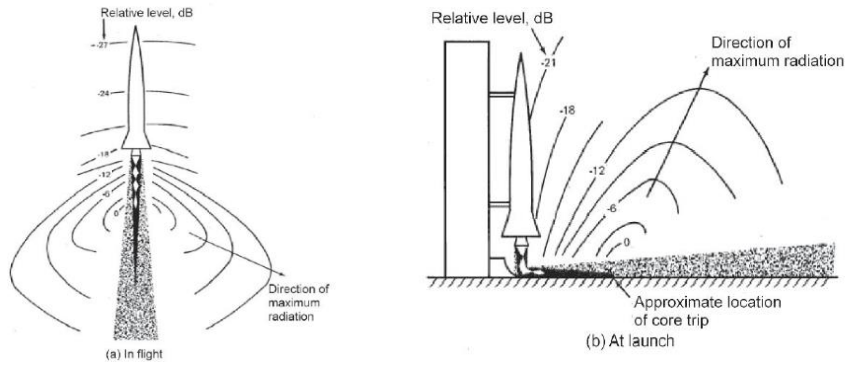


Figure 18: Acoustic loads [Ref.12]

4.1.4 Shocks

Shock events take place in the very early orbit phase. In these moments different relevant events occur, for instance stages separation, deployment of appendages or fairing jettisoning. Peculiarity of these events is the high energy content, high frequency and magnitude. It can induce non negligible solicitations to the structure and instruments.

In fact, potential damaging effects are:

- Structural impact
- Mechanism impact
- Electronics impact

For this reason, design process shall be conducted in terms of derivation of S/C shock environment and verification approach. The aim is to verify that structures, equipments and instruments are able to satisfy the shock environmental requirements.

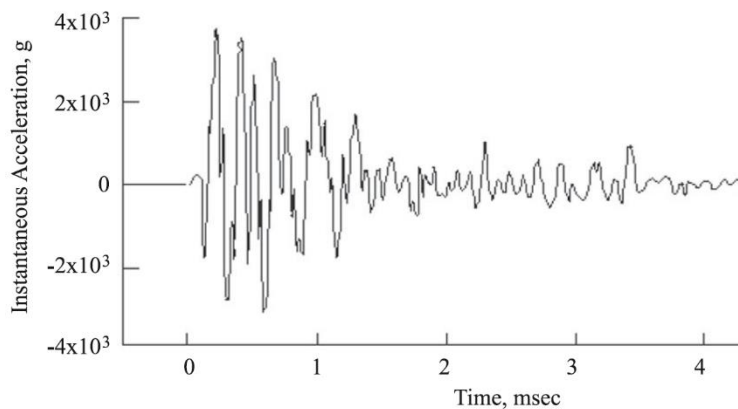


Figure 19: Example of time history for shock loads [Ref.12]

4.2 Example of launch loads through Ariane 5

Nowadays, Ariane 5 is the most powerful LV of Ariane family (in near future will be Ariane 6). It is provided by two solid booster that supply 90% of thrust at lift-off and a cryogenic core stage, ignited and checked on ground. It is able to place heavy payloads in GTO and ideally suited for launching the space tugboat or Automated Transfer Vehicle (ATV) towards the International Space Station.

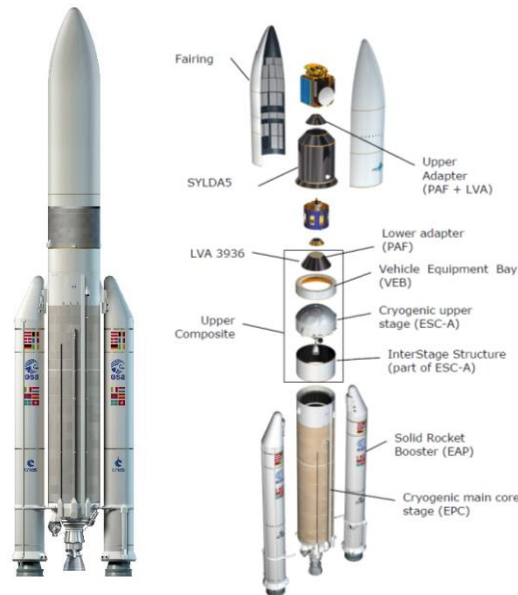


Figure 20: Close-up (on left) and exploded view of the LV (on right) [Ref.30]

Payload fairing		Solid rocket booster (EAP)	
Diameter	5.4 m	Size	Φ3.05 m x 31.6 m
Height	17 m	Structure	Stainless steel case
Mass	2675 kg	Propulsion	Solid propellant motor (MPS)
Structure	Two halves - Sandwich CFRP sheets and aluminium honeycomb core	Propellants	240 t of solid propellant per EAP
Acoustic protection	Foam sheets	Mean thrust	7000 kN (Vacuum)
Separation	Horizontal and vertical separations by leak-proof pyrotechnical expanding tubes	Isp	274.5 s
		Combustion time	130 s

(a)

Cryogenic upper stage (ESC-A)		Cryogenic main core stage (EPC)	
Size	Φ 5.4 m x 4.711 m between I/F rings	Size	Φ 5.4 m x 23.8 m (without engine)
Dry mass	4540 kg	Dry mass	14700 kg
Structure	Aluminium alloy tanks	Structure	Aluminium alloy tanks
Propulsion	HM7B engine - 1 chamber	Propulsion	Vulcain 2 - 1 chamber
Propellants loaded	14.9 t of LOX + LH2	Propellants loaded	170 t of LOX + LH2
Thrust	67 kN	Thrust	960 kN (SL) 1390 kN (Vacuum)
Isp	446 s	Isp	310 s (SL) 432 s (Vacuum)

(b)

Table 12: Some technical information (a), (b) about Ariane 5 [Ref.30]

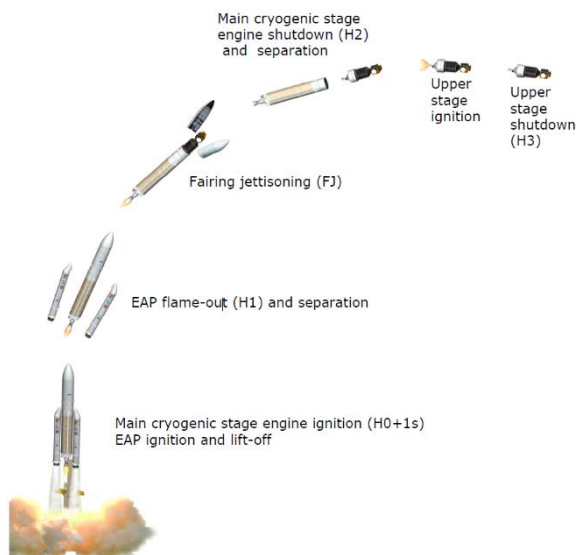


Figure 21: Ariane 5 typical mission profile [Ref.30]

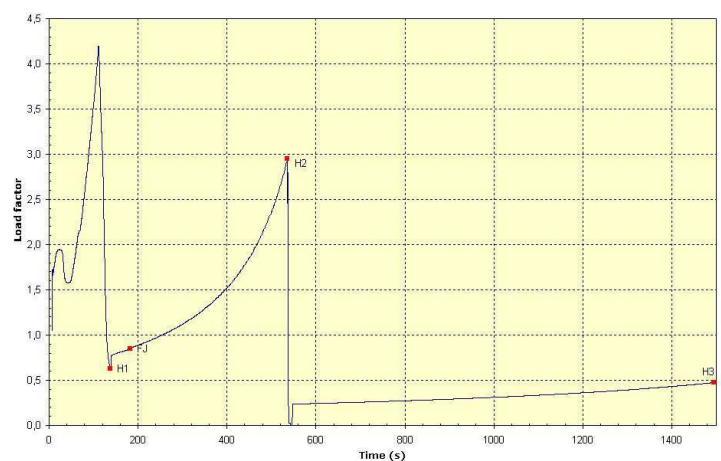


Figure 22: Quasi-static longitudinal acceleration during time [Ref.30]

In Figure 21 a typical mission profile for Ariane 5 is shown. In this context, during launch, LV it self and its payloads shall be whitstand to the following mechanical loads, how is shown in the previous paragraphs.

Firstly, static and quasi-static acceleration due to gravity, aerodynamic and propulsion systems is shown in Figure 22. During the ascent, the peak is reached before than 200 s after the lift-off and its values is 4.55g for longitudinal acceleration. The highest lateral static acceleration is up to 0.25g

Secondly, during powered flight sinusoidal excitation (or sine-equivalent) levels at the spacecraft base does not exceed the values given in Table 13

Direction	Frequency band (Hz)	Sine amplitude (g)
Longitudinal	2-50	1.0
	50-100	0.8
Lateral	2-25	0.8
	25-100	0.6

Table 13: Sine excitation at spacecraft base [Ref.30]

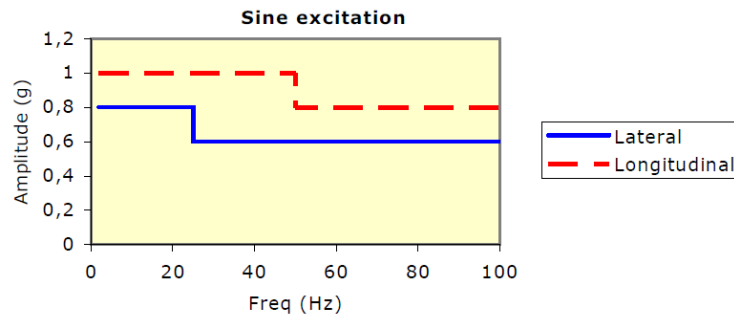


Figure 23: Sine excitation at spacecraft base [Ref.30]

How is possible to see, sinusoidal vibrations are defined up to 100 Hz.

Thirdly, according to random vibrations, they are covered by the sine vibration under 100 Hz.

Above 100 Hz, the acoustic spectrum covers the random vibration at the spacecraft base, particularly for flight conditions. In this case, acoustic pressure transmitted to the structure produces noise.

Octave center frequency (Hz)	Flight limit level (dB) (ref: 0 dB= 2x10E-5 Pa)
31.5	128
63	131
125	136
250	133
500	129
1000	123
2000	116
OASPL (20 – 2828 Hz)	139.5

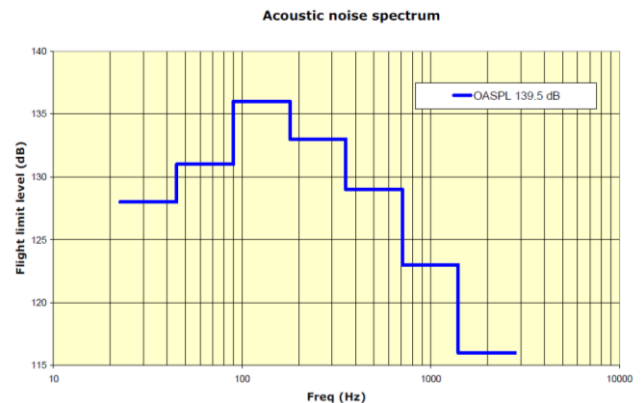


Table 14: Acoustic noise spectrum under the fairing [Ref.30]

Figure 24: Acoustic noise spectrum [Ref.30]

The last mechanical source is shock. They propagate through structural path and caused by different events.

The spacecraft separation shock is directly generated at the base of the spacecraft and its levels depend on the adapter type, since the interface diameter and the separation system have a direct impact. For a clampband adapter the envelope of shock response spectrum is given in the below curve.

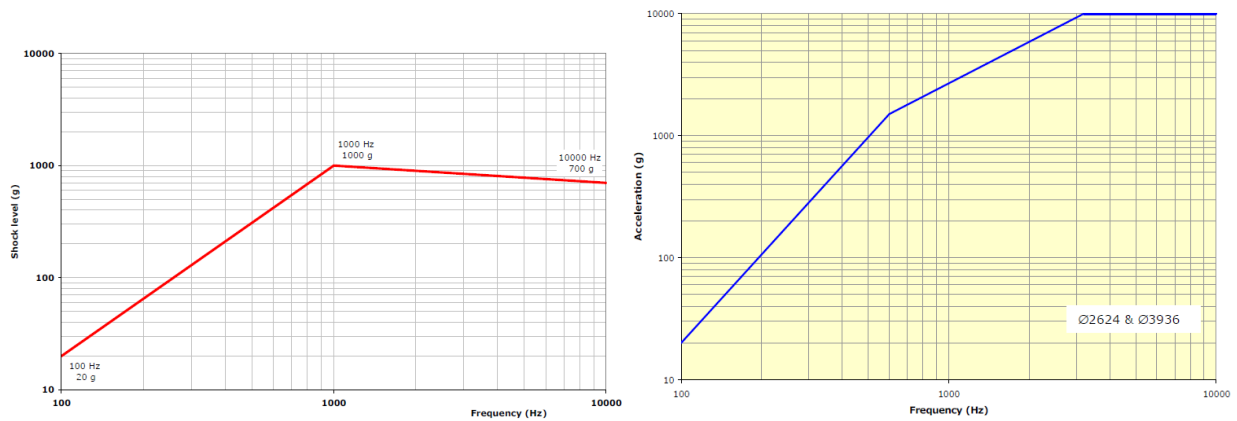


Figure 25: Envelope shock spectrum for clamp-band release at spacecraft interface and for fairing and L/V stage separation events (left) L/V acceptable shock spectrum at launcher bolted interface (right) [Ref.30]

Then, how is easy to understand, each load case is combined to a precise kind of analysis or tests dedicated to examining the response of the considered structure, Table 15.

Load	Verification by analysis	Verification by test
Static and Quasi-static	Static analysis	Static test
Transient environment	Transient analysis	Sine burst test
in low frequency range	Frequency response analysis	Sine vibration test
Quasi harmonic loads in low	Transient analysis	Sine vibration test
frequency range	Frequency response analysis	Sine vibration test
Broad band vibration	Random vibration analysis	Random vibration test
(random and acoustic)	Vibro-acoustic analysis	Acoustic noise test
Shock & high	Transient analysis	
frequency transient	Shock propagation assessment	Shock test
	Semi-analytical approaches	
	Static analysis	
Pressure	Thermal-functional analysis	Proof pressure test
	Venting analysis	Thermal-functional test
Thermo-elastic	Thermo-elastic analysis	Thermo-elastic test

Table 15: Verification by analysis and test for each load cases [Ref.14]

Chapter 5: Sine vibration

How is well known, launch environment is a sum a various contribution. In fact, take place different solicitations coming from different sources and events.

Low and high frequency vibration affect the LV and the S/C during the ascent from lift off to the fairy jettisoning. They are usually classified as in Figure 15 and Figure 16.

From the low frequency point of view, is typical to identify this kind of vibrations as “sine vibration”. Above all, sine wave excitation is a useful approach for tests and allow the simulation of transient phenomena, at system and subsystem level, using the so-called “sine sweep”.

Setting adequately frequency up to 100 Hz and magnitude of the sine wave is possible to represent the hypothesized transient phenomenon, as low frequency random or acoustic and vibrations coming from booster ignition.

In this context take place the sine wave, with constant frequency and amplitude. However, in practical use, a “swept sine wave” is preferred to a simple sine wave. It has the peculiarity related to the increasing of its frequency and usually constant amplitude, how Figure 266 shows.

This approach allows the simulation of the frequency response of the system when it is attached to a mounting structure, with an enforced motion, particularly an acceleration, at the base of the spacecraft. This procedure, coupled with the physical shaker body modelled through CAD and FEM, is the prelude of the VST.

In addition, from a time point of view, using swept sine wave analysts are able to conduct the so called CLA in which S/C and LV are coupled together. This allows the imposition of a transient analysis whereby is reconstructed the time domain behaviour due to the coupling.

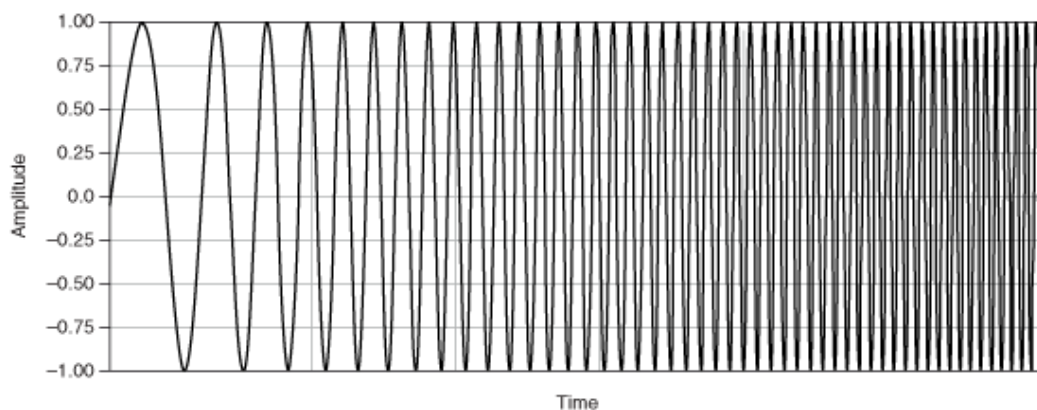


Figure 26: Swept sine wave [Ref.31]

Particularly, working on this framework, is typical to consider a swept sine as a function of time as,

$$l(t) = l_0 \sin(E(t) + \phi) \quad (5.1)$$

In which

- ϕ : the phase, generally zero
- $E(t)$: function of time characteristic of the sweep mode
- $l(t)$: generally, is an acceleration, but it could be a displacement, a velocity or a force
- l_0 : magnitude of $l(t)$

In addition, we can define the pulsation of the swept sine wave as

$$\Omega = 2\pi f = \frac{dE}{dt} \quad (5.2)$$

In this case is possible to define two swept mode, at least:

- Linear sweep:

$$f = \alpha t + \beta \longrightarrow \Omega(t) = \Omega_0 + \left(\frac{K_1}{60}\right)t \quad (\text{for practical use}) \quad (5.3)$$

- Logarithmic-exponential sweep:

$$f = f_1 e^{\frac{t}{T_1}} \longrightarrow \Omega(t) = \Omega_0 2^{\left(\frac{K_e}{60}\right)t} \quad (\text{for practical use}) \quad (5.4)$$

In which $K_e[\frac{\text{octaves}}{\text{minute}}]$ is the exponential sweep rate and $K_1[\frac{\text{Hz}}{\text{minute}}]$ is the linear sweep rate.

These two could be an increasing or decreasing frequency. Specially, linear and logarithmic sweep are usually used during sine testing. In fact, during vibration tests, sine swept is largely used in order to simulate the envelope of the environment in a given frequency range.

Moreover, the concept of “octave” is widely used. It represents interval between two frequencies whose ratio is 2. The number of octaves ranging between two frequencies f_1 and f_2 is such that:

$$\frac{f_2}{f_1} = 2^n \implies n = \frac{\ln \frac{f_2}{f_1}}{\ln 2} \quad (5.5)$$

However, is a common practice to introduce the sweep rate as the number of octaves per minute R_{om} and octaves per seconds R_{os} as

$$R_{os} = \frac{n}{t_s} = \frac{\ln f_2/f_1}{t_s \ln 2} \quad (t_s \text{ in seconds}) \quad (5.6)$$

$$R_{om} = \frac{60 n}{t_s} = 60 R_{os} \quad (5.7)$$

With some mathematical manipulation is possible to write

$$f = f_1 2^{R_{om} \frac{t}{60}} \quad (5.8)$$

So, how is possible to recognize, the equivalence between (5.4) and (5.9). It follows that

$$R_{om} = K_e \quad (5.9)$$

In aerospace field, the most used sweep rates

Sweep rate	Aim
0.5	Modal survey
2	Qualification level
4	Acceptance level

Table 16: sweep rate in aerospace field

This means that every 60 seconds frequency grows of 2^{K_e} [Hz].

Observing the user's manual of Ariane 5 the sine vibration environment is defined for different units.

Axis	Units less 100 kg			Units greater 100 kg		
	Frequency (Hz)	Qualification	Acceptance	Frequency (Hz)	Qualification	Acceptance
Out of plane	5-20	15mm	9.9 mm	5-20	9.3 mm	7.5 mm
	20-100	24 g	16 g	20-60	15 g	12 g
				60-100	5 g	4 g
In plane	5-20	9.9 mm	6.6 mm	5-20	7.8 mm	6.6
	20-100	16 g	10.7 g	20-60	12.5 g	10 g
				60-100	5 g	4 g
Sweep rate		2 Oct/min 1sweep up	4 Oct/min 1sweep up		2 Oct/min 1sweep up	4 Oct/min 1sweep up

Table 17: Sinusoidal environment for different units [Ref.14]

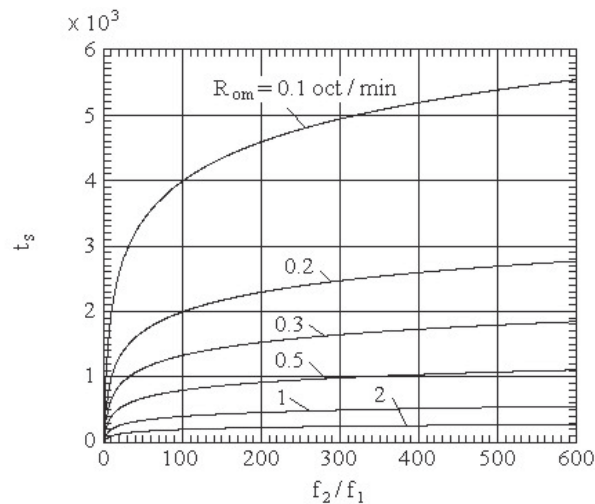


Figure 27: Time vs frequency ratio for different exponential rate of sweep [Ref.31]

Previously has been said that (5.1) represent the typical sine law. For this reason, assuming $l(t)$ as acceleration, phase ϕ equal to zero and exponential sweep, is possible to deduce the complete equation of motion, as

$$E(t) = \int_0^t \Omega(t) dt = \Omega_0 \int_0^t 2^{\frac{K_e}{60}t} dt = \Omega_0 \frac{60}{K_e} \int_0^t \frac{K_e}{60} 2^{\frac{K_e}{60}t} dt = \Omega_0 \frac{60}{K_e} \frac{2^{\frac{K_e}{60}t}}{\ln 2} + cost \quad (5.10)$$

For initial condition: $t = 0 \implies E(t = 0) = 0 \implies cost = -\frac{\Omega_0 60}{K_e \ln 2}$

Then

$$\phi(t) = \frac{\Omega_0 60}{K_e \ln 2} \left(2^{\frac{K_e}{60}t} - 1 \right) \quad (5.11)$$

Therefore,

$$l(t) = l_0 \sin \left[\frac{\Omega_0 60}{K_e \ln 2} \left(2^{\frac{K_e}{60}t} - 1 \right) \right] \quad (5.12)$$

In addition, l_0 is not constant a priori. In fact, in case of testing, is common practice to modulate the amplitude in case of overtesting. This is the concept of primary notching and will be explored later.

Usually, sine sweep is common applied during sine test on shaker. In fact, a satisfactory correspondence is reached only at low frequency using this procedure

5.1 Shock response spectrum (SRS), equivalent sine dynamics and equivalent sine level (ESL)

Shock response spectrum is a useful tool largely used for simulation and analysis of transient phenomena. In fact, despite Fourier transform is one of the most used in signal processing, it is lack in terms of notion of severity. For this reason, SRS is preferred to FT in order to have a better knowledge of severity required to elaborate specifications.

It should be noted that, term “Shock” can be misleading, its definition is general and applicable to different sources, not only for shocks.

In general, SRS represents the maximum response of a 1-DOF system as a function of its natural frequency, for a given damping ratio or quality factor “ $Q = 1/(2\zeta)$ ”.

Recalling what has been done in paragraph 1.2, in terms of enforced acceleration on a SDoF

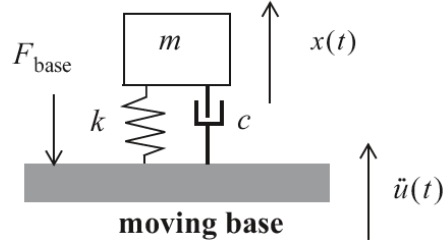


Figure 28: Enforced motion at the base [Ref.13]

The relative displacement

$$z(t) = x(t) - u(t) \quad (5.13)$$

In which $z(t)$ represents the relative motion; $x(t)$ the displacement of the mass; $u(t)$ the displacement of the base.

The equation of motion in terms of relative displacement

$$\ddot{z}(t) + 2\zeta\omega_n\dot{z}(t) + \omega_n^2z(t) = -\ddot{u}(t) \quad (5.14)$$

The absolute acceleration can be calculated as

$$\ddot{x}(t) = \ddot{z}(t) + \ddot{u}(t) = -2\zeta\omega_n\dot{z}(t) - \omega_n^2z(t) \quad (5.15)$$

Particularly, SRS calculation requires homogenous condition, then

$$z(t) = -\int_0^t e^{-\zeta\omega_n\tau} \left(\frac{\sin \omega_d \tau}{\omega_d} \right) \ddot{u}(t-\tau) d\tau = -\int_0^t e^{-\zeta\omega_n(t-\tau)} \left(\frac{\sin(\omega_d(t-\tau))}{\omega_d} \right) \ddot{u}(\tau) d\tau \quad (5.16)$$

Hence, the absolute acceleration

$$\ddot{x}(t) = 2\zeta\omega_n \int_0^t e^{-\zeta\omega_n(t-\tau)} \cos(\omega_d(t-\tau)) \ddot{u}(\tau) d\tau + \omega_n(2\zeta^2 - 1)z(t) \quad (5.17)$$

Using (5.17) the calculus of the SRS is possible for a given natural frequency $\omega_n = 2\pi f_n$ [Rad/s] of the SDof system. In case of MDoF system is necessary to tune the natural frequency and damping coefficient in order to analyse each SDof.

After all time history, in terms of acceleration, are known, the SRS is the envelope of the peaks (g-peaks) of each SDof.

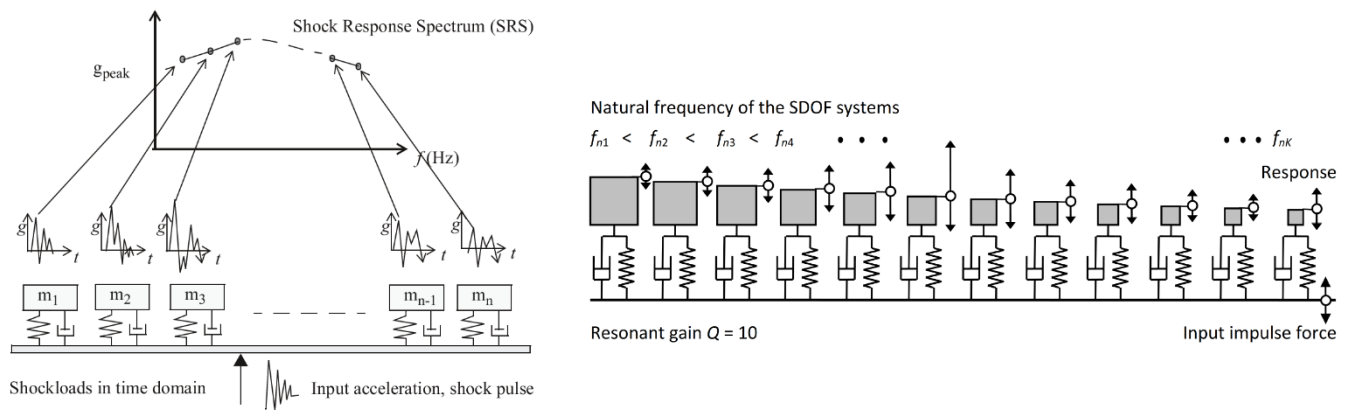


Figure 29: Construction of SRS [Ref. 12, 32]

Figure 29 shows in a graphical way the introduced procedure. Particularly, on the horizontal axis are present the frequency. These are an infinitive set of frequency, but every g-peak are defined for a precise natural frequency that correspond to a precise SDOF.

Drawback:

- SRS is a priori mathematically very complex and high nonlinear
- SRS is irreversible. For a given time history is associate a unique SRS but not vice versa

In addition, exists other problems relates to SRS, as:

- Being it is a theory just appropriate for a SDOF, the modal superposition cannot be strictly applied resulting in an appropriate combined response with the risk of obtaining significant difference in amplitude
- The damping in the structure could be different between the quality factor used for SRS

In general, the purpose of SRS can be divided in:

- To perform structural analysis: input SRS, output response of the system
- To perform a shock synthesis: elaboration time history for testing

Some useful relationship involved with the calculus of SRS are presented below

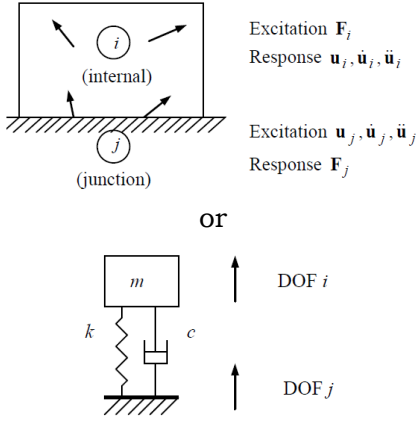


Figure 30: Simplified 1 DoF models [Ref.14]

$$\begin{Bmatrix} \ddot{u}_i(\omega) \\ F_j(\omega) \end{Bmatrix} = \begin{bmatrix} -\omega^2 G_{ii}(\omega) & T_{ij}(\omega) \\ -T_{ij}(\omega) & M_{jj}(\omega) \end{bmatrix} \begin{Bmatrix} F_i(\omega) \\ \ddot{u}_j(\omega) \end{Bmatrix}$$

$$G_{ii}(\omega) = H_k(\omega) \frac{1}{k}$$

$$T_{ij}(\omega) = T_{ji}(\omega) = T_k(\omega):$$

$$M_{jj}(\omega) = T_k(\omega)m$$

$$H(\omega) = H\left(\frac{\omega}{\omega_k}\right) = \frac{1}{1 - \left(\frac{\omega}{\omega_k}\right)^2 + i2\zeta_k \frac{\omega}{\omega_k}}$$

$$Tr_k(\omega) = Tr_k\left(\frac{\omega}{\omega_k}\right) = \frac{1 + i2\zeta_k \frac{\omega}{\omega_k}}{1 - \left(\frac{\omega}{\omega_k}\right)^2 + i2\zeta_k \frac{\omega}{\omega_k}}$$

$$h_k(t) = \omega_k e^{-\zeta_k \omega_k t} \frac{1}{\sqrt{1 - \zeta_k^2}} \sin\left(\omega_k \sqrt{1 - \zeta_k^2} t\right)$$

$$t_k(t) = \frac{-\ddot{h}_k(t)}{\omega_k^2}$$

The system (5.17)

Dynamic flexibility
(displacement/force) (5.18)

Dynamic
transmissibility for
forces and
displacements (5.19)

Dynamic
mass (5.20)

Dynamic
amplification (5.21)

Dynamic
transmissibility (5.22)

Inverse Dynamic
amplification (5.23)

Inverse Dynamic
transmissibility (5.24)

After SRS has been introduced, another basic and useful concept is the “Sine equivalent dynamic”. This idea concerned test, and the capability of the used tool. In fact, the use of equivalence in order to perform an adequate simulation of the operational service.

In this framework a relevant significance is assumed by low frequency transient load defined in time domain and harmonic excitation in frequency domain. This represent the so-called “Sine equivalent level” (ESL) or “Equivalent sinusoidal input” (ESI).

Particularly, this idea allows an equivalent way able to simulate flight loads cannot be easily simulated on the electro-dynamic shaker. Indeed, using ESI or ESL technicians are able to setup and perform an adequate vibrational shaker test reducing the sine input despite the aims are preserved.

In order to better understand the Equivalent sine input and the relationship between ESI and SRS, let consider a SDOF system having natural frequency f_k (e.g. 10 Hz) and being excited at the base with a transient acceleration $\ddot{u}(t)$.

How is well prescribed by “ECSS-E-HB-32-26A Spacecraft mechanical loads analysis handbook”: “The equivalent sine input $ESI(f^*)$ at a generic frequency f^* , of $\ddot{u}(t)$, can be defined as the amplitude of the sinusoidal acceleration at the base, with an excitation frequency equal to f^* , which makes the SDOF system with natural frequency $f_k = f^*$ reach, at steady-state condition, the acceleration amplitude $SRS(f^*)$ which is the shock response spectrum of $\ddot{u}(t)$ at the frequency f^* . The value $SRS(f^*)$ is, by its definition, equal to the maximum that would be reached by applying $\ddot{u}(t)$ at the base of the SDOF system”.

From a mathematical point of view ESI is defined as

$$ESI(f^*) = \frac{SRS(f^*)}{Q} \quad \text{Low damping ratios} \quad (5.25)$$

$$ESI(f^*) = \frac{SRS(f^*)}{\sqrt{Q^2 + 1}} \quad \text{High damping ratios} \quad (5.26)$$

Figure 31 gives a practical illustration about ESI level

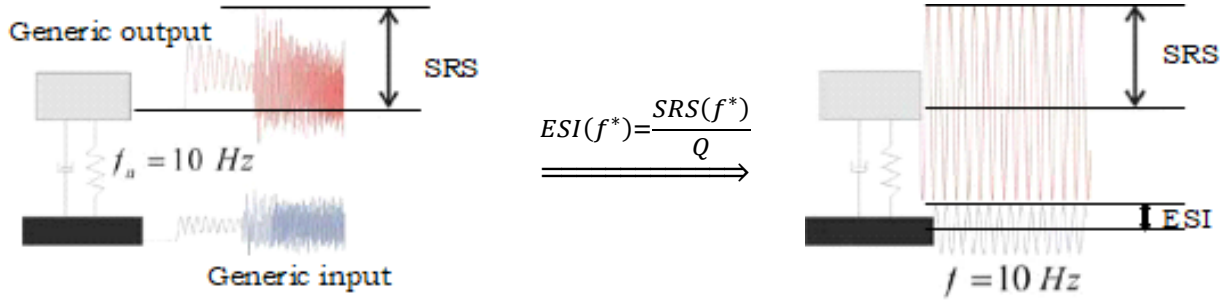


Figure 31: Brief scheme of ESI definition [Ref.9]

In this way, we are able to define the ESI level for each frequency involved when damping ratio or quality factor “Q” are known or assumed a priori for all real SDoF or modal SDoFs. A qualitative result is shown in Figure 31 and Figure 32.

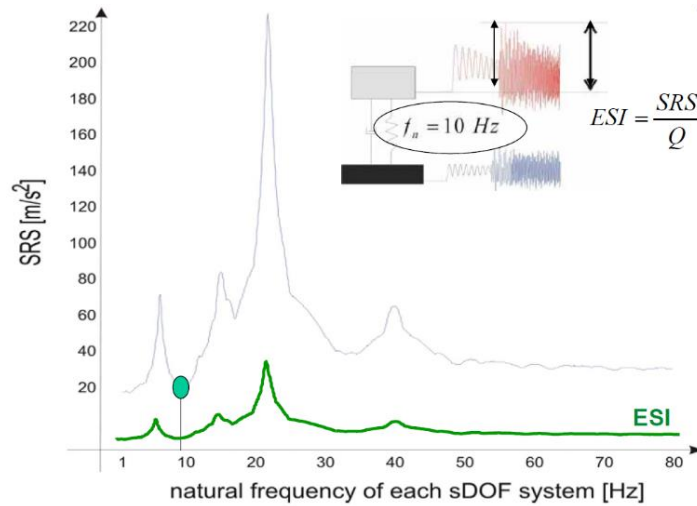


Figure 32: Comparison between ESI and SRS curves [Ref.9]

Observing the curves shown in Figure 32, ESI and SRS looks like similar. In fact, the value or “Q” behaves as shatter facto for each SDoF.

How introduced before, ESI represent the needed value to use during test in order to be representative of a given environment (sinusoidal, low frequency random, low frequency

acoustic, etc..). However, at the same time, ESI is the minimum requested input necessary to perform a test, in this case shaker test.

Despite the definition of ESI from SRS is a useful tool, particularly during CLA simulations with enforced accelerations, it has different inconsistencies, as:

- CLA-ESI-SRS is a rigorous approach only for SDoF systems. Their use for MDoF introduce a large approximation. In fact, if MDoF is subjected to an enforced ESI level, the steady-state vibration maximum accelerations reached are different from the ones reached by enforcing the base with the transient acceleration and, above all, also the internal forces are different
- The sweep rate could disturb the equivalence between transient time history and ESI level, in terms of structural response. Using a sweep rate, is usually difficult to reach a steady state input
- From a theoretical point of view, the comparison between ESI and the specified sine vibration level is inconsistent because the latter is a Fourier spectrum on the contrary of ESI spectrum.

Chapter 6: Sine testing for S/Cs

Testing procedures are the unique ways in which engineers could understand the real responses that occur during the simulated flight conditions or during the qualification campaign, afterwards all the deep conducted analysis. In addition, the aim of a test is to confirm or deny the provisions proposed by a mathematical model and the analytical assumptions.

Indeed, how is well known, in aerospace field tests are divided in two main categories: qualification tests and acceptance test.

The first one, is conducted at the “design limit loads” and used in order to prove that the structure can withstand the “qualification loads”. Vice versa, acceptance tests are carried out at the “flight limit loads” and it is executed in order to analyse the effects of production deviation not discovered during the inspections.

For an appropriate overview, Table 18 gives a brief description of the commonly mechanical test

Test	Description
Static test	The aim is to verify the strength and stiffness requirements of the primary structure and critical structural interfaces
Modal survey	The aim is to verify the dynamic requirements in terms of modal characteristic as natural frequencies and mode shapes. Usually performed with small exciters or shaker
Shaker vibration sine test	The aim is to verify and qualify the adequacy of the secondary structure when subjected to a dynamic environment
Shaker vibration random test	Support the verification of the S/C units subjected to a random dynamic environment.
Shock test	Support the verification and qualification of the S/C structure and instruments when they are subjected to a shock environment
Acoustic test	Support the verification of the S/C against the specified acoustic loads under the fairing

Table 18: Mechanical test usually performed

In this framework assumes a particular importance the sine vibration test. It shall simulate the low frequency sinusoidal dynamic loads, as introduced in “Chapter 5: Sine vibration”.

In fact, the common range of frequency involved in this procedure is usually included between 0 and 100 Hz.

Typically, this kind of test is performed on a electrodynamic shaker and carried out in three spatial direction separately with swept sine vibration. During the test the technicians compare the curves deriving from FE analysis and those coming from the vibration test. Obviously, according to the aim of the test (qualification or acceptance) how is shown in Table 17 just for example.

The main goals and objectives of the sine vibration test are:

- To demonstrate that the spacecraft structure (including flexible appendages) can withstand the low frequency dynamic environment (qualification or acceptance loads) without failure or structural degradation
- To characterise the spacecraft dynamic behaviour (resonance search) in order to validate the spacecraft dynamic model used for CLA
- To confirm the equipment level mechanical environmental specifications
- Prediction of the global integrity of the spacecraft when exposed to sine vibration, prediction of the loads at the spacecraft/launcher I/F, prediction of the sine load specifications for payload and equipment
- Notch assessment identification of areas for potential notching

One of the most critical factors during sine vibration test compared to FE frequency response analysis are the boundary conditions. In fact, the main used BC during a vibration test, and the analogous simulation, are represented by “*hard mounted*” in which 6 DoF are constrained, or “*simply supported*” in which 3 translational DoFs are constrained. Such BC represent a sort of criticalities when differences exists between the real conditions of interface S/C- LV, S/C-shaker and FE model. Particularly, this kind of differences appear in terms of natural frequency and mode shapes.

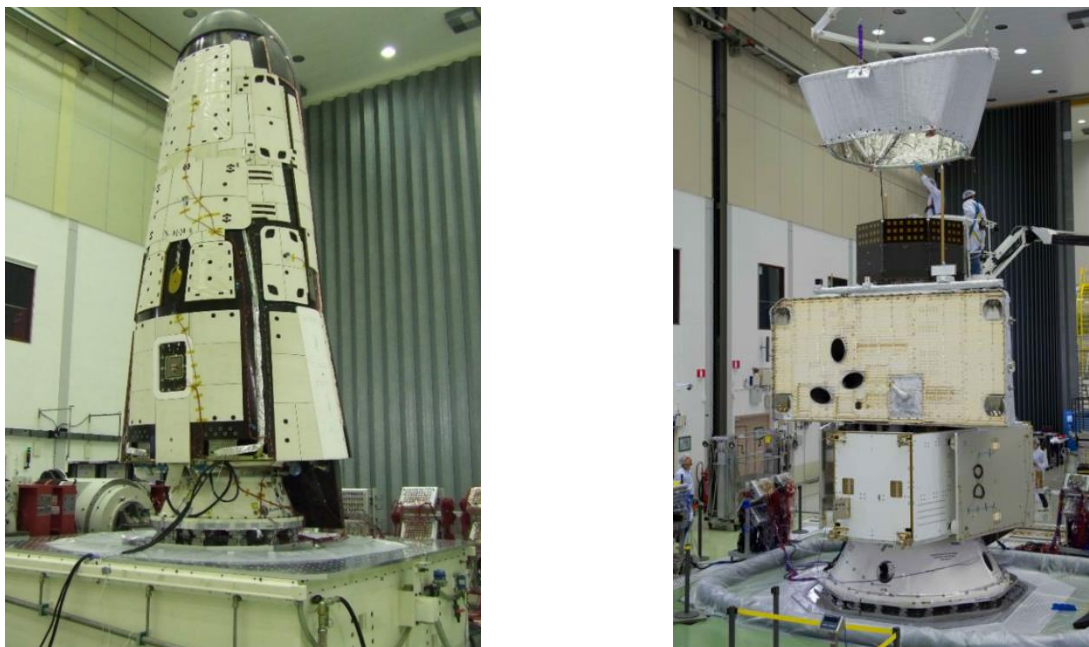


Figure 33: IXV (left) and Bepi Colombo (right) on shaker [Curtesy of ESA]

6.1 Test preparation: configuration and sequence

Before carry out of a sine test some general guide lines and procedures must be clear, in order to:

- Anticipate and avoid possible difficulties during test
- Improve the performance thanks to enhanced predictions
- To have a best test input with to the test objectives

Futhermore, despite the best choice is to test the S/C in launch configuration, sometimes, for different reasons (technical or programmatics) is not possible. In this case is necessary to accept some discrepancy compared to the ideal configuration and the actually prosecutable.

The effects of these discepancies should be verified.

In addition, two different philosophie are available: Structural model (SM) or Flight model (FM or PFM). How is known, the choice of one of them impose different levels of results achivables. In fact, SM should be flight representative and in this case equipment and instruments units might be replaced by mass dummies. On the contrary, FM or PFM should be tested in a fully integrated and flight- representative configuration.

According to the sequence of the test, usually it consist for each axis in (from Ref.14: ECSS-E-HB-32-26A Spacecraft mechanical loads analysis handbook) :

- Low level run (resonance search): during this taks, the aims are the identification of the resonance frequencies and comparison with FEM analysis, estimation of Q-factors and damping factors associated to the main modes, verify the structural integrity and enstablish firs notch prediction
- Intermediate level run: it allows to adjust the initial evaluations
- Full level run (qualification or acceptance level): it permit the demonstration that the test objectives have been achieved with respect to structure qualification or acceptance and identify the dynamic characteristics at flight-representative load levels in case of significant structural nonlinearities
- Low level run: resonance search for purpose of structural integrity check
- Following activities: random vibration test, functional test, visual inspection

6.2 Primary and secondary notching during sine vibration test

During a sine vibration test is a common practice to test the S/C with representative masses attached to the primary and secondary structure, or with the real and representative configuration.

When the frequency of the swept sine vawe reaches the natural frequencies of the S/C mounted on the shaker the response, in terms of global/local accelerations, moments and foces increases sligthly.

This is the reason why, during the sine vibration test is applied the notching criterion. Actually, it is valid in vibro-acoustic and random vibration tests too, but in this case, the discussion is focused on sine vibration.

In general, notching is the reduction of acceleration input levels around resonant frequencies, to avoid over testing.

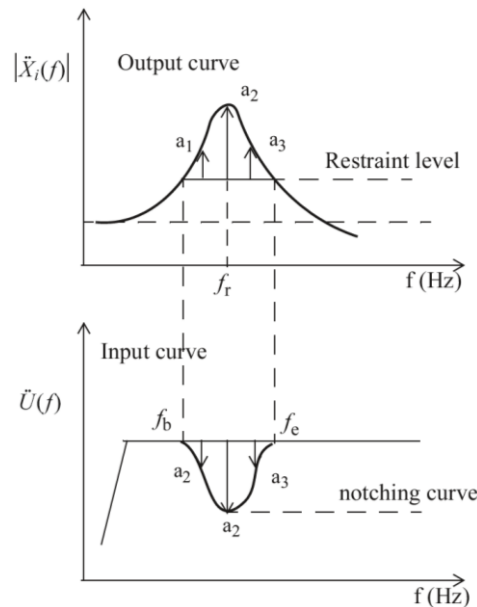


Figure 34: Representation of a notched profile [Ref.12]

In fact, how Figure 34 shows, after the brief part of the input curve (on the bottom) in which it increases, itself remain constant in amplitude for the considered frequency range. In this case the frequency response has a peak. Particularly, if its value is greater than a certain threshold during the test, is necessary to reduce the input magnitude of the swept sine wave in order to preserve the integrity of the mechanical interfaces between the IUT-slip table or the inner components of the S/C.

For this reason, during the test, when the input frequency is close among the natural frequency of the IUT and its output become greater than a certain level the “notching curve” shown in Figure 342 is followed in order to reduce the output and avoid the overtest.

From a theoretical point of view, nothing can be distinguished in (from Ref.14 and Ref 37):

- Primary notching
- Secondary notching

The first one, “primary notching” is performed to limit the shaker-test specimen interface forces and moments to the target values, normally qualification or acceptance loads. This is basically the same as to limit the equivalent accelerations to the centre of gravity of the test item.

Usually, is (or “may be”) allowed.

The latter, “secondary notching” performed to limit local accelerations with the purpose of protecting equipment, instruments or sub-systems. In these terms, it is related to level reduction on critical areas inside the spacecraft.

Generally, is not allowed and shall be approved by the customer.

Moreover, in sine testing, primary notching is justified by the fact that the real lunch environment has a transient nature and it is simulated on a shaker by a sine sweep.

These potential level reductions are due to high test item dynamic mass at the interface which reduces the effect of the exciting forces. This dynamic mass is generated by eigenmodes with high effective masses with respect to the interface. However, in general, the

application of notching (primary or secondary) on the input spectrum shall not jeopardize the aim of the test.

Generally, during a vibration test, different approaches are applicable to primary/secondary notching. They are based on the loads acquisition (e.g. forces and moments) at the interface between L/V and S/C.

In this context we are interested on (Ref.14 ECSS-E-HB-32-26A):

- Accelerations: this approach is applicable only if the F.E.M is sufficiently accurate in order to simulate and anticipate the dynamic behaviour of the IUT. In this case the accelerations of certain points are acquired and is necessary to relate these accelerations with the forces and moments interface.
- Force Measurement Devices (FMD): it measures the loads at interface between S/C and shaker during the vibration test. Is a direct measure of the force and moment.

Part III

Application to a Spacecraft

Chapter 7: The issue of the coupling between shaker and test-item

Sine tests is a critical milestone during the S/C design and validation. Its aim is to qualify the IUT with respect to the low frequency launch environment in order to demonstrate the compliance. In addition, it confirms or deny the FE analysis as Frequency Response Analysis (FRA, SOL 111) and modal analysis (SOL 103).

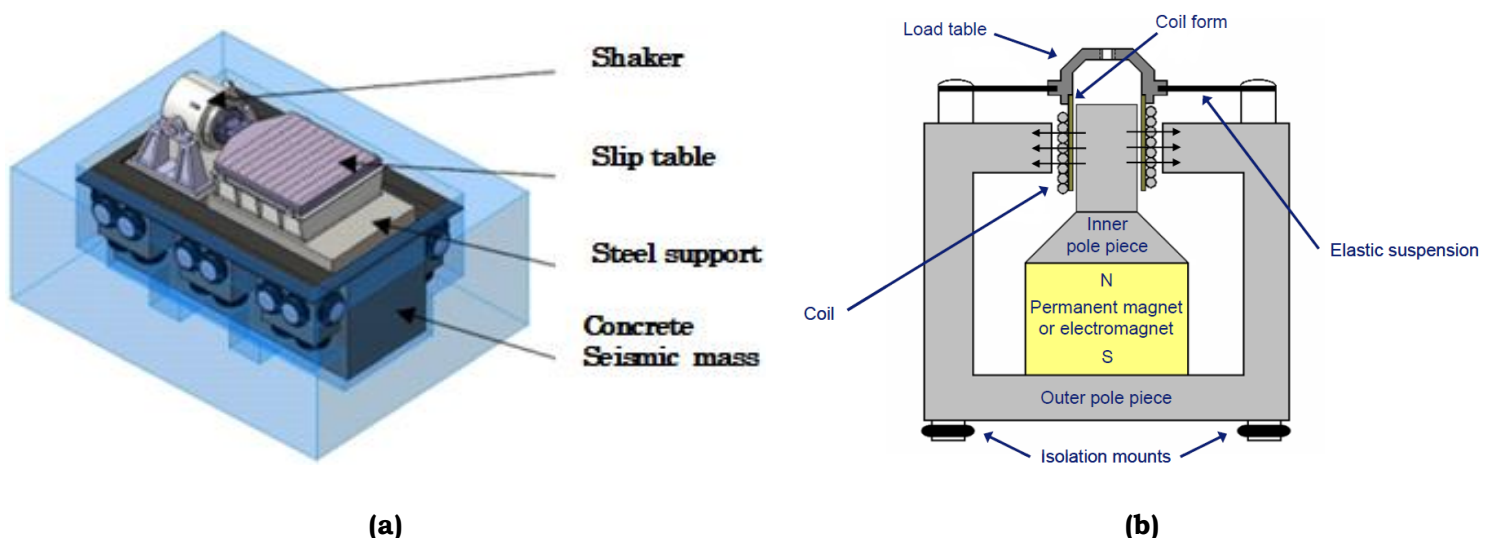
In fact, how introduced in paragraph 6.1, when the IUT is mounted on top of the slip table it is usually constrained as “hard mounted” and the adopted procedure consist in different passages in order to describe the dynamic of the analysed object and validate that the system is able to withstand to the dynamic environment. In addition, using this procedure, is possible to identify the issues coming from machining process.

However, when the test is finished, and the FE/test results are compared, they are different between them. These discrepancies are assigned, from many authors, to:

- Sine sweep excitation and characteristics of the excitation generated by vibration control
- Influence of notching
- Mechanical (elastic) and dynamic coupling between shaker and IUT
- Presence of possible nonlinearities

In this context, possible nonlinearities are neglected because space structure are designed for to be considered as linear.

These discrepancies resulting after the comparison between the analytical and experimental results could induce direct effect on the identification of modal parameters as natural frequencies, modal shapes, effective masses or modal damping.



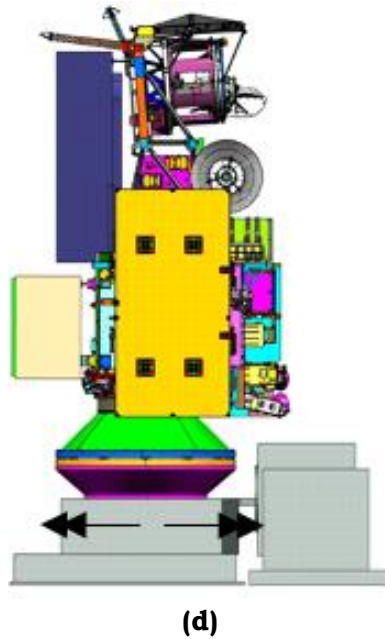


Figure 35: Views of the shaker facility, (a)-(b) describes the keys elements involved, (d) shows a hypothetical IUT mounted on top of the slip table [Ref.36, Ref. 8]

In order to have a better comprehension about the effects of the coupling between shaker and IUT, a brief description of the vibration system is provided. Figure 35 shows the architecture of this device.

Firstly, it is well constrained on ground with “steel supports” in order to avoid rigid body motions. They are mounted on top of a “seismic mass” with which reduce and isolate the vibrations.

The heart of the system is provided by a coil, floating on a radial magnetic field produced by a permanent magnet or an electromagnet. In addition, the axial acting force, tanks to which is possible to carry out a sine test, pass through the coil and guarantee the movement of the slip table.

In this way, the IUT is mounted on top of the slip table with an appropriate head expander/adapter. In this framework assumes important relevance the boundary conditions introduced in the previous chapters.

7.1 Sine sweep excitation

Swept sine input differs from a frequency response analysis, useful tool during the S/C verification and design, because it does not satisfy the steady state requirement involved during the calculation of the frequency response (displacement, velocity or acceleration).

In fact, FRA supposed that the analysis is conducted at a given frequency value using a sine wave input with fixed amplitude and frequency. The value contained into frequency response is that corresponds at the response in time domain when the steady state condition is reached (for the considered value of frequency). The full FRA is achieved when the introduced procedure is conducted for all the frequency involved into the considered spectrum.

On the contrary, how introduced in “Chapter 5: Sine vibration”, swept sine input is governed by the “exponential rule” expressed in “Equation (5.4)”. In this case the steady state requirement is not satisfy because every minute the frequency vary with the octave rule. In this case, just one sine wave input is involved.

Particularly, these discrepancies produce several effects in the dynamic response between the theoretical/analytical and the experimental.

7.1.1 The effect of sweep rate

The first cause of discrepancies from FRA to swept sine vibration is the effect of the sweep rate. In fact, how introduced before the difference between steady state conditions and transient environment produce a transient behaviour, how is shown in Figure 364.

In this case a SDoF is analysed, but the essay is general.

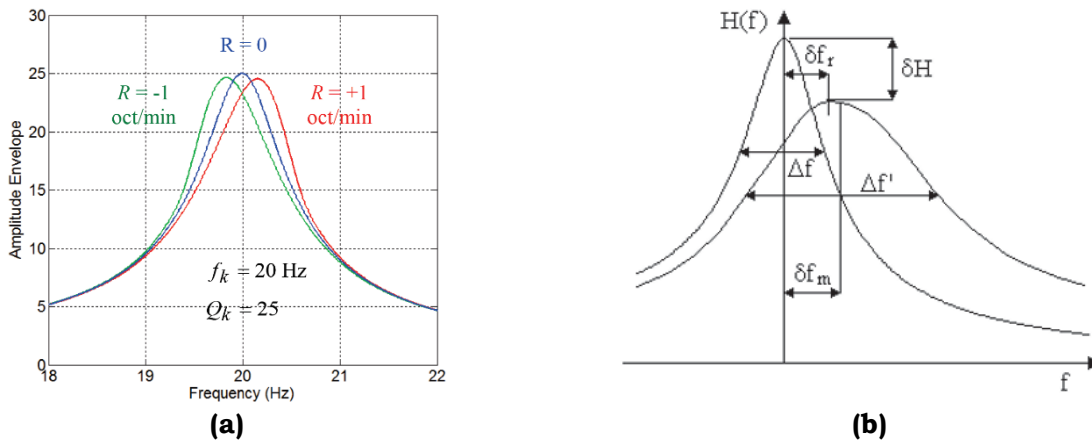


Figure 36: Peak shift caused by the sweep rate [Ref. 4]

Particularly, “ $R=0$ ” means the FRA output, “ $R=\pm 1$ ” means sweep rate up and down.

As can be seen, compared with the steady state conditions, the peak shift it self in the same direction of the sweep rate (i.e. if $R>0$ the peak moves towards right and vice versa).

In addition, the peak of the response decreases its magnitude in terms of “ Q ”, quality factor, and reduces its sharpness because a fictitious value of damping ratio appears.

Moreover, equation (7.1) provided by Lalanne, offers a useful model, for exponential sweep, thanks to which quantify the amount of deviation from steady state response.

$$\eta = \frac{Q^2 R \ln(2)}{60 f_k} \quad (7.1)$$

Particularly, if $\eta \simeq 0.1$ the swept response is close to the steady state. Else, if η grows it deviates from theoretical condition.

In fact, observing the considered equation, it depends with a direct proportionality to the sweep rate “ R ”, and inverse proportionality to the natural frequency and the square of the damping ratio being $Q = 1/(2\zeta)$. This suggest that if the damping ratio is low the low frequency modes are greatly influenced for a given sweep rate.

7.1.2 Beating phenomena

Beating phenomena represent one of the most common issues during vibration test, caused, particularly, by the effect of sweep rate introduced in the previous subparagraph. These problems appear around the main resonant frequency. Indeed, it is a transient phenomenon caused by the un-steady state condition typical during the swept sine wave imposed at the base of IUT. In addition, these un-steady conditions produce a severe perturbation of the FRA analysis (steady state analysis).

Moreover, is possible to divide them in three different classes:

- Beating from two close frequency oscillations
- Beating from transient excitation with frequency content close to a resonant frequency
- Beating due to sine sweep rate

Firstly, according to “Beating from two close frequency oscillations” they are modelled in a simplified way using two sinusoidal excitations of unitary amplitude.

That is, the structure undergoes vibrations of frequency equal to the half of the frequencies sum, which are modulated by a function having frequency equal to the half of the frequency difference.

$$\sin(2\pi f_1 t) + \sin(2\pi f_2 t) = 2 \cos[\pi(f_1 - f_2)t] \sin[\pi(f_1 + f_2)t] \quad (7.1)$$

Where f_i is the i-th frequency and “t” is the time.

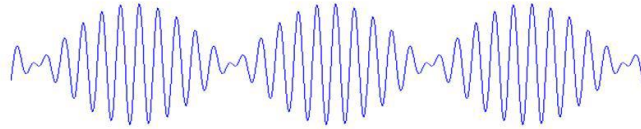


Figure 37: Beating from the superposition of two frequency sinusoidal excitations [Ref. 4]

However, this type of phenomenon rarely appears during vibration test.

Secondly, “Beating from transient excitation with frequency content close to a resonant frequency” is analysed considering different levels of damping ratio and frequency input at given natural frequency.

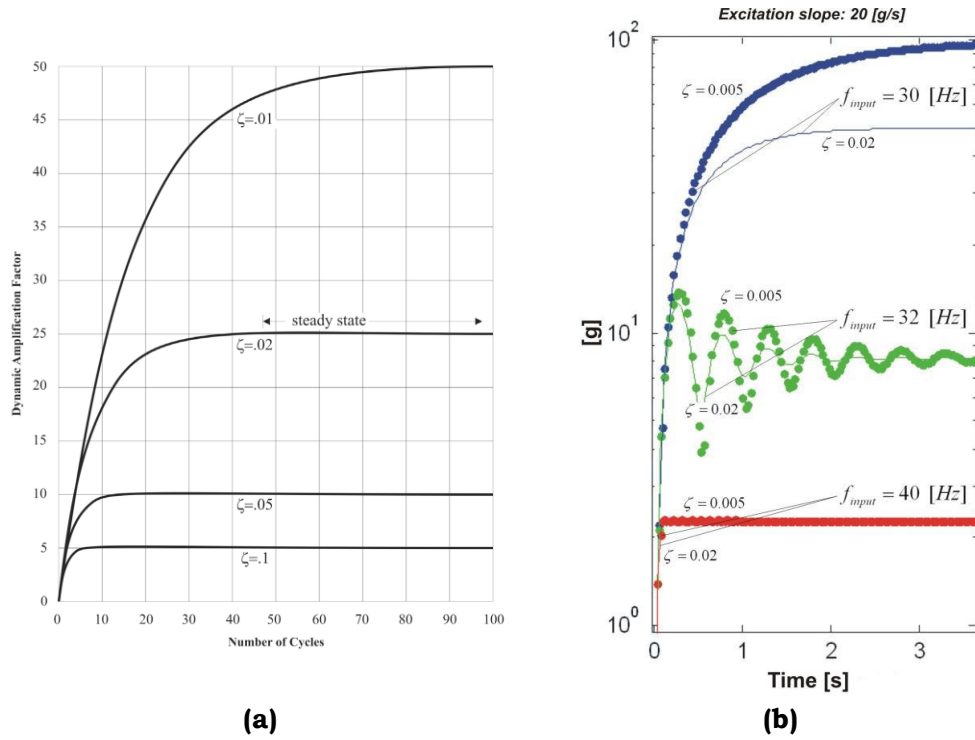


Figure 38: Dynamic amplification factor at different damping ratio (a), Response at various damping and input levels (b) [Ref. 4]

Particularly, structure with low damping ratio stressed by a sinusoidal input with frequency content close to that of the natural frequency reach the steady state conditions when the amplitude is constant. Being beating phenomenon is transient and it appear before the steady state and around the initial phase.

Lastly, about “Beating due to sine sweep rate”, Figure 39 and Figure 40 show the typical differences between the effect of the sweep rate, in terms of sweep up and sweep down, with the influence of damping ratio considering the natural frequency coming from FRA about 30 Hz. The ratio \ddot{U}/\ddot{Z} in y-axis is the transmissibility (input- output are accelerations).

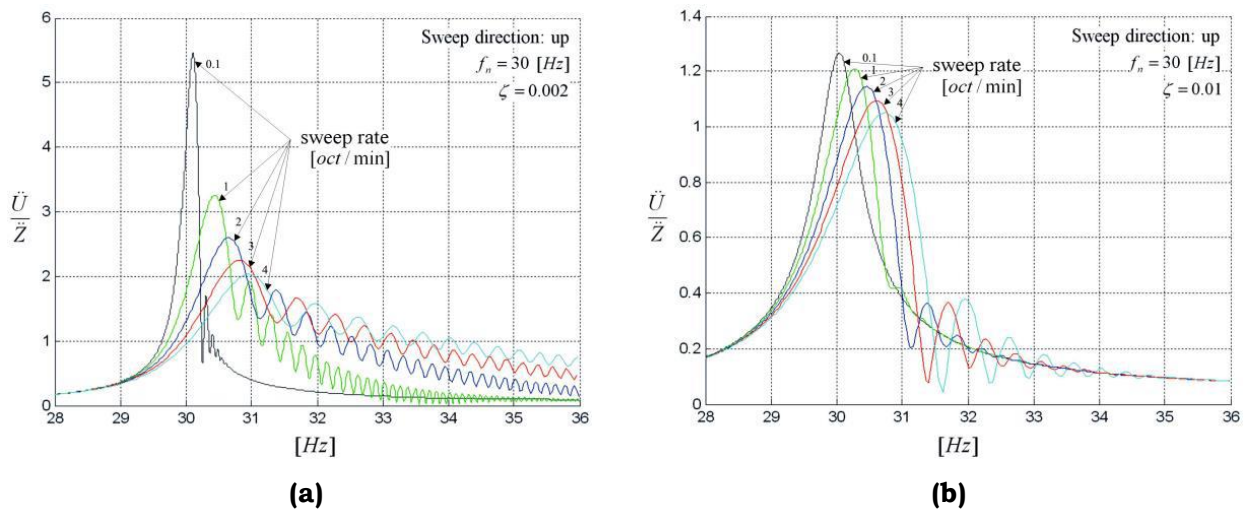
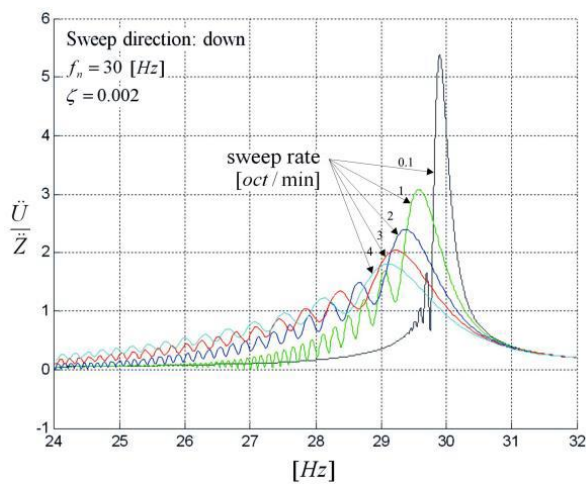
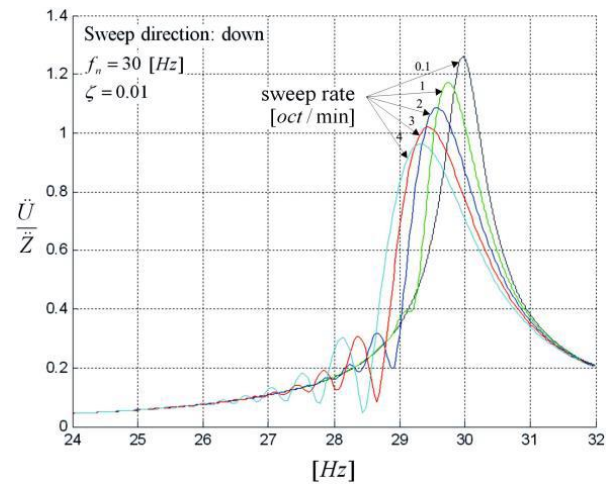


Figure 39: The effect of sweep rate (up) and damping [Ref. 4]



(c)



(d)

Figure 40: The effect of sweep rate (down) and damping [Ref. 4]

How is possible to see, comparing (a) and (b), a positive and increasing sweep rate produce a positive shift of the frequency at which the peak is reached with a lower value among the natural one coming from FRA. Vice versa, (c) and (d) show the same phenomena with a negative rate of sweep.

However, the main particularity concerned the pattern oscillation after the peak value. They are the beating or the so called “ringing”.

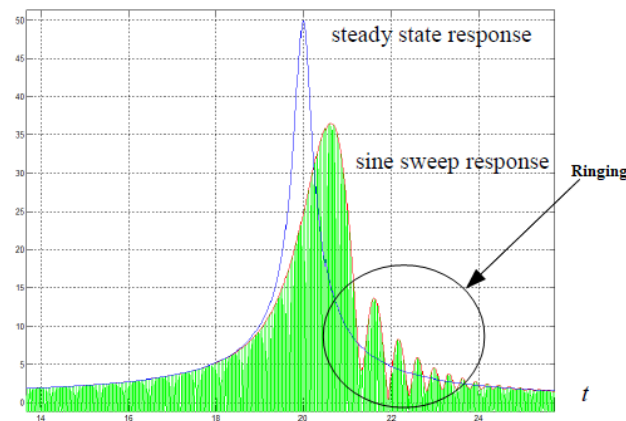


Figure 41: Ringing after the peak [Ref. 4]

This ringing is a result of the system responding at two frequencies of nearly the same value comprising the transient response at the natural frequency and the harmonic response at the swept excitation frequency.

To sum up, the most important remarks concerning the sine sweep excitation:

- i. It produces the peak shifting in terms of magnitude, sharpness and frequency at which the peak is reached
- ii. Beating phenomena affect the swept sine response, caused by the interference between the peak at the natural frequency and the transient response caused by the excitation
- iii. These two effects show a direct proportionality to the sweep rate “R”, and inverse proportionality to the natural frequency and the square of the damping ratio.

7.2 Mechanical and dynamic coupling between shaker and IUT

One of the most challenging issues is represented by the “cross-talks”. It represents the consequence of the mechanical coupling between both of them and, particularly, is the response along the direction i -th during the vibration test is performed along the direction j -th.

Usually, this phenomenology depends on the type of the vibration test: longitudinal or lateral test.

In fact, during these two configurations, the shaker is oriented differently, the “cross-talks” happens anyway but is due to different causes.

For a lateral vibration test the main cause comes from the dynamic coupling between the shaker assembly, the IUT and, above all, the seismic mass. It has its natural frequencies and during the swept sine it is excited.

On the contrary, during the longitudinal vibration test the “cross-talks” are caused by offsets between the CoG and the axis along the vibration is imposed. That induce bending on top of the slip.

In addition to “cross-talks”, also other coupling phenomena exist: “saddle”, “bending” and “rockling” modes. They are mainly caused by the seismic mass that interacts with the IUT during the sine sweep.

Chapter 8: The Virtual Shaker Testing

approach (VST)

Virtual shaker testing is a novel and innovative approach thanks to is possible to predict the dynamic behaviour affecting an IUT. It allows to anticipate possible criticalities during vibration test considering the dynamic coupling between the shaker and the object of the analysis. Since from the first VST made by Mr. Appolloni and Mr. Cozzani (2007) the potentiality of this procedure was evident.

It consists in a dynamic real time simulation of the condition during the test, modelling the IUT and the shaker together. In the other words, we are modelling the boundary conditions (B.C). In fact, a simple analysis with clamped edge, or hard mounted, is not sufficient because we are forgetting the elasticity of the head of the shaker that is capable to deform itself too. The interaction between those systems produces differences among the expected by FE frequency response and transient analysis compared with the extracted results.

Moreover, VST is an appropriate procedure thanks to which is possible to eliminate a huge number of problems during the vibration test, as the test abort, suggesting the appropriate values of the relevant parameters and operating procedure/ sequence to follow during the test. In fact, it has been an important topic during the ECCSMET 2016 and 2018 in which the progress and the future trends were shown.

Obviously, VST is a simulation of a ground test, and capable to demonstrate the overall structural integrity under a precise load case as is sine sweep.

Classically, using FE method a sine sweep simulation should run in order to predict the response of the item and the coupling with the platform.

In this way, reconstructing the typical curves as FRFs or time domain response, is easy to recognize the reaction of different degrees of freedom in terms of over accelerations or displacements. Hence, if a structure is subjected of over acceleration or over displacement it risks to be *overtested*. This can cause unwelcome ruptures or damages to the structure. This is a prelude of an important criterion, the “notching” criterion.

In this framework, a new procedure, based on the simulation of the control system (HIL) coupled with FE model of the IUT and the shaker, is developed. This procedure allows a very close analysis of the dynamic phenomena, identifying the response of all degrees of freedom and gathering if one or more of them are overtested. In this case, the control system reacts modulating in amplitude the sine forcing function at the base of the S/C.

Using this procedure test engineers are capable to perform an excellent test setup from which to lead and extrapolate consistent results avoiding any damage due to overtesting and reducing the margin of safety (MoS).

At the same time, one of the main reasons why to perform a VST is the possibility to save time and costs related to the use of the test facility.

In addition, a better knowledge about the response of the IUT coupled with the shaker allows a precise satisfaction of the launcher frequency requirements when related criticalities appear.

Furthermore, it has an economic consequence represented by the cost saving of the facility and time saving of the operations.

Many research works in this context of VST are focused on post-correlation, but the real power of this topic is the possibility of its application to pre-correlation. It means a real prevision of the execution of vibration test.

In the following sections and chapters the discussion will be addressed firstly analysing some reduced analytical models, and secondly applying the basic concept to a real case of study. In this context, is typical to divide the “DoFs” based on their application. The difference between “pilots” and “notchers” is given in Table 19.

<u>Pilots</u>	<u>Notchers</u>
<p>Accelerometers/degrees of freedom applied to the slip table of the shaker head. They are particularly useful for the monitoring of its dynamic during the vibration test.</p> <p>If the response of the pilots is different among a certain fixed value, probably a coupling is taking place between shaker and IUT</p>	<p>Accelerometers/degrees of freedom representing different point of the IUT. The monitoring response is that of the analysed structure</p>

Table 19: Difference between pilots and notchers

At the same time, Figure 42 gives an idea about the collocation of notchers and pilots on top of a shaker and the structure.

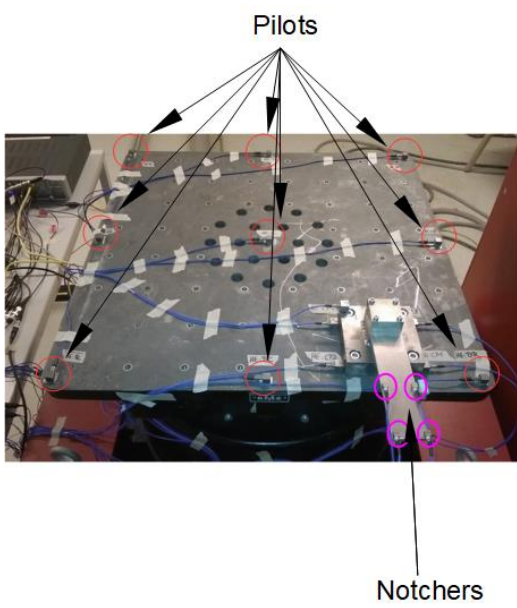


Figure 42: Example of collocation of pilots and notchers on a platform [Ref.26]

As introduced before, classically the VST was performed using the modal analysis and the frequency response analysis of the assembly composed by the shaker and the IUT. Particularly, the first step was the separated study of each system thanks to which their properties were stored. The second was the coupling between them and the same analysis were performed. In this term, the modal analysis and the frequency response analysis were used in order to anticipate the dynamic behaviour of the complete system during the test.

Figure 43 (work of Mr. Aglietti) explain in a simply way the concept of couplign between the shaker and IUT.

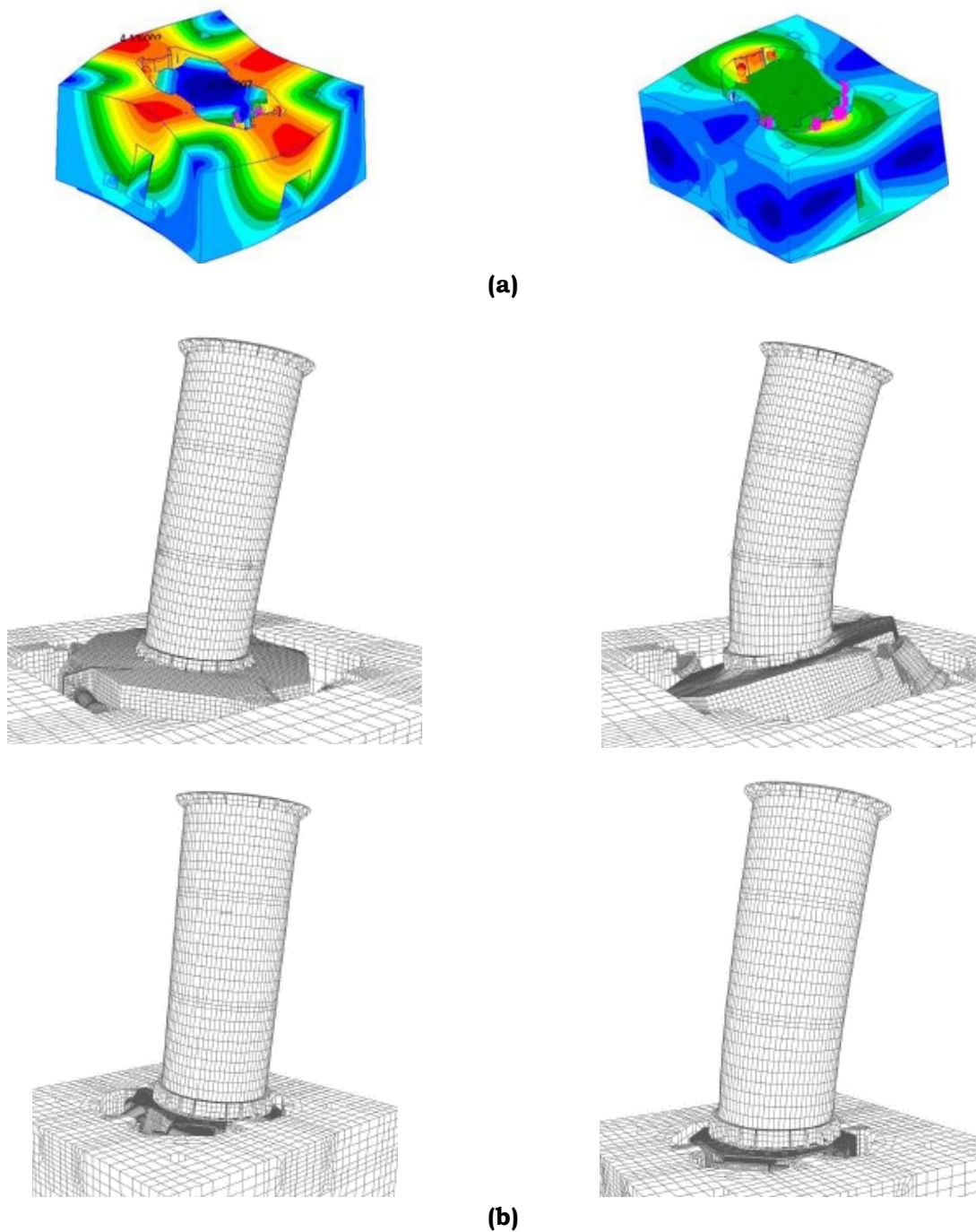


Figure 43: VST based on modal analysis [Ref. 27, 26] saddle, bending and rockling modes

In fact, how is shown, the assembly composed by the two systems has its natural frequencies, related mode shapes, effective masses and in general its dynamic properties.

In this term, when the vibration test occurs and the swept sine run up against one, or more, natural frequencies of the new introduced assembly, the response of the IUT is obviously affected by the mechanical and dynamic coupling with the shaker.

However, up to now, the unique solution used in order to mitigate the coupling between them were to perform the vibration test, usually more than one during the campaign, was to modulate the parameter that affect the dynamic, but during the test.

Recently, a new procedure based on the implementation of the structural model (lumped model based on mass- spring- damper systems, or condensed model using a dynamic reduction) into a HIL closed loop system, is developed.

8.1 Electro-mechanical lumped analytical model of the shaker

In order to develop an analytical and simplified model, with which to examine and compare more in details following results, Figure 44 shows an example of the desired shaker.

In fact, VST does not requires a priori a particular complex model as can be FE model or reduced FE.

Particularly, this approach is used in order to approaching to the MatLab/ Simulink code and the global procedure

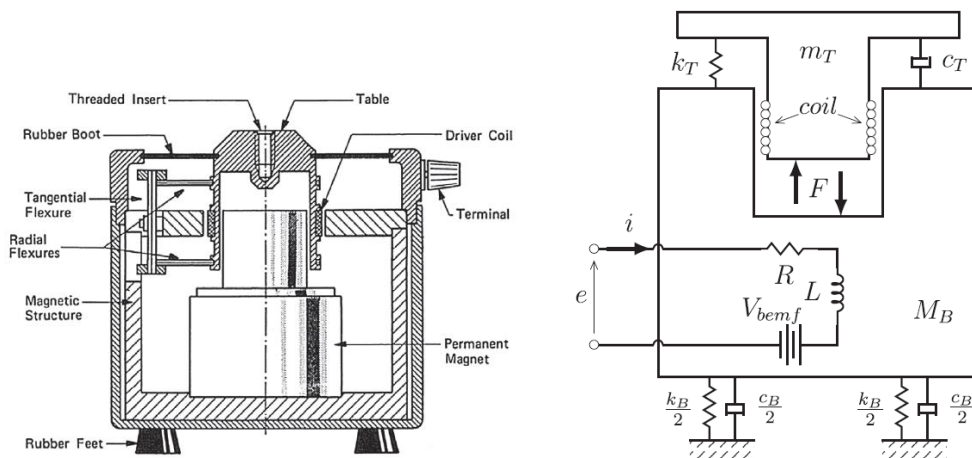


Figure 44: Cross section of the shaker (left), example of electromechanical model (right) [Ref.5]

How is well described in “Chapter 7: ”, the main components of an electrodynamic shaker are:

- Rubber feet;
- Permanent magnet;
- Coil;
- Table;
- Rubber boot.

Particularly, a 4 DoFs has been considered. In fact, an appropriate modelling is represented by 3 mechanical vertical DoFs and 1 electrical DoF, at least.

In this way, is possible to appreciate the response of the 3 mechanical DoFs, in terms of displacements, speeds and accelerations, during the variation of the voltage.

Some equations,

3 Mechanical
Equations

$$m_i \ddot{x}_i + d_i \dot{x}_i + k_i x_i = F_i \quad (8.1)$$

1 Electrical
Equation

$$e(t) = Ri(t) + L \frac{di(t)}{dt} + V_{bemf}(t) \quad (8.2)$$

In which $F = Blni = \mu_F i$ and $V_{bemf} = \mu_F (v_T - v_B)$ is the back electromotive force induced by the velocity of the coil in the magnetic field. Together are the expression of Lorentz's law.

Practically, the electrical equation generates the source, in terms of applied force, that allows the coil motion.

Moreover, the relationship between the electrical and mechanical domains is not a “one-way street.” In fact, When the coil moves within the magnetic field, a voltage is generated across the coil in proportion to the velocity.

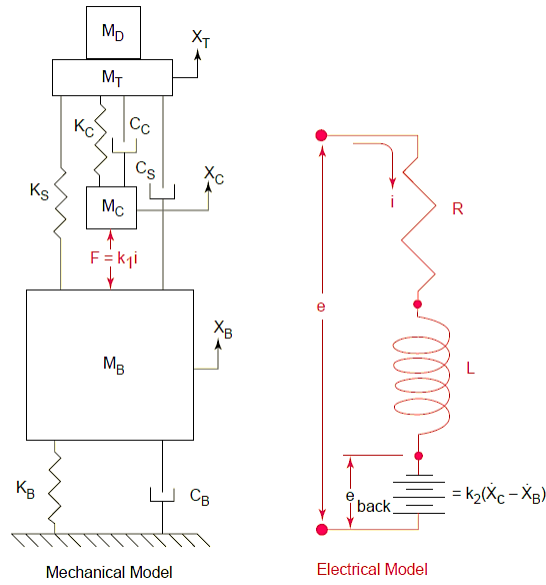


Figure 45: The implemented electro-mechanical model [Ref.33]

Observing the equation (8.1). the external force is composed by the unknown “i”, the current. However, they will be pick up with the other unknowns.

Rewriting in matrix form, the mechanical equation of the analysed model, shown in Figure 45 appears as

$$\begin{bmatrix} m_t + m_{iut} & 0 & 0 \\ 0 & m_c & 0 \\ 0 & 0 & m_b \end{bmatrix} \begin{Bmatrix} \ddot{x}_t \\ \ddot{x}_c \\ \ddot{x}_b \end{Bmatrix} + \begin{bmatrix} d_c + d_s & -d_c & -d_s \\ -d_c & d_c & 0 \\ -d_s & 0 & d_b + d_s \end{bmatrix} \begin{Bmatrix} \dot{x}_t \\ \dot{x}_c \\ \dot{x}_b \end{Bmatrix} + \begin{bmatrix} k_c + k_s & -k_c & -k_s \\ -k_c & k_c & 0 \\ -k_s & 0 & k_b + k_s \end{bmatrix} \begin{Bmatrix} x_t \\ x_c \\ x_b \end{Bmatrix} = \begin{Bmatrix} 0 \\ \mu_F i \\ -\mu_F i \end{Bmatrix} \quad (8.3)$$

Introducing the electrical equation,

$$\begin{bmatrix} m_t + m_{iut} & 0 & 0 & 0 \\ 0 & m_c & 0 & 0 \\ 0 & 0 & m_b & 0 \\ 0 & 0 & 0 & 1 \end{bmatrix} \begin{Bmatrix} \ddot{x}_t \\ \ddot{x}_c \\ \ddot{x}_b \\ 0 \end{Bmatrix} + \begin{bmatrix} d_c + d_s & -d_c & -d_s & 0 \\ -d_c & d_c & 0 & 0 \\ -d_s & 0 & d_b + d_s & 0 \\ 0 & \mu_v & -\mu_v & L \end{bmatrix} \begin{Bmatrix} \dot{x}_t \\ \dot{x}_c \\ \dot{x}_b \\ \frac{di}{dt} \end{Bmatrix} + \begin{bmatrix} k_c + k_s & -k_c & -k_s & 0 \\ -k_c & k_c & 0 & -\mu_F \\ -k_s & 0 & k_b + k_s & \mu_F \\ 0 & 0 & 0 & R \end{bmatrix} \begin{Bmatrix} x_t \\ x_c \\ x_b \\ i \end{Bmatrix} = \begin{Bmatrix} 0 \\ 0 \\ 0 \\ e \end{Bmatrix} \quad (8.4)$$

Or in more compact form

$$\begin{bmatrix} [\mathbf{M}_{mech}] & 0 \\ 0 & 1 \end{bmatrix} \begin{Bmatrix} \{\ddot{x}\}_{mech} \\ 0 \end{Bmatrix} + \begin{bmatrix} [\mathbf{D}_{mech}] & 0 \\ 0 & 0 \end{bmatrix} \begin{Bmatrix} \{\dot{x}\}_{mech} \\ \frac{di}{dt} \end{Bmatrix} + \begin{bmatrix} [\mathbf{K}_{mech}] & 0 \\ 0 & 0 \end{bmatrix} \begin{Bmatrix} \{x\}_{mech} \\ i \end{Bmatrix} = \begin{Bmatrix} 0 \\ 0 \\ 0 \\ e \end{Bmatrix} \quad (8.6)$$

Then, calling $\{q\} = \begin{Bmatrix} \{x\}_{mech} \\ i \end{Bmatrix}$

$$[\mathbf{M}_{EM}]\{\ddot{q}\} + [\mathbf{D}_{EM}]\{\dot{q}\} + [\mathbf{K}_{EM}]\{q\} = \bar{\mathbf{F}} \quad (8.7)$$

In Table 20 the most relevant symbols, are recollected

Symbols	Description
m_b, d_b, k_b	Mass, damping and stiffness of the body of the shaker
m_t, m_{iut}	Mass of the table and IUT
m_c, d_c, k_c	Mass, damping and stiffness of the coil
d_s, k_s	Damping and stiffness of mechanical connection between shaker body and table (suspension)
R [Ω], L [H]	Resistance and inductance of the coil.
μ_v [V/(m/s)], μ_F [N/A]	Coupling constants (typically, with the same value)

Table 20: Adopted symbols

Then, the State- Space system is obtained using the standard nomenclature

$$\begin{aligned} \{\dot{x}\} &= [A]\{x\} + [B]\{u\} \\ \{y\} &= [C]\{x\} + [D]\{u\} \end{aligned} \quad (8.8)$$

Where

$$[A] = \begin{bmatrix} \begin{bmatrix} 0 & \dots & 0 \\ \vdots & \ddots & \vdots \\ 0 & \dots & 0 \end{bmatrix} & \begin{bmatrix} 1 & \dots & 0 \\ \vdots & \ddots & \vdots \\ 0 & \dots & 1 \end{bmatrix} \\ [M_{EM}]^{-1}[K_{EM}] & [M_{EM}]^{-1}[D_{EM}] \end{bmatrix} \quad (8.9)$$

$$[B] = \begin{bmatrix} \begin{bmatrix} 1 & \dots & 0 \\ \vdots & \ddots & \vdots \\ 0 & \dots & 1 \end{bmatrix} & \begin{bmatrix} 0 & \dots & 0 \\ \vdots & \ddots & \vdots \\ 0 & \dots & 0 \end{bmatrix} \\ \begin{bmatrix} 0 & \dots & 0 \\ \vdots & \ddots & \vdots \\ 0 & \dots & 0 \end{bmatrix} & [M_{EM}]^{-1} \end{bmatrix} \begin{Bmatrix} 0 \\ 0 \\ 0 \\ 0 \\ 0 \\ 0 \\ 1 \end{Bmatrix} \quad (8.10)$$

$$\{u\} = e \quad (8.11)$$

The remaining matrices depends on which I want to observe.

In this case, I suppose to observe the acceleration, so

$$\{y\} = \begin{Bmatrix} \ddot{x}_t \\ \ddot{x}_c \\ \ddot{x}_b \end{Bmatrix} \quad (8.12)$$

$$[C] = [[M_{mech}]^{-1}[K_{mech}] \quad [M_{mech}]^{-1}[D_{mech}]] \quad (8.13)$$

$$[D] = \begin{bmatrix} 0 & \dots & 0 \\ \vdots & \ddots & \vdots \\ 0 & \dots & 0 \end{bmatrix} \begin{Bmatrix} 0 \\ 0 \\ 0 \\ 0 \\ 0 \\ 0 \\ 1 \end{Bmatrix} \quad (8.14)$$

Obviously, in this case the damping values are supposed as known, but in general these quantities are difficult to impose. For this reason, is a common practice to propose the damping mechanical matrix as composed by “modal damping” in which the damping is assigned to the modes of the structure, or “proportional damping” in which the matrix is a linear combination of mass and stiffness whit appropriate coefficients.

$$[D_{mech}] = \begin{bmatrix} 2\zeta_1\omega_1 & 0 & \dots & 0 \\ 0 & 2\zeta_2\omega_2 & \dots & 0 \\ \vdots & \vdots & \ddots & \vdots \\ 0 & 0 & \dots & 2\zeta_n\omega_n \end{bmatrix} \quad (\text{modal damping}) \quad (8.15)$$

$$[D_{mech}] = \alpha[M_{mech}] + \beta[K_{mech}] \quad (\text{proportional damping}) \quad (8.16)$$

In this framework, the pilot was the assembly composed by the IUT and the table into eq. (8.3) and the notcher is the coil.

In these terms, during the virtual test when the frequency of the swept sine increases according to the sweep rule, if the acceleration level of the considered notcher exceeds its maximum

allowable, the control system reduces the magnitude of the input. Particularly, the input in this electro-mechanical model is a force able to impose an acceleration level to the pilot. However, from a control point of view, it has to reach and maintain a predefined acceleration level.

The following pictures, related with the introduced mathematical, model are extracted using the control system provided by Siemens and described in “Chapter 9: Description of Siemens LMS Vibration Control Routines in Simulink environment”.

Quantity	Value
m_t [kg]	4
m_{iut} [kg]	1
m_c [kg]	3.5
m_b [kg]	150
d_c [N/s]	484
d_s [N/s]	643
d_b [N/s]	20
k_c [N/m]	546000
k_s [N/m]	145000
k_b [N/m]	5000000
C	5
Ref.prof [g]	1
Notch level (global) [g]	0
S [oct/min]	2

Table 21: Implemented values

The simulation doesn't consider the presence of notching. In this term, the output curves is the unnotched motion.

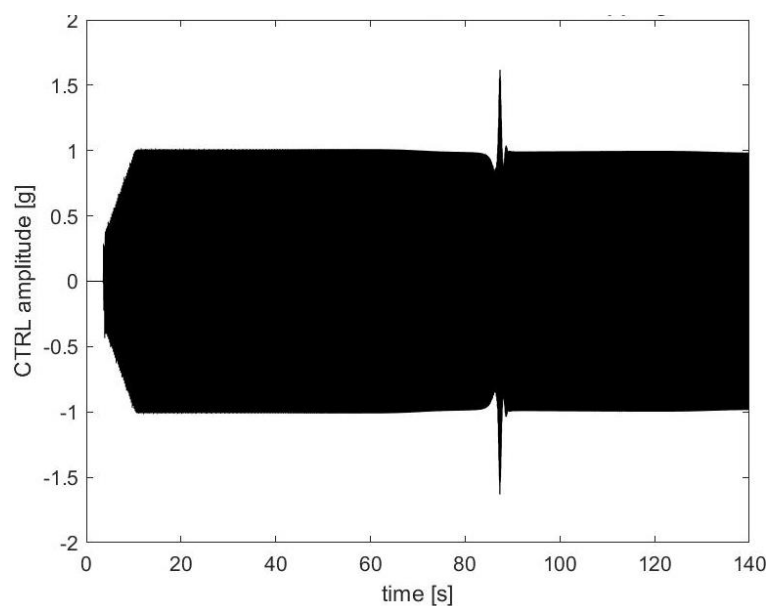


Figure 46: Pilot curves

Figure 46 shows the sinusoidal trend of the pilot curves. How it appears, all the curves are overlapped. This is exact, in fact, just one pilot is considered and the curve represents the same output. Actually, how will be examined in the next chapter, the Simulink model requires 4 signals coming from at least 1 input.

However, being the natural frequencies are about 20 Hz, 30 Hz, 90 Hz, pilots are able to maintain the required acceleration profile (1g) except around 30 Hz. Figure 47.

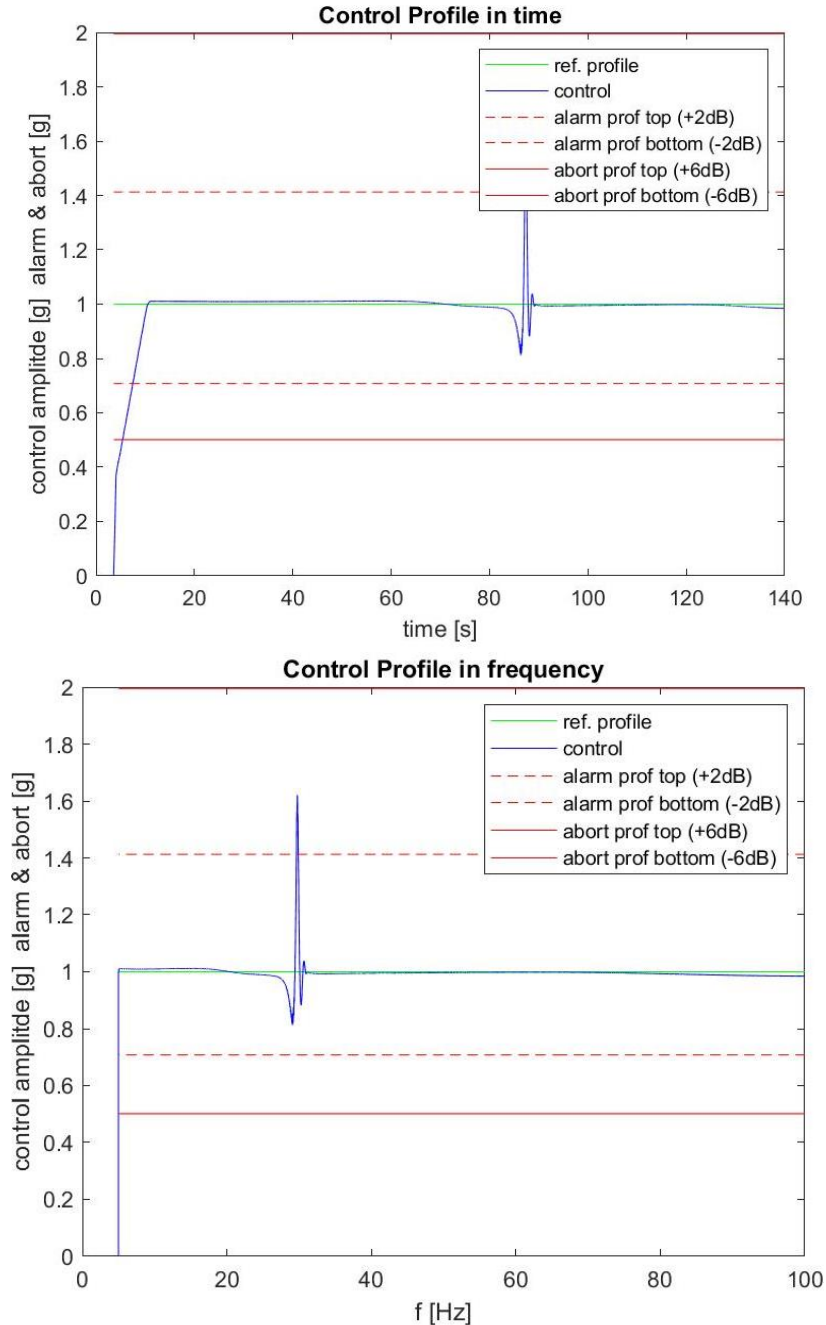


Figure 47: Acceleration profile reached up from the pilots (time and frequency)

On the other hand, the time variation of the remaining DoFs is presented in Figure 48.

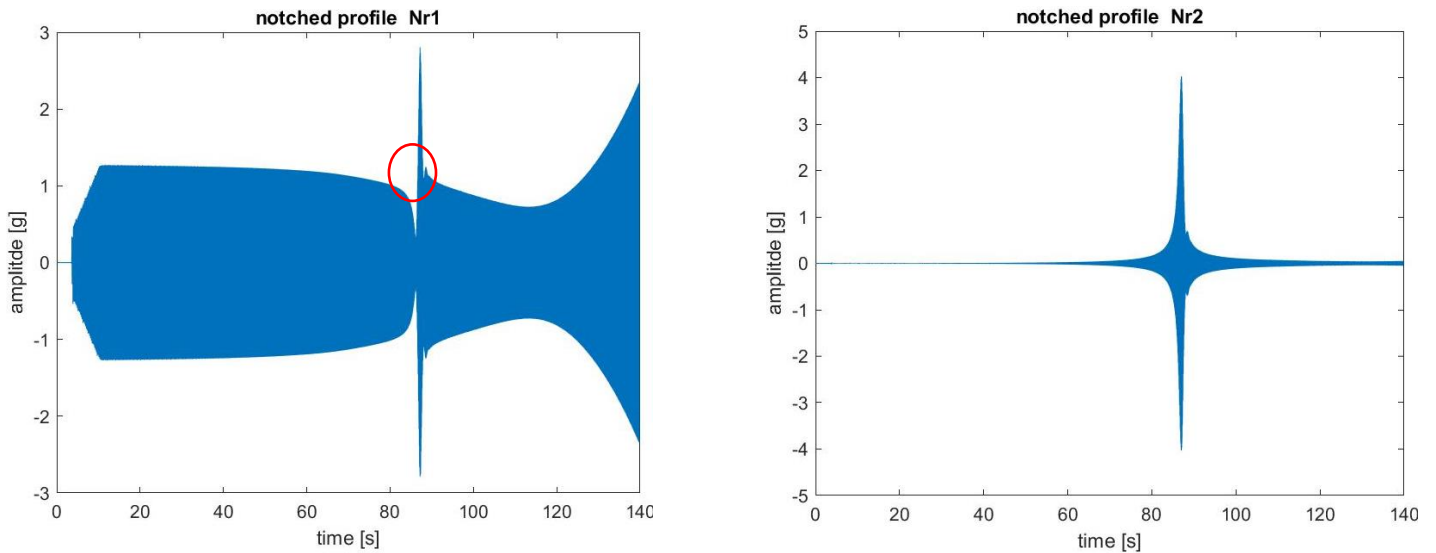


Figure 48: Coil and Body time variation

It shows the time response of the Coil and the shaker body. Particularly, how is possible to see, a great peak appears during the body response. Particularly, it appears at about 30 Hz in accordance with the second natural frequency. In fact, the first is not considered because the implemented model forces the structure between the shaker body and the coil. This is equivalent as the constraint imposition between these two.

Lastly, Figure 49 shows the time and frequency variation of these unnotched DoFs. Again, the greatest peak appears if the input has the frequency of the second natural frequency of the global system

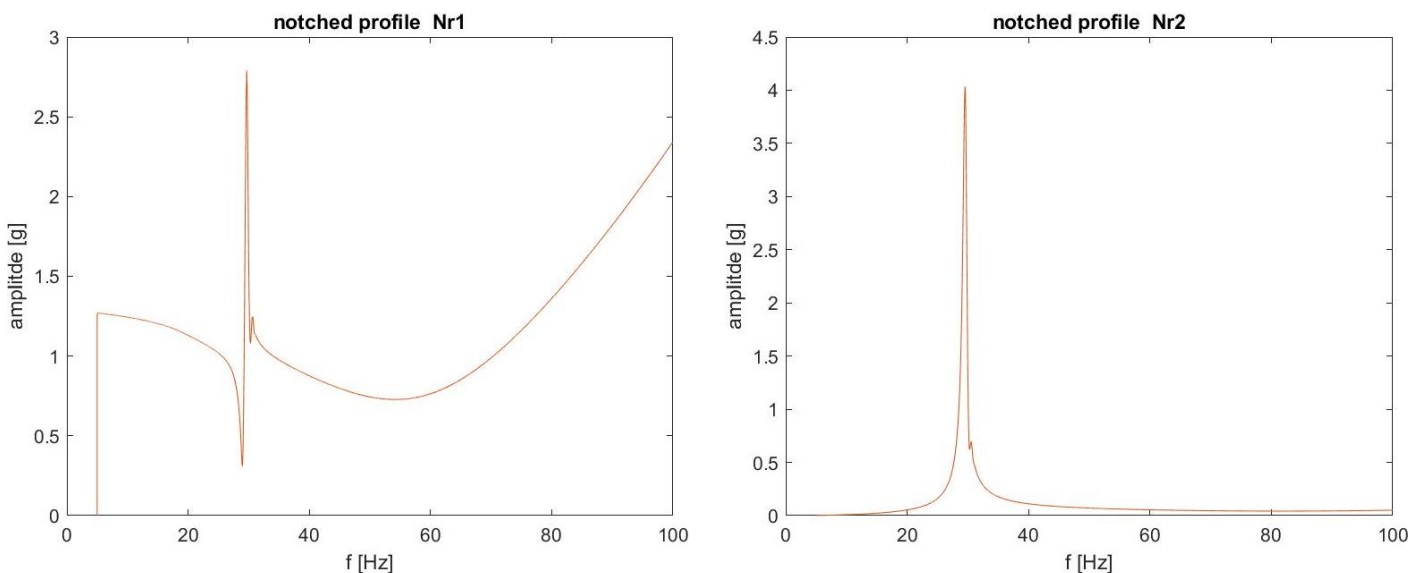


Figure 49: Coil and Body frequency variation

In fact, considering the previous mechanical system, the imposition of a force between the shaker body and the coil means to constraint a reduced system composed by only the coil and the sum of IUT and table. This concept is expressed by erasing the row and the relative column into the mass and stiffness matrix related to the shaker body. Then, performing a modal analysis, the natural frequency about 30 Hz is reached.

Chapter 9: Description of Siemens LMS

Vibration Control Routines in Simulink

environment

The vibration control routine provided by Siemens is the equipment thanks to which is possible to carry out the virtual vibration test -the virtual shaker test-.

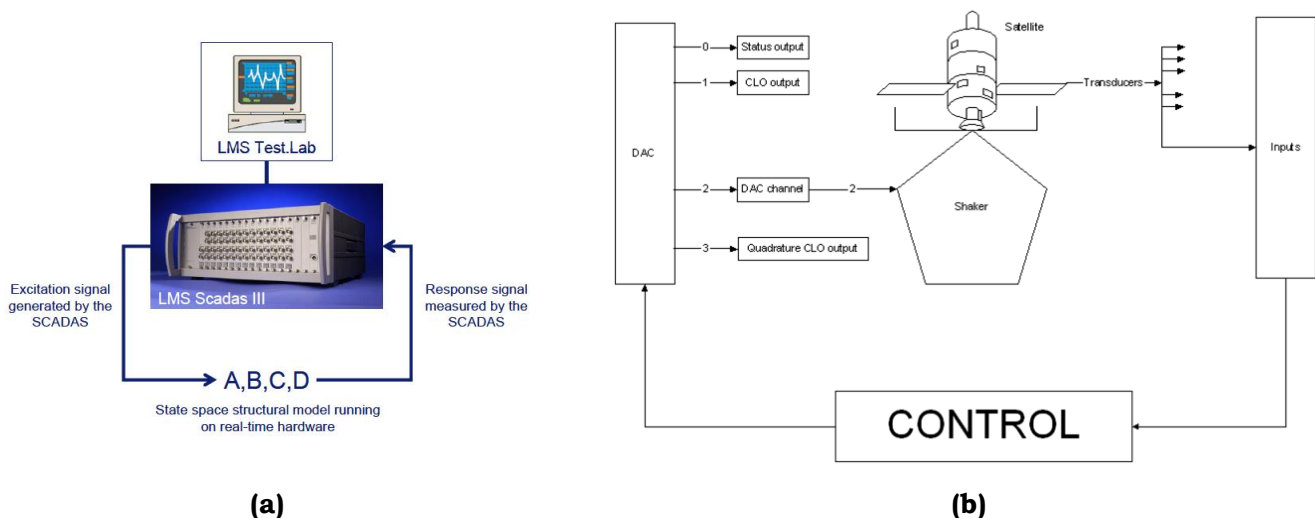
It is designed using Simulink, the MatLab tool, being adequate in the handling, management and processing of signals with different natures. In fact, in this context it will be useful for the transient analysis during the test phase.

Its strong peculiarity is related to the capability to keep both hardware and software issues and aspect in order to better simulate the control's behaviours during the real vibration test.

However, it is able to perform only the sine sweep approach, then is not able to analyse and predict other behaviours as the random or shock response.

Figure 50 shows in a short and schematic way what the LMS Vibration routine do. Firstly, it requires that the user load the mathematical model (condensed or analytical) into the Simulink environment as discrete state space model. It represents the IUT connected with the shaker assembly. In the same preliminary process is necessary that all the simulation parameters are declared (e.g. notch profile, reference acceleration profile, etc..) in order to set up an adequate virtual test. They will be discussed and described subsequently.

After that, when the simulation starts, the control system imposes a sinusoidal input to the base of the shaker (or elsewhere according to the mathematical model). Particularly, the Simulink model doesn't require any electro- mechanical formulation. Nevertheless, if we are treating an assembly composed by the shaker, its parts and the IUT, is a useful approach to include the electrical DoF as responsible to induce the movement between different parts. Monitoring the response of the considered structure in terms of acceleration, it is capable to modulate in magnitude the next sine input characterized by a specific frequency.



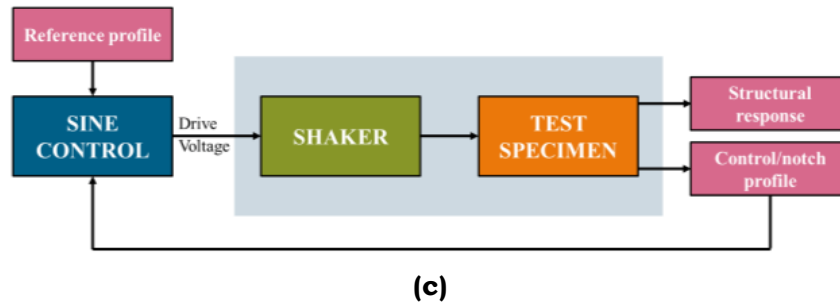


Figure 50: Hardware and software in the loop (a), Simple scheme of the vibration controller (b) [Ref.7], Principle control-loop virtual shaker testing (c) [Ref. 25]

Speaking in terms of the LMS Vibration, as it provided by Siemens, it is composed by three different part:

- Two MatLab files: “Flow.m” and “Set_Control_parameters.m”
- One Simulink model

Obviously, they carry out different tasks.

In addition to these files, another dedicated routine were written in order to read the Nastran file “.op4” and setup the vibration control from the state space point of view. Its name is “S_S_Converter.m”. It will be discussed in the following chapter because its writing is a general, but dedicated, approach outside the LMS environment

9.1 LMS- MatLab files description

MatLab files are necessary in order to perform the virtual test using the Simulink model. How is said before, they are “Set_Control_parameters.m” and “Flow.m”.

Particularly, the first is allocate into the second one.

In fact, into the different insert (distinguished by the marker “%%”) proposed into “Flow.m” different actions follow one another.

9.1.2 “Set_Control_parameters.m”

It manages the input of the simulation in terms of reference acceleration and notching profiles, frequency span to cover and other simulation parameter. Table 22 describes the involved parameter.

9.1.2 “Flow.m”

This routine provides the setup of the virtual test. In fact, it initializes “Set_Control_parameters.m” and save its values into the MatLab Workspace.

Moreover, it is endowed of other parameters as described in Table 23.

In addition, it recalls and starts the Simulink model and, when the simulation stops, it prints the output in terms of control profile and time and frequency response of the notchers.

<u>MatLab parameter</u>	<u>Full name</u>	<u>Dimension</u>	<u>Description</u>
S	Sweep rate	Oct/min (exponential law) Hz/sec (linear law)	Represent the increasing or decreasing of the frequency during the test. At low sweep rates better control and more control update are achievable
f0 f_max	Start frequencies end frequencies	Hz	They represent the start and the end simulation frequencies
c	Compression factor	dimensionless	Typically, the appropriate values are 1 to 20 during the test. It possible to consider it as a constant value ore with different shapes. Low factors allow a better control. High factors allow a stable control in terms of the smooth of the spectrum and beating phenomena
but	Build up time	s	It Defines the rate at which the drive amplitude is increased at the beginning of the simulation, keeping the frequency constant, before the sweep is started
itf0	Inverse transfer function amplitude at f0	V/g	It Defines the drive level that makes the structure response to meet the specified on at the starting frequency
Fs	Sampling frequency	Hz	It Defines the sampling frequency used into Simulink model
Refp	Reference amplitude profile (acceleration)	g	It Defines the amplitude reference profile in term of acceleration that the control system should achieve
Shift	Abort and alarm profiles at each frequency	dB	It Defines the amplitude of the abort and alarm profile according to the reference profile
Nn	Notching channel	Dimensionless	It Defines the number of notching channel achievable from the control system. Into Simulink model the maximum number is 40
Ref_notch	Reference notching level	g	It Defines the values of maximum acceleration for each notchers during the frequency span

Table 22: Set_control_paramenters.m

<u>MatLab parameter</u>	<u>Full name</u>	<u>Dimension</u>	<u>Description</u>
p	Number of periods	dimensionless	Number of periods in which the control system generates its control. Low number of periods allows a better control, but the amplitude of the signal is noisier. Using this option more control update is reachable
Delay	Amplitude delay	s	It Defines the delay at which the amplitude starts. It represents the time at which the system reached for the first time the 50% of the final response
E_s	Estimation strategy	dimensionless	It Defines the strategy with which is possible to evaluate the output during the simulation. It could be: Harmonic, Peak, RMS or Average
Ctrl_strategy	Control strategy	dimensionless	It Defines the strategy with which is possible to control the input signal. It could be Minimum, average or maximum
Number_channels	Number of channels	dimensionless	It Defines the number of control channel (up to 4) with which analyse the control signal
m	Sweep mode	dimensionless	It defines the sweep mode. It could be linear or exponential, up or down

Table 23: parameters into Flow.m

From the control and future simulations point of view, a very important parameter is provided by the compression factor. It represents part of the “heart” of the control algorithm (un-visible into the MatLab/Simulink model that we will discuss. If the compression factor is high, the control algorithm and the control of system takes more time and become slow. On the contrary, if it is low, the control algorithm is reactive and sharp.

From a theoretical point of view, the unique knowledge of this criterion could induce the test facility (or the designer) to select low compression factor. Nevertheless, a more reactive control could induce extra-excitation undesired and stronger corrections than the necessary, particularly in case of beatings of near modes of the system.

Typically, we are interesting, in terms of compression factor, to suggest to the test facility a suitable compression factor though is possible to reduce the usual low-level runs at varying to different compression factors. They are necessary to understand, in the absence of a chosen compression factor, which could be the suitable one capable to reduce overshoots and beatings.

9.2 Simulink model description

The Simulink model represents the real “heart” of the control system. It is a very complex system in term of logic and implemented functions. It is composed by different blockset drowned at each level as Mux, Demux, MatLab embedded functions, switch and transfer functions and it is written in order to be an HIL closed loop system, capable to reproduce the same characteristics and behaviours of the test facility control system.

The main control environment is endowed of appropriate “scopes” in order to see the output in real time. In Figure 51 and Figure 52 the Simulink environment at different levels is shown.

How is possible to see, the control system shows different masks. They shadow control logic, but, going deeper, there are some function impossible to analyse in order to better understand the logic.

In these terms, the Simulink model will be considered as a “black box” when the simulation run.

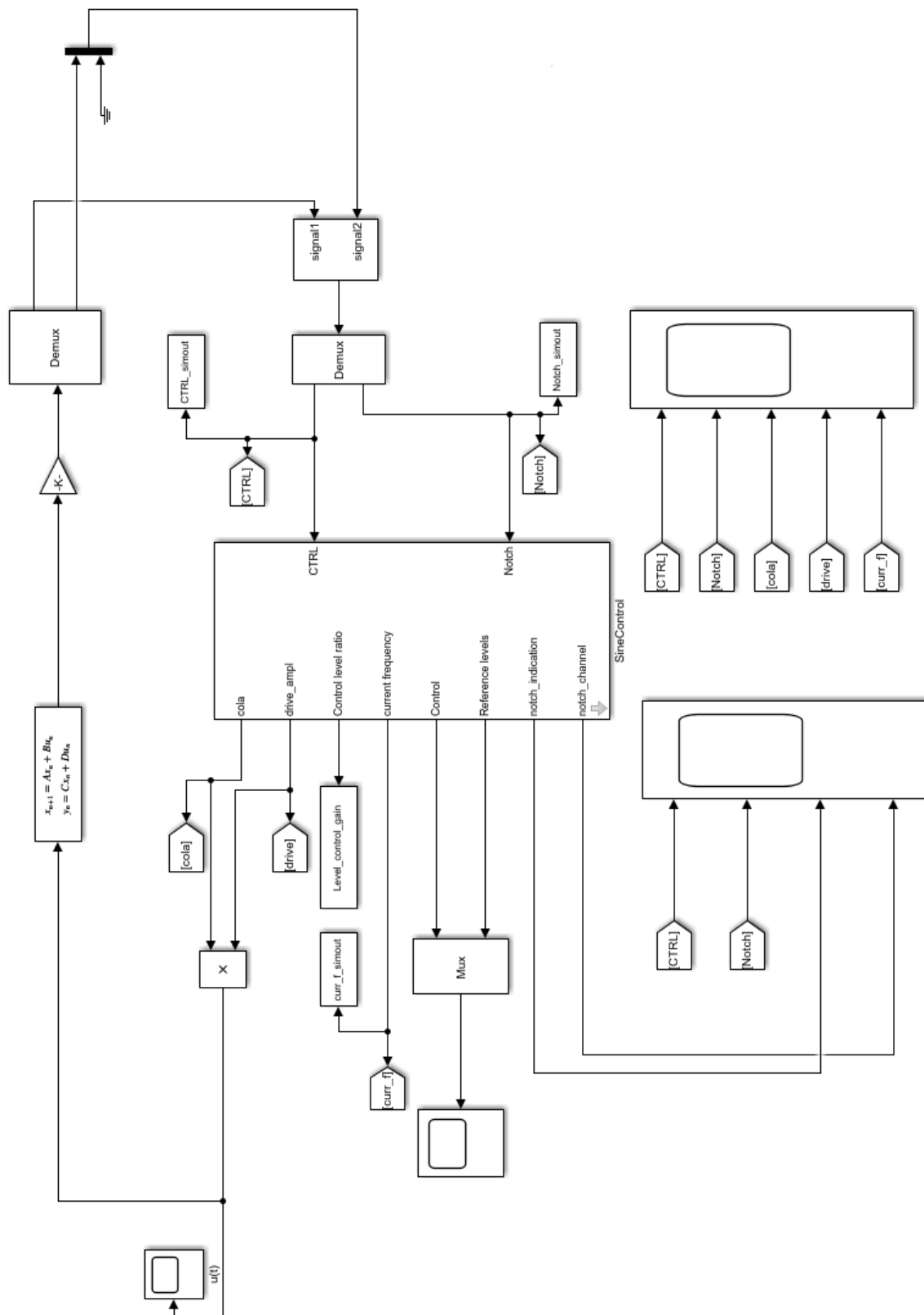


Figure 51: Main control environment

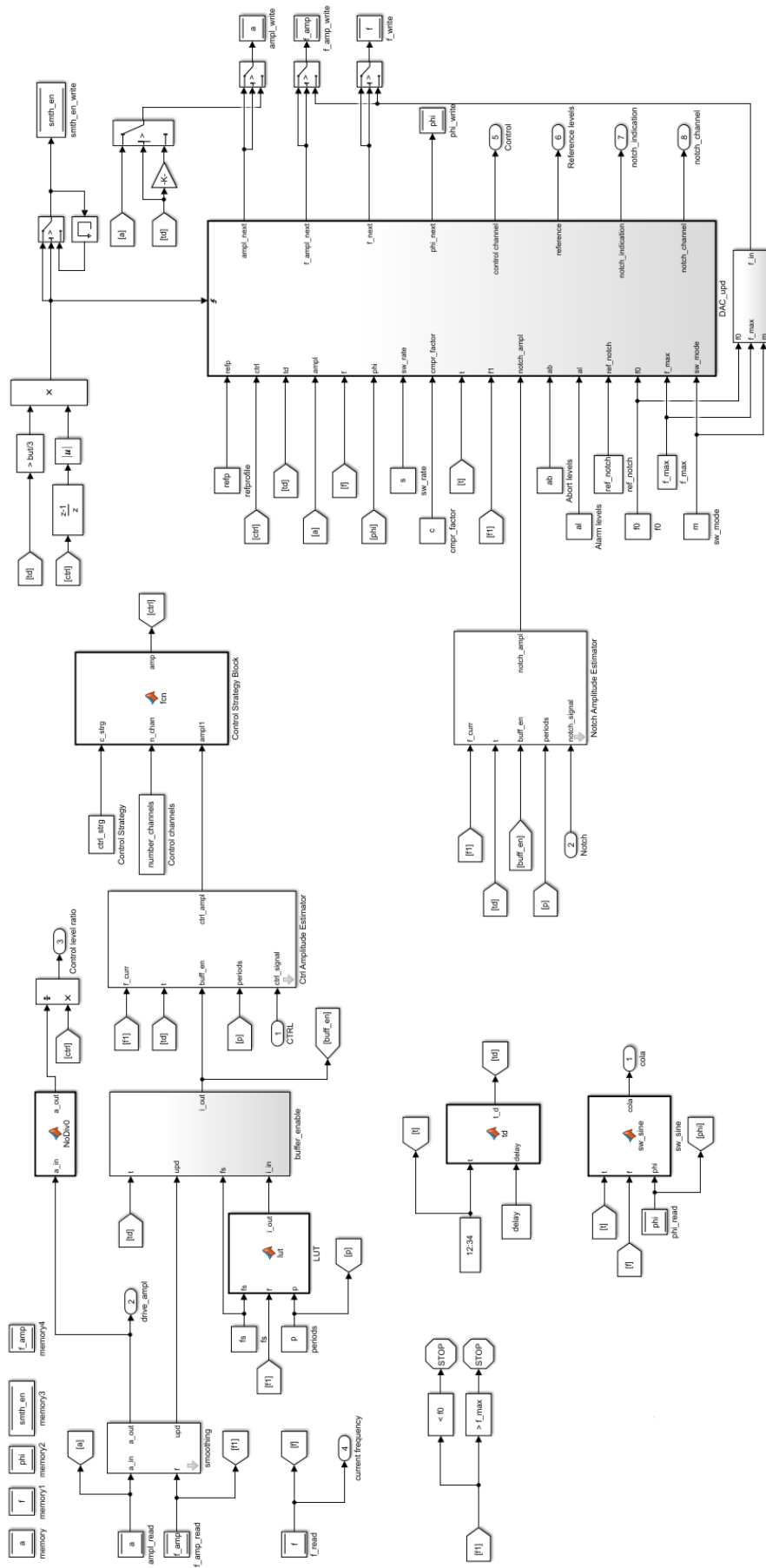


Figure 52: Detailed sine control environment

However, from a system point of view, is possible to describe the qualitative way in which the control system operates.

The code is able to perform the vibration control of a loaded system or device using up to 40 notchers (or DoFs) in order to monitoring their response.

It is written in order to guarantee always 4 pilot curves. In fact, the original version of the model considered provide just one output coming from DEMUX.

It is repeated considering 3 gain factors that amplifies the input signal. Subsequently, it becomes composed by 4 output. Then, is provided to the following MUX that recollect them with the other 40 signals coming from notchers in which some of them comes from the “C” matrix of the state space system and the remaining part from the “ground”. Figure 53 (a)

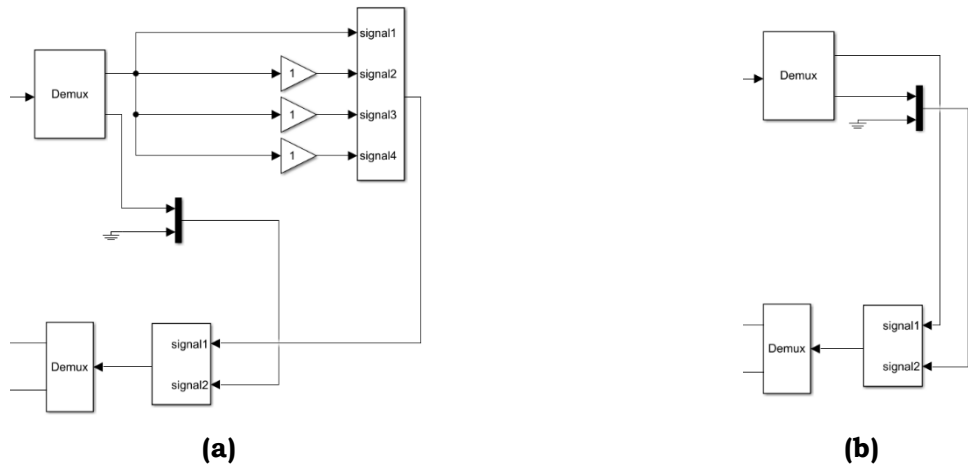


Figure 53: Modification to the Simulink model: before (a), after (b)

This implemented modelling strategy were tested with the reduced models mass- spring-damper described in “Chapter 8: The Virtual Shaker Testing approach (VST)” but is not appropriate in order to perform the VST using a condensed model in which the pilots are extracted with the Craig- Bampton theory, according to the location of the physical accelerometers attached to the vibration platform.

For this reason, the Simulink model were modified in order to extract exactly 4 signals from DEMUX. Particularly, they refer to the pilots of the Craig- Bampton theory located into the first four position of the “C” matrix. Figure 53 (b).

After that, the signals come into the real “sine controller” which, for each time step, perform actions as notching level calculation, control amplitude, time delay or sinusoidal input means cola.

In Figure 54 is shown as is appear the mask of the sine control in which the input variables are recalled.

One of the key points of the sine control are the control and estimation strategy.

The first one represents the way in which the control takes place. It concerns the trend, and the values, of the pilots. Particularly, three possibilities are available:

- Maximum: the control signal generates a control profile characterized by the maximum value of the pilots
- Average: the control signal generates a control profile characterized by the sum of the pilot signals divided by the number of control channel, chosen in “Flow.m”

- Minimum: the control signal generates a control profile characterized by the minimum value of the pilots

The second one gives the way in which all the signals are evaluated. Basically, there are four possibilities:

- Peak: it takes the greatest amplitude of the sample signal. If the system is characterized by noisy, this kind of evaluation could introduce some instabilities
- Average: if the signal is characterized by “N” sample time, it calculates the average of the absolute value of them. It takes the complete signal.
- RMS: it calculates the average of the squared values of “N” sample time during one period. As the average method, it evaluates the complete signal. It is able to produce a low drive signal
- Harmonic: it is considered as the appropriate valuer for fundamental frequency research. It provides magnitude and phase response

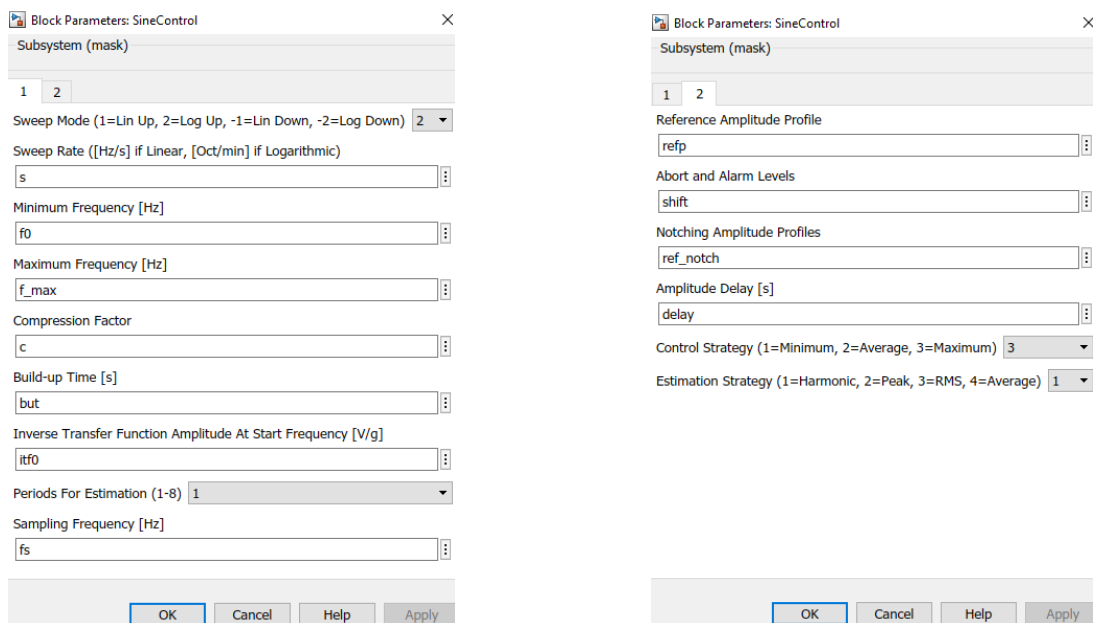


Figure 54: Sine control block parameters

When the simulation starts, it requires the initial condition in order to join into the loop. They usually are the homogeneous conditions in which, using the formulation of a dynamic second order system, are displacement and speed equal to zeros.

However, the block scheme implemented in Simulink is the “Discrete State Space”, shown in Figure 55. It come from the “Continuous State Space” system. In fact, how is described in “

Chapter 2: The State space systems”, this kind of mathematical formulation represent the best way in which to perform the control of a dynamic or electro-dynamic system.

Particularly, the discrete formulation comes from the continuous quantizing the matrix operator with the " t_s " sampling time consistent of the data acquisition system of the vibration facility.

Nevertheless, from the algorithm point of view, it is able to solve the differential equation using the same procedure of the finite difference.

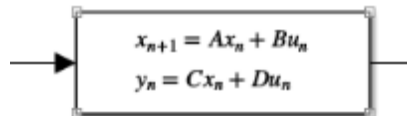


Figure 55: Simulink block for Discrete State Space

On the other hand, the code is not able to undergoes to modification in terms of solver. In fact, it is written usign a “discrete logic”, so is not possible to replace the “Conotinuuous state space block” using the Runge-Kutta method.

For sake of clarity, if Runge- Kutta is the exact approximation of a differential equation in time domain, the discrete state space solver is the approximation of this. In these term, the extracted curves using the discrete method will match in some points with them extrated using the continuous method.

When the simulation advance up to the maximum value of the frequency (typically 100 Hz for sine sweep) the Simulink model send out two matrix: “spectra.mat” and “spectra_notch.mat” in which are recollect the requested output and classified by columns in term of time, frequency related notcher values and control profiles.

The output that is possible to extract to the sine control system are:

- 4 pilot curves: they describe the variation in time domain of the considered pilot. How we said before, talking in terms of signals, is necessary to guarantee 4 signals to the control system. They could be overlapped or not
- Up to 40 notched curves in frequency and time domain
- The control signal profile compared to the abort and alarm limits
- Two “on/off diagram” in which are shown if one, or more Dofs are notched and which of them
- The drive amplitude of the input
- The cola: it shows the sinusoidal input imposed to the coil
- The enhancement of the frequency during the simulation

Particularly, the control curve (i.e. the acceleration of the pilots handles by one of the controls and strategy criteria) is compared to the upper and lower abort and alarm limit.

Usually, during a vibration test if the control curve exceeds one of the two abort limit (± 6 dB) it is interrupted. However, into the LMS vibration control environment we are to see the control curve during all the simulation span, in frequency or time domain, even if it exceeds the upper or the lower value.

Probably, in fact, the aim of do not interrupt the running simulation is to permit to the engineer to observe where and when the control “burst” or “disappears”. This, in order to apply the required modification to the control environment in terms of compression factor, notch profile, control strategy or damping model if the FEM model is unprovided.

In this way, the sine control lives in a wide set of simulation distinguished by the possible variation of each control parameter and under a precise strategy to distinguish the type of control.

Obviously, the final result of the VST activity is to suggest the more appropriate value at each control parameter, before the real vibration test into the facility centre, in order to observe some specified behaviours during the base excitation and guarantee that them do not provoke any rupture. For these reason does not exist a unique and unequivocal result, but it depends on what the test facility engineers want to observe. In these terms, the VST shall emanate a variety of output, based on what they want.

Chapter 10: Setup and definition of VST methodology and framework using pre-existing experimental data

10.1 MatLab state space converter description: S_S_Converter.m

This automated routine is able to convert the mechanical matrices into a State Space electromechanical system.

In order to achieve this purpose different subroutines are written:

- Damping_model.m;
- Proportional_damping.m;
- Observation_matrix_accelerations.m;
- Observation_matrix_fmd_accelerations.m.

In this context, a brief overview is provided.

Firstly, the main routine “S_S_Converter.m” import the NASTRAN matrices in “.op4” format transforming them into MatLab variables.

After that, is necessary to impose the position of the bobine and shaker body DoFs in order to attach the forcing function. Is necessary to define the number of condensed (interface) DoFs and the observed acceleration of the notchers.

Subsequently, the electrical parameters shall be defined. How will be shown in the following passages, the electrical parameters do not influence dramatically the results. For this reason, the user can maintain the pre-imposed ones.

Thereafter, the routine will define automatically the mass, stiffness and damping electrical vector starting from the electrical parameters.

Going deeper into the code, natural frequencies are extracted from the stiffness matrix in Craig Bampton formulation. In this way using “Proportional_damping.m” the viscous damping matrix is defined and imposes according to different models and approaches provided into Chapter 10.2. Basically, the user should select the frequency band and the damping ratio (proportional and modal) to apply.

Coming back to “S_S_Converter.m”, the mass matrix is inverted and the state matrix (A) and control matrix (B) are built according to equation from (8.9) to (8.11).

Now the time has come to build the control matrix. In this context two separated routines, “Observation_matrix_accelerations.m” and “Observation_matrix_fmd_accelerations.m”, are written in order to implement different observation strategies.

They are quite similar because they are able to prepare the final control matrix allowing to observe one or more pilots (up to 4) DoFs for each one. However, the first four positions are available only for control pilots namely the pilots used for control the dynamic of the system. Other position, typically from 5th to the 12th, are dedicated to the observed DoFs in order to observe their cross talks.

Nevertheless, subsequently to the pilots, is possible to impose the observation of the notchers in X and Y direction. In this case Z is careless.

This is a common part for both routines. The additional part is just of the “Observation_matrix_fmd_accelerations.m” in which is possible to define two fictitious DoFs used in order to observe the moment at the base starting from the rotational DoFs of eventual springs.

Coming back to “S_S_Converter.m”, the continuous state space system is build using the pre-implemented function “sysc”. It requires the four matrices (A, B, C, D) only. The interesting part is represented by the discrete state space in which is necessary to provide to the algorithm a sampling time “Ts” used for sample the A and C matrix. In this case a Ts= 0.00015625 [s] is implemented how suggested by SIEMENS.

After this instruction, the “Flow.m” routine, introduced before is able to perform the VST.

10.2 Evaluations based on different damping models

In this section some evaluations about the behaviours expressed through the use of different damping models, are shown.

The first approach is based on the preparation of the damping matrix using mass and stiffness matrices extracted by the condensed FEM model. In this context six models are taken into account under the viscous formulation: Raleigh (or proportional) and modal.

The second point of view is based on enhanced and improved damping models, built “ad-hoc” for condensed FEM, using the structural damping matrix (K4AA), output of NASTRAN, trying to deduce an equivalent viscous formulation, useful for transient analysis.

Firstly, how is well known, damping is a critical mechanical quantity that produces energy dissipation due to internal friction into the material sub-structure. Its phenomenology is complex and typically difficult to understand, reproduce and modelling.

For this reason, considering linear-elastic materials, two kinds of models are classically employed and taken into account: viscous and damping formulations. The following definitions are in agreement with “NASTRAN user guide”.

$$\text{Viscous damping} \quad f_{viscous} = b\dot{u} \quad (10.1)$$

$$\text{Structural damping} \quad f_{structural} = iGku \quad (10.2)$$

Where:

- a) b : viscous damping coefficient
- b) \dot{u} : speed
- c) $i = \sqrt{-1}$: imaginary unit (phase change of 90 degrees)
- d) G : structural damping coefficient
- e) k : stiffness
- f) u : displacement
- g) $f_{viscous}, f_{structural}$: viscous and structural damping force, respectively

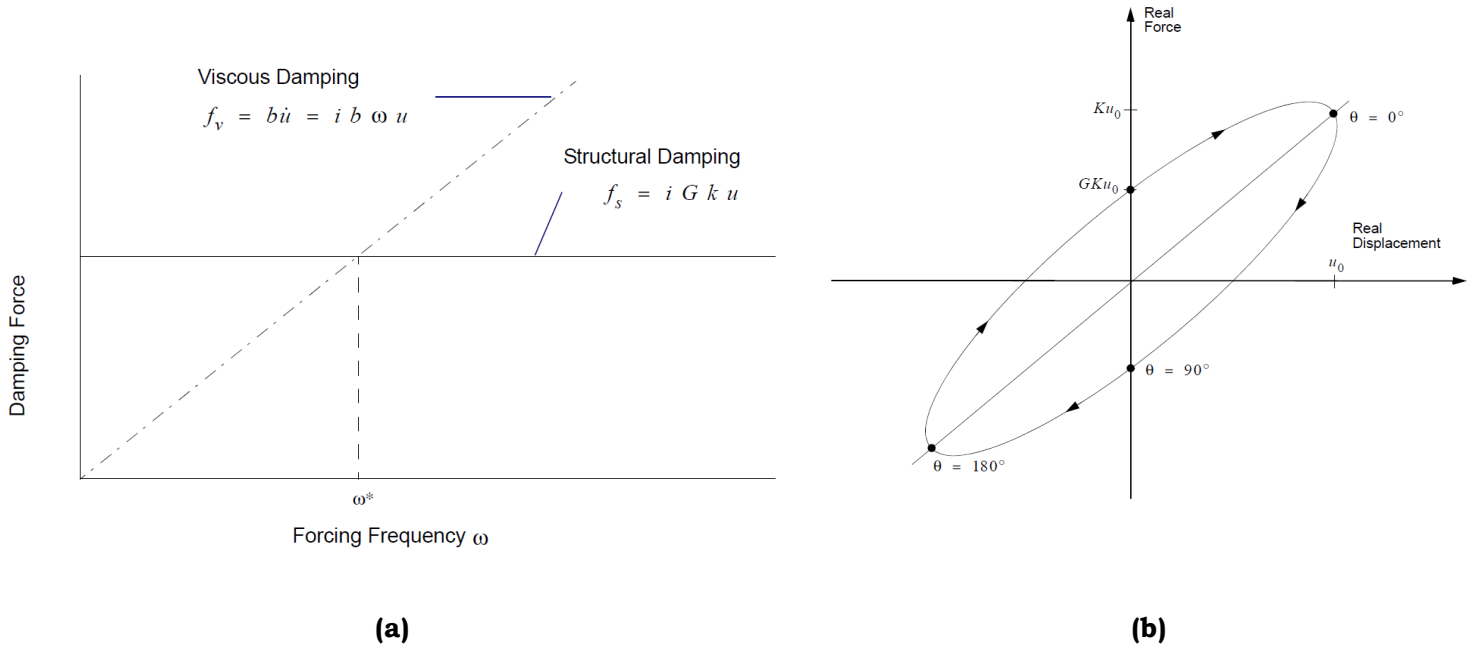


Figure 56: Viscous vs structural damping force (a), equivalent hysteresis process in structural damping (b) [Ref.34]

How is known, viscous damping is related to the speed of the system, instead structural to the strain state of the systems, then in frequency domain to the displacement. In terms of damping force, expressed by the used formulations, using the relationship between speed and displacement, in Figure 56 (a) we can understand that in frequency domain viscous damping force increases compared to the structural in which the value is constant.

Interesting characteristic, at a given forcing frequency, the following equivalence is given

$$ib\omega u = iGku \quad (10.3)$$

Then, if $\omega = \omega^*$

$$b = \frac{Gk}{\omega^*} \quad (10.4)$$

Is possible to deduce an equivalent viscous relationship

$$b_{cr} = 2\sqrt{km} = 2m\omega_n \Rightarrow \frac{b}{b_{cr}} = \zeta = \frac{G}{2} \quad (10.5)$$

We deduce the so called “quality factor” or “dynamic magnification factor”

$$Q = \frac{1}{2\zeta} = \frac{1}{G} \quad (10.6)$$

Talking about viscous damping two main and conventional techniques will be useful, the so called “*modal damping*” and “*proportional (or Raleigh) damping*” usually developed for mechanical MDOF systems.

For this purpose, recalling the equation (8.15), (8.16) the two formulation are shown

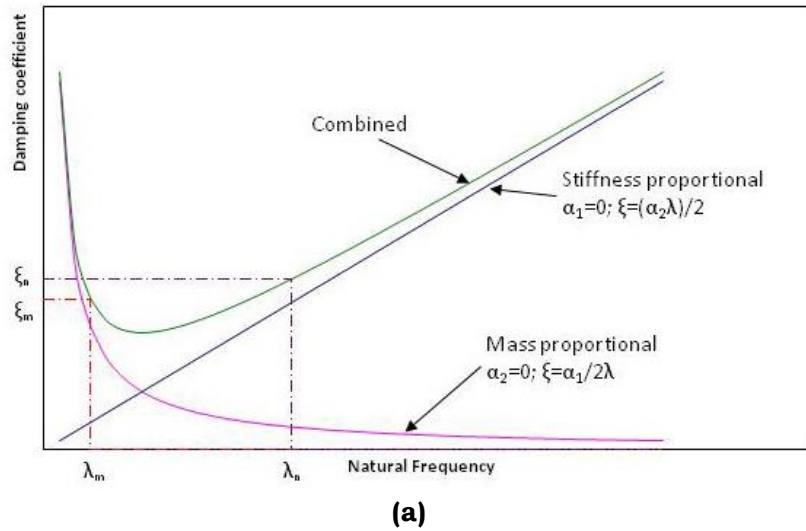
$$[D_{mech}] = \begin{bmatrix} 2\zeta_1\omega_1 & 0 & \dots & 0 \\ 0 & 2\zeta_2\omega_2 & \dots & 0 \\ \vdots & \vdots & \ddots & \vdots \\ 0 & 0 & \dots & 2\zeta_n\omega_n \end{bmatrix} \quad (\text{modal damping}) \quad (10.7)$$

$$[D_{mech}] = \alpha[M_{mech}] + \beta[K_{mech}] \quad (\text{proportional damping}) \quad (10.8)$$

Basically, working with a proportional model we assume to assign a precise contribution in terms of mass and stiffness as a liner combination adequately combined by α and β coefficients. Typically, the resultant matrix is full and it is based on the physical system.

On the other hand, modal damping model shows a diagonal matrix, where the elements are defined, and defined themselves, the i-th mode of vibration (and i-th natural frequency). In this way, we assume a decoupling in terms of mode and the damping contribution is a function of the frequency.

It is a very efficient approach when coupling affects are negligible or absents, however the values of ζ_i are extracted by tests (e.g. hammer tests).



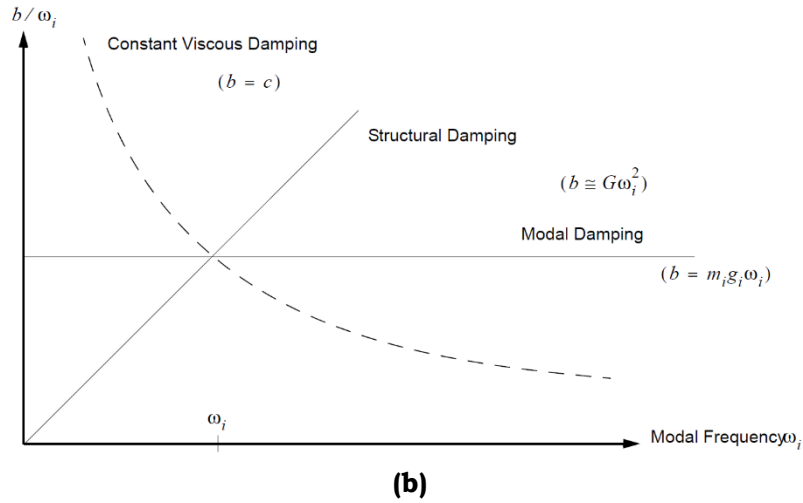


Figure 57: Variation of viscous damping with natural frequencies (a), damping coefficients Vs natural frequency [Ref.34]

The other fundamental, and widely used, damping model is the so called “Structural damping”. It refers of a hysteretic damping process inside the materials and related to the displacement. Particularly, from a mathematical and physical point of view, it results in 90 degrees out of phase displacement with a stiffness matrix related to complex value. Practically, structural damping is an useful approach in order to represent the hysteretical process in frequency domain. However, due to the presence of the complex value, is necessary to deduce an equivalent linear viscous approach.

Mathematically, we usually write the structural damping matrix, in terms of FEM, as

$$K_{new} = (1 + iG)K + i \sum_1^{N_{elements}} G_e K_e \quad (10.9)$$

Where

- a) K : entire stiffness matrix
- b) K_e : elemental stiffness matrix

In this context more precise damping models will be discussed subsequently.

To sum up, the difference between viscous and damping models.



	<div style="border: 1px solid black; padding: 5px; display: inline-block;"> $M\ddot{x}(t) + Kx(x) + F_{diss}(t) = F(t)$ </div>	
<p>Structural damping</p> $F_{diss}(\omega) = iK_S x(\omega)$ $K_S = \eta_G K + \sum_1^{N_{elements}} G_e K_e$ $[-\omega^2 M + (K + iK_S)]x(\omega) = F(\omega)$		<p>Viscous damping</p> $F_{diss}(t) = B\dot{x}(t)$ <p>B: viscous damping matrix</p> $[-\omega^2 M + i\omega B + K]x(\omega) = F(\omega)$

Table 24: Differences between structural and viscous damping

Due to the importance of the appropriate damping model, in terms of value of damping coefficient and frequency span, is reasonable to expect several differences between the different response of the system in accordance to the implemented model, but also differences between analytical/numerical predictions and test outputs.

Lastly, few words about the format file thanks to which is possible to extract the mass, stiffness and damping matrices: the “op4”. The op4 file contains the requested matrices generated by Dmap alters, in NASTRAN. Alters are particular routines by which is possible to deduce condensed models (e.g. Craig-Bampton) and their storage scheme may be dense or sparse formulation in ASCII or binary codification.

10.2.1 Notch prediction using viscous damping models with mass and stiffness matrices extracted from the condensed model

Into the VST context, the mathematical model loaded inside of the Simulink environment is represented by the “Craig- Bampton” dynamic reduction thanks to which is possible to reduce the size of a Finite Elements Model (FEM) preserving its dynamic characteristics. In addition to this, a “Discrete State Space” formulation will be used in order to allows an effective simulation.

Particularly, the use of “Craig- Bampton” formulation makes it non-trivial due to the presence of physical (or boundary where the condensation takes place) and modal DoFs into the unknown, as well as into the mass and stiffness matrices in which coupling sub-matrices are present. The aim, how expressed before, is to prepare a damping viscous matrix.

Then recalling its formulation for an undamped system as shown by equation (3.15)

$$\begin{bmatrix} M_{rr} & L^T \\ L & [m_p] \end{bmatrix} \begin{Bmatrix} \ddot{x}_j \\ \ddot{\eta}_p \end{Bmatrix} + \begin{bmatrix} \widetilde{K}_{jj} & 0 \\ 0 & <\lambda_p> [m_p] \end{bmatrix} \begin{Bmatrix} x_i \\ \eta_p \end{Bmatrix} = \begin{Bmatrix} F_j \\ 0 \end{Bmatrix}$$

In which:

- $\{x_j\}$: the external or boundary degrees of freedom ($j \leq 6$)
- $\{\eta_p\}$: the generalised coordinates
- $[M_{rr}]$: the 6x6 rigid body mass matrix with respect to the boundary DOFs
- $[\widetilde{K}_{jj}]$: the Guyan reduced stiffness matrix (j-set) (=0 if a statically determined structure)
- $[m_p]$: diagonal matrix of generalised masses
- $[M_{jp}] = [L]^T$: matrix with the modal participation factors

We want to introduce the damping using different approaches based on Rayleigh formulation: proportional and modal damping, as shows the equations (8.15), (8.16), in which the coefficients are calculated as in (10.1), (10.2).

$$\zeta = \frac{\alpha}{2\omega} + \frac{\beta\omega}{2} \quad (10.1)$$

Considering the frequency span between f_1 , f_2 and ζ^*

$$\alpha = \frac{2\zeta^*(2\pi f_1)(2\pi f_2)}{2\pi(f_1 + f_2)}$$

$$\beta = \frac{2\zeta^*}{2\pi(f_1 + f_2)}$$
(10.2)

The effects expressed by α , β are shown in Figure 57 **(a)**.

In these terms the damping matrix is built following the following models/ approaches:

$$1. \quad \text{"Pure proportional"} \quad [D] = \alpha \begin{bmatrix} M_{rr} & L^T \\ L & [m_p] \end{bmatrix} + \beta \begin{bmatrix} \widetilde{K}_{JJ} & 0 \\ 0 & <\lambda_p> [m_p] \end{bmatrix} \quad (10.3)$$

$$2. \quad \text{"Pure modal"} \quad [D] = \begin{bmatrix} 0 & 0 \\ 0 & <\lambda_p> [m_p] \end{bmatrix} = \begin{bmatrix} 0 & 0 & \dots & 0 \\ 0 & 2\zeta_1 \omega_1 & \dots & 0 \\ \vdots & \vdots & \ddots & \vdots \\ 0 & 0 & \dots & 2\zeta_n \omega_n \end{bmatrix} \quad (10.4)$$

$$3. \quad \text{"Partial proportional Case 1"} \quad [D] = \begin{bmatrix} \alpha * M_{rr} & 0 \\ 0 & 0 \end{bmatrix} + \begin{bmatrix} \beta \widetilde{K}_{JJ} & 0 \\ 0 & 0 \end{bmatrix} \quad (10.5)$$

$$4. \quad \text{"Partial proportional Case 2"} \quad [D] = \begin{bmatrix} \alpha M_{rr} & \alpha L^T \\ \alpha L & 0 \end{bmatrix} + \begin{bmatrix} \beta \widetilde{K}_{JJ} & 0 \\ 0 & 0 \end{bmatrix} \quad (10.6)$$

$$5. \quad \text{"Partial proportional Case 3"} \quad [D] = \begin{bmatrix} \alpha M_{rr} & L^T \\ L & 0 \end{bmatrix} + \begin{bmatrix} \beta \widetilde{K}_{JJ} & 0 \\ 0 & 0 \end{bmatrix} \quad (10.7)$$

$$6. \quad \text{Hybrid} \quad [D] = \begin{bmatrix} \alpha * M_{rr} & \alpha L^T \\ \alpha L & [m_p] \end{bmatrix} + \begin{bmatrix} \beta \widetilde{K}_{JJ} & 0 \\ 0 & <\lambda_p> [m_p] \end{bmatrix} \quad (10.8)$$

Particularly α, β were calculated using a frequency range between $f_1=25$ Hz, $f_2=70$ Hz considering $\zeta^*=2\%$ of the critical damping. The same value of ζ were used into modal damping.

How is possible to see, a simple "pure proportional" damping model involves all the terms into the mass and stiffness damping matrices, operating in the same way on both physical and modal DoFs.

This inconsistency is investigated introducing other damping models capable to influence only physical DoFs, only modal or a prescribed combination of both.

From a structural point of view, Figure 58 **(a)** shows the upper stage of the physical model adopted and **(b)** represents the location of the accelerometers.

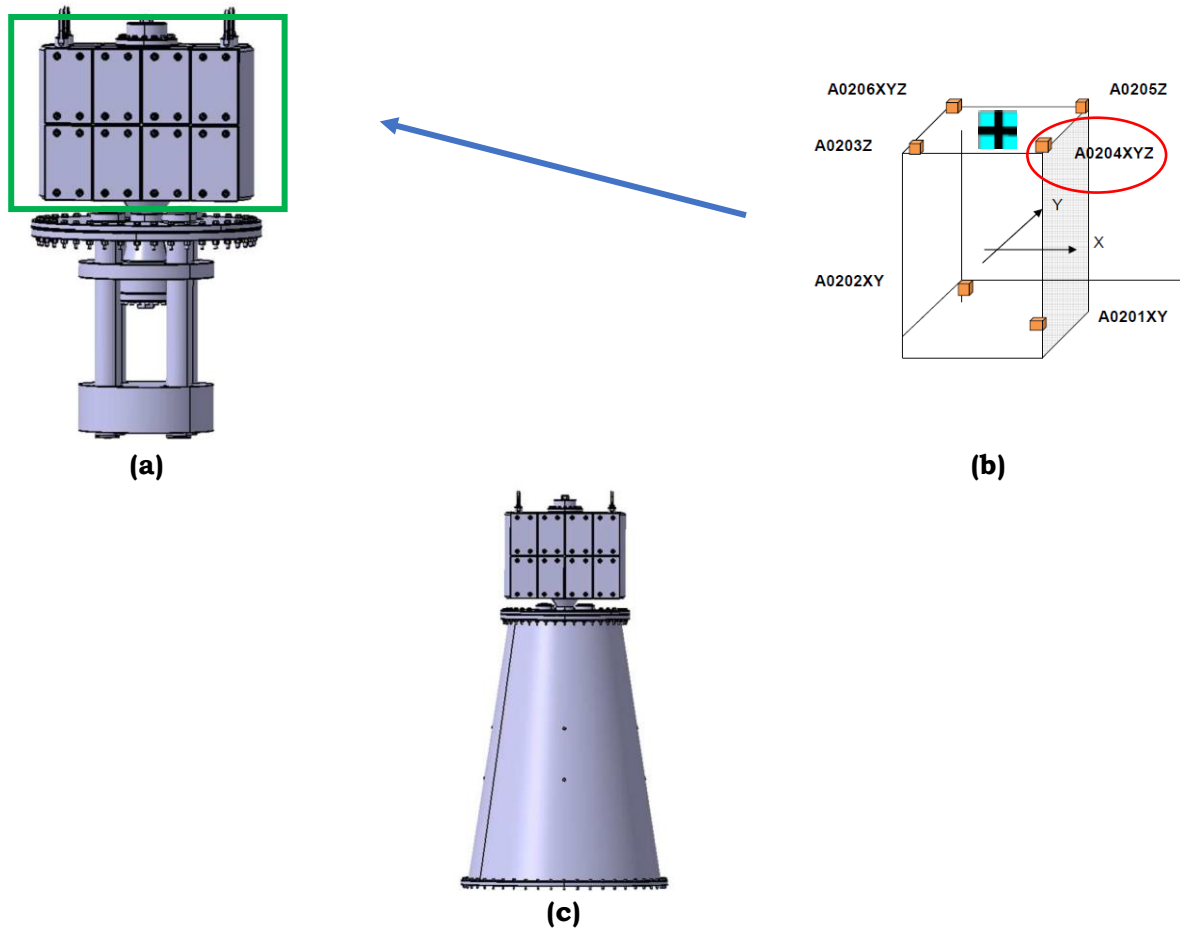


Figure 58: DTM structural model as a reference (a), location of accelerometers and condensed node, entire structure (c) [Courtesy of Thales Alenia Space IT]

Particularly, the red curve highlights the accelerometers in which during the vibration test were notched at about 19 Hz. On the other hand, the blue and black square indicate the FEM node in which the model was dynamically condensed.

Despite we are using just a part of the entire structural model considering this condensed node which represent the upper structure, we expect that:

- The control algorithm is able to notch the acceleration profile during the virtual test
- The depth of the valley induced by the controller should be similar compared to the experimental one

For the sake of clarity, during this first approach and correlation analysis/test we are interested only in the first “notch valley” and the related following overshoot being the condensed dynamic node represents the first notching DoF whose response is greater than the prescribe acceleration threshold.

In addition, the frequency span in which the mode shapes are involved arrives up to 120 Hz in order to expand as much is possible with a reasonable sense, the modal base. In this way, using a fixed number of DoFs, we are using a

For this reason, we expect that the control acceleration profile should be similar between 5 Hz and 35 Hz because in this range only the condensed node affects the control behaviours. Figure 59 shows the experimental data available. It represents the acceleration profile of the control system during a sine sweep vibration test along Y+ direction and acquisition along the same direction

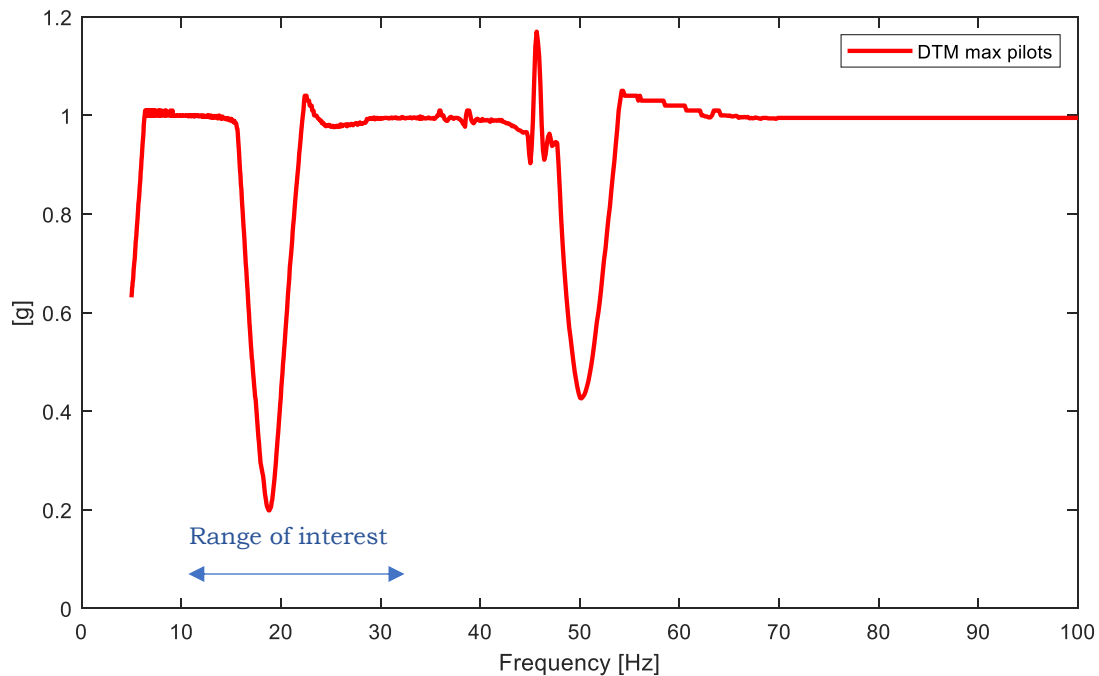


Figure 59: Pre-existing experimental data. Excitation along Y+ and acquisition along Y+ and frequency range of interest (5-35 Hz) [Courtesy of Thales Alenia Space IT]

Input/output quantities (from test)	Value
Notch level [g]	3.9 (direction Y+) (condensed node)
Reference profile [g]	1
S [Oct/min] (sweep up, log)	2
Compression factor [/]	4
Frequency range [Hz]	5- 100
Peak notch valley [g]	0.2
Peak overshoot [g]	≈ 1.02

Table 25: Input/ output parameters from test

➤ Test 1: “Pure proportional damping model”

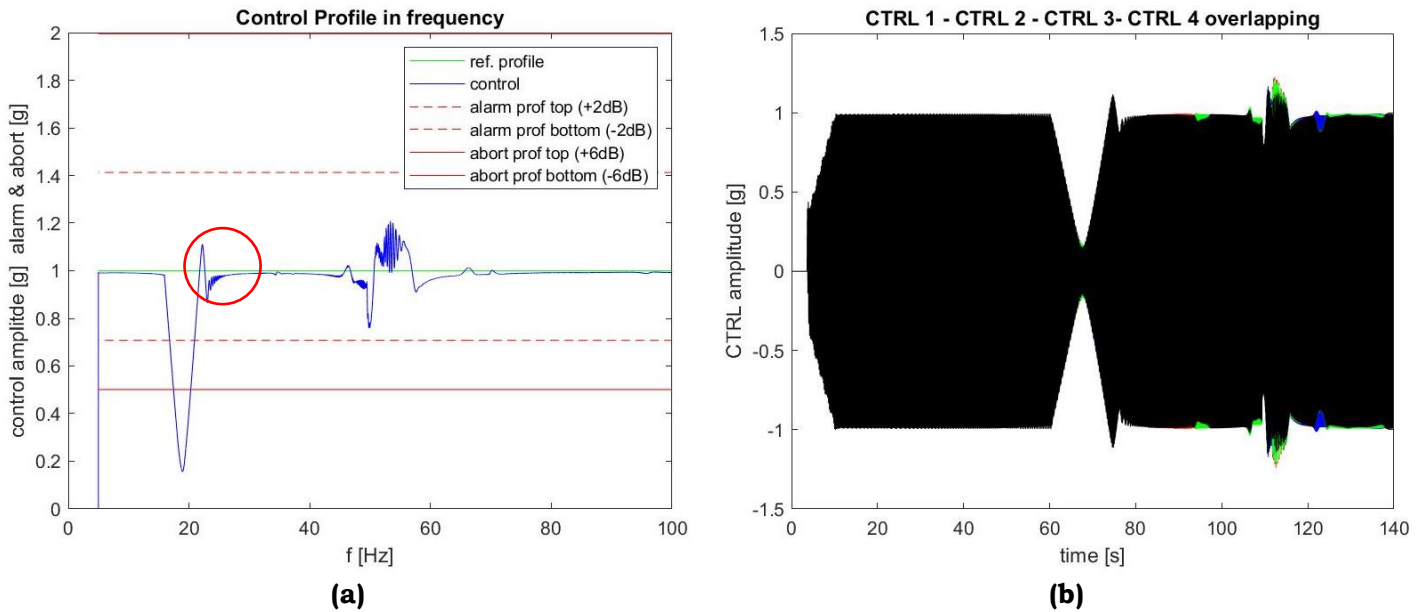


Figure 60: Acceleration control profile in frequency domain (a), pilot curves in time domain (b)
{Pure proportional damping model}

The output result, in the considered frequency range, shows with a considerable precision the similarity with the experimental curve. In fact, the lowest values of the valley is reached at 0.2 g, approximately. Subsequently, the controller produces an overshoot due to the extra acceleration imposed at the base of the shaker in order to re- reach the reference control profile in terms of “g”.

In addition, an important phenomenon appears and it is highlighted into the red circle: the beating of the control profile. Typically, this kind of event appears after the peak of an overshoot, from the control point of view, or after the peak of the notcher response. This beating phenomenon imposes an important discrepancy compared to the experimental results.

How introduced before, these curves come from the condensation procedure where the considered modes at 120 Hz of a single node located as in Figure 60 (b). For this reason the expected curve/result is acceptable into its “region of influence” where it express the highest contribution to the response, neglecting the frequency content up to 35 Hz in the related profile.

➤ Test 2: “Pure modal damping model”

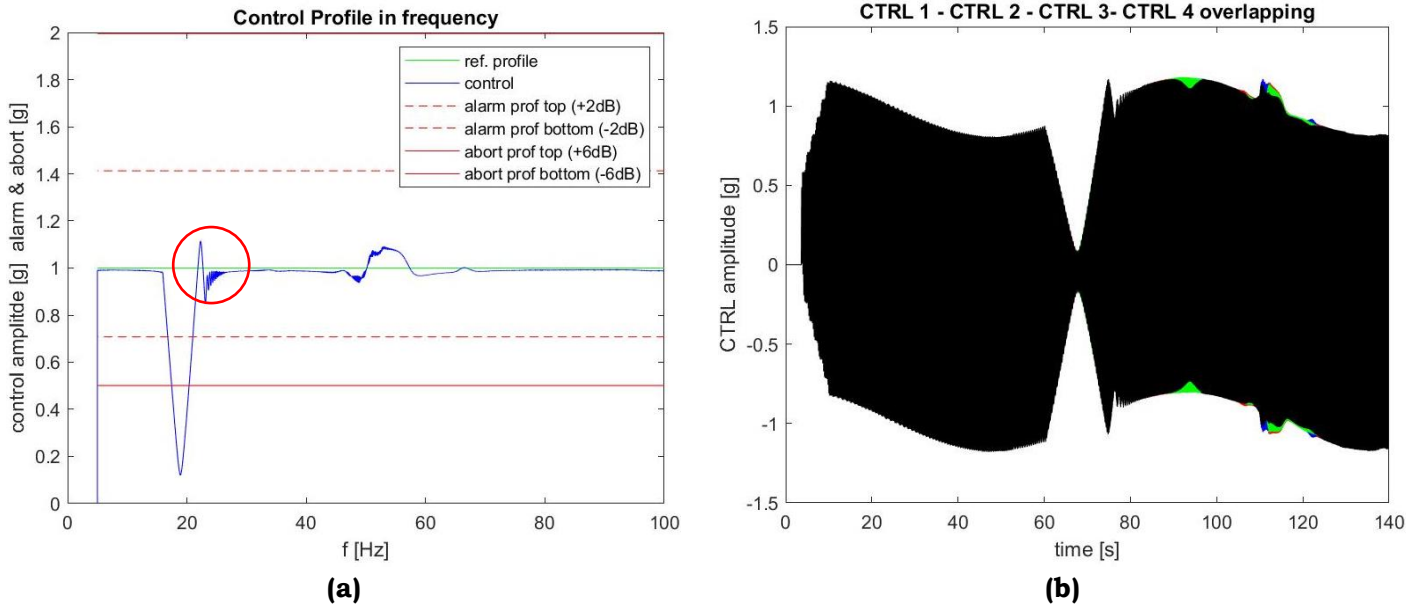


Figure 61: Acceleration control profile in frequency domain (a), pilot curves in time domain (b)
{Pure modal damping model}

Analogous consideration are effective for this case.

As well as for the previous case, the “pure proportional damping model”, a similar trend is reached by the “pure modal damping model” up to 40 Hz.

In fact, the unique discrepancy is related by the lowest peak value of the control profile at the IUT resonance. In this case its value is slightly lower 0.2 g.

In addition, the beating phenomenon occurs with deeper oscillations than before.

➤ Test 3: “Partial proportional Case 1”

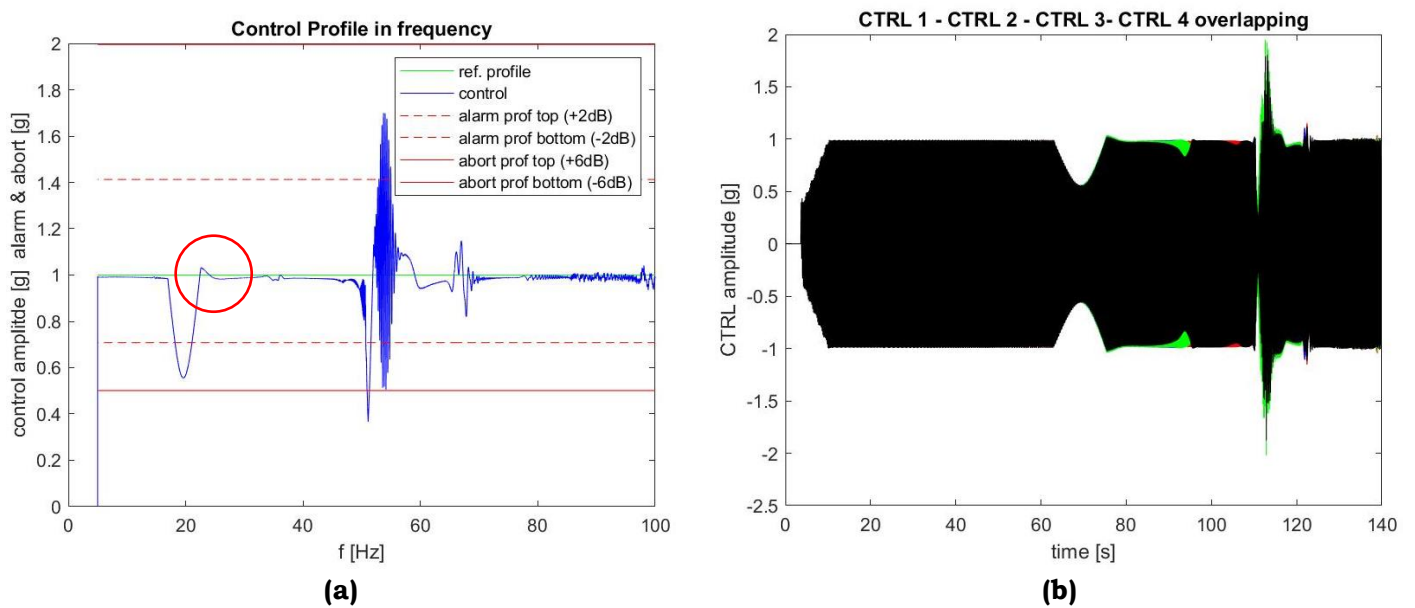


Figure 62: Acceleration control profile in frequency domain (a), pilot curves in time domain (b)
{Partial proportional Case 1}

“Partial proportional case 1” introduces significant differences. In fact, modelling the damping matrix, as composed by only physical DoFs, the lowest peak is very higher than the experimental value, reaching about 0.5 g. In addition, the beating after the overshoot disappear leaving place to the trend shown into the red circle highlighted into the red circle in Figure 62 (a). Particularly, this curve is very close to the experimental one, in term of trend and values.

➤ Test 4: “Partial proportional Case 2”

The control algorithm isn’t able to achieve convergence. In fact, the simulation goes for more than 20 minutes and it was stopped. On the contrary, the other considered simulations work for less the 5 min. Probably, the control algorithm isn’t able to perform the virtual test with this particular damping model.

➤ Test 5: “Partial proportional Case 3”

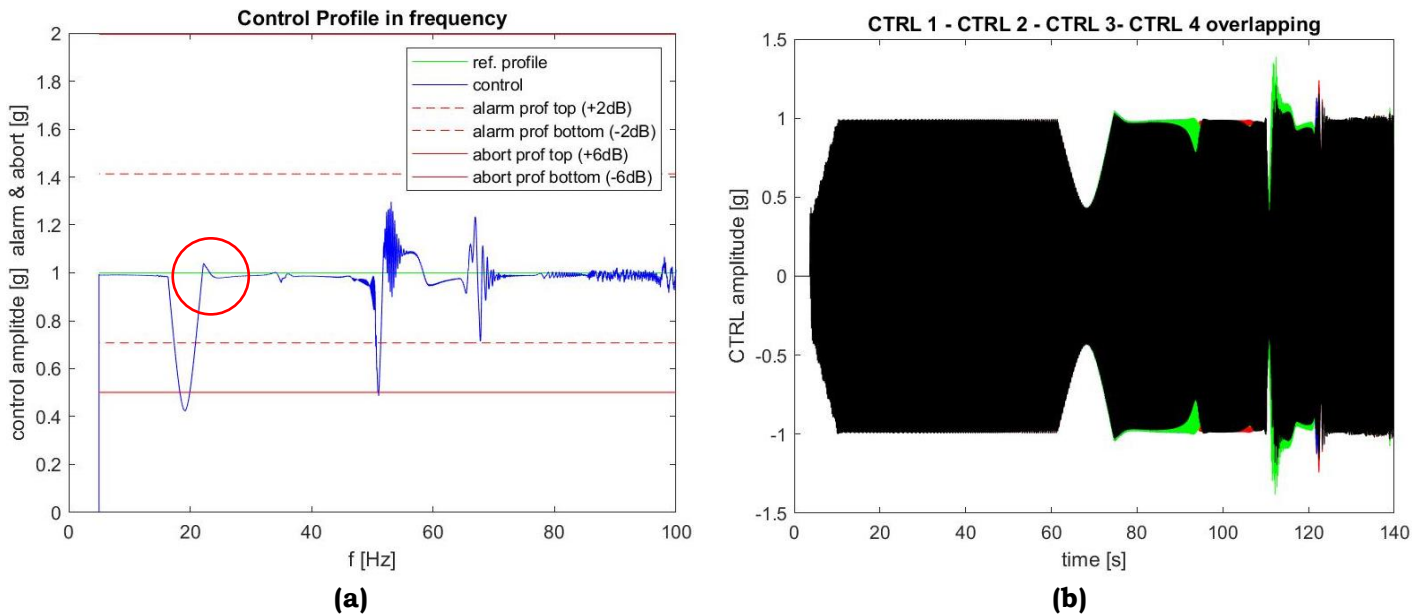


Figure 63: Acceleration control profile in frequency domain (a), pilot curves in time domain (b)
{Partial proportional Case 3}

Analogous consideration are effective for this case as well as for “Partial proportional Case 1”. In this case, the appreciable difference is the value of the lowest peak at which the control profile arrives in terms of acceleration profile. In fact, despite the comparison with the experimental curve shows a negative difference, the notching prevision gets better.

At the same time, the beating doesn’t appear, leaving place to a similar trend after the overshoot.

➤ Test 6: “Hybrid”

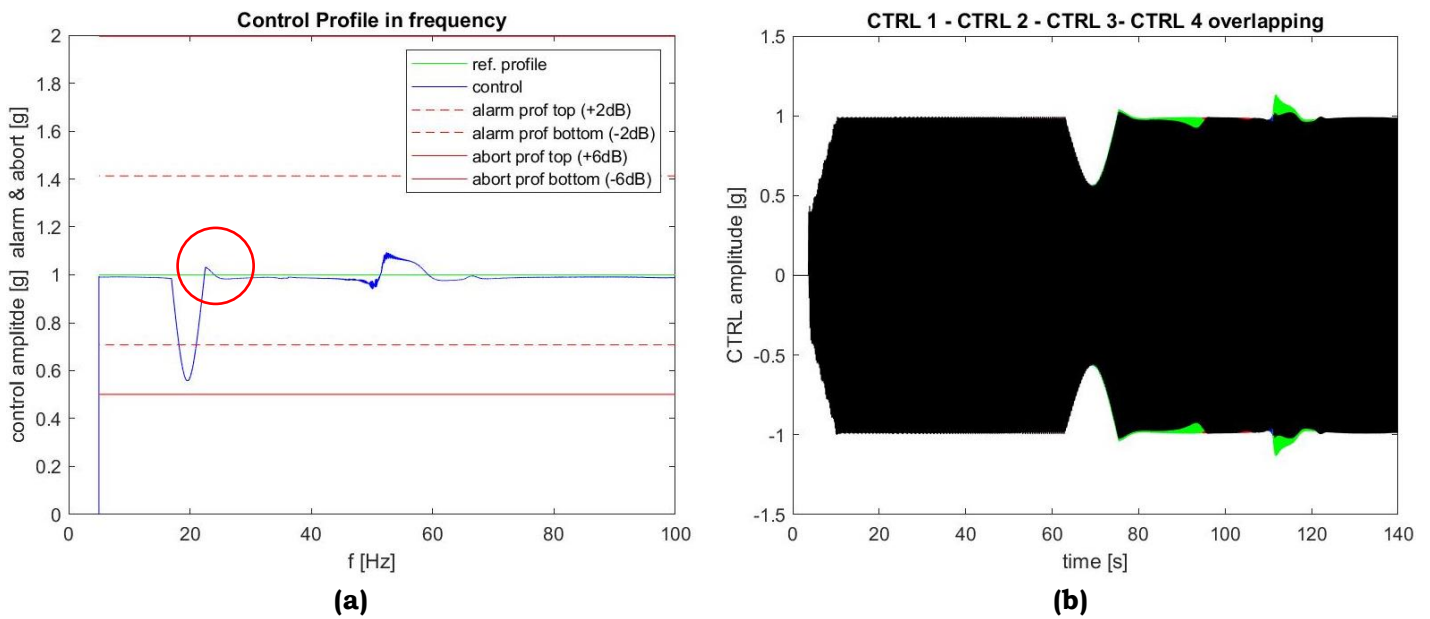


Figure 64: Acceleration control profile in frequency domain (a), pilot curves in time domain (b)
{Hybrid case}

The last damping model, the “Hybrid”, appears as a mix between “Partial proportional Case 1” up to 40 Hz and “Pure modal damping model” from the same value to the end of the considered range of frequency despite we are working up to 40 Hz.

In fact, the lowest peak is greater than 0.5 g and the overshoot peak, and its trend, are in accordance to the experimental curve.

10.2.2 Notch prediction updating using viscous damping models with mass and stiffness matrices from the condensed model

Next step into VST computational methodology development is the updating of the simplified model used in the previous paragraph.

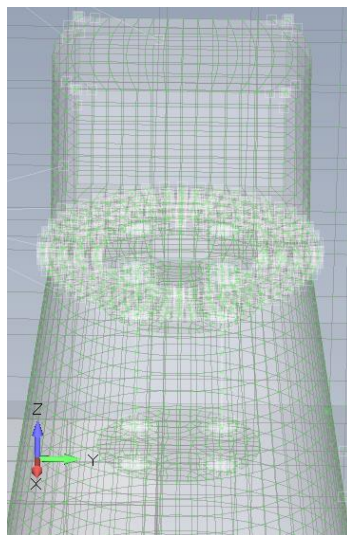
Particularly, this case considers the adjunction of other notchers located, as is shown in Figure 65 and Figure 66, using the comparison between the CAD model and a schematic drawing, without simulating a condensed node capable to resume the global effect of the upper stage of the IUT.

In addition, these notchers represent not only the accelerometers thanks to which is possible to measure the response of the structure, but they are involved during the condensation procedure using the Craig-Bampton method.

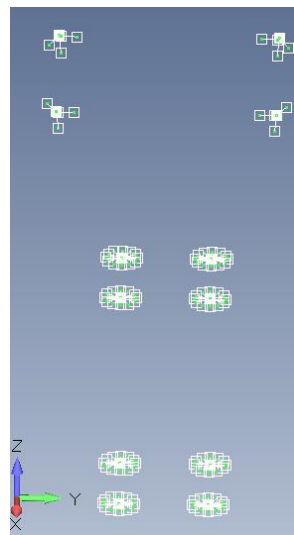
Practically, in this way, the mathematical model is more detailed than before being consistent with the physical model. For this reason, the frequency range is extended up to about 60 Hz after the second notch valley and the following overshoot.



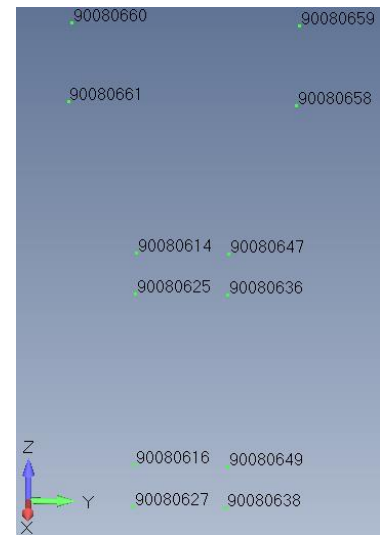
Figure 65: Location of the notching Dofs attached on the DTM structure



(a)



(b)



(c)

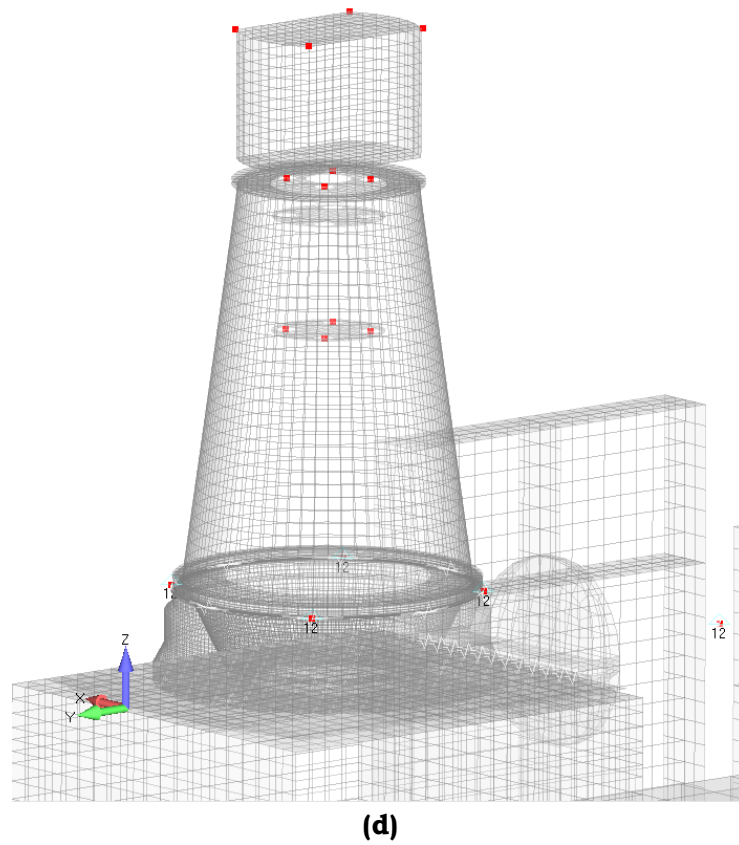


Figure 66: View of the DTM FEM model (a), nodes used for the dynamic condensation using Nastran superelements (b) and (c), global view of the structure with the nodes used for the condensation (d)

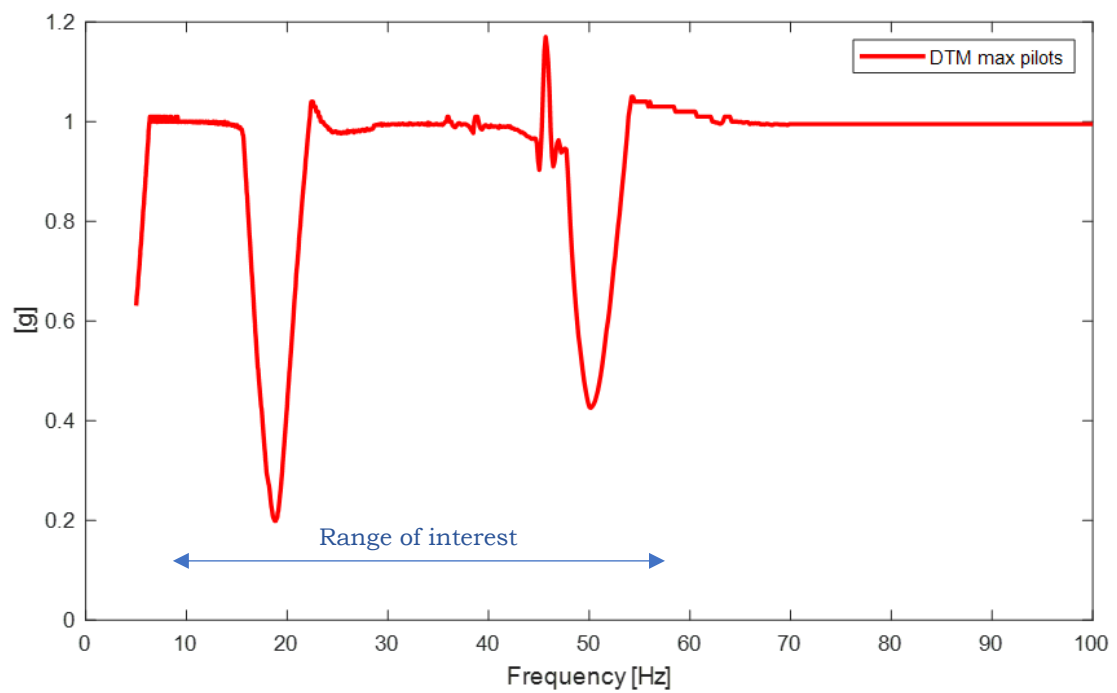


Figure 67: Frequency range of interest of the updating model

➤ Comparison and evaluation of different damping models

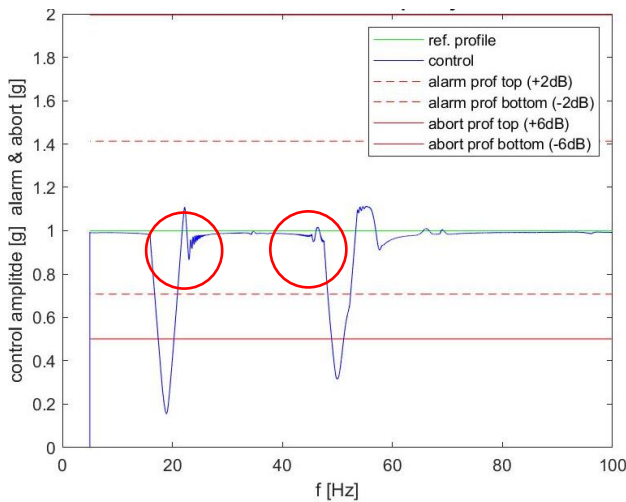


Figure 68: Pure proportional damping model

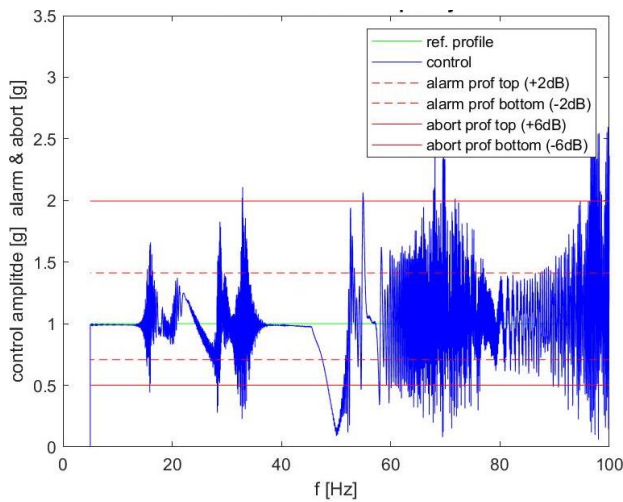


Figure 69: Pure modal up to 150 Hz

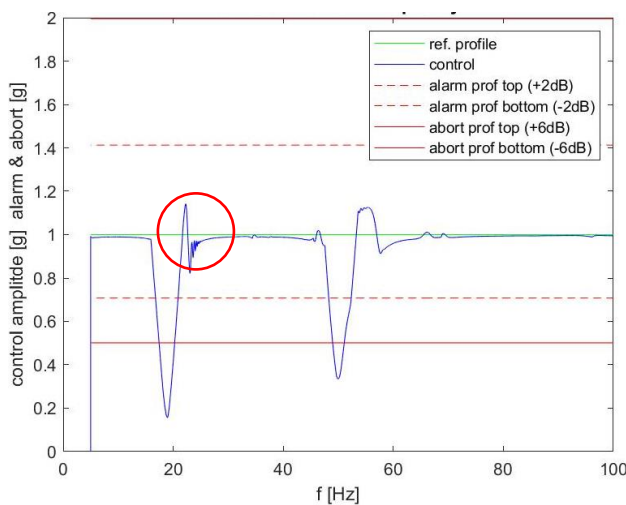


Figure 70: Pure modal up to 200 Hz

Using a “pure proportional” damping model is possible to reach the value of the first valley at the first resonance ($\approx 19\text{Hz}$) and the overshoot appears.

However, after the first overshoot, a beating phenomenon appears in contrast to what is shown by the experimental data.

Moreover, after a frequency range in which the acceleration profile is flat, another overshoot appears in accordance to the existing data.

The following valley of the second exceeding resonance ($\approx 50\text{Hz}$) reach a value slightly greater than the real datas.

In this case a “pure modal” damping model with a modal base up to 150 Hz is not sufficient in order to predict the dynamic behaviours of the structure. In fact the acceleration profile (unique term of comparison between the VST and the experimental data) is completely different appearing jagged, Figure 69. Probably, the analysis with this low modal base (i.e. included modes) are not sufficient for the dampen the motion.

For this reason, another condensed model has been developed considering a greater modal base, in this case up to 200 Hz, Figure 70.

Is evident how the acceleration profile becomes better, presenting a smooth curve. In fact, in this case the unique difference between the “pure proportional” expressed in Figure 68 is the trend of the beating after the first overshoot

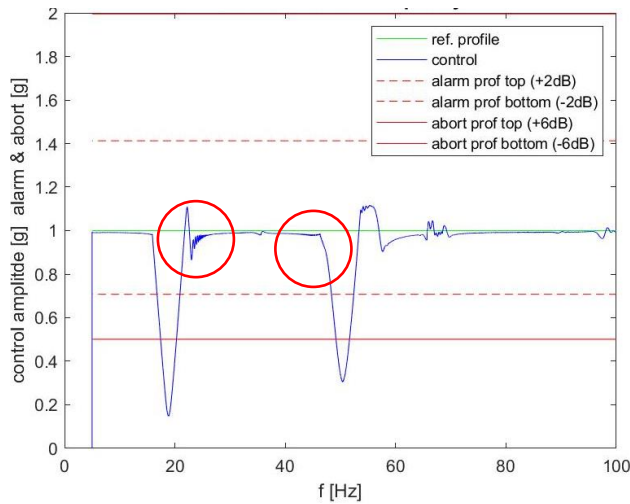


Figure 71: Partial proportional Case 1

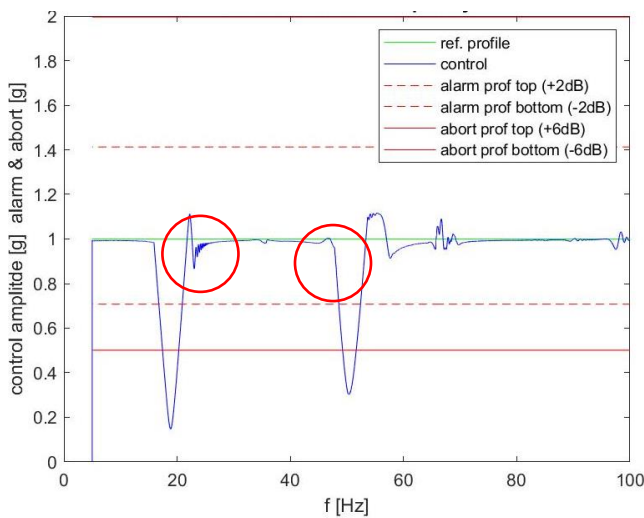


Figure 72: Partial proportional Case 3

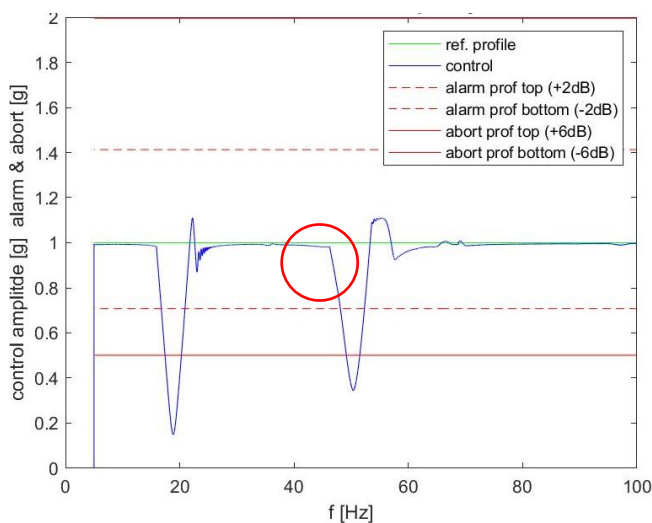


Figure 73: Hybrid model

The “Partial proportional Case 1”, in this case too, is able to predict the two main valley at $\approx 19\text{Hz}$ and $\approx 50\text{Hz}$.

However, using this damping model is possible to predict just the first overshoot, the second doesn't appears. In fact, the acceleration profile goes below the acceleration profile.

Also in this case, “Partial proportional Case 3”, the lowest peaks are reached but the overshoot at about 50 Hz doesn't appears. In fact, despite the acceleration profile has bending upwards, the curve doesn't exceed the reference profile.

Lastly, the “Hybrid” model, generates a smooth curve, but is not able to provide the overshoot before the second valley, as for “Partial proportional Case 1”.

However, as for the previous damping models, the two valley appear as expected.

As it possible to see, each damping model is able to predict the global behaviours of the structure in terms of the control profile.

This because the unique comparison manageable is between the control profile extracted by the real test and the VST. A detailed analysis based on notchers response (in time or frequency domain) is not available caused by the absence of the test curves.

However, the experimental curve and the VTS curves are in good agreement despite the presence of the beating after the first overshoot and the absence of the second overshoot before the second valley. Probably this overshoot requires many others point of condensation around a detailed location of the real model, in order to appear.

10.2.3 Notch prediction using structural damping matrix provided by NASTRAN

How introduced previosly, structural damping model is directly related to the displacement in frequency domain by means the imaginary unit. Infact, considering the structural damping force $f_{structural} = iGku$ is possible to deduce the equation (10.9)

$$K_{new} = (1 + iG)K + i \sum_1^{N_{elements}} G_e K_e$$

In which “K” is the stiffness matrix of the system.

Typically, this approach has a drawback: structural damping doesn’t allows its use during the transient response analysis (time domain analysis). For this reason is necessary to deduce and equivalent viscous formulation. However, usually this request is not trivial.

In fact, for a SDoF system, in frequency domain,

Force balance

Structural damping	$[-\omega^2 m + (1 + i\eta)k]x(\omega) = F(\omega) = [-\omega^2 m + i\omega c + k]x(\omega)$	Viscous damping
-----------------------	----------------------------------------------------------------------------------------------	--------------------

Then, is possible to deduce an equivalent formulation

$$\zeta = \frac{\eta \omega_p}{2 \omega} \tag{10.9}$$

Where ω_p is a resonant frequency. This is the so called “*modal equivalent viscous damping approach*”

However, in general, for a MDoF system, if the structural damping is constant and global

$$B = \frac{\eta}{\omega} K \tag{10.10}$$

The equivalent viscous matrix “B” is frequency dependent.

For the sack of clarity and completeness, an extraction of structural and viscous modal parameters, based on complex eigenvalues analysis, exists. Nevertheless, in this context is neglected.

In order to extract an equivalent viscous damping matrix, capable to reproduce the damping behaviours during the transient simulation, into the *Simulink Vibration controls* the K4AA

matrix will be take into account. Particularly, K4AA is the structural damping matrix provided by NASTRAN during the “op4” generation of the Craig-Bampton condensed model. It is a full matrix, due to the condensation procedure. However, in accordance to the theory, it is defined at a given frequency. This will be a significant point of weakness related to this methodology. In fact, despite the structural factor and the stiffness matrices are constant, “B” change in frequency. However, the Simulink vibration controls aren’t able to impose this change in frequency during the running simulation. For this reason, we assume as a contrast the K2AA.

To manage and treat the Craig-Bampton formulation coupled with the structural damping formulation is not trivial. In fact, recalling the equations in Table 24

$$K_s = \eta_g K + \sum_1^{N_{elements}} \eta_e K_e \quad (10.11)$$

Then is possible to write

$$M\ddot{x} + (K + iK_s)x = F + R \quad (10.12)$$

In accordance to this model, the Craig-Bampton formulation in terms of structural damping is

$$\begin{bmatrix} M_{rr} & L^T \\ L & [m_p] \end{bmatrix} \begin{Bmatrix} \ddot{x}_j \\ \ddot{\eta}_p \end{Bmatrix} + \left(\begin{bmatrix} \widetilde{K}_{jj} & 0 \\ 0 & <\lambda_p> [m_p] \end{bmatrix} + iD_{CB} \right) \begin{Bmatrix} x_i \\ \eta_p \end{Bmatrix} = \begin{Bmatrix} F_j \\ F_p \end{Bmatrix} + \begin{Bmatrix} R_j \\ 0 \end{Bmatrix} \quad (10.13)$$

Where

$$D_{CB} = \Psi^T K_s \Psi = \begin{bmatrix} D_{jj} & D_{jp} \\ D_{pj} & D_{pp} \end{bmatrix} \quad (10.14)$$

$$D_{jj} = K_{s_{jj}} + K_{s_{ji}} \phi_{ij} + \phi_{ij}^T K_{s_{ij}} + \phi_{ij}^T K_{s_{ii}} \phi_{ij} \quad (10.15)$$

$$D_{jp} = K_{s_{ji}} \phi_{ip} + \phi_{ij}^T K_{s_{ii}} \phi_{ip} \quad (10.16)$$

$$D_{pp} = \phi_{ip}^T K_{ii} \phi_{ip} \quad (10.17)$$

How introduced previously, structural damping is unadoptable for time dependent problems. For this reason, the following methodologies will be discussed in accordance to Ref. [34]:

- 1) Methodologies based on modal components
 - a) EqVD: equivalent viscous damping methodology
 - b) Decoupled methodology
- 2) Methodologies for assembled Craig-Bampton components at system level
 - a) SDCB methodology
 - b) System EqVD

In Table 26 the condensation strategy and the control parameters are recollected.

<u>Condensation strategy</u>		
Quantity	Description	
Number of FEM nodes	18	<ul style="list-style-type: none"> • 4: pilots • 1: bobine • 1: body • 12: on IUT
Number of degrees of freedom per node	2	Directions: x,y
Number of condensed DoFs	36	
Frequency band	0- 300 Hz	
<u>Control parameters</u>		
Quantity	Description	
Sweep rate [oct/min]	2	
Sweep mode	Log up	
Notch treshold [g]	3.9 (Y+)	
Estimation strategy	Harmonic	
Contol strategy	Maximun	
Tested frequency band	5- 100 Hz	
Compression factor	4	

Table 26: condensation and control parameters

➤ Methodologies based on modal components

The “*equivalent viscous damping methodology*” takes into account only the modal components related to the Craig Bampton formulation, considering that the matrix substructure I clamped. In this way the “EqVD Matrix” is deducted through the amplification factors at each natural frequency.

Then, considering the modal contribution of the equation (10.13) in case of mass normalized modes

$$I_{pp}\ddot{\eta}_p + \Lambda_{pp}\dot{\eta}_p + iD_{pp}\eta_p = \phi_{ip}^T F_i = f_p \quad (10.14)$$

Particularly, these modal DoFs are not decoupled caused by D_{pp} is complete and fully populated.

Assuming a sinusoidal response and excitation, is possible to desume the complex transfer function

$$H_{pp}(\Omega) = \frac{1}{-\Omega^2 I_{pp} + \Lambda_{pp} + iD_{pp}} \quad (10.15)$$

How introduced, this methodology defines an equivalent matrix starting from the amplification factors at each frequency. In this case, the point of interest is for the p^{th} diagonal term of the transfer function.

$$Q(\omega_p) = \frac{|H_{pp}(\omega_p)|}{1/\omega_p} \quad (10.16)$$

Lastly, the equivalent viscous damping coefficient

$$\zeta_{pth}^{eq} = \zeta(\omega_p) = \frac{1}{2Q(\omega_p)} = \frac{1}{2\omega_p^2 |H_{pp}(\omega_p)|} \quad (10.17)$$

And the “EqVD matrix”

$$\text{EqVD matrix} = B_{CB_{eqvd}} = \begin{bmatrix} 0_{jj} & 0_{jp} \\ 0_{pj} & \beta_{pp} \end{bmatrix} \quad (10.18)$$

In this way, the Craig Bampton formulation

$$\begin{bmatrix} M_{rr} & L^T \\ L & m_p \end{bmatrix} \begin{Bmatrix} \ddot{x}_j \\ \ddot{\eta}_p \end{Bmatrix} + \begin{bmatrix} 0_{jj} & 0_{jp} \\ 0_{pj} & \beta_{pp} \end{bmatrix} \begin{Bmatrix} \dot{x}_j \\ \dot{\eta}_p \end{Bmatrix} + \begin{bmatrix} \widetilde{K}_{jj} & 0 \\ 0 & <\lambda_p> [m_p] \end{bmatrix} \begin{Bmatrix} x_i \\ \eta_p \end{Bmatrix} = \begin{Bmatrix} F_j \\ 0 \end{Bmatrix} + \begin{Bmatrix} R_j \\ 0 \end{Bmatrix} \quad (10.19)$$

Typically, this approach is determined mode by mode and imply an important computational cost. In addition, damping has been neglected at the interface and the result depends on the modal truncation.

Other methodology is represented by *“the decoupled methodology”*. Its aim is to deduct, in this case too, the equivalent matrix focusing only on the modal components of K4AA considering the principal diagonal.

In this case, the following relationship exists

$$iD_{pp} = i\omega_p \beta_{pp} \quad (10.20)$$

Directly, the damping factor

$$\zeta_p^{dec} = \frac{\text{diag}(|D_{pp}|)}{2\omega_p^2} \quad (10.21)$$

Finally,

$$\text{Decoupled matrix} = B_{CB_{dec}} = \begin{bmatrix} 0_{jj} & 0_{jp} \\ 0_{pj} & \beta_{pp} \end{bmatrix} \quad (10.22)$$

➤ Methodologies for assembled Craig-Bampton components at system level

The first methodology considered is *“SDCB methodology”* (system damping Craig-Bampton). The idea is to consider the energy dissipation at the interface of the DoFs. The procedure foresees a viscous damping value related to these Dofs. Particularly, performing a normal modes analysis in order to extract a reduced modes base of “M” dimension

$$[-\omega^2 M_{CB_{SxS}} + K_{CB_{SxS}}] \phi_{SxM} = 0 \quad (10.23)$$

Projecting the damping matrix K4AA (or D_{CB}) on the modal base, dividing each diagonal term for the natural frequencies preserved on the modal part of K_{CB}

$$C_{CB_{MxM}} = \text{diag}(\phi_{MxS}^T D_{CB_{SxS}} \phi_{SxM}) * \text{diag}(\sqrt{\Lambda_{MxM}}) = \begin{bmatrix} 0_{6x6} & & \\ & \ddots & \\ & & 2\zeta_k \omega_k \\ & & & \ddots \end{bmatrix} \quad (10.24)$$

Where 0_{6x6} if the condensed model is in free-free conditions.

Using a product between matrix is possible to extract damping matrix in which are considered interface and modal damping respectively.

$$B_{CB_{SxS}} = M_{CB_{SxS}} * \phi_{SxM} * C_{CB_{MxM}} * \phi_{SxM}^T * M_{CB_{SxS}}^T \quad (10.25)$$

Finally, the last approach “*System EqVD*” is a combination between the EqVD and the SDCB. Practically, using a reduced modal base, we obtain new mass, stiffness and damping matrices as a projection of the extracted by the condensed modes. Moreover, using an analogous definition of transfer function is possible to deduce the damping factor. Then, built a damping matrix as in (10.25).

Performing a modal analysis as in (10.23), new matrices are derived using the projection

$$\bar{M}_{MxM} = \phi_{MxS}^T M_{CB} \phi_{SxM} = \bar{I}_{MxM} \quad (10.26)$$

$$\bar{K}_{MxM} = \phi_{MxS}^T K_{CB} \phi_{SxM} = \bar{\Lambda}_{MxM} \quad (10.27)$$

$$\bar{D}_{MxM} = \phi_{MxS}^T D_{CB} \phi_{SxM} \quad (10.28)$$

The complex transfer function

$$H_{pp}(\Omega) = \frac{1}{-\Omega^2 \bar{I} + \bar{\Lambda}_{pp} + i \bar{D}_{pp}} \quad (10.29)$$

Extracting the quality factor at each resonant frequency

$$Q_k(\omega_k) = \frac{|H_k(\omega_k)|}{1/\omega_k^2} \quad (10.30)$$

Then the equivalent damping coefficient

$$\zeta_k = \zeta(\omega_p) = \frac{1}{2Q(\omega_k)} = \frac{1}{2\omega_k^2 |H_{pp}(\omega_k)|} \quad (10.31)$$

And the equivalent viscous matrix

$$C_{CB_{MxM}} = \begin{bmatrix} 0_{6x6} & & \\ & \ddots & \\ & & 2\zeta_k \omega_k \\ & & & \ddots \end{bmatrix} \quad (10.32)$$

In this case too, the matrix in (10.32) depends on the modal truncation after the normal mode analysis.

Lastly, using (10.25) the equivalent viscous matrix at system level is obtained.

In term of notched curves of the pilots, the results in frequency domain

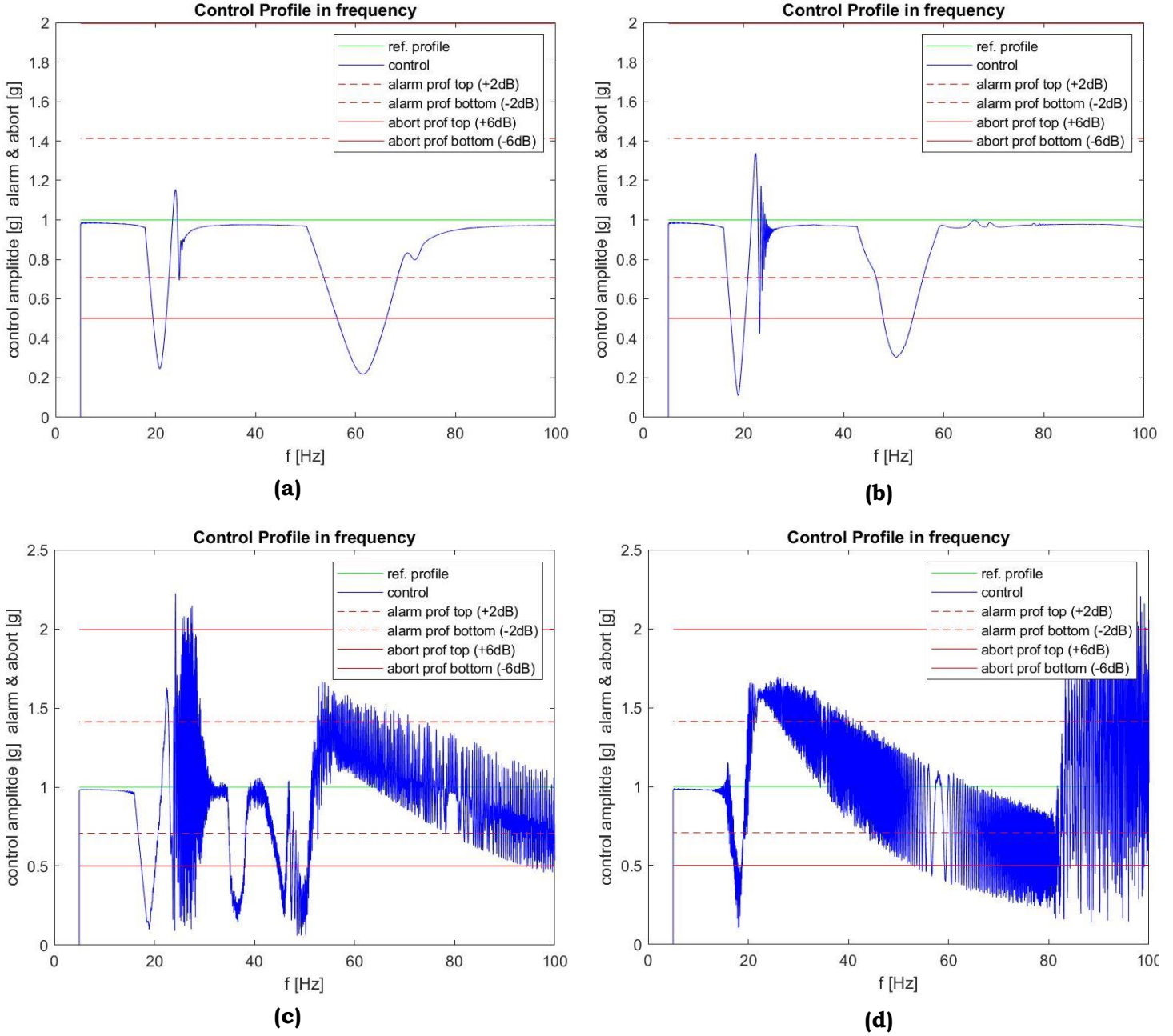


Figure 74: Pilots curves: EqVd on components (a), decoupled method (b), SDCB method (c), EqVd on system (d)

How Figure 74 (a), (b), (c), (d), show the influence of the damping model is not negligible. In fact, trying and applying increasingly complicated models step by step, the result worsens its correspondence with the experimental output. Figures (a) and (b), despite some global and local differences, are able to reproduce the first notch valley and the first overshoot above all. However, the present fictitious beating phenomena after the overshoot.

Interesting comparison, always between (a) and (b), is represented by the second valley: the “EqVD” methodology on components introduces a shift component thanks to which we could think that the resonance at which the notch threshold is exceeded is about 60 Hz, instead 50

Hz. In addition, this model doesn't capture the increasing trend after the second valley. Decoupled method is not affected by these two described problems.

Talking about of **(c)** and **(d)**, they are completely unable to reproduce and simulate the dynamic behaviours during the vibration test. Probably these damping models need a greater frequency span for the condensation in order to include many modes.

To sum up, the intense and deep activity about the implementation, development and characterization of damping models confirm that this is a very critical quantity. Working with viscous damping approach we build automatically the damping matrix starting only from mass and stiffness matrices extracted from Craig-Bampton model. In this environment, six damping models were tested. In term of average, all of these six models are adequate to reproduce the dynamic behaviours during the vibration test. Particularly, despite the despite its simplicity, a proportional damping is a proper option. Easy to build and not heavy mathematical calculus is requested. Using structural damping models, described before, the results are not completely sufficient despite four model were tested with

10.3 Evaluations based on several control and testing parameters

In this section some evaluations about the most influential control and electro- mechanical parameters are addressed in order to clarify the computational environment and prepare for future applications.

Condensation strategy	
Quantity	Description
Number of FEM nodes	18 <ul style="list-style-type: none"> • 4: pilots • 1: bobine • 1: body • 12: on IUT
Number of degrees of freedom per node	2 Directions: x,y
Number of condensed DoFs	36
Frequency band	1- 300 Hz
Control parameters	
Quantity	Description
Sweep mode	Log up
Notch treshold [g]	3.9 (Y+)
Estimation strategy	Harmonic
Contol strategy	Maximun
Tested frequency band	5- 100 Hz

Table 27: General parameters simulation independent

In Table 27 the parameters independent to the case of study are taken into account. They are valid independently to the aim of the simulation.

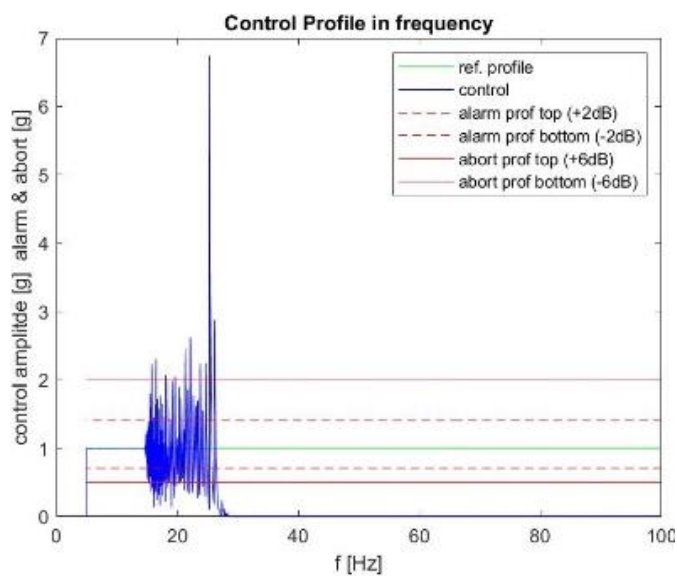
Basically, the main interest is to understand the effect on the response of the system related to the variation of the “compression facto,” “sweep rate”, “electrical parameters”.

In addition, the simplest damping model, the proportional is taken into account as fixed. Obviously, the solution, will change as explained in paragraph 10.2.

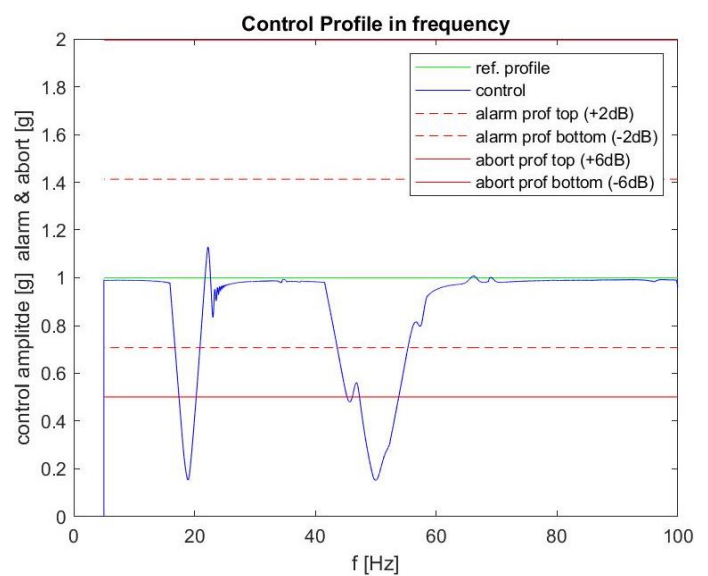
10.3.1 Influence of the compression factor

Fixed parameters		Parameter under test	
	Value		Test value
Sweep rate [oct/min]	2	Compression factor	0, 5, 10, 15, 20
Electrical parameters	• $R = 0.16 \text{ } [\Omega]$		
	• $L = 81 \text{ } [H]$		
	• $\mu_v = 38 \text{ } [V/(m/s)]$		
	• $\mu_F = 38 [N/A]$		

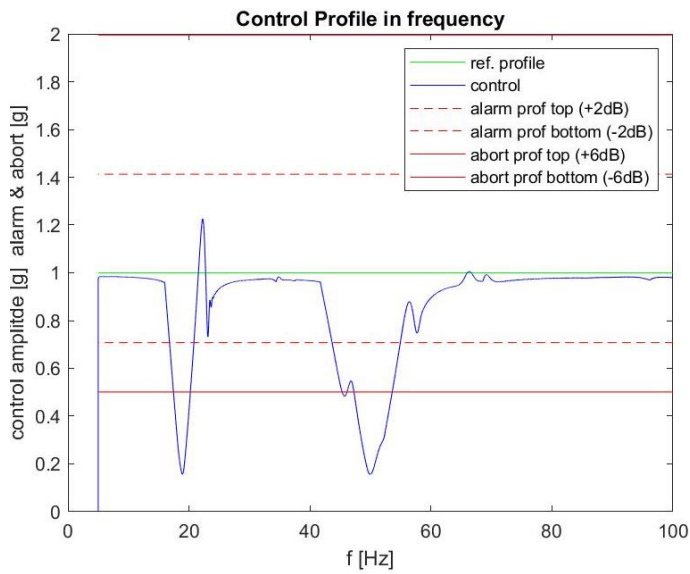
Table 28: Fixed and variable parameters, first case of study



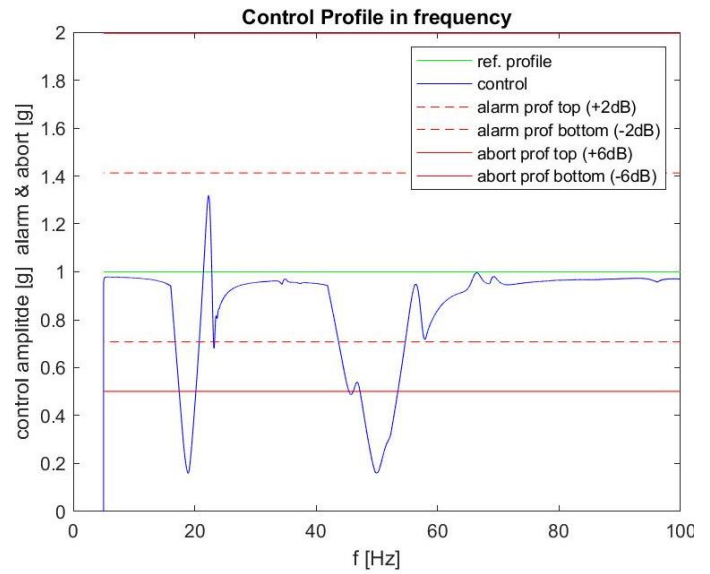
(a)
C=0



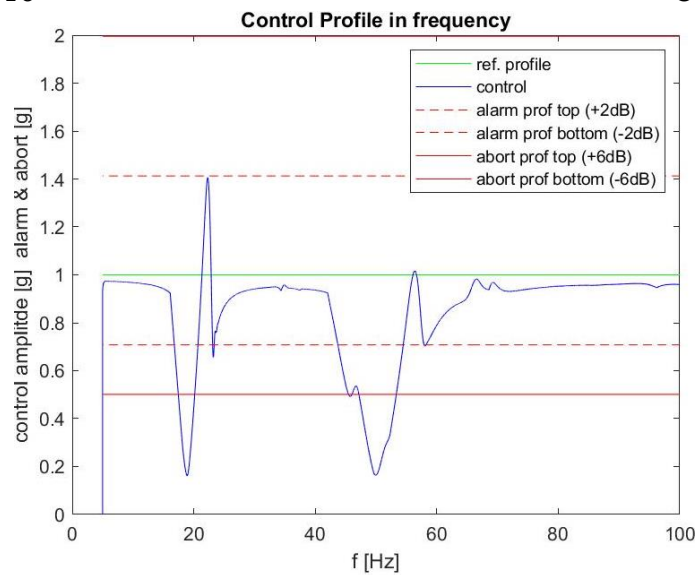
(b)
C=5



(c)
C=10



(d)
C=15



(e)
C=20

Figure 75: Analysis with variable compression factor.

The first important parameter of which is interesting to monitoring the effect on the system response is the compression factor. It works as a “filter”. If the compression factor is low, it guarantees better control. On the contrary, if the factor is high a better control (smoother spectrum) with less beating is reached.

Taken into account the curves from **(a)** to **(e)** we can observe that they change rapidly. Obviously, the first is not adequate to reproduce a VST. Practically it means that the system has no control.

The discussion about the curves **(c)**, **(d)**, **(e)** is difficult because they are related to an hypothetical VST considering a precise compression factor. We can monitor the variation of the curves but in these case we are performing another physical and virtual vibration test with other compression factors.

10.3.2 Influence of the sweep rate

Fixed parameters		Parameter under test	
	Value		Test value
Compression factor	4	Sweep rate [oct/min]	0.5, 1, 2
Electrical parameters	<ul style="list-style-type: none"> $R = 0.16 \text{ } [\Omega]$ $L = 81 \text{ } [H]$ $\mu_v = 38 \text{ } [V/(m/s)]$ $\mu_F = 38 \text{ } [N/A]$ 		

Table 29: Fixed and variable parameters, second case of study

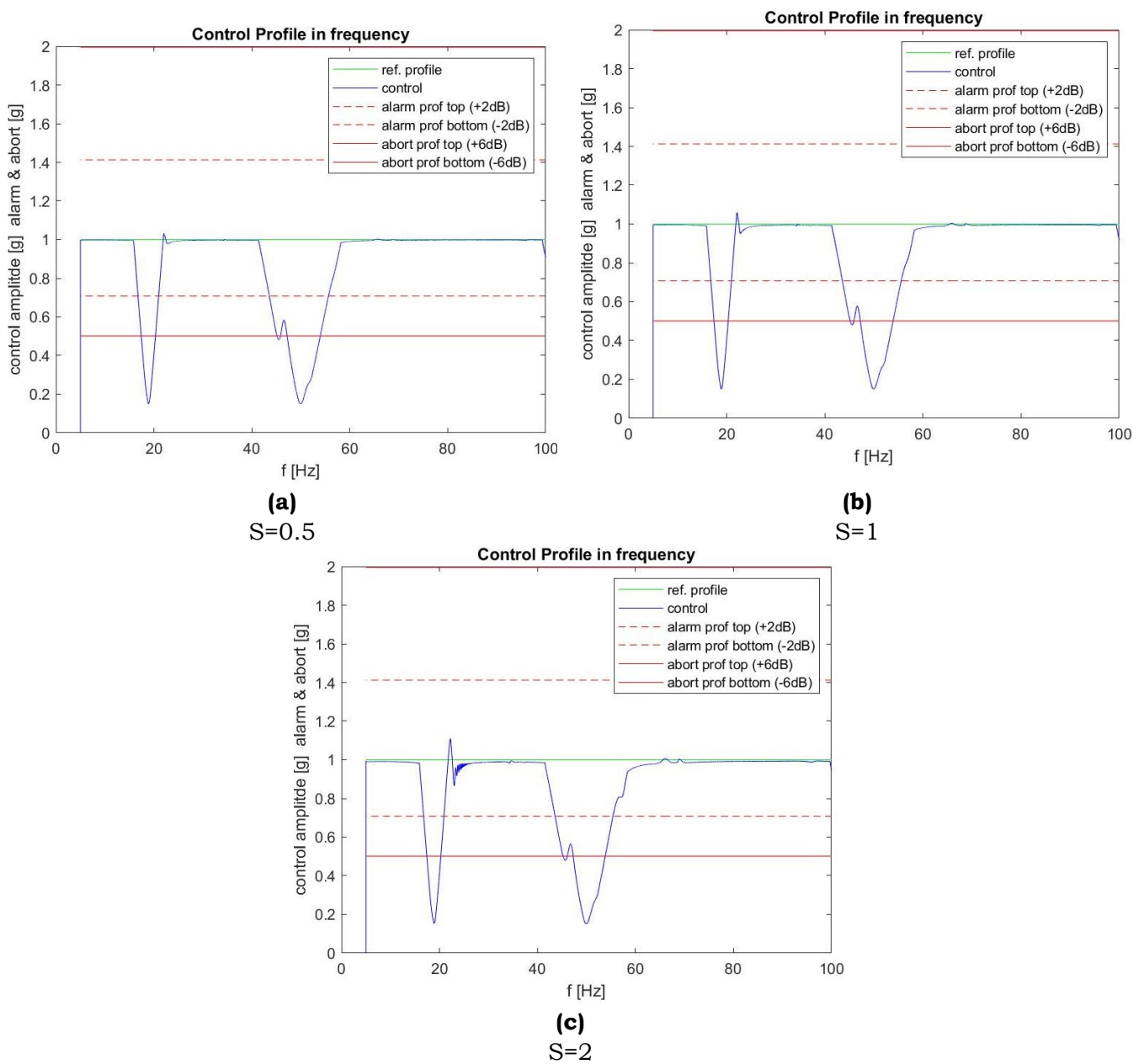


Figure 76: Analysis with variable sweep rate [oct/min]

After the compression factor, the sweep rate is one of the most important quantities during a vibration test, but also during a VST.

Basically, if the sweep rate is low the transient solution is “close” compared with the FRA. For this reason the frequency at which the peak value appears is close with the natural frequency identified during a FRA and normal modes.

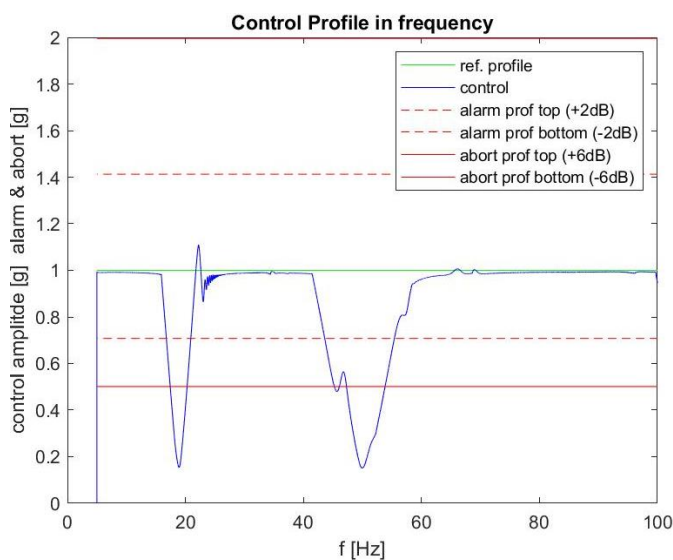
In these cases, the frequencies at which the peaks are minimum, they do not move visibly being the frequency response the exact quantity to measure.

In addition, is possible to see that when the sweep rate increase the shape of the first overshoot changes. Particularly, in case **(c)**, fictitious beating appears. Moreover, after the second valley, the dynamic system takes more time to reach the nominal reference value at 1 [g].

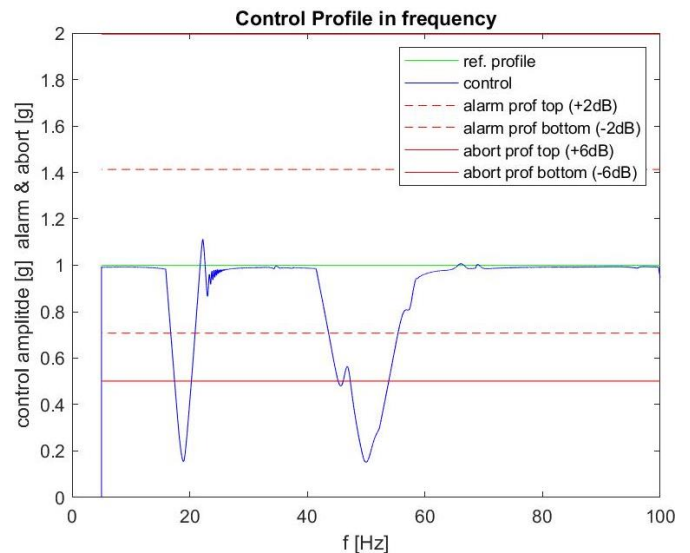
10.3.3 Influence of the electrical parameters

<u>Fixed parameters</u>		<u>Parameter under test</u>			
	<u>Value</u>	<u>Test values 1</u>	<u>Test values 2</u>	<u>Test values 3</u>	
Compression factor	4	Electrical parameters	<ul style="list-style-type: none"> R= 1.6 [Ω] L= 810 [H] μ_v= 380 [V/(m/s)] μ_F = 380 [N/A] 	<ul style="list-style-type: none"> R= 32 [Ω] L= 1620 [H] μ_v= 760 [V/(m/s)] μ_F = 760 [N/A] 	
Sweep rate [oct/min]	2				

Table 30: Fixed and variable parameters, third case of study



(a)



(b)

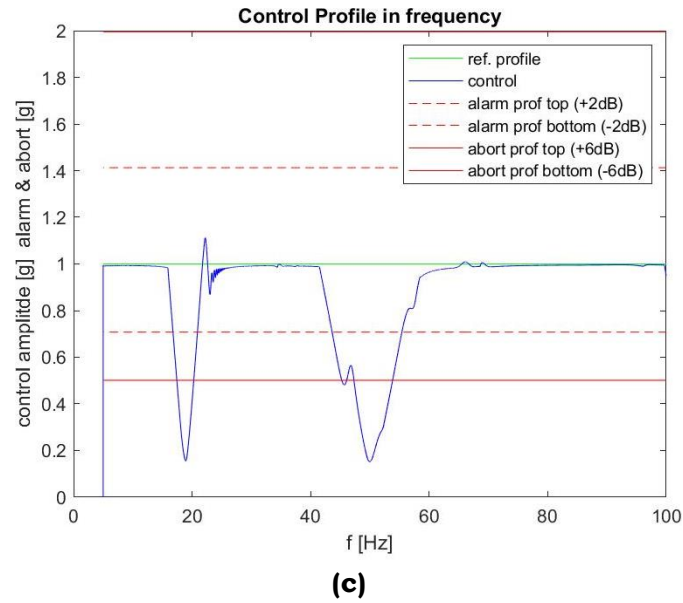


Figure 77: Analysis with variable electrical parameters

The electrical parameters seem a negligible quantity. In fact, considering three multiplicative factors (x_1 , x_{10} , x_{20}) we can affirm that the variation of the response in terms of pilot profiles is negligible. For this reason, for the following simulation we will consider the standard parameters as in “test values 1”.

However, the exact knowledge of these, related to a generic facility, they remove any doubts about possible errors due to incorrect input values

Chapter 11: Application of VST to a S/C and results

In this chapter the structural results in term of response profiles will be shown and provided using the practical background developed in the previous chapters. Due to property reasons, the analysed S/Cs are called “S/C_01” and “S/C_02”.

Differently from what developed in Chapter 10, in this case two real prediction are approached and take into account. Obviously, also in this case, will be necessary to consider some approximation, as for instance, for damping model and coefficients. However, the theory and approximation about “light damping structures” are valid and take into account. For this reason, damping values about 2% and 3% are considered.

11.1 Transient analysis into VST environment of S/C_01

In this paragraph the transient analysis using the VST approach will be discussed for S/C_01.

Briefly, some information about it. It is an Italian S/C and take part into a constellation of satellite. Its aim is to improve the quality of the images, enhancing the possibilities and capabilities of a higher number of images respect to a similar previous constellation. Figure 79 shows an extended view of the satellite with solar panel in open position.

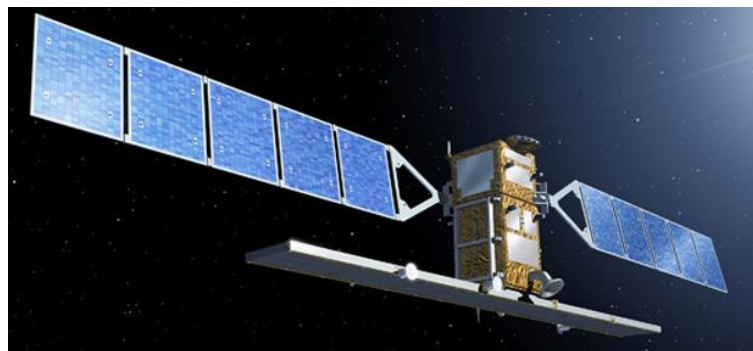


Figure 78: S/C_01 artist impression [Curtesy of spacenews.com]

In Table 31 and Table 32 the notching plan and the sine input level are reported. Here the fundamental instruction about how VST takes place are available.

Label	FEM ID node	Condensation DOFs	Global order	<u>Notch threshold /profile</u>
Pilot 1	129	123		<u>Sine input in Table 32</u>
Pilot 2	177	123		
Pilot 3	225	123		
Pilot 4	273	123		
Notcher 1	23262	123	1,2	4g on [5-10] Hz; 3g on [10-19] Hz; 4g on [19-100] Hz Along X and Y equally
Notcher 2	24223	123	3,4	4g on [5-10] Hz; 3g on [10-19] Hz; 4g on [19-100] Hz Along X and Y equally
Notcher 3	61363	123	5,6	3g on [5-100] Hz along X
Notcher 4	264495	123	7,8	11.2g on [5-100] Hz along X
Notcher 5	750121	123	9,10	5.5g on [5-100] Hz along X
Notcher 6	1316718	123	11,12	3.9g on [5-100] Hz along Y
Notcher 7	40159411	123	13,14	3.52g on [5-100] Hz along Y
Shaker Body node	90021845	123	15,16	NA
Bobine node	90021846	123	17,18	NA

Table 31: Notching plan for "S/C_01"

Frequency range [Hz]	Level [g]
5 – 20	0.78
20 – 40	0.52
40 – 100	0.4

Table 32: Proposed sine input level along X and Y axis

How is possible to see, according to the notching plan, the considered notchers could notch along X and Y direction during the VST along X or Y. For this reason, for instance, if the VST is performed along the Y direction, one or more notcher could notch along X direction, and vice versa.

In addition to the notching plan, other important instruction and information about the VST run are available on Table 33.

Quantity	Value
Compression factor	4
Sweep rate [Oct/min]	4
Damping model	$f_1 = 20 \text{ Hz} \rightarrow \zeta_1 = 5\%$ $f_2 = 100 \text{ Hz} \rightarrow \zeta_2 = 3\%$

Table 33: Further instruction about S/C_01 VST

For simplicity reasons, “proportional damping” is taken into account.

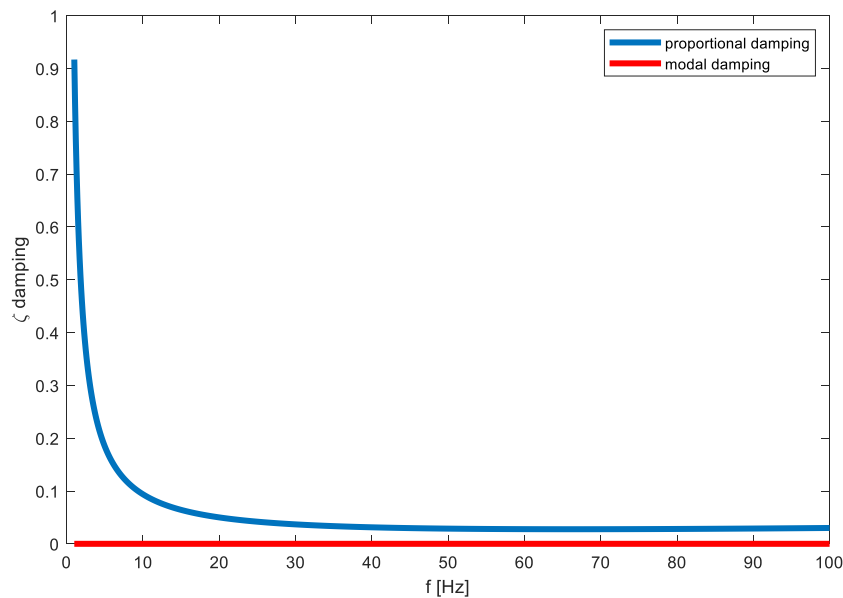


Figure 79: Damping ration for S/C_01

In addition, despite the sine input table requires that the input vary instantaneously at 20Hz and 40Hz, the analysis (along X and Y respectively) are performed considering 3 unique sine input level for all the frequency span. In this case the response is the one that is competence of sine input considered.

This approach is due to a “limit” of Simulink model that doesn’t allows that the input vary at a given frequency, but it requires a constant level input.

In fact, the simple application of a required input into its frequency range (e.g. 0.52 g between 20 Hz and 40 Hz) did not keep track and memory of the time history previously followed.

11.1.1 S/C_01 notching prediction using H.M. boundary conditions

First of all, in case of H.M. condition, i.e. neglecting the contribution of the shaker, its characteristics and devices, using the normal modes analysis (SOL 103) the natural frequencies, mode shapes and modal effective masses, are extracted. In Table 34 the main

contributions to the effective masses, where only the most severe behaviours are highlighted in yellow.

Is easy to recognise that the main contributions are provided by the first three modes along three different axes: bending mode on X, bending moment on Y and torsional mode on Z. Respectively, the first one involves 59.2% of mass (14.6 Hz), the second 63% (14.2 Hz) and the third 84.5% (24.63 Hz).

For this reason, the primary notch, along each axis, is applied in order reduce the magnitude of bending and torsional moment along the involved axes at S/C-shaker interface.

Subsequently, the other main contributions in terms of effective masses (mode 6th, 9th and 11th) are secondary notch in which the aim is to preserve the integrity of the equipment without overtested.

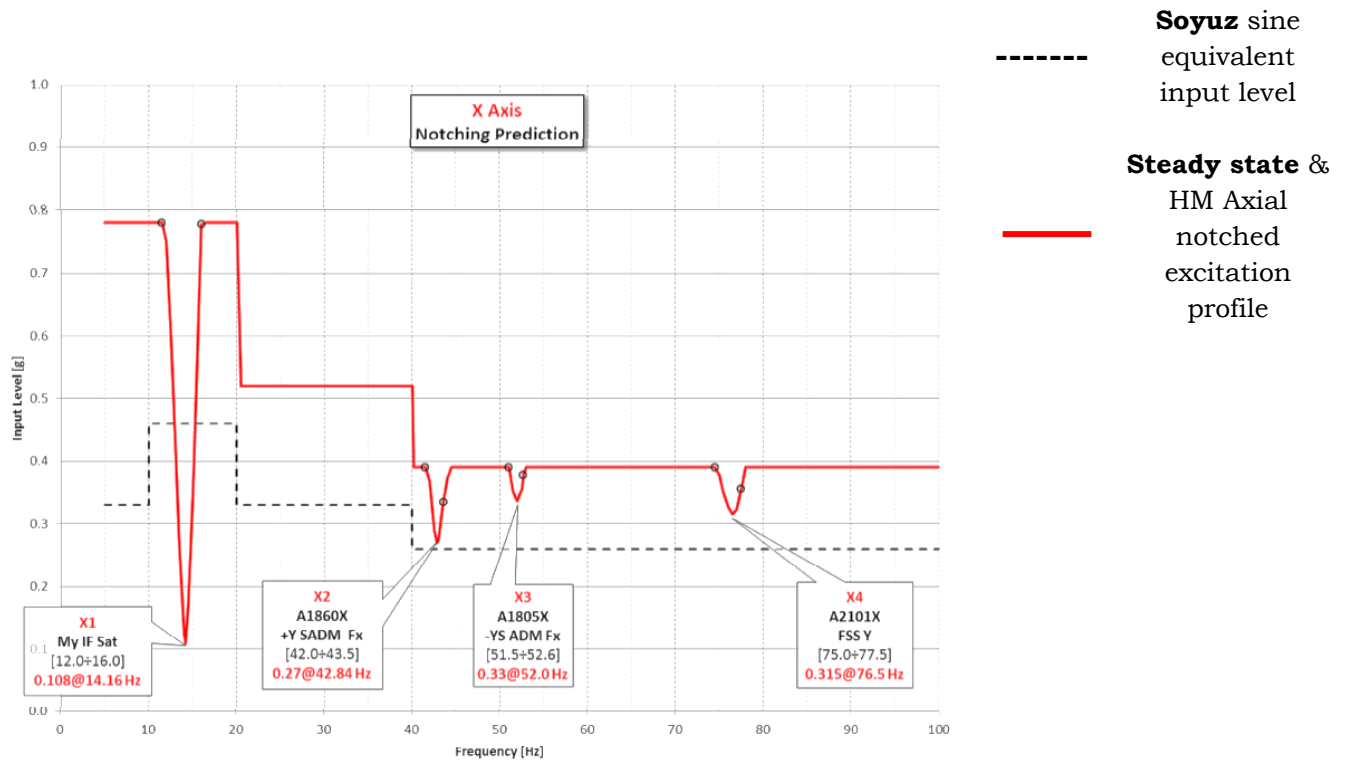
Our future purposes, in terms of VST analysis, are based only for X and Y direction because along them the coupling phenomena appear.

Mode #	Freq. [Hz]	M _{xx}		M _{yy}		M _{zz}		I _{xx}		I _{yy}		I _{zz}		Description
		[Kg]	[%]	[Kg]	[%]	[Kg]	[%]	[Kg·m ²]	[%]	[Kg·m ²]	[%]	[Kg·m ²]	[%]	
1	14.16	1237.6	59.2%	70.7	3.4%	0.0	0.0%	505.8	5.1%	9689.7	93.4%	0.2	0.0%	S/C Main Lateral Mode Along X Axis
2	14.20	67.5	3.2%	1317.4	63.0%	0.0	0.0%	9279.2	93.2%	517.7	5.0%	0.6	0.0%	S/C Main Lateral Mode Along Y Axis
3	24.63	0.0	0.0%	0.0	0.0%	0.0	0.0%	0.0	0.0%	0.1	0.0%	1151.0	84.5%	S/C Main Torsion Mode around Z Axis
4	37.70	0.6	0.0%	0.0	0.0%	0.0	0.0%	0.0	0.0%	0.5	0.0%	0.5	0.0%	STT Support IP (X-Y) Bending
5	40.18	0.0	0.0%	0.4	0.0%	4.7	0.2%	0.8	0.0%	0.0	0.0%	0.0	0.0%	FSS Support OOP Bending
6	42.84	293.4	14.0%	0.3	0.0%	5.2	0.3%	4.5	0.0%	52.2	0.5%	1.2	0.1%	SAR Lateral Panels OOP + SAW IP + SADM OOP 2nd S/C Lateral Mode along X Axis
7	43.56	59.3	2.8%	2.9	0.1%	1.1	0.1%	34.0	0.3%	15.4	0.1%	0.0	0.0%	SAR lateral Panels IP + SAW OOP
8	44.64	6.2	0.3%	0.1	0.0%	3.1	0.1%	0.0	0.0%	1.0	0.0%	77.2	5.7%	
9	46.34	2.6	0.1%	0.2	0.0%	989.9	47.4%	0.3	0.0%	0.7	0.0%	3.0	0.2%	S/C Main Longitudinal Mode along Z Axis
10	46.72	0.1	0.0%	0.1	0.0%	210.8	10.1%	0.1	0.0%	0.0	0.0%	6.5	0.5%	
11	48.00	1.9	0.1%	214.2	10.2%	1.7	0.1%	47.4	0.5%	0.8	0.0%	1.6	0.1%	2nd S/C Lateral Mode along Y Axis
12	48.59	0.0	0.0%	33.9	1.6%	2.0	0.1%	11.9	0.1%	0.4	0.0%	11.2	0.8%	
13	48.97	0.7	0.0%	28.0	1.3%	18.5	0.9%	6.2	0.1%	0.2	0.0%	0.4	0.0%	SADA +Y
14	49.89	0.1	0.0%	7.5	0.4%	3.5	0.2%	0.5	0.0%	0.8	0.0%	0.5	0.0%	SADA -Y
15	50.80	26.3	1.3%	2.3	0.1%	0.0	0.0%	0.9	0.0%	11.0	0.1%	7.0	0.5%	SAWs OOP Out of Phase

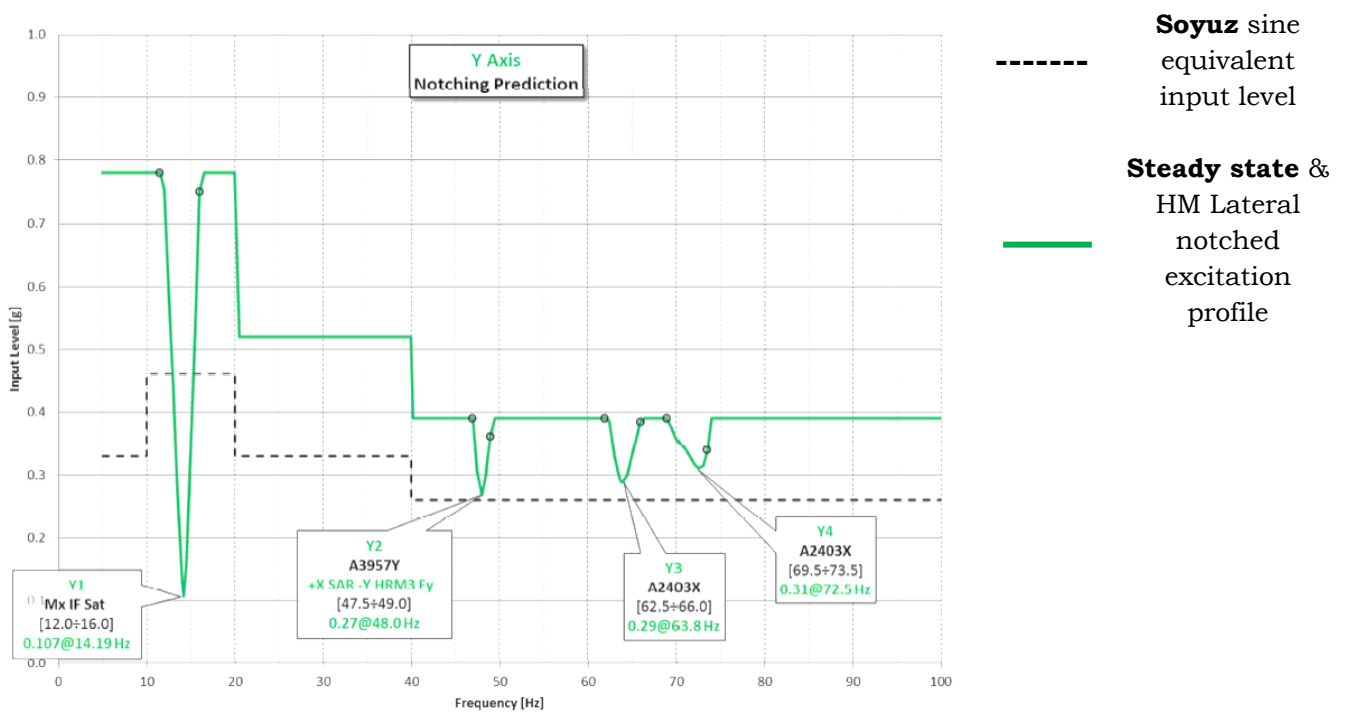
Table 34: Modal effective masses with the main contributions

In Figure 80 the HM sine prediction based on steady state approach, are provided.

In dashed black curve the Soyuz sine equivalent input level



(a)



(b)

Figure 80: Hard Mounted (HM) sine prediction, X (a), Y (b)

	Frequency requirement	S/C_01 PFM Prediction
First lateral mode	>15	14.16
First Longitudinal Mode	>35	43.6

Table 35: Frequency requirement imposed by the launcher and S/C_01 PFM Prediction

Lastly, the following VST analysis for S/C_01 are based on the accelerations criteria described in 6.2. In this case, primary and secondary notch appears caused by their overcoming with respect certain thresholds.

11.1.2 S/C_01 VST along Y direction

After the setup and definition of the analysis in terms of matrix extraction from the “.op4” file, conversion into the state space (continuous and discrete) system and imposition of the control parameters, the VST provides the results, in terms of acceleration profiles of the pilots reported in Figure 81, and the response in frequency of the notchers. Particularly, in this case, only the notched notchers are shown in Figure 82

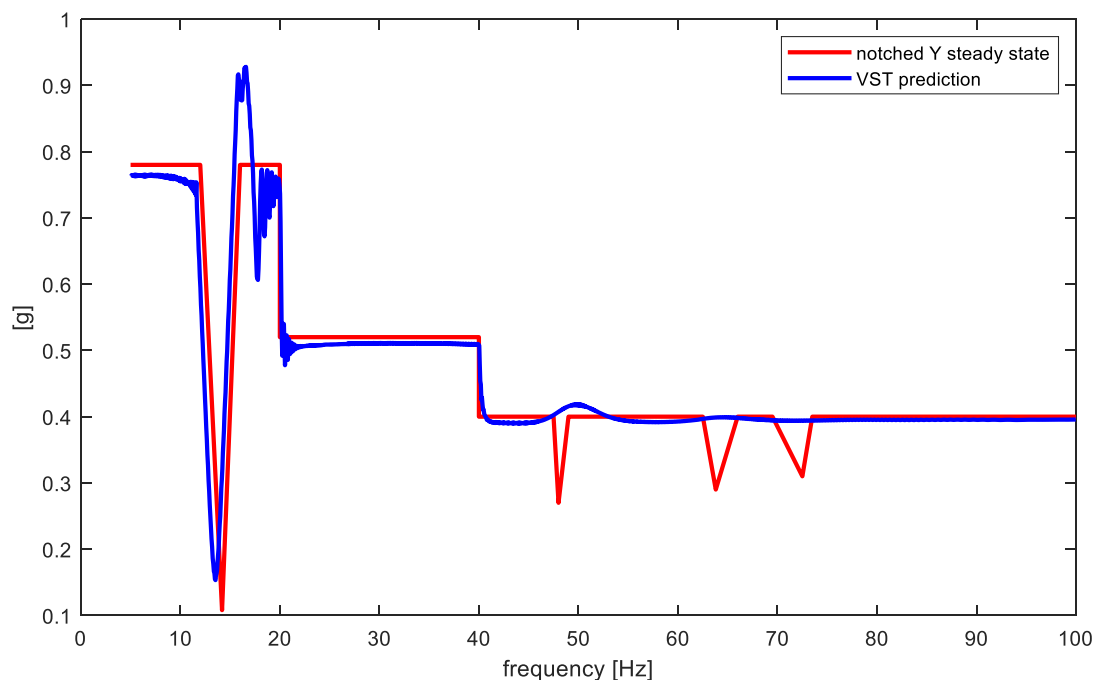


Figure 81: Pilot curves during VST along Y direction of S/C_01: comparison with steady state

Is easy to observe that the most critical excitation, from the notchers point of view, is 0.78g during which a primary notch appears at about 13.47 Hz. Common issues as overshoot and beating appear. Particularly, how is well known the FRA analysis do not take into account the overshoot, and also the beating, after the increasing to the nominal input (0.78g) related to the primary notching. The VST analysis predict an overshoot up more than 0.9g. Subsequently, an important beating occurs after the overshoot itself.

Another interesting phenomenon is represented by the fact that the VST assumes no notching than predicted by the FRA between 40-100 Hz. This could be related to the sweep rate effect that at high frequencies imposes less excitation, in terms of time, to the critical frequencies of the structure, and to the damping model. In this case the imposed structural damping to the FEM model is difficult to reproduce by a global model as into the VST environment.

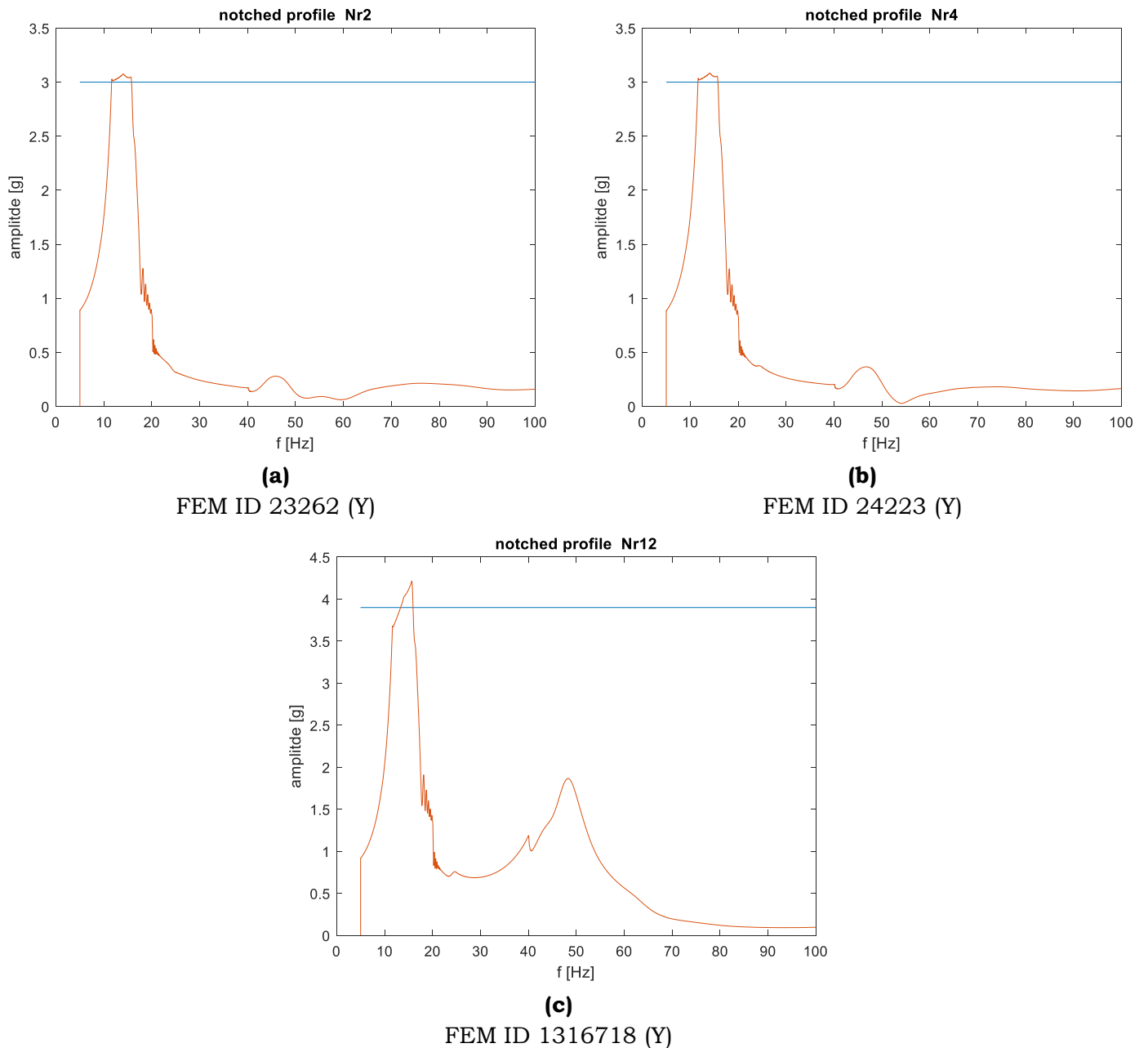


Figure 82: Notched responses for Sine Y

In Figure 82 the notched response of the notchers are shown. Due to is a transient like phenomenon, when the notching threshold is exceeded the control algorithm imposes the control actions in order to reduce the response of the structure. Then the overshoot on the notchers responses occur.

11.1.3 S/C_01 VST along X direction

Using the same approach adopted for VST along Y direction, the VST analysis along X is performed.

In Figure 83 the extracted results for pilots oscillations are shown.

First of all, the frequency at the lowest value for the notch valley is 13.47 Hz, as for VST on X, with a value equal to 0.15g. The related overshoot has its max value at 16.59 Hz with a value equal to 0.92g. Moreover, the input at 0.52g between [20 - 40] Hz is flat as for the Y VST case of study.

Lastly, from pilots point of view, with 0.4g of input, different control overshoots appears despite the notch valleys are absent with respect to the steady state prediction.

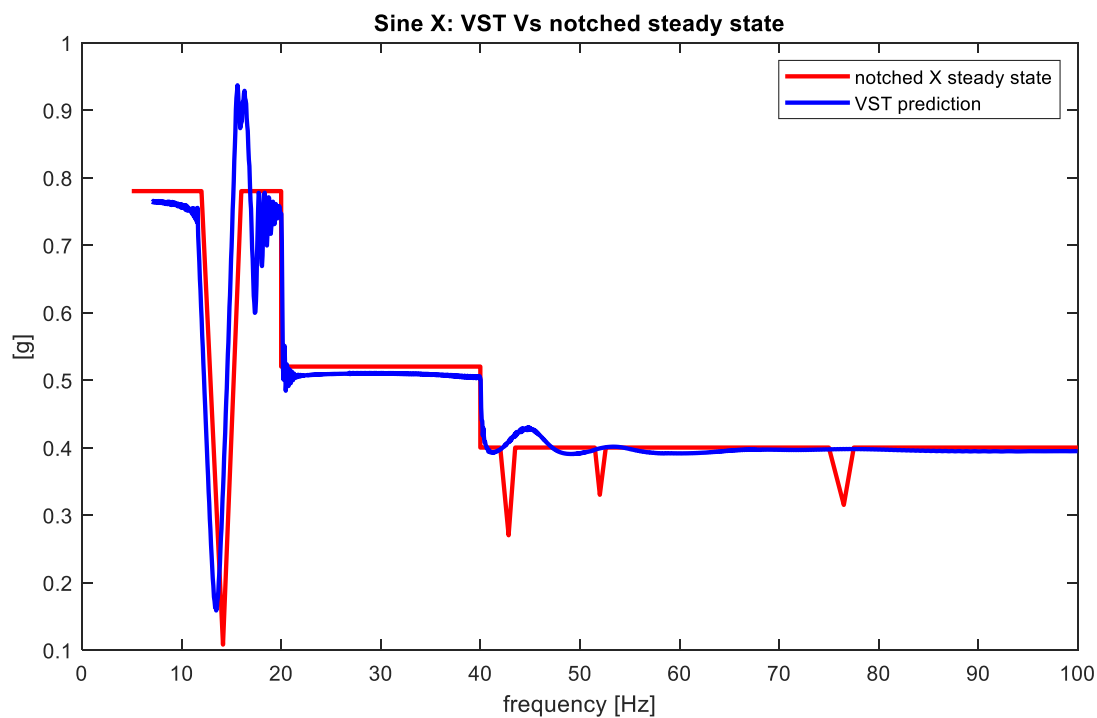


Figure 83: Pilot curves during VST along X direction of S/C_01: comparison with steady state

These notch absences are probably related to the sweep rate and the adopted damping model, as for VST along Y. Particularly, at high frequencies the damping is very “hard” and the response is dramatically reduced. In fact, due to the transient phenomena, we expected more oscillation to high frequencies.

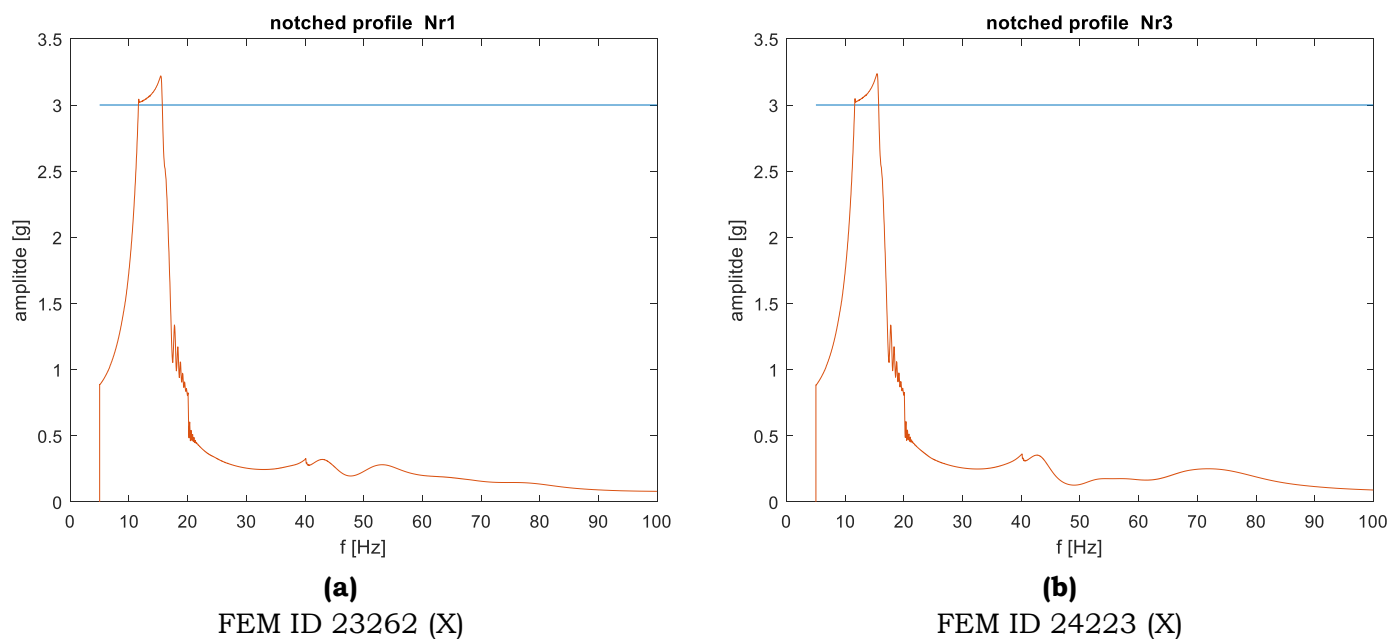
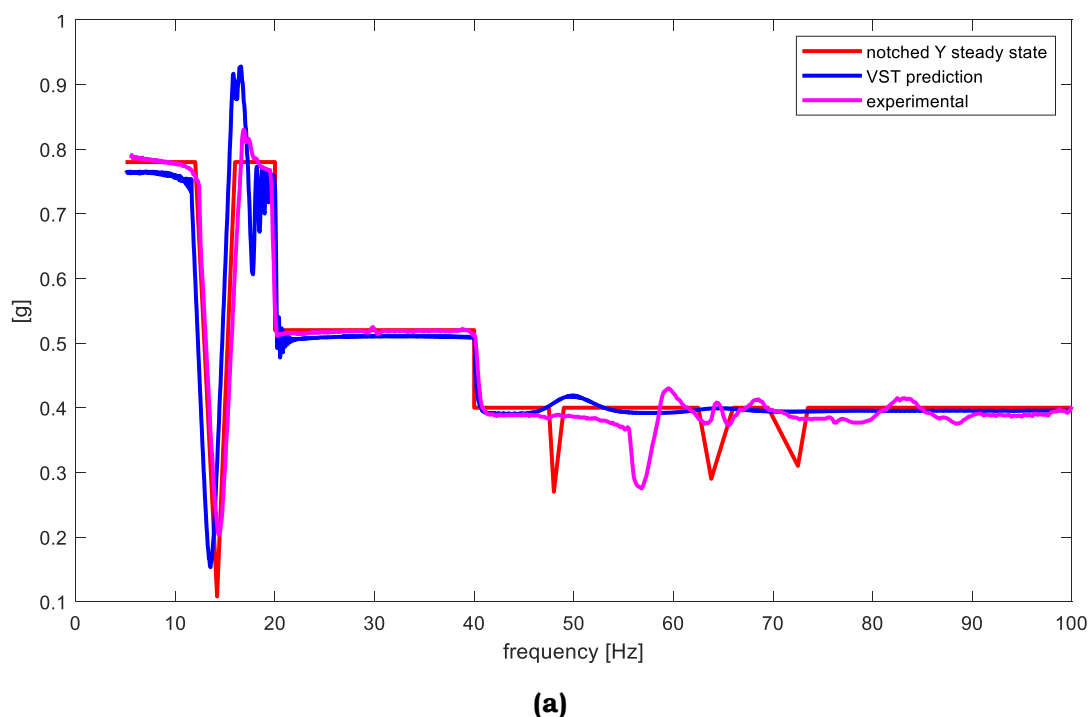
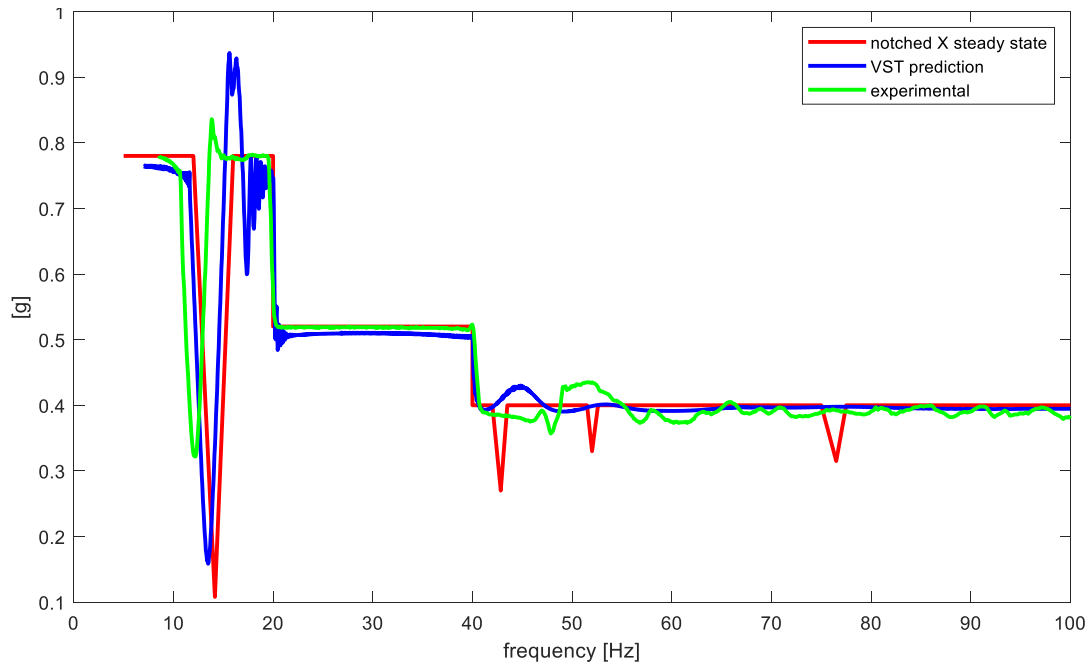


Figure 84: Notched responses for Sine X

The notched response of some DoFs are shown. Also in this case, due to the threshold exceeding the control algorithm imposes the control actions capable to reduce the response at the critical frequency. An overshoot appear with a similar value equal to 0.25g with respect to the threshold fixed at 3g.

11.1.4 S/C_01 Comparison between notched input from FRA, VST prediction and experimental test results





(b)

Figure 85: Notched steady state HM Vs VST prediction Vs experimental test: Sine Y (a), Sine X (b)

In this section we will discuss about the comparison between the experimental data from test Vs the FRF and VST analysis.

Firstly, talking about the VST along Y Figure 85 (a) the three curves are in good agreement in term of primary notching. Table 36 shows numerical results for primary notching prediction.

	Frequency [Hz] at notching	Valley [g] at notching	Frequency [Hz] at peak overshoot	Value [g] at peak overshoot
FRF with HM conditions	14.16	0.108	<u>Not expected</u>	<u>Not expected</u>
VST	13.47	0.15	16.59	0.93
Experimental	14.31	0.204	16.84	0.83

Table 36: Sine Y comparison between experimental, VST and FRA with HM conditions

Subsequently, the overshoot appears in VST and experimental result, but obviously not expected by the FRA caused by is a steady state analysis. Is possible to see that the overshoot is shifted in frequency between VST and experimental, reaching the peak how is shown always in Table 36.

A beating phenomenon is expected by the VST, probably caused from damping model, is absolutely absent into the real vibration test. However, VST analysis and the experimental are

able to follow the step input at 20 Hz, and the flat one from 20 Hz to 40 Hz. Nevertheless, the main criticality is represented by the trend from 40 Hz to 100.

Is easy to recognize that the three profile are very different between them. The red profile, based on the FRA, predicts three notch valleys at different frequencies. On the other hand, the VST suppose the absence of the notching, oscillating around to the input profile. The real difference is represented by the test curve. The control system had the need to notch at 56.81 Hz. This is an unexpected behaviour of the structure.

A possible reason and explanation mostly lies on the stiffness, but also to the and damping of the real structure. In fact, notching frequency depends on natural frequencies who themselves depends on mass and stiffness. Mass is not a critical quantity, but stiffness it is caused by the uncertainty.

This could mean that the real structure is more rigid around that frequencies that move the natural frequencies.

Secondary, talking about the VST along X Figure 85 **(b)** the three curves are not in good agreement in term of primary notching. Table 37 shows numerical results for primary notching prediction.

	Frequency [Hz] at notching	Valley [g] at notching	Frequency [Hz] at peak overshoot	Value [g] at peak overshoot
FRF with HM conditions	14.1	0.107	<u>Not expected</u>	<u>Not expected</u>
VST	13.47	0.158	15.62	0.936
Experimental	12.16	0.322	13.84	0.836

Table 37: Sine X comparison between experimental, VST and FRA with HM conditions

As for sine Y, also in this case the unreal bearings appear. However, VST analysis and the experimental are able to follow the step input at 20 Hz, and the flat one from 20 Hz to 40 Hz. Nevertheless, also in this case, the main criticality is represented by the trend from 40 Hz to 100. In fact, despite how expected from VST, an overshoot from the experimental test appears at about 50 Hz. The same phenomenon appears also in VST analysis at about 45 Hz.

This is another indication about the real characteristics of the structure. Probably, the stiffness of the real tested structure is greater than the imposed into the FRA, than into VST, due to the unexpected behaviours.

11.2 Transient analysis into VST environment of **S/C_02**

The second case of study is represented by S/C_02. Its mission involves the study, analysis and research of the dark matter's nature. It will answer to some fundamental questions about the Univers expansion and the source of the dark energy.

It will be lauched on 2022 through Soyuz, starting its travel from the European space centre in Kourou (French Guiana).

In order to satisfy its mission, the mechanical arquitecture is very complex, full of elements with a detailed design coming from several industrial partners. However, TAS-I is the prime contractor

Figure 87 and Figure 88 show an artist impression and a lateral view of the CAD model. In addition, Figure 88 shows the mechanical assembly composed by the Service Module (SVM) and Payload Module (PLM).

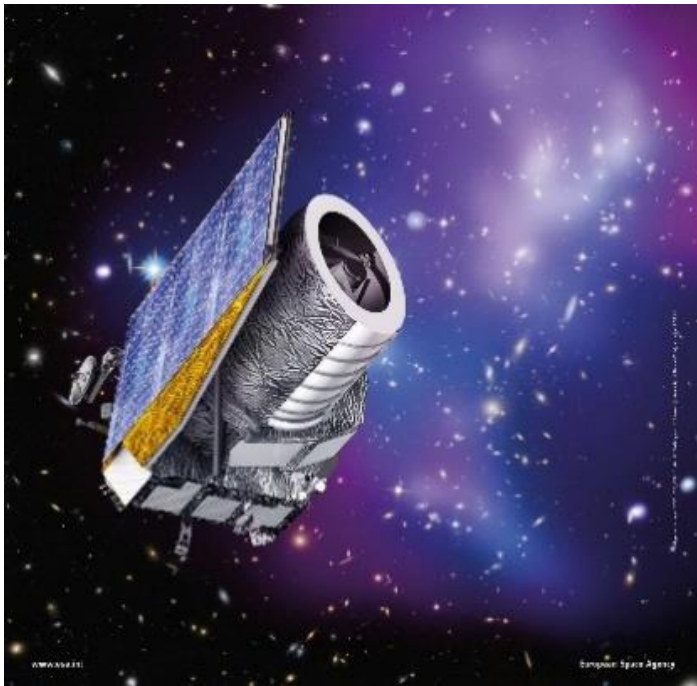


Figure 86: S/C_02 Courtesy of ESA

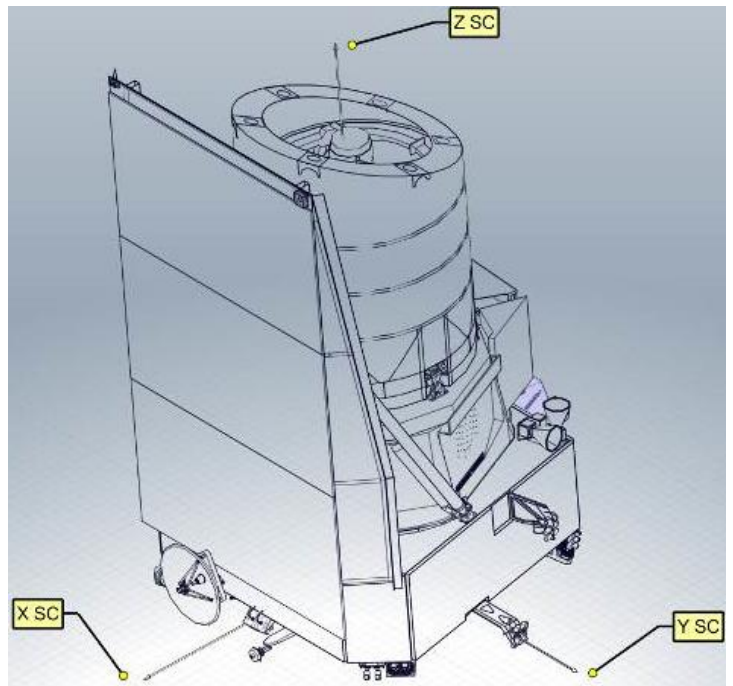


Figure 87: S/C_02, Courtesy of TAS-I

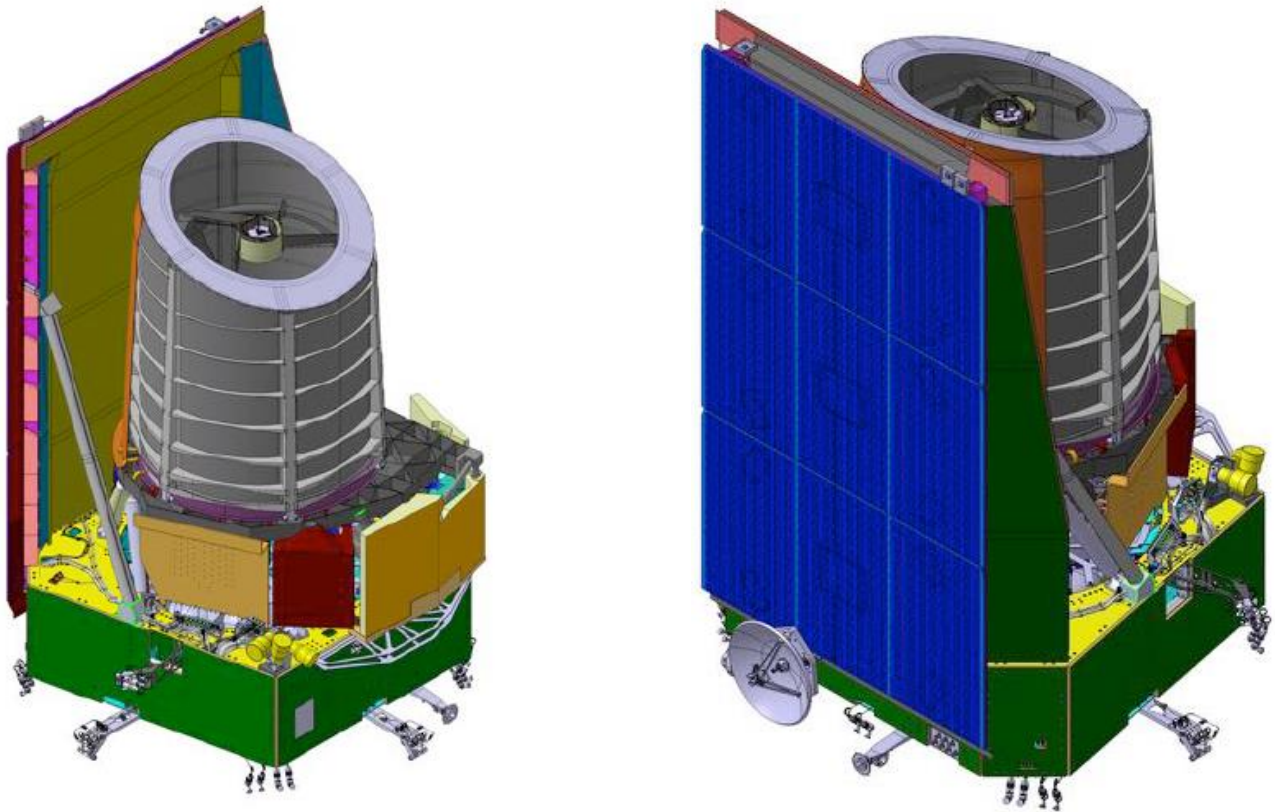


Figure 88: S/C_02 overview [Ref. 38]

The first one, the Service Module (SVM), accommodates the instruments, electronics, and all the fundamental subsystem as, for instance, the propulsion system. One of the most important parts is the Sun shield (SSH) that protects the PLM from the sun rays and provide the electrical devices as the photovoltaic cells. The second, the Payload Module (PLM), is composed by a Korsh telescope and different instruments.

11.2.1 S/C_02 notching prediction using H.M. boundary conditions

First of all, before the VST, the Normal modes analysis, with hard mounted conditions, is carried out in order to deduce the natural frequencies, mode shapes and the effective masses for each mode. Table 38 shows the modal mass contribution up to the 30th mode. Considering the H.M conditions the first global mode is the 12th (in this case global mode is considered for a mass contribution greater of 10%). Is easy to understand that it is the most critical, along the X axes, due to its mass participation. Similarly, the 14th mode is critical for the entire structure caused by the global mode along the Y axes.

Table 39 provides a brief description for the most critical modes.

MODE	EFFECTIVE	MASS (%TOTAL)					
MATRIX	ELEMENT	M11	M22	M33	M44	M55	M66
TOTAL	MASS	1867.06	1867.06	1867.06	2828.97	2989.33	2136.19
MODE	FREQ (Hz)						
1	2.16	0.00	2.67	0.00	1.37	0.00	0.00
2	2.16	2.66	0.00	0.00	0.00	1.30	0.00
3	3.15	0.00	0.00	0.00	0.01	0.00	0.00
4	3.20	0.00	0.00	0.00	0.01	0.00	0.00
5	5.95	0.00	0.00	0.00	0.00	0.00	0.00
6	7.07	0.00	0.00	0.14	0.00	0.11	0.00
7	7.07	0.00	0.16	0.00	0.55	0.00	0.09
8	7.08	0.18	0.00	0.00	0.00	0.51	0.00
9	7.08	0.00	0.00	0.00	0.03	0.01	0.01
10	7.12	0.02	0.00	0.01	0.00	0.01	0.00
11	7.15	0.00	0.02	0.00	0.04	0.00	0.01
12	16.96	23.10	0.00	0.11	0.04	42.74	0.03
13	17.60	0.23	0.01	0.00	7.11	0.20	1.23
14	20.90	0.12	50.71	0.02	41.30	0.05	2.48
15	22.97	27.70	0.13	0.03	0.17	8.10	0.01
16	23.52	0.04	0.00	0.26	0.00	0.02	0.00
17	26.38	0.00	0.10	0.00	0.02	0.00	0.15
18	27.10	0.37	0.00	0.00	0.01	0.13	0.11
19	28.76	0.05	0.12	0.04	2.12	0.18	2.84
20	28.77	0.04	0.04	0.04	0.95	0.12	0.40
21	29.02	0.06	0.63	0.25	8.15	0.01	9.11
22	30.76	0.00	0.02	0.11	0.14	0.15	0.21
23	34.03	0.02	0.00	0.06	1.87	2.22	1.35
24	35.32	0.04	0.00	1.87	1.23	2.02	0.07
25	35.69	0.00	0.00	0.93	0.10	0.60	0.52
26	36.68	0.01	0.00	3.56	5.68	1.57	0.00
27	39.03	0.01	0.02	0.05	0.04	1.34	1.61
28	39.15	0.00	0.02	0.00	0.02	0.01	0.01
29	39.63	0.05	0.00	0.00	0.04	0.09	0.01
30	40.29	0.04	0.01	0.17	0.05	0.25	0.73

Table 38: Modal effective mass table (up to 30th mode) and normal modes

# MODE	EFFECTIVE	MASS (% TOTAL)					
MATRIX	ELEMENT	M11	M22	M33	M44	M55	M66
TOTAL	MASS	1867.06	1867.06	1867.06	2828.97	2989.33	2136.19
MODE	FREQ. (Hz)						
12	16.96	23.1	0	0.11	0.04	42.74	0.03
14	20.9	0.12	50.71	0.02	41.3	0.05	2.48
15	22.97	27.7	0.13	0.03	0.17	8.1	0.01
21	29.02	0.06	0.63	0.25	8.15	0.01	9.11
38	47.91	0.1	0.02	22	0.3	0.03	0.49
45	51.58	0.08	0.02	22.13	0.2	1.82	0

Table 39: Most critical modes and the effective masses involved HM

# Mode	Frequency	Description
12	16.96	X main SSH Bending Mode
14	20.9	Main Lateral Mode in Y direction
15	22.97	Main Lateral Mode in X direction, PLM and SSH Out-of-Phase
21	29.02	SSH Torsional Mode
38	47.91	HGAMA Z mode, SSH wing Y mode, upper and middle panel Out-of-Phase
45	51.58	SSH wing Y mode, upper panel Out-of-Phase / SVM Z mode

Table 40: Description of the characteristics of each mode HM

These are the first information thanks to which is possible to start a real dynamic analysis. In this case we will consider the FRA with H.M conditions.

Fundamental milestone is the definition of the damping model. Precisely, in order to build the FEM the following damping ratio are taken into account:

- 1% C/Ccr (Q=50) on PLM
- 2% C/Ccr (Q=25) on SVM
- 4% C/Ccr (Q=12.5) on SSH

In this case, the structural damping has been chosen. This will imply huge difficulties into the VST damping model in order to perform the analysis.

Figures from 91 to 94 are very interesting. They show the modal displacement (modal shape) of the structure at give frequency. Particularly, the main global mode and those characterized by high effective mass, are represented. Particularly, considering Figure 89 and Figure 91, despite they are similar, the first one involves the Sun shield mainly. The second is related to the out of phase movement of the PLM with the SSH.

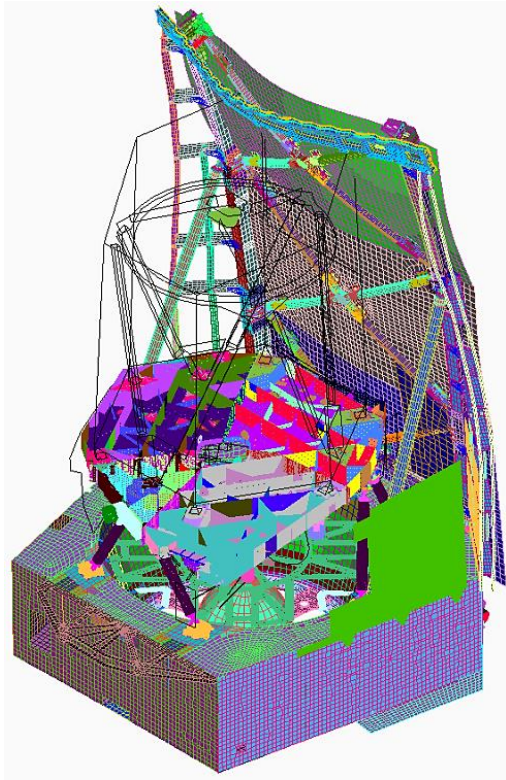


Figure 89: SSH main X bending mode ($f=16.96$ Hz)

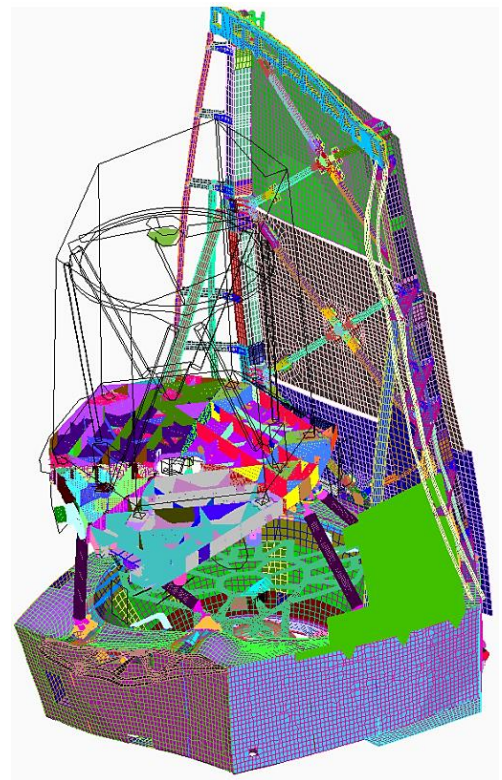


Figure 90: Global mode Y ($f= 20.9$ Hz)

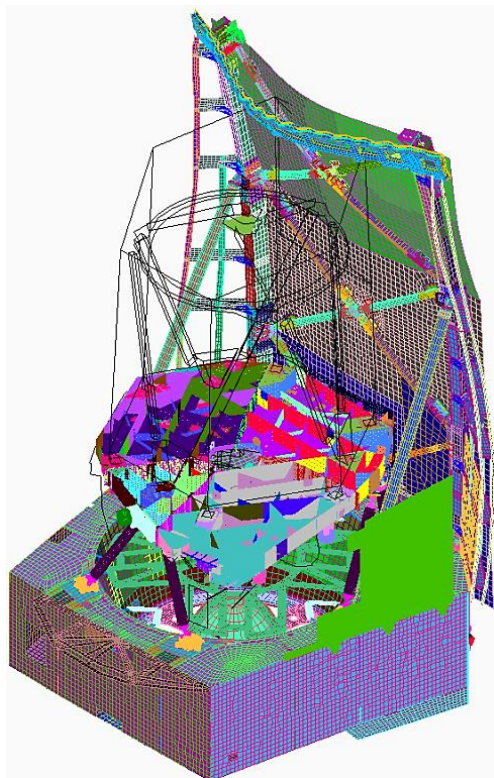


Figure 91: Main PLM lateral mode X with SSH out-of-phase ($f=22.97$ Hz)

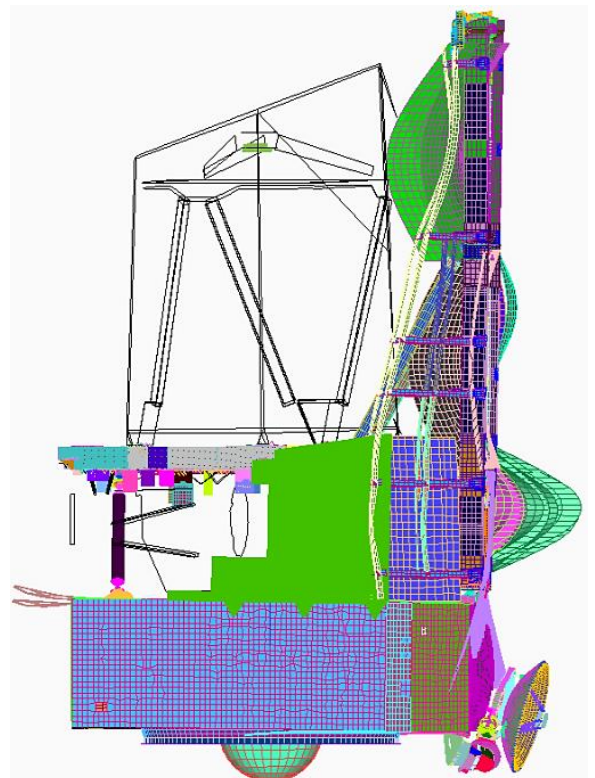


Figure 92: HGAMA Z mode, SSH wing Y mode, upper and middle panel Out-of-Phase ($f=47.91$ Hz)

Second step of the dynamic analysis is represented by the Frequency Response Analysis (FRA). The aim of the FRA, in this case, is to predict and anticipate the acceleration and forces in

some interesting locations of the S/C_02 due to the sinusoidal qualification input along X, Y and Z. However, our purposes are related only for X, Y excitation.

First of all, the amplification factors are calculated with unitary input. Then, using DynaWorks software the output has been extrapolated considering the input level represented in Figure 93 that is valid for both X and Y direction.

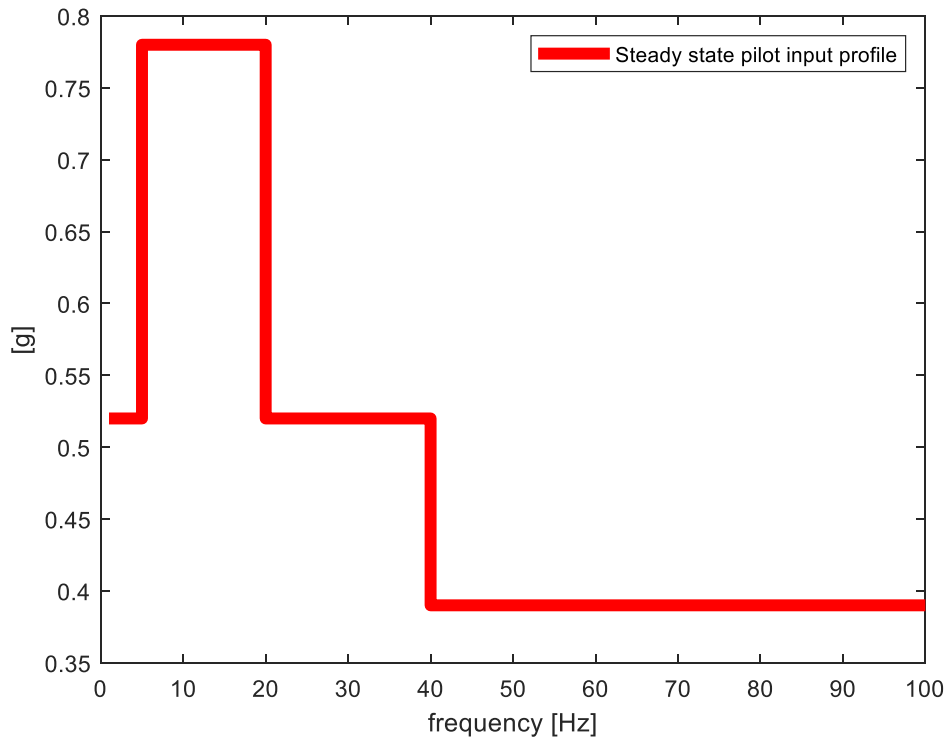


Figure 93: Lateral (X-Y) HM input profile

Sine	Frequency range [Hz]	Qualification levels (0-peak) [g]
Lateral X-Y	1-5	0.52
	5-20	0.78
	20-40	0.52
	40-100	0.39

Table 41: Nominal qualification Lateral input profile (X-Y)

At the end of the extrapolations, the peaks of the responses, for all the considered locations (DoFs), are known. In this context the notching philosophy, and its plan, is written down.

Particularly, for S/C_02 the primary notching approach is based on Force Measurement Device (FMD) thanks to which the excitation is reduced when the imposed moment thresholds are exceeded during the test. Secondary notching is always based on the acceleration criteria introduced in Chapter 6.

Frequency [Hz]	ITEM REQUESTING TO NOTCHING X	DIRECTION	NOMINAL INPUT [g]	NOTCHED INPUT
17	Acceleration at CoG X (MY)	RY	0.78	0.24
23.0	Acce CoG X (MY)	X	0.52	0.25
48.4	PCDU	Z	0.39	0.33
49	HYDRAZINE TANK	Radial	0.39	0.32

Table 42: Notched qualification input in X

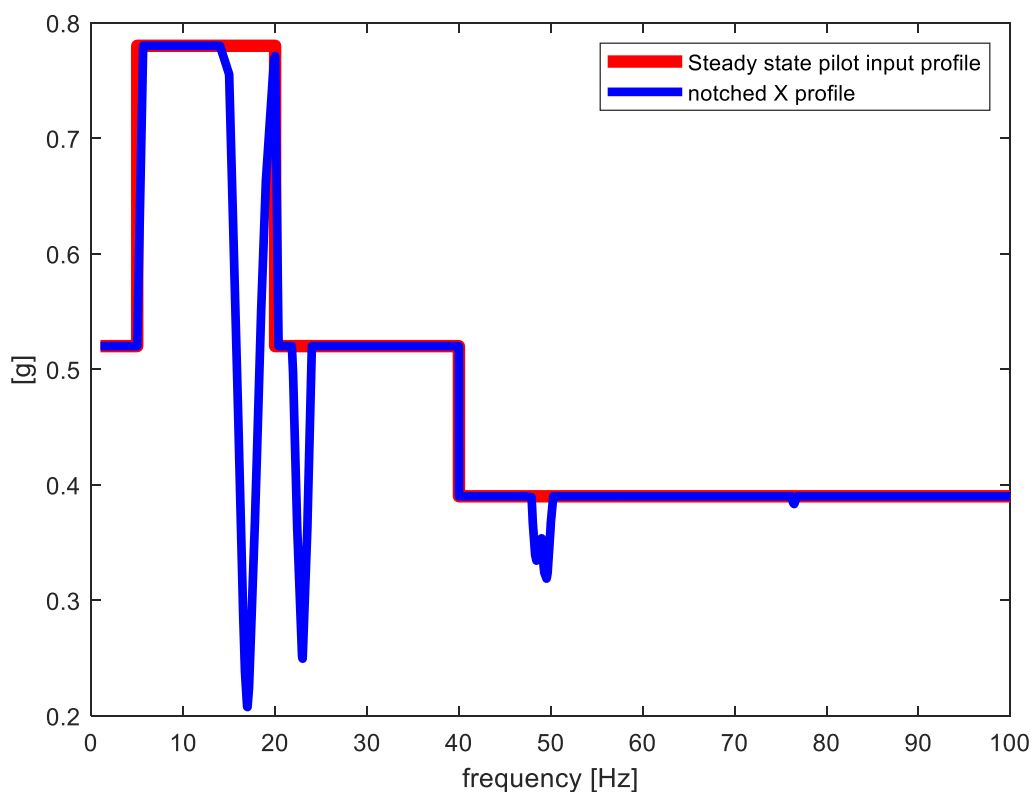


Figure 94: Lateral (X) Steady state HM notched input profile

Frequency [Hz]	ITEM REQUESTING TO NOTCHING Y	DIRECTION	NOMINAL INPUT	NOTCHED INPUT
20.9	Acceleration at CoG Y (MX)	RX	0.52	0.09
49.3	HYDRAZINE TANK	Radial	0.39	0.30

Table 43: Notched qualification input in Y

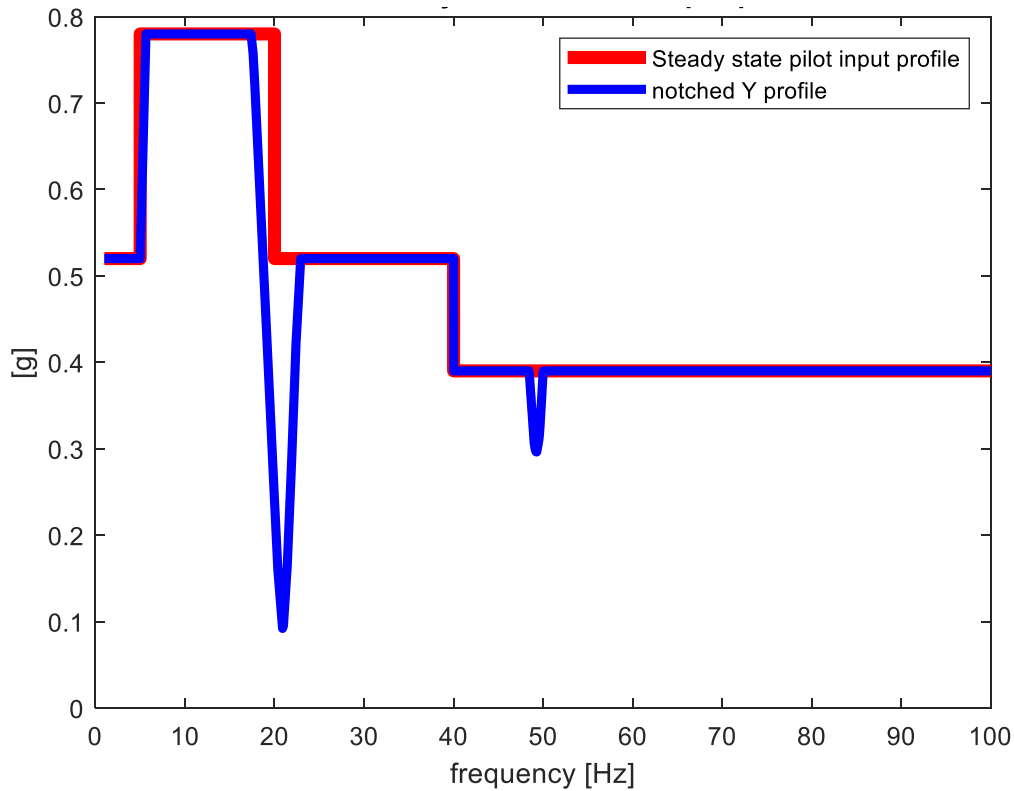


Figure 95: Lateral (Y) Steady state HM notched input profile

11.2.2 S/C_02 VST setup and analysis

Also in this case, as for S/C_01, before running the VST analysis is necessary to impose all the control and analysis parameters.

First of all, the condensed model is downloaded into the MatLab/Simulink model. Precisely, the condensation strategy is based on 28 boundary (or Physical) DoFs with a modal base from 0 Hz up to 250 Hz. In this case, 774 modes are taken into account.

Particularly, talking bout the boundary DoFs, they are divided into:

- 4 Pilots at the base of the S/C (Tx, Ty,Tz) = 12 DoFs
- 1 Bobine node (Tx, Ty,Tz) = 3 DoFs
- 1 Shaker body node (Tx, Ty,Tz) = 3 DoFs
- 2 CBUSH nodes (Rx,Ry) = 4 DoFs
- 1 SunShield (SSH) node (Tx,Ty) = 2 DoFs
- 1 Tank node (Tx,Ty) = 2 DoFs
- 1 PDCU node (Tx,Ty) = 2 DoFs

=====

28 boundary DoFs

Figure 96Figure 96 shows the mass and stiffness matrices in terms of their pattern. The green line located on the bottom and on the right side of the matrices means the presence of the electrical vector in order to compute the electromechanical model.

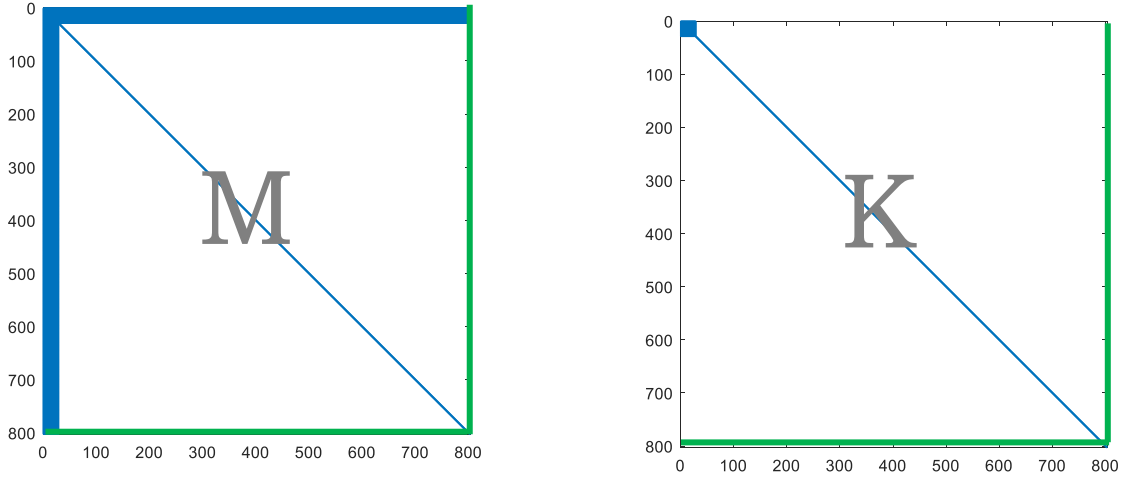


Figure 96: Mass and stiffness matrix from NASTRAN Craig-Bampton condensation, pattern visualization

Second main step into the VST setup is represented by the preparation of the damping matrix “D”. Typically, damping is one of the most difficult quantity to impose and predict. For this reason, structural responses could have important variation if damping model vary. In case of S/C_02 different damping models, based on Chapter 10, has been tested.

After several dry run of the MatLab/Simulink model, the most suitable damping model is the Hybrid in which boundary, modal and coupling blocks are considered together.

$$[D] = \begin{bmatrix} \alpha * M_{rr} & \alpha L^T \\ \alpha L & [m_p] \end{bmatrix} + \begin{bmatrix} \beta \widetilde{K}_{JJ} & 0 \\ 0 & <\lambda_p> [m_p] \end{bmatrix} \quad (11.1)$$

Particularly, the damping ratio and the frequency span used for extract the α and β coefficients, and the modal damping, are:

- $f_1 = 25 \text{ Hz} \rightarrow \zeta_{prop_1} = 3\%$
- $f_2 = 100 \text{ Hz} \rightarrow \zeta_{prop_2} = 0.75\%$
- $\zeta_{modal} = 2\%$

We remark that this particular damping model was build in order to consider into a global damping model different characteristics that appear into a local model, as the imposed structural model into FEM tools.

Figure 97 shows the damping ratios (modal and proportional coefficients) involved into the Hybrid damping model.

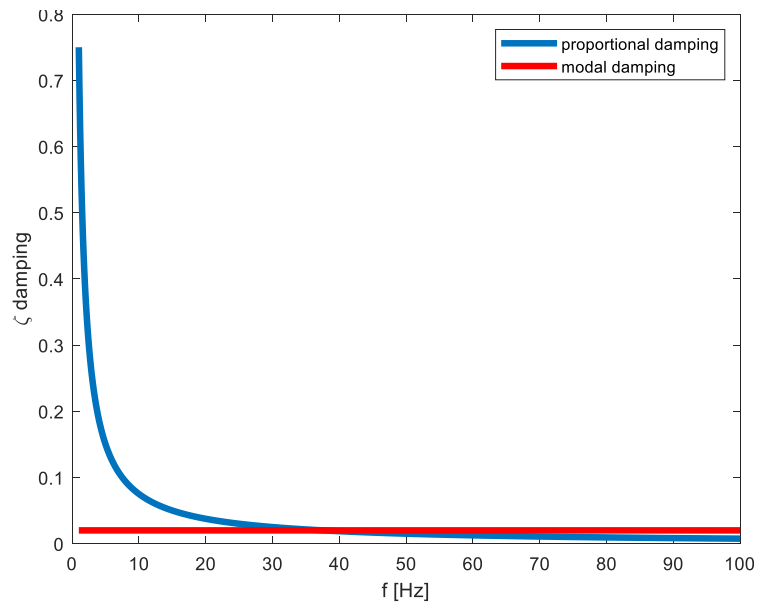


Figure 97: Proportional damping ratio (ligh blue), modal damping ration (res) at given frequency

Lastly, after the State-space conversion (from continuous to discrete) is necessary to impose the control parameters as, for instance, sweep rate, compression factor, estimation/control strategy. At the same time, notching plan shall be declared in order to impose the suitable notching threshold to the DoFs.

Control parameters/ instructions

Control strategy	maximum
Sweep mode	Log up
Estimation strategy	Harmonic
Sweep rate [Oct/min]	4
Frequency band	1-100 Hz
Compression factor	Sensitivity on CF= [2, 4, 6, 8, 10]

Table 44: Control parameter and instruction into S/C_02 VST analysis

Item	FEM ID	Condensed DoFs	Threshold
Moment at the base of the SC (X)	Fictitious, built from CBUSH DoFs	\	50720.6 Nm
Moment at the base of the SC (X)	Fictitious, built from CBUSH DoFs	\	50720.6 Nm
PCDU	1140654	1,2	15 [g] along X, Y
TANK	3310610	1,1	5.57 [g] (X), 5.7 [g] (Y)

Table 45: Notching plan for S/C_02

11.2.2.1 S/C_02 VST along Y direction

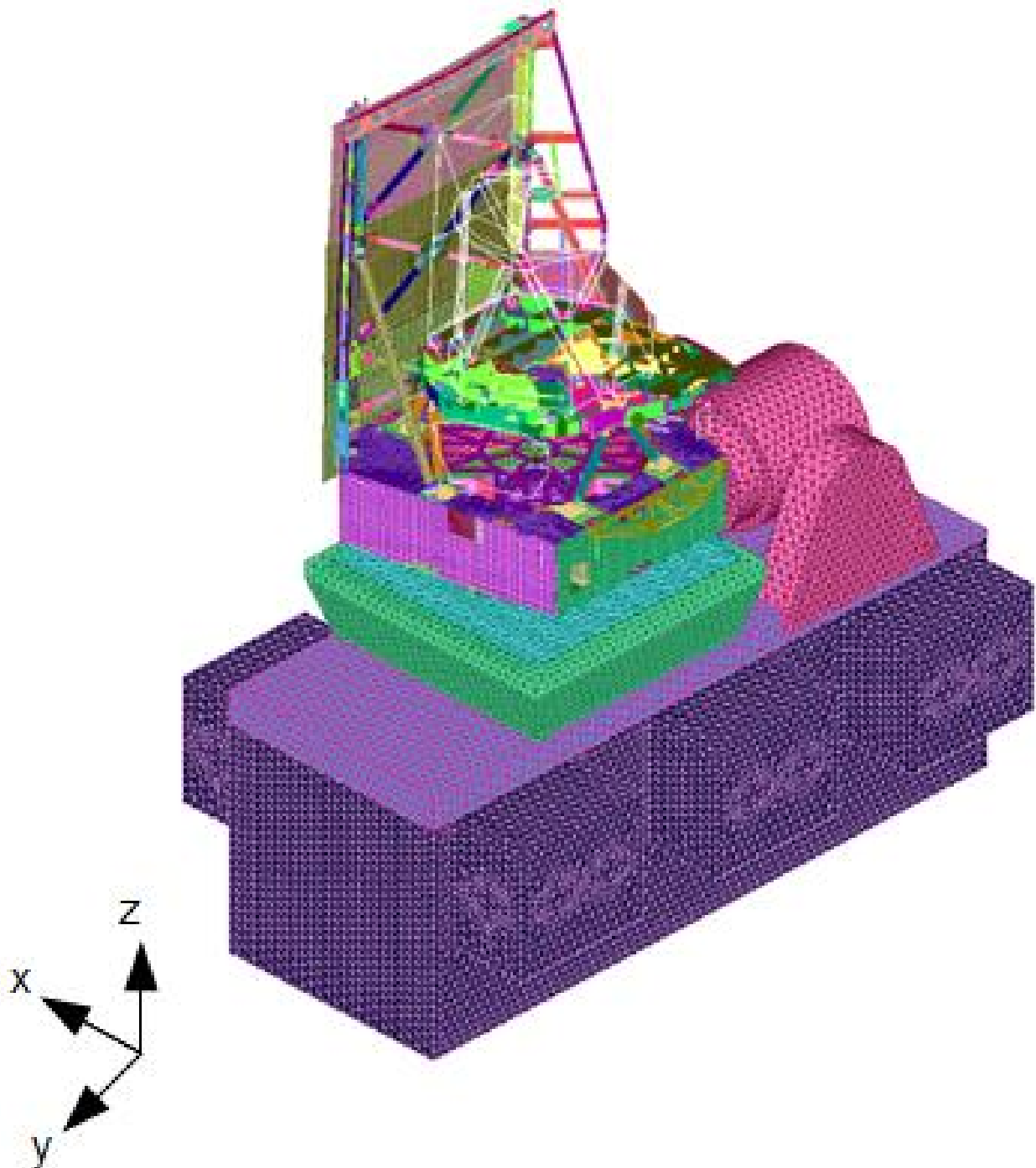


Figure 98: S/C_02 mounted on shaker along Y

Figure 98 shows the triptych of S/C_02 mounted on top of the shaker along Y.

In order to suggest to the facility, where the vibration test will be performed, the proper compression factor to apply during the test, a sensitivity analysis is conducted. Practically, the amplitude of the overshoot and the importance of the beating phenomena are taken into account during the sensitivity, as a guide. A suitable compression factor shall produce a “small” overshoot in terms of amplitude and a few beating phenomena.

Figure 99 shows the output results coming from this sensitivity.

It's easy to understand that if during the vibration test a compression factor equal to 2 or 10 the beating (due to CF=2) and the overshoot (CF=10) are maximized. For these reasons they are automatically discarded.

The remaining are evaluated based on the same criterion. For this reason, a compression factor equal to 6 appears as a good solution.

Figure 100 shows the overlapped representation between the steady state HM solution to the pilots compared to the solution provided by the transient VST.

Overall, considering that the real phenomenon is a transient structural behaviour, it appears as a reasonable solution. In fact, the VST solution, in terms of pilot curve, follows the steady state solution with typical oscillation that are common during the vibration test.

Comparing the steady state HM with the VST curve, there are interesting phenomena that appears in addition to the oscillation around to the steady state solution.

First of all, the presence of a ramp into the VST solution, rather than a perfect step increase. This is a typical practice during a real test in order to avoid initial and undesired overshoot.

Secondary, when the structure is notched, the minimum value of the valley suffers the so called frequency shift. Particularly,

	S/C_02 STM HM	S/C_02 VST
f1 [Hz]	20.9	20.28
Main Lateral Mode in Y direction		
Δf	0.62	

Table 46: Frequency shift along sine Y

This means that the coupling between shaker and S/C produces the reduction at which the notch valley reaches its minimum value. This is a fundamental information, above all for S/C with a first natural frequency very close to the frequency requirement. If a frequency (down) shift appears, this means that the shaker with its mass, stiffness, and geometrical characteristics, is able to impose a frequency reduction to the S/C oscillation peak. For this reason, a S/C could be unaccepted, in terms of frequency requirement, caused by the down shift in frequency imposed to the shaker, despite the S/C in HM condition satisfy the launcher frequency requirement.

Thirdly, to the ascent from the notch valley (Main Lateral Mode in Y direction) an important overshoot, followed by a series of beating, appears. This behaviour take place, probably, due to the presence of a considerable amount of effective mass involved during the first fundamental mode. In fact, more than 50% of the mass along the Y (translation) direction and more than 40% along the RY (rotation) are involved. Due to the presence of this amount of involved mass is necessary to reduce the peak of the overshoot in order to protect the structure to undesired overstress.

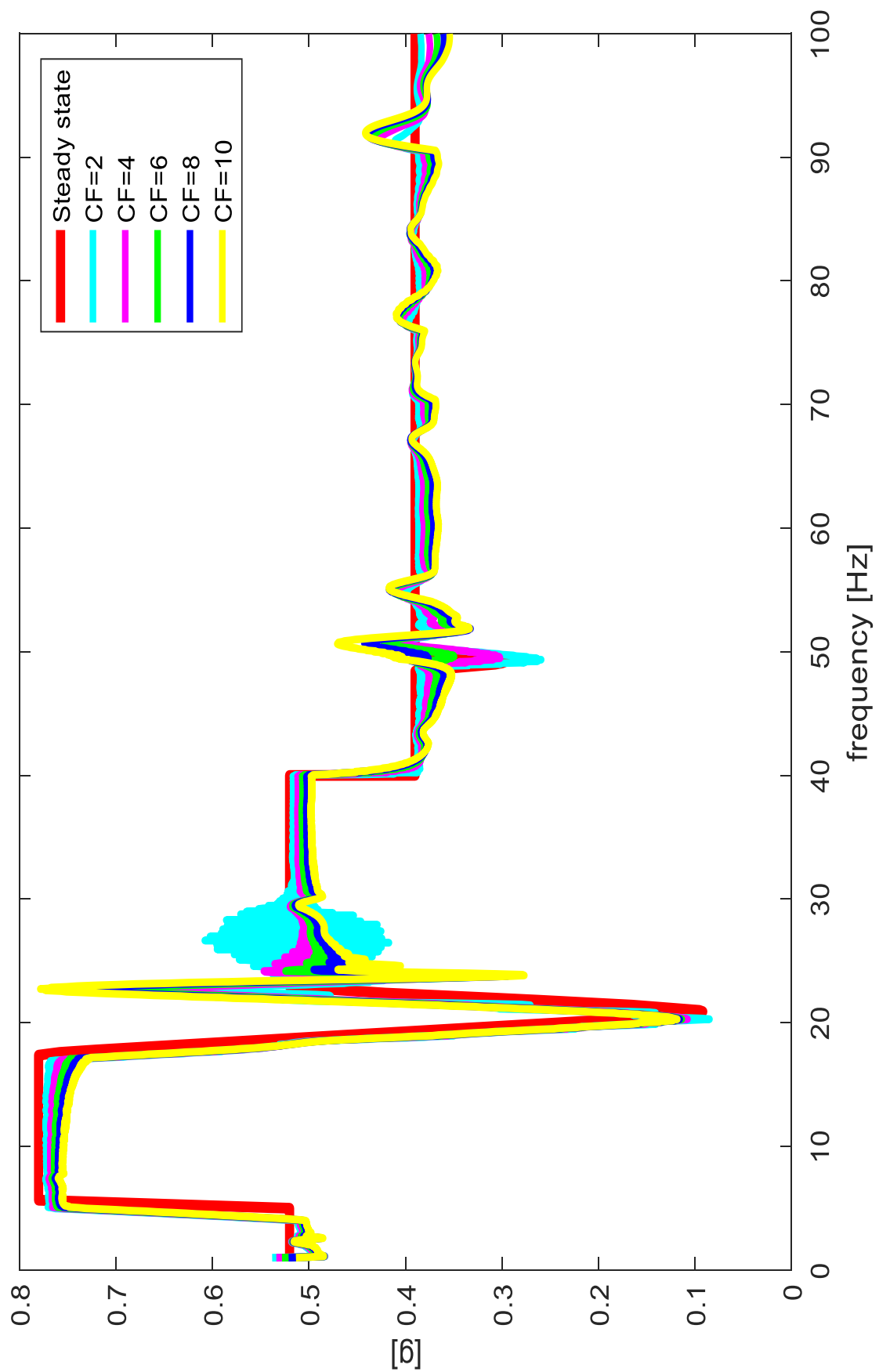


Figure 99: Sensitivity analysis to different VST compression factor Vs Steady state HM input on Y

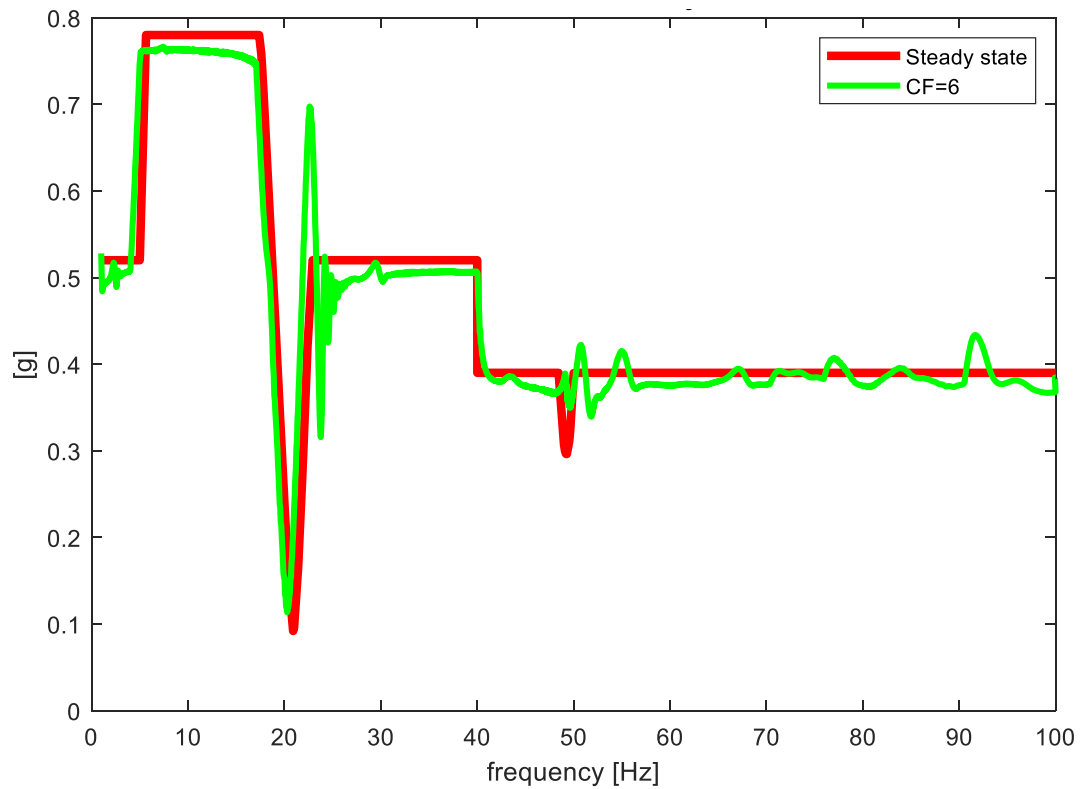
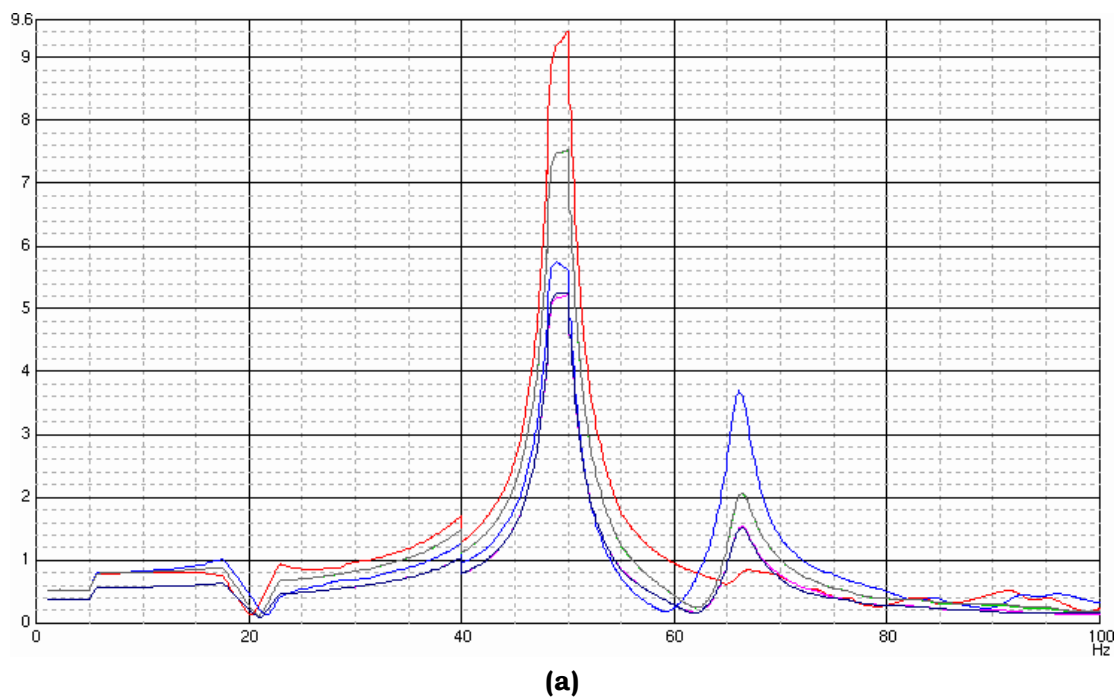


Figure 100: VST Y curve at CF=6 Vs steady state HM

Lastly, at about 50 Hz the hydrazine tank is expected to notch at 5.75g according to the steady state solution. How is possible to see in Figure 100, the tank will be notched. However, its valley is less deep than expected by the steady state.

Figure 101Figure 101 shows the comparison of the tank response between the steady state HM solution with the VST curve.



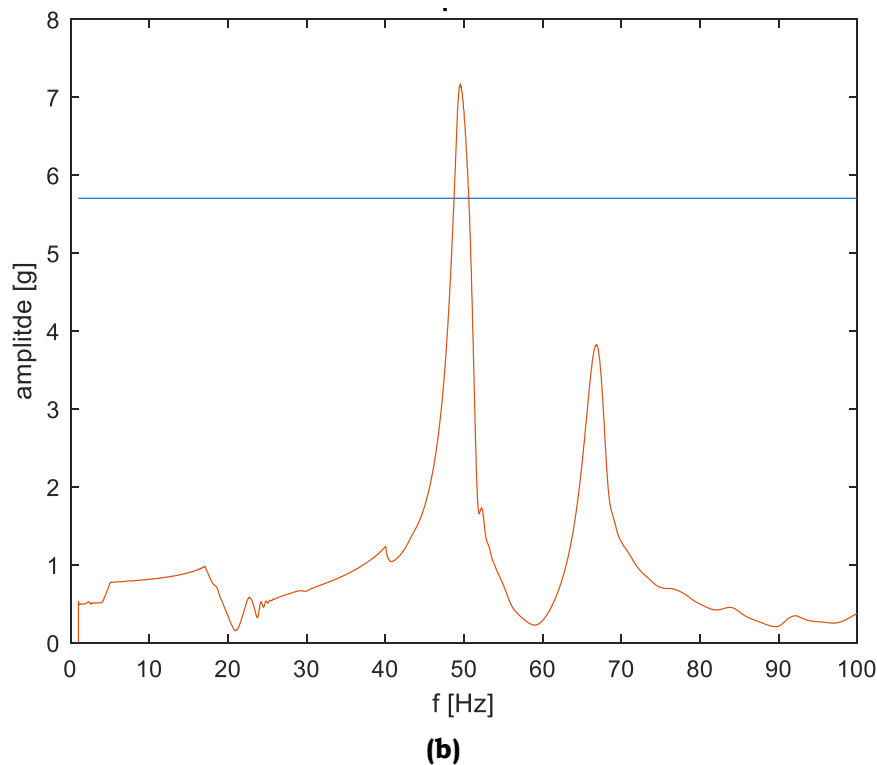


Figure 101: Tank response on Y, Steady state from NASTRAN/SYNEPOST (a) Vs VST (b)

It is easy to recognize that the curves are in good agreement. In fact, the VST curve is able to reproduce all of the most important behaviours present into the steady state HM curve.

Particularly, considering that the steady state curves are related to the 4 different pilots, we should consider the so called “max pilot” that is the max value of the four at different frequency. In this case we will consider the red curve up to 50 Hz and the blue up to 100 Hz.

For this purpose, the notched valley at about 20 Hz, the flexion at 40 Hz, the two peaks at about 50 Hz and 65 Hz, are present.

The unique point of discrepancy is represented by the sharpness of the first peak at 50 Hz.

This discrepancy is originated, with good confidence from the damping value at the frequency near 50 Hz. In general, from the damping model. However, as a global result, the curve provided by the VST appears as a good a reasonable result.

Together to the tank response, also the sun shield and the PCDU are interesting to evaluate. Nevertheless, in this case the sunshield response is shadowed by the moment. In fact, according to the base moment we will notch. On the other side, the PCDU response is near to be zero due to the excitation is perpendicular to its direction. In addition, the response along X is also low. This probably means that no coupling effects appears.

In Appendix are shown the observed pilots along the X and Z direction. In general, they are no critical curves caused by their values is lower than 20%. This means that no critical coupling effects foreseen.

11.2.2.2 S/C_02 VST along X direction

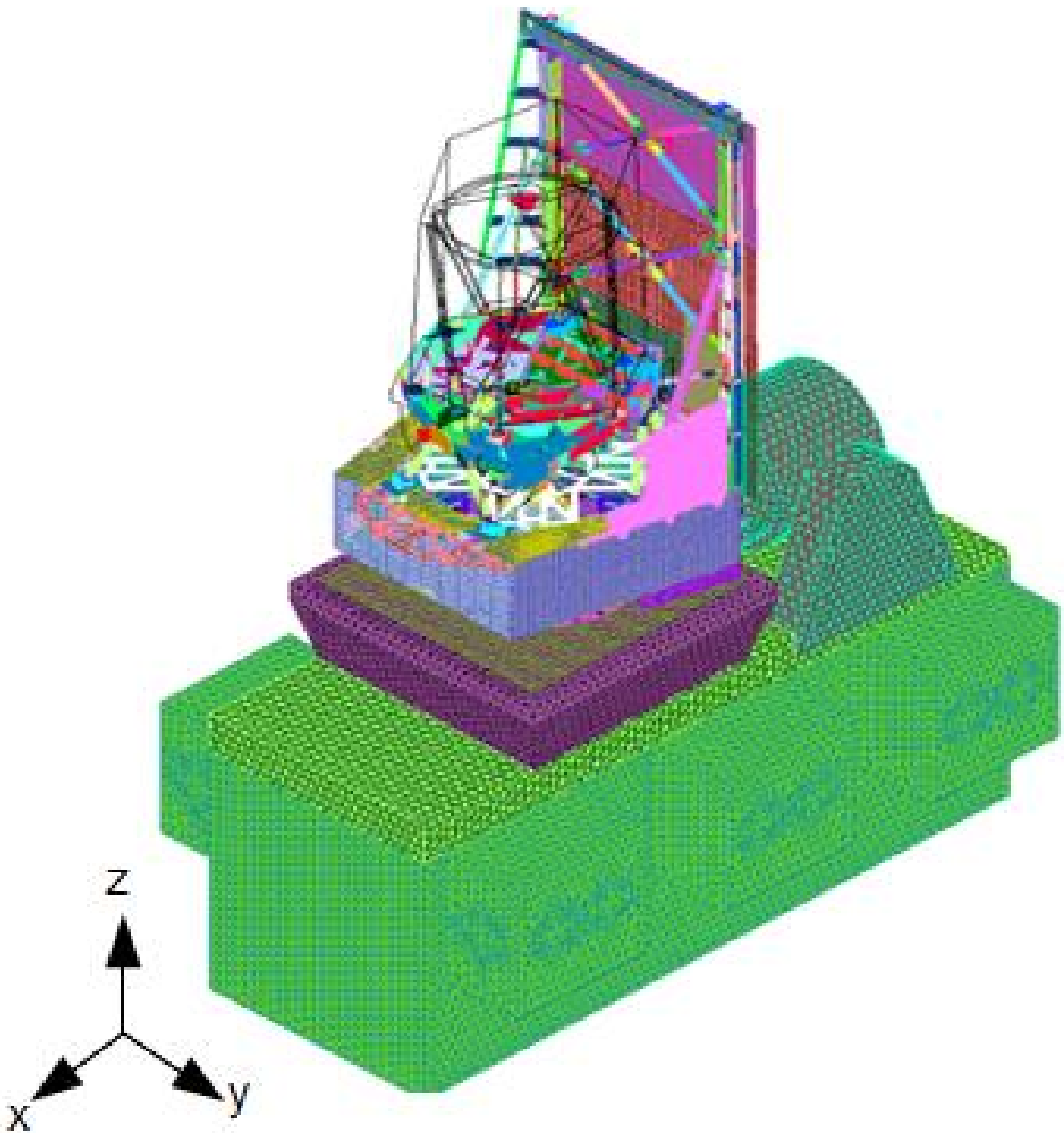


Figure 102: S/C_02 mounted on shaker along X

Figure 102 shows the triptych of S/C_02 mounted on top of the shaker along X. Precisely, into the FEM tool the shaker has been rotated.

Even in this case, as for VST along X direction, a sensitivity analysis, in terms of compression factor, is performed in order to anticipate criticalities as beating and overshoot phenomena.

Figure 103 shows the overlapped curves from the steady state with HM conditions to the CF=10. Referring to the curves at vary to the compression factor (CF), they are quite similar in terms of shape except at about 50 Hz where the shapes change showing different behaviours.

Even in this case, a CF=10 is an unreasonable value due to the huge overshoot produced. Particularly, its value is grater tha the nominal input equal to 0.52g.

Making a trade off, also in this case a CF=6 has been chosen in order to reach and produce a reasonble transient structural response.

Figure 104 shows the selected curve wit CF=6 compared to the steady state. Many oscillations are recognizable. Particularly, after the second primary notch at 23 Hz, an important overshoot, followed by beating, appears.

As for VST along Y, also in this case, the frequency down shift is foreseen. Table 47 quantify this phenomenon.

	Euclid STM HM	Euclid VST
f1 [Hz]		
X main SSH bending mode	16.96	16.74
Δf	0.22	
f2 [Hz]		
Main Lateral Mode in X direction	23	22.93
Δf	0.07	

Table 47: Frequency shift along sine X

However, the most important criticality appears at about 50 Hz. In fact, despite a notch valley is planned with a precise depth, the VST provides a most severe behaviour. In this case the unique explanation is based on the adopted damping model. In fact, in the previous paragraph we mentioned that the applied damping model on FEM is based on structural damping, a typical way in order to apply the damping to a specific part of the structure. Probably this approach is poor at about 50 Hz producing an over response of the structure.

For this reason, the structure along the X direction could be more damped respect to the Y direction, or in general, the damping along these two is different.

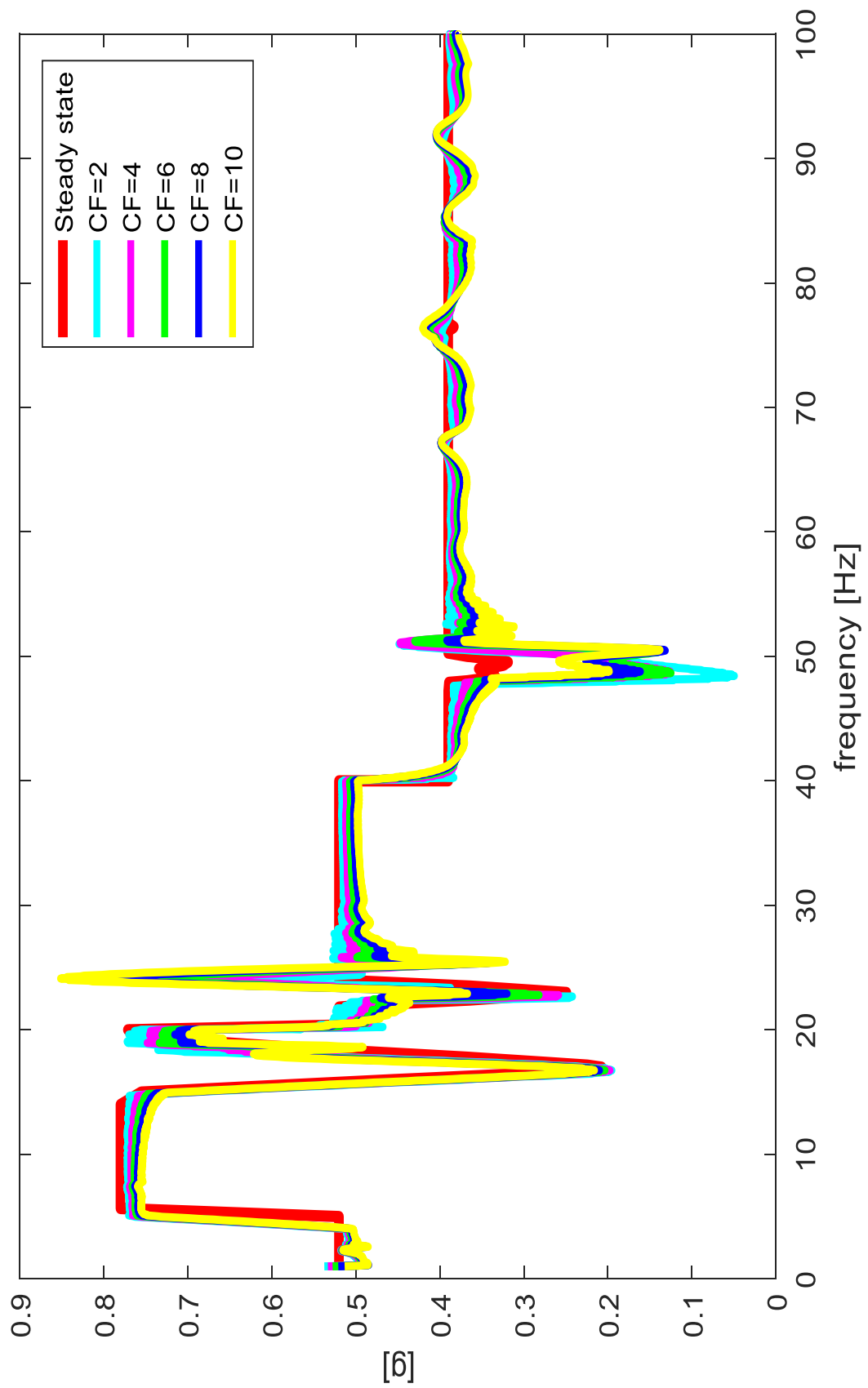


Figure 103: Sensitivity analysis to different VST compression factor Vs Steady state HM input on X

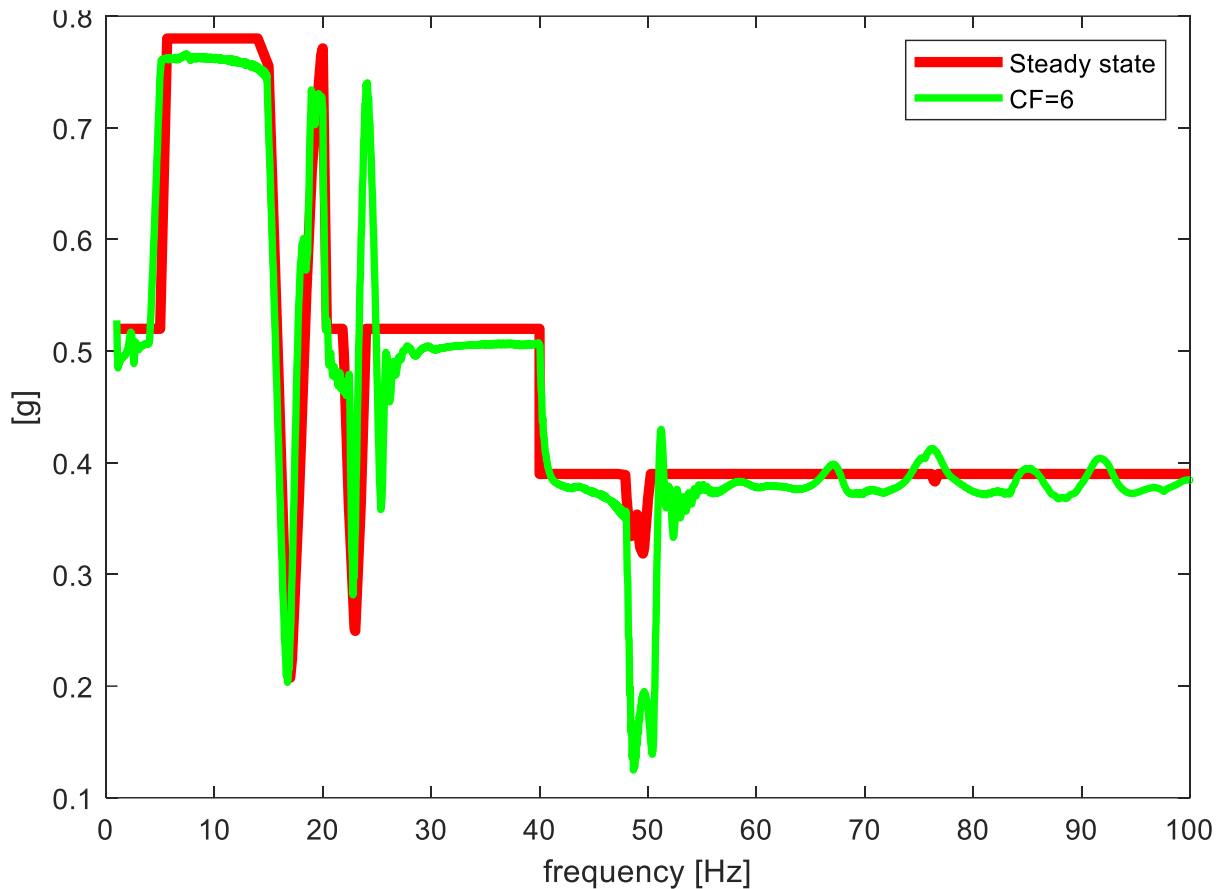


Figure 104: VST X curve at CF=6 Vs steady state HM

Considering the most important responses, Hydrazine tank and PCDU, they are shown in Figure 105 and Figure 106. They provide a comparison between the steady state unnotched HM curves with the transient VST notched curves.

Talking about the first one, the tank response, Figure 105, the two curves are different. Actually, being the first (a) is unnotched and the second (b) is notched, due to the overcoming of the PCDU acceleration threshold, the peak at about 50 Hz of the VST is lower than its acceleration threshold and divided into three peaks. Precisely, this happens because the notching of the PCDU is foreseen before than the tank. In this case the tank notched response is shadowed from PCDU.

In addition to this, observing the peak values at about 70 Hz, they are in good agreement between the steady state HM with the VST.

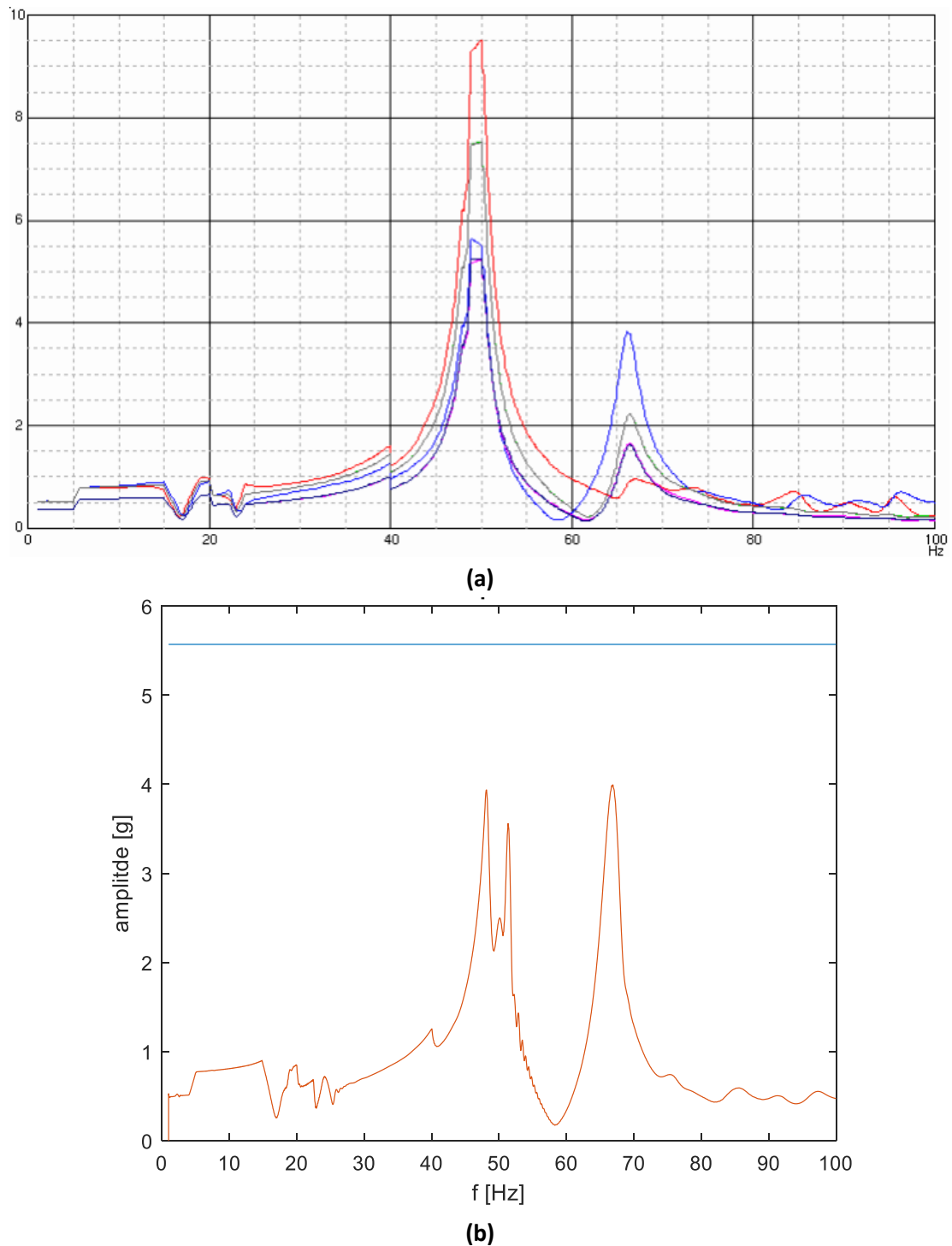


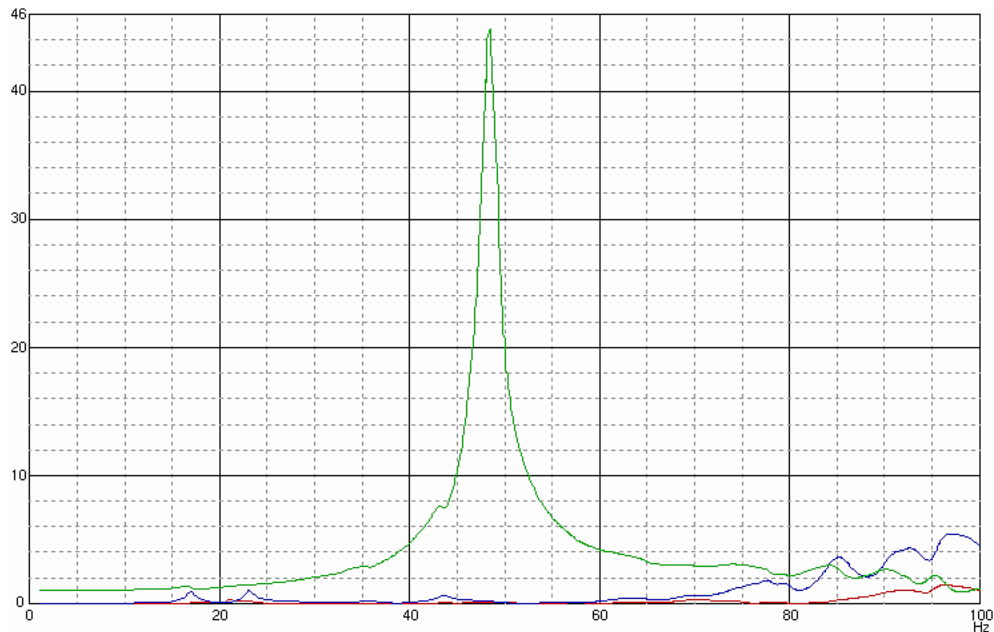
Figure 105: Tank response on X, Steady state from NASTRAN/SYNEPOST (a) Vs VST (b)

On the other hand, Figure 106 shows the response of the PCDU, always in frequency domain providing also in this case the comparison between the steady state HM unnotched case respect to the notched transient VST.

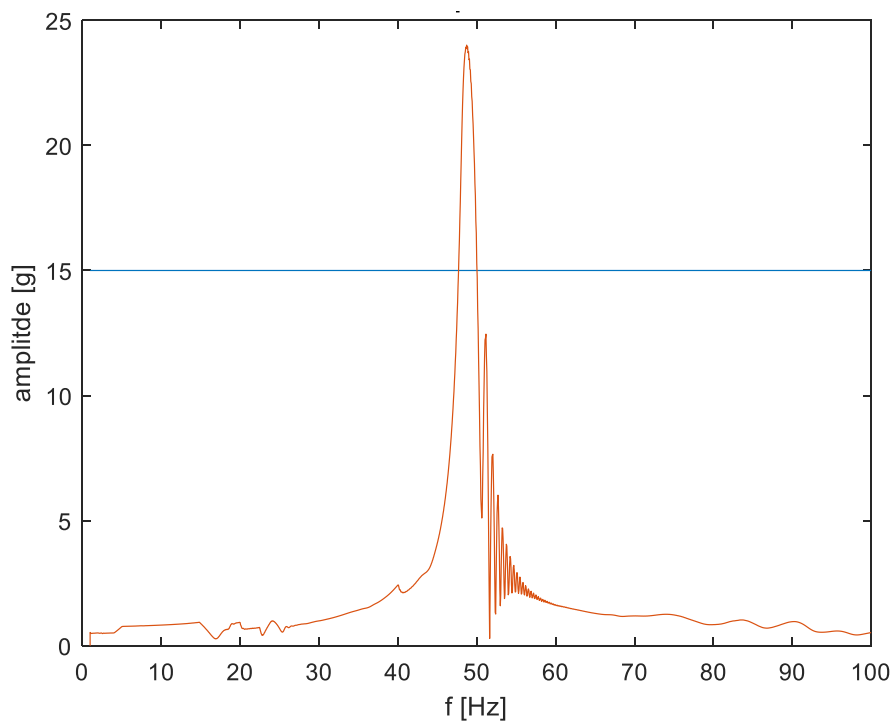
It is easy to recognize that the principal differences between the two curves is represented by the peak value and the beating after the peak.

The first one is affected by the damping, and its value, at the main resonance. In fact, how represented in the control pilot curve, the notch valley is deeper than the steady state.

This means that the control algorithm imposes most severe actions in order to reduce the amplitude of the PCDU response. In addition, usually the peak after the notching and its overshoot, should be smoother.



(a)



(b)

Figure 106: PCDU response on X, Steady state from NASTRAN/SYNEPOST (a) Vs VST (b)

Secondary, the beating after the resonance is a common issue during a vibration test. For this reason, is reasonable to have this behaviour due to the interaction of the excitation and the response

In Appendix are shown the observed pilots along the X and Z direction (from Figure 107 to Figure 110). In general, they are no critical curves caused by their values is lower than 20%. This means that no critical coupling effects foreseen. Always in Appendix, Figure 111 is shown the VTA device. On top of it will be placed the S/C_02. On the bottom the FMD devices are connected.

Overall, the VST analysis of S/C_02 shall be an appropriate anticipation of the sine vibration test that will be performed. How introduced, the main point of discordance is represented by the applied damping model to the structure as whole.

Next step will be the comparison of future experimental curve in order to confirmed or refute the expected results and their assumption.

Chapter 12: Future trends and applications

After the analysis of VST in terms of sine sweep test, its capabilities are clear and the application for the near future could be many and technically challenging.

First of all, VST was approached as a single axis problem performing the virtual test only along X or Y direction. For this reason, in order to have a better and complete representation of the dynamic behaviours that the S/C could meet during launch, an extension to a multi axis approach could be useful.

Particularly, in this context, we are referring to a 6-DoFs shaker (e.g. Hydra, available in ESA-ESTEC facility). In this case, using a multi axis VST is possible to couple different kinds of loads together, as for instance two translations and one rotation, or other combinations.

However, in order to realize the aim, a modification of the Simulink model and MatLab script is required. Nevertheless, talking about Simulink, only people who produce the model are capable to solve the problem due to the presence of masks that hidden some routines. At the same time, the modification of MatLab is quite easy. In fact, is necessary to change the B and D matrices into the state space representation.

Another kind of future application is the extension to random loads. How is well known, random loads are possible to study only in statistical way regarding the load amplitude and its frequency. The analogous test procedure in term of VST shall take into account their peculiarities. For this reason, also in this case, only the Siemens guys are able to modify the Simulink because they know the hidden laws of the load application into the VST framework.

A separate other possibility for next applications and tests is to extract the “PAA” vector from NASTRAN in order to impose the loads directly from the condensed FEM model to the state space representation. In this case body and bobine are directly connected not only from the mass and stiffness matrices, but also from the output loads.

A more challenging application is based on the interaction between NASTRAN and MatLab/Simulink. In fact, due to the structural damping matrix is calculated at a given frequency, is theoretically possible to put in communication the two different softwares into a loop. Basically, at each loop step NASTRAN provides as input for MatLab/Simulink the structural damping a different frequency in order to produce the equivalent viscous damping matrix that takes place into the VST simulation. However, this procedure could take many hours to finish the simulation compared to a low increasing in term of calculus precision.

Lastly, an easy but important application is the use of the VST for many and many predictions. In this case, the editing of technical tables could help engineers and technicians involved into the real vibration test for better understand if the S/C is compliance in term of capability to withstand the reactive forces or coupling phenomena from the hypothesized facility point of view. It deals with the preparation of technical database.

Chapter 13: Conclusions

As shown in the previous chapters, the Virtual Shaker Testing (VST) confirms its important and significant contribution to predict the dynamic behaviours of a test item, during a sinusoidal (low vibration) test, avoiding the overtesting. VST is also a general approach and leaves aside the type and the nature of the test article though the imposition of external load and excitations.

Talking about the aerospace environment, using the VST approach is possible to impose to the test item, the acceleration level at its base, in accordance to the acceptance or qualification philosophy, preserving its structural integrity without ruptures or damages at the end of the lateral or axial test.

Not only, a good prevision allows the program manager to apply the most appropriate test parameters, abort and alarm levels or compression factor, during the real test, reducing risks. Furthermore, using the VST analysis the manager is able to decide if the planned test facility is an acceptable choice, or not, from the coupling between shaker and S/C point of view.

From an applicative standpoint, its approach considers an extension of the Hard Mounted (HM) Boundary Conditions (BCs) beyond the S/C taking into account the entire assembly composed by the shaker-S/C into a global Finite Element Model (FEM).

Particularly, using the Vibration Controls, provided by SIEMENS®, written in MatLab/SIMULINK®, the VST approach allows to anticipate, into a transient environment loaded into a sine control algorithm, the common issues that could appear during a vibration test as beatings, dynamic coupling effects, sweep rate effects as frequency shifts, and overshoots.

In addition, with respect to the classical sine prediction based on the Frequency Response Analysis (FRA), the transient point of view proposed into this work analyses the responses of different structures starting from the mechanical matrices (mass and stiffness) as NASTRAN output into Craig-Bampton formulation. Then, the State Space approach, in order to be able to perform the VST analysis, is written and implemented as automatic add-on scheme to the provided MatLab/SIMULINK © model.

Going deeper into the work, a first approach with mass-spring-damper models whose studied and tested in order to evaluate the quality of the structural responses.

After that, an important virtual test campaign, focused on the response at varying to different damping models, compression factor, sweep rate effects and electrical parameters has been performed as a post-correlation with test data.

Taking about the damping models, basically, two ways were followed.

The first one is related to damping models based on the classical proportional and modal approaches. This just because the Craig- Bampton formulation takes into account the physical (or boundary) DoFs as well as the modal DoFs and coupling DoFs into the same matrix. This means a dedicated damping formulation for physical, modal and coupling submatrices.

The second considers the NASTRAN structural damping matrix. In this way, an equivalent viscous damping with different methodologies: based on modal components and based on assembled Craig-Bampton components at system level, is implemented.

Subsequently, analysing the effect of the sweep rate, the response of the notchers increases when the sweep decreases because the conditions go towards the steady state conditions proposed by the FRA theory. At the same time, if the sweep rate increases, the frequency shift of the primary and secondary notching increases itself.

On the other side, the effect of the compression factor implies dramatically the response of the structure, in terms of the pilots control curve. In fact, overshoots with different amplitude of the peaks appear. Particularly if the compression factor increases the overshoot after the notch valley increases. This could be the source of the overtest producing ruptures and damages.

Finally, the evaluation of the response of the electrical parameters confirms that they are negligible in terms of structural response.

At the end of this phase, the real sine test prediction to different S/Cs has been performed: S/C_01 and S/C_02.

In general, starting from the natural frequency and the modal effective mass is possible to quantify the severity of the considered mode. In this way, observing the amplitude of the responses of some key elements, that have to be monitored during the test, the notchers, the notching plan is written and applied as input to the VST.

In this framework, for each considered S/Cs, a sensitivity analysis, based on compression factor at fixed sweep rate, was performed along the X and Y axes, caused by possible coupling effects. The related simulations show that at vary to different compression factor the severity of the beating phenomena and the amplitude of the overshoot change.

Observing the overlapped curves, the most appropriate value of the compression factor has been suggested to the test facility in order to apply to the real sine vibration test.

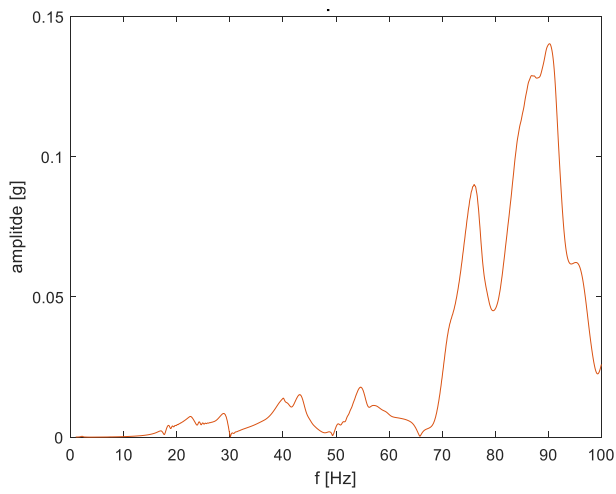
Actually, for each S/C a preliminary analysis based on damping models was performed to anticipate and understand their responses with different approaches. In this phase a knowledge update about the criticality represented by the damping has been possible.

In fact, starting from damping, possible future works are related to the updating of its models, using NASTRAN structural matrix output, in order to build an appropriate viscous damping formulation.

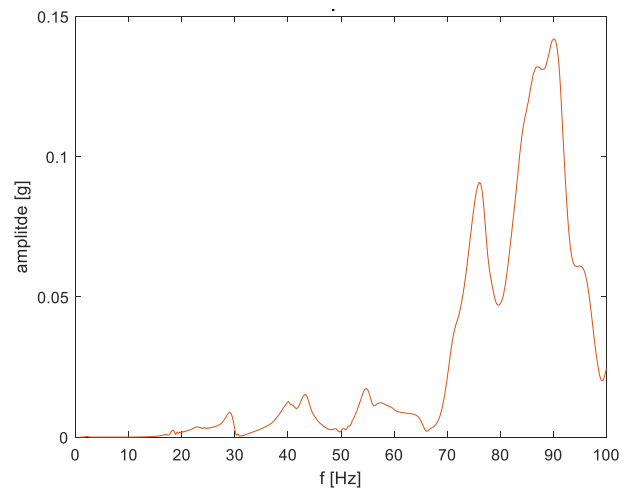
In addition to this, a future step for the VST is related to its application to different loads, as for instance, the random loads.

Furthermore, another possible step is to extend this practice to the multi-axial shaker. In this way, during the same test the S/C will be subjected to the real input profile expressed to the launcher.

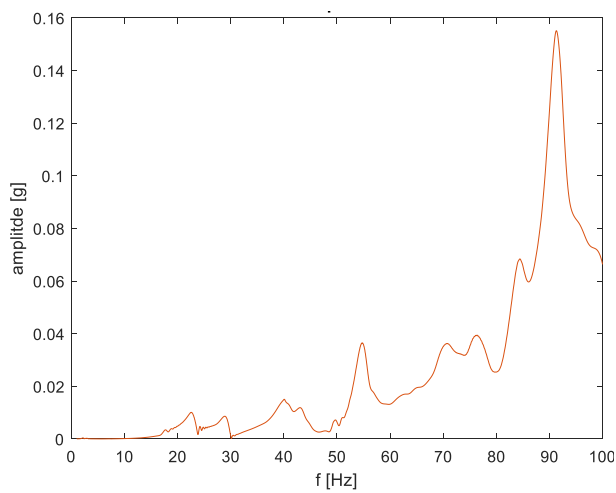
Appendix



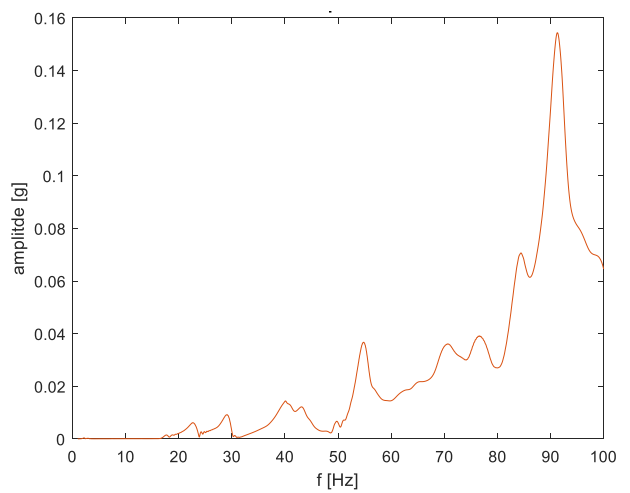
(1)



(2)

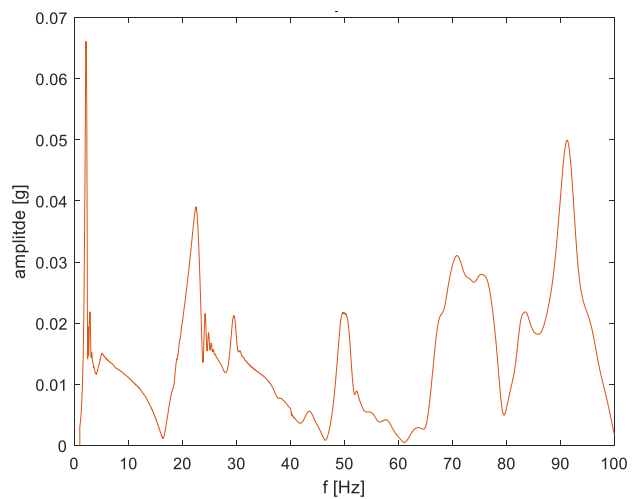
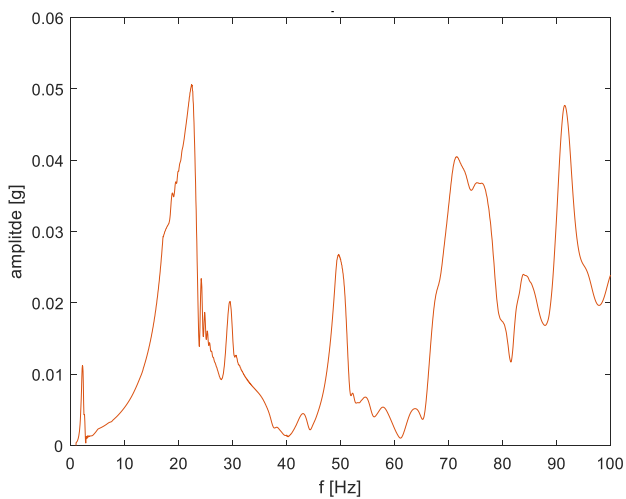


(3)



(4)

Figure 107: Sine Y - Pilots along X (Cross talks)



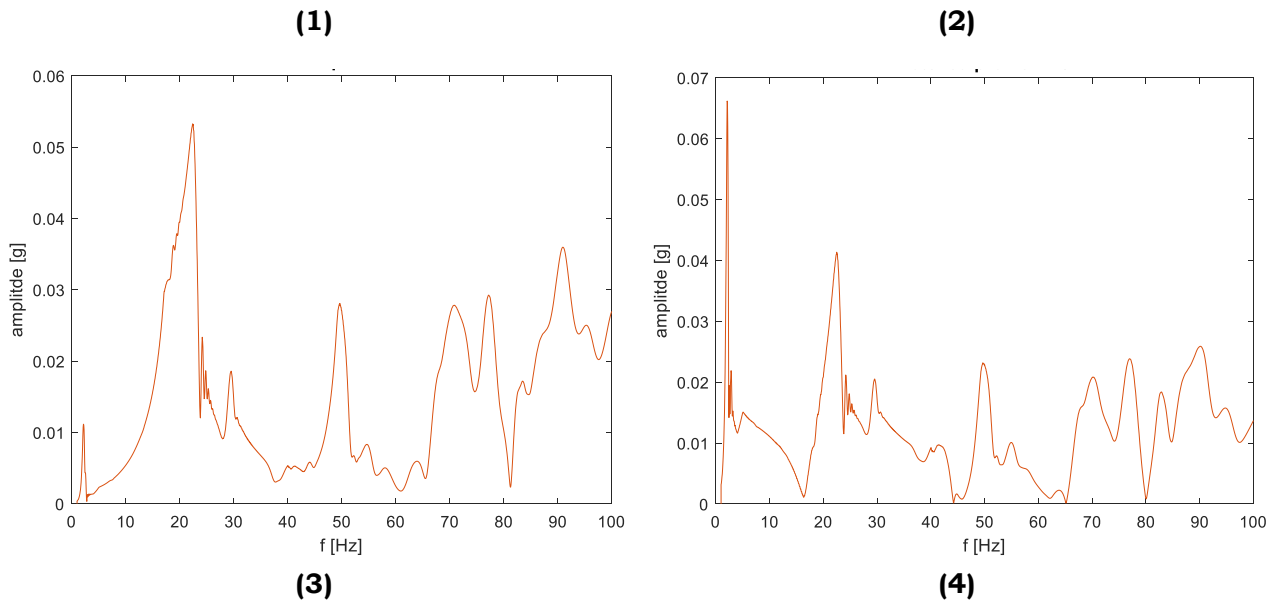


Figure 108: Sine Y - Pilots along Z (Cross talks)

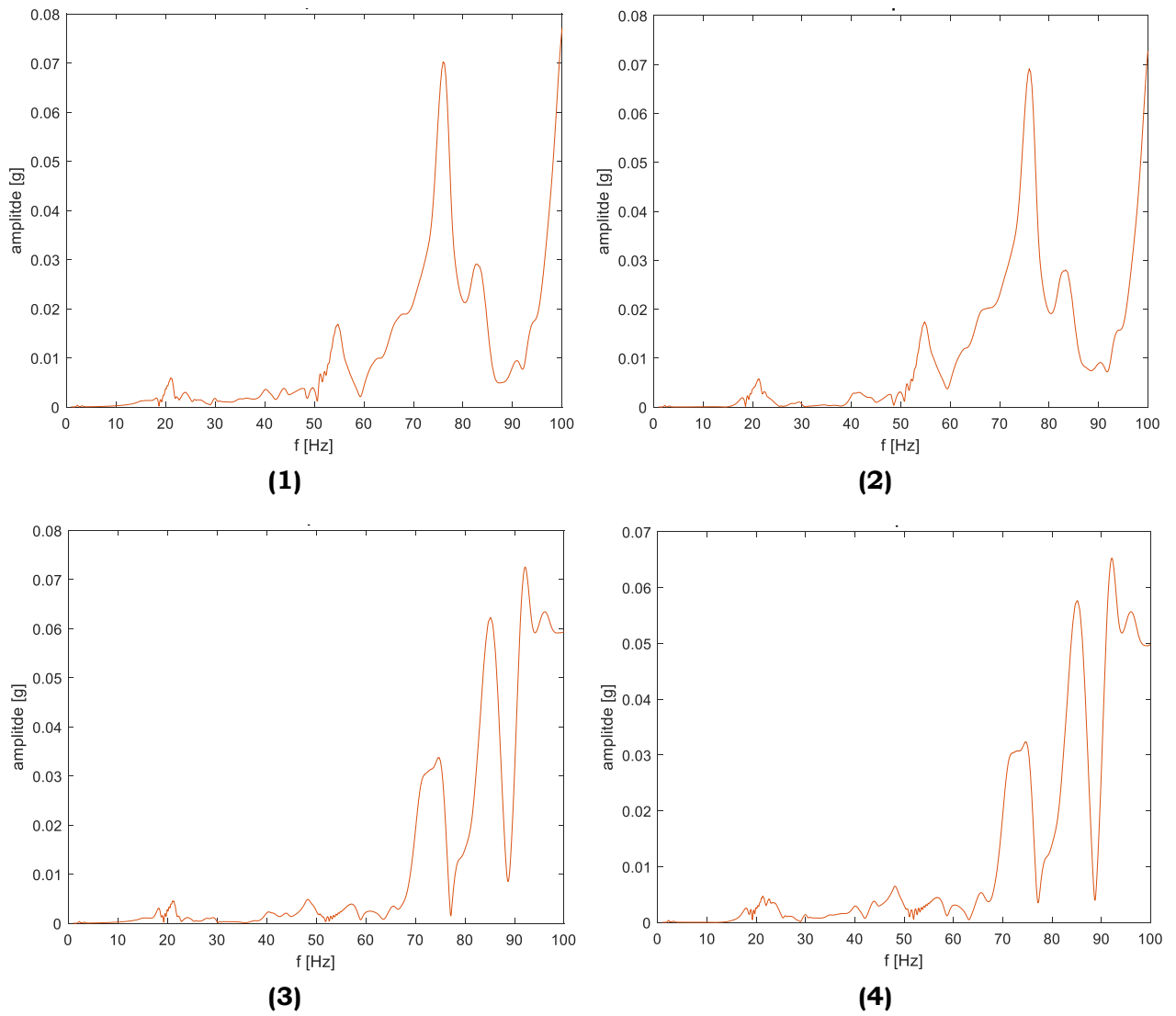


Figure 109: Sine X - Pilots along Y (Cross talks)

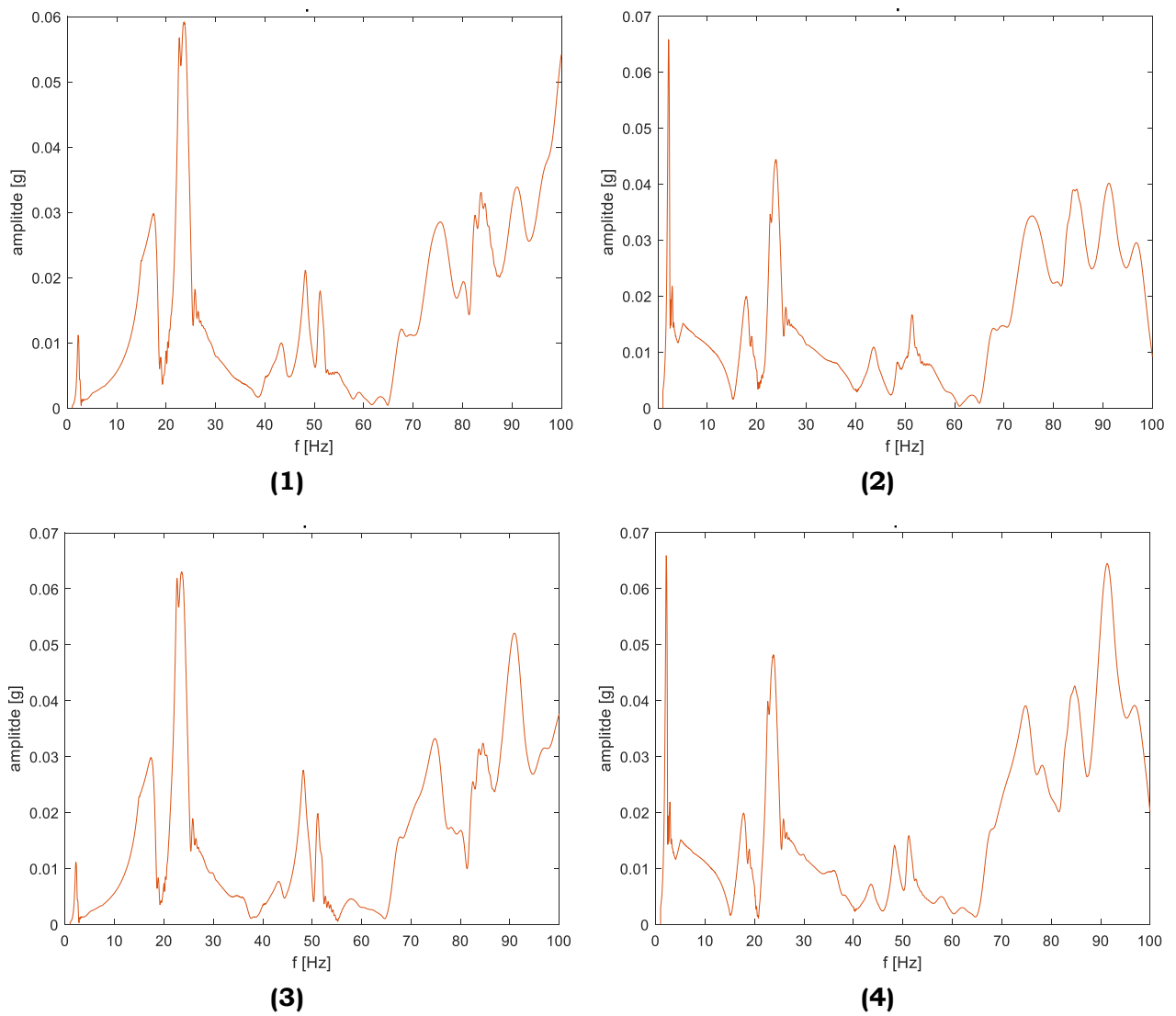


Figure 110: Sine X - Pilots along Z (Cross talks)

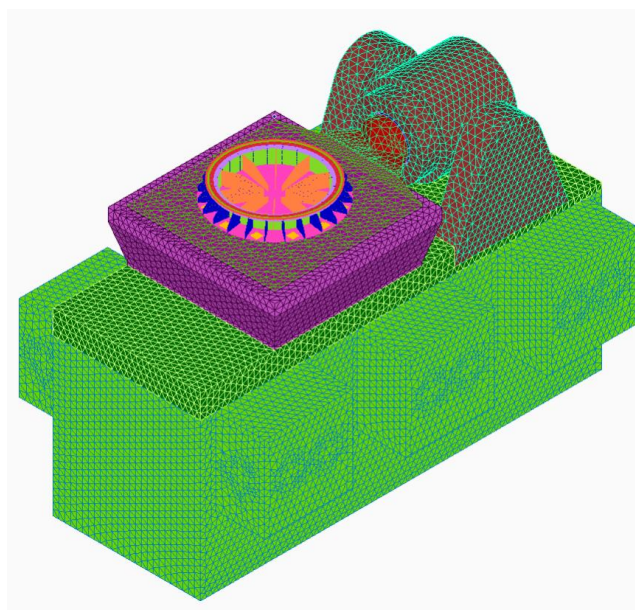


Figure 111: VTA adapter on shaker

References

1. Reduction of overtesting during base-drive random vibration tests for the euclid spacecraft hardware, Adriano Calvi, European Space Agency Keplerlaan 1, Noordwijk, the Netherlands.
2. Spacecraft base-sine vibration test data uncertainties investigation based on stochastic scatter approach, S. Laborde, A. Calvi
3. Virtual shaker testing: actual achievements in TAS and future prospects, P. Nali, V. Di pietro, P. Ladisa, G. Bitetti, F. Lumaca, A. Bettacchioli
4. Beating phenomena in spacecraft sine testing and an attempt to include the sine sweep rate effect in the test-prediction, Nali, Bettacchioli
5. Virtual shaker modeling and simulation, parameters estimation of a high damped electrodynamic shaker, Jonathan Martino, Kristof Harri
6. Understanding the Physics of Electrodynamic Shaker Performance by G.F. Lang and D. Snyder
7. Measured-based shaker model to virtually simulate vibration sine test, sébastien hoffait, frédéric marin, daniel simon, bart peeters, jean-claude golinval
8. Virtual shaker testing for predicting and improving vibration test performances, Ricci, b. Peeters, r. Fetter, d. Boland, j. Debille
9. Spacecraft Loads Analysis, Adriano Calvi PhD, ESA-ESTEC
10. Aircraft and Space Vehicles Structures, An Introduction to Modelling, Analysing and Testing Marco Di Sciuva
11. Mechanical Vibrations in Spacecraft Design, Jaap Wijker - Springer-Verlag Berlin Heidelberg (2004)
12. Spacecraft Structures, Jacob Job Wijker
13. Random Vibrations in Spacecraft Structures, Jaap Wijker
14. ECSS-E-HB-32-26A 19 February 2013 Spacecraft mechanical loads analysis handbook
15. ECSS-E-ST-32C Rev.115 November 2008 ST Structural general requirements
16. Modal Testing, A Practitioner's Guide, Peter Avitabile university of Massachusetts Lowell, USA
17. Modal Testing: Theory, Practice and Application, D. J. Ewins
18. Structural Dynamics in Industry, Alain Girard and Nicolas Roy
19. Harris_Shock_And_Vibration_Handbook
20. Structural Dynamics, Craig
21. Primer on the Craig-Bampton method. Introduction to boundary node functions, base shake analyses, load transformation matrices, modal synthesis and much more, John T. Young, October 2000.
22. Control System Design – An Introduction to State- Space Methods. Bernard Friedland
23. Sine sweep effect on specimen modal parameters characterization, Nicolas Roy, Maxime Violin, Etienne Cavo
24. The effect of swept sinusoidal excitation on the response of a single degree of freedom oscillator, J.A. Lollock, 2002
25. LMS Virtual Sine Controller, Bart Peeters
26. Experimental data driven approach for numerical spacecraft vibration test prediction, Waimer, Manzato, Peeters, Carrella, Wagner, Guillaume
27. On the spacecraft structure model validation and test philosophy, Aglietti, Remedia, Appolloni, Kiley
28. An enhanced methodology for spacecraft correlation activity, Remedia, Aglietti, Appolloni, Cozzani, Kiley

29. Lezioni di guida e controllo del velivolo. E.Battipede
30. Ariane5_Users-Manual_October2016
31. Mechanical vibration and shock analysis. Volume 1, Lalanne, Christian, Sinusoidal Vibration
32. Calculation of a Shock Response Spectra, Tuma
33. Understanding the Physics of Electrodynamic Shaker Performance by G.F. Lang and D. Snyder
34. MSC Nastran 2014 dynamic analysis user's guide
35. Validation of equivalent viscous damping methodologies, Xavier Vaquer Araujo, Mater thesis, ESA-ESTEC/ ISAE SUPAERO.
36. The Virtual Shaker Testing Approach in Spacecraft Sine Testing: Critical Overview and Assessments, Marco Gnoffo
37. Force limited random vibration testing: the computation of the semi-empirical constant C2 for real article and unknown supporting structure, Thesis of Jaap Wijker
38. The Euclid mission design, Giuseppe D. Racca et al.